LEABHARLANN CHOLÁISTE NA TRÍONÓIDE, BAILE ÁTHA CLIATH | TRINITY COLLEGE LIBRARY DUBLIN
Ollscoil Átha Cliath | The University of Dublin

**Terms and Conditions of Use of Digitised Theses from Trinity College Library Dublin**

**Copyright statement**

All material supplied by Trinity College Library is protected by copyright (under the Copyright and Related Rights Act, 2000 as amended) and other relevant Intellectual Property Rights. By accessing and using a Digitised Thesis from Trinity College Library you acknowledge that all Intellectual Property Rights in any Works supplied are the sole and exclusive property of the copyright and/or other IPR holder. Specific copyright holders may not be explicitly identified. Use of materials from other sources within a thesis should not be construed as a claim over them.

A non-exclusive, non-transferable licence is hereby granted to those using or reproducing, in whole or in part, the material for valid purposes, providing the copyright owners are acknowledged using the normal conventions. Where specific permission to use material is required, this is identified and such permission must be sought from the copyright holder or agency cited.

**Liability statement**

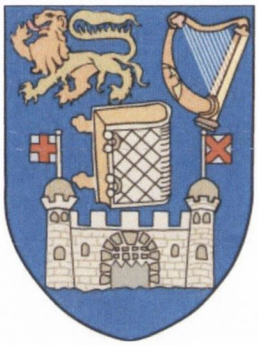
By using a Digitised Thesis, I accept that Trinity College Dublin bears no legal responsibility for the accuracy, legality or comprehensiveness of materials contained within the thesis, and that Trinity College Dublin accepts no liability for indirect, consequential, or incidental, damages or losses arising from use of the thesis for whatever reason. Information located in a thesis may be subject to specific use constraints, details of which may not be explicitly described. It is the responsibility of potential and actual users to be aware of such constraints and to abide by them. By making use of material from a digitised thesis, you accept these copyright and disclaimer provisions. Where it is brought to the attention of Trinity College Library that there may be a breach of copyright or other restraint, it is the policy to withdraw or take down access to a thesis while the issue is being resolved.

**Access Agreement**

By using a Digitised Thesis from Trinity College Library you are bound by the following Terms & Conditions. Please read them carefully.

I have read and I understand the following statement: All material supplied via a Digitised Thesis from Trinity College Library is protected by copyright and other intellectual property rights, and duplication or sale of all or part of any of a thesis is not permitted, except that material may be duplicated by you for your research use or for educational purposes in electronic or print form providing the copyright owners are acknowledged using the normal conventions. You must obtain permission for any other use. Electronic or print copies may not be offered, whether for sale or otherwise to anyone. This copy has been supplied on the understanding that it is copyright material and that no quotation from the thesis may be published without proper acknowledgement.

# Investigation and Theoretical Modeling of the Nonlinear Optical Properties of 5,10-$A_2B_2$ Porphyrins



*Submitted by*

**Monika Zawadzka**

School of Chemistry, Trinity College Dublin, Ireland

*A thesis submitted to the University of Dublin, Trinity College for the degree of*

**Doctor of Philosophy**

*University of Dublin, Trinity College*

*2012*

TRINITY COLLEGE
2 4 MAY 2013
LIBRARY DUBLIN

Thesis 10163

## Declaration

This thesis has not been submitted as an exercise for a degree at this or any other university. Except where otherwise indicated, the work described herein has been carried out by the author alone.

The author agrees that the library may lend or copy this thesis upon request.

Monika Zawadzka

Monika Zawadzka

## Summary

An optical limiter is a device which is transparent to ambient light but becomes opaque upon high intensity laser irradiation. Such irradiation is dangerous to human eyes and light sensitive detectors. Porphyrins, which are a group of conjugated macrocyclic dyes, are interesting candidates for optical limiting (OL) applications. This is because they exhibit strong positive nonlinear absorption (NLA) in the spectral window between Soret and Q-bands in the visible range. The NLA arises due to the sequential absorption of photons and is referred to as reverse saturable absorption (RSA). RSA occurs when the excited states absorb light more efficiently than the ground state, which is phenomenally expressed as transmission drop with intensity. Although much is known about the linear and nonlinear optical properties of porphyrins, it is still not fully understood how the structural features of these macrocycles impact their OL performance.

First, the research focused on the investigation of the linear and nonlinear absorptive properties of structurally diversified free base and metallated meso substituted porphyrin monomers, dimers and trimers in different meso configuration patterns, in order to identify correlations between the compound structure and its OL performance. It was found that the introduction of meso substituents with strong electron-withdrawing or –donating character, or the incorporation of zinc into the central cavity of the porphyrin ring, improved OL performance. Generally, compounds with substituents connected to porphyrin ring *via* multiple bonds provided better OL efficiency than similar compounds with directly bound substituents. The trimethylsilylethynyl (TMS-ethynyl) meso substituent was identified to be especially promising for OL uses. In addition to the character of the substituents, the meso configuration pattern also impacted the NLA properties of the compounds studied.

Based on the above findings new porphyrins in the yet unexplored 5,10-$A_2B_2$ substitution pattern, were designed and synthesized. The target compounds comprised of two series of 5,10-$A_2B_2$ porphyrins with varied central metal. For the first series A = bromine and for the second series A = TMS-ethynyl, while B = *p*-tolyl for both series. 5,10-Di(*p*-tolyl)porphyrin precursor was subjected to bromination and to further metallation to yield the first (brominated) series of compounds. Bromoporphyrins were then coupled with TMS-acetylene in a Sonogashira coupling reaction to obtain the second series of compounds. Alternatively, metallation of TMS-ethynyl substituted free base was applied to obtain some of metal complexes of the TMS-ethynyl series.

Nonlinear absorptive properties of the two series of 5,10-$A_2B_2$ porphyrins were studied

(open Z-scan technique). Some of the compounds exhibited more complex responses than a simple drop in transmission with the input intensity, typically observed under similar experimental conditions. A transmission drop in the lower intensity regime turning over to a transmission increase in the higher intensity range (RSA/SA switch), or an increase in transmission in the lower intensity regime turning over to a drop in higher intensities (SA/RSA switch) was detected. Although the character of the responses varied between compounds, modeling studies revealed that the four-level model with simultaneous two-photon absorption arising from the higher excited state (1 + 1 + 2 photon absorption) best fitted all of the responses. This suggested that 5,10-$A_2B_2$ porphyrins exhibited photophysical properties different from those of compounds in other substitution patterns.

With regard to OL performance of the two series of 5,10-$A_2B_2$ porphyrins, the TMS-ethynyl meso substituent was found to be a more promising OL group than a bromine atom at the equivalent positions. Except for lead, the effect of the metal on the OL performance was not consistent for the two series of compounds. With regard to the central metal, the OL performance showed the following trends: 2H ~ Pd(II) < Sn(IV) ~ Zn(II) ~ In(III) < Pb(II) for the brominated series, and: 2H < Sn(IV) < Pd(II) < In(III) ~ Zn(II) ~ Pb(II) for the TMS-ethynyl one. This showed that the effect of the substituent was significant.

Finally, the effect of the solvent on nonlinear optical properties of the 5,10-$A_2B_2$ compounds was studied. Generally, most of the compounds exhibited better OL performance in toluene compared to DMF or chloroform. This was attributed to the enhanced two-photon absorption in toluene. Nonlinear scattering contributed strongly to the open Z-scan responses for many compounds in chlorobenzene and chloroform/chlorobenzene solutions but did not occur in other solvents studied. This was associated with the photodegradation of chlorobenzene. Additionally, it was demonstrated that free base porphyrins in chloroform were protonated upon illumination with laser light, which enhanced their OL performance. It was proposed that upon illumination with focused laser beam chloroform undergoes photodegradation, which generates protonic species reacting with the free base porphyrin to give its protonated form.

To conclude, 5,10-$A_2B_2$ porphyrins were identified as an interesting group of nonlinear optical materials exhibiting unique photophysical properties. It was also demonstrated that type of the substituents and their regiochemical rearrangement, as well as the chemical environment must be fine-tuned simultaneously to maximize the optical limiting efficiency of porphyrins.

# Publications

Mathias O. Senge, Claudia Ryppa, Marijana Fazekas, Monika Zawadzka and Katja Dahms, "5,10-$A_2B_2$-type meso-substituted porphyrins a unique class of porphyrins with a realigned dipole moment" *Chem. Eur. J.*, **2011**, 17, 13562-13573.

Mathias O. Senge, Marijana Fazekas, Monica Pintea, Monika Zawadzka and Werner J. Blau, "5,15-$A_2B_2$– and 5,15-$A_2BC$–type porphyrins with donor and acceptor groups for use in nonlinear optics and photodynamic therapy" *Eur. J. Org. Chem.*, **2011**, 5797-5816.

Monika Zawadzka, Jun Wang, Werner J. Blau and Mathias O. Senge, "Correlation studies on structurally diverse porphyrin monomers, dimers and trimers and their nonlinear optical responses" *Chem. Phys. Lett.*, **2009**, 477, 330-335.

Marijana Fazekas, Monica Pintea, Mathias O. Senge and Monika Zawadzka, "Synthetic strategies and porphyrin building blocks for unsymmetrical multichromophores" *Tetrahedron Lett.*, **2008**, 49, 2236-2239.

Mathias O. Senge, Marijana Fazekas, Eleni G. A. Notaras, Werner J. Blau, Monika Zawadzka, Oliver B. Locos, Eimhin M. Ni Mhuircheartaigh, "Nonlinear optical properties of porphyrins" *Adv. Mater.*, **2007**, 19, 2737-2774.

## Conference Abstracts

Monika Zawadzka, Jun Wang, Mathias O. Senge and Werner J. Blau, "Open Z-scan studies on 5,10-$A_2B_2$ porphyrins" International Conference on Organic Photonics and Electronics 2011 / The 12th International Conference on Organic Nonlinear Optics, Trinity College Dublin, Dublin, Ireland, 6 – 9 September **2011**.

Monika Zawadzka, Jun Wang, Mathias O. Senge and Werner J. Blau, "Open Z-scan studies on structurally diverse porphyrins" The 9th International Symposium on Advanced Organic Photonics, Shannon, Ireland, 3 – 4 September **2009**.

Monika Zawadzka, Jun Wang, Mathias O. Senge and Werner J. Blau, "Open Z-scan studies on structurally diverse porphyrins" International Symposium on Materials and Devices for Nonlinear Optics, Ile de Porquerolles, France, 26 June – 1 July **2008**.

Monika Zawadzka, Mathias O. Senge and Werner J. Blau, "Open Z-scan studies on porphyrins systems" CSCB Symposium, Health Sciences Centre, University College Dublin, Ireland, 12 December **2008**.

Monika Zawadzka, Jun Wang, Mathias O. Senge and Werner J. Blau, "Optical limiters – Porphyrins" The Tetrapyrrole Discussion Group, Trinity College Dublin, Dublin, Ireland, 12 - 14 September **2008**.

Monika Zawadzka, Marijana Fazekas, Monica Pintea, Mathias O. Senge and Werner J. Blau, "Optical limiters – Porphyrins", HRSMC Summer School "Photochemistry 2008: Fundamentals and Applications" Maastricht, The Netherlands, 31 May – 4 June **2008**.

Monika Zawadzka, Marijana Fazekas, Monica Pintea, Mathias O. Senge and Werner J. Blau, "Porphyrins as materials for optical limiting" CSCB Symposium, Dublin, Ireland, 14 December **2007**.

*"It is important to become aware of interdependence by realizing that a phenomenon occurs owing to multiple causes and conditions. Reducing it to one single factor would lead to a fragmentation of reality."*

*The Dalai Lama in My Spiritual Autobiography*

# Acknowledgements

First of all I would like to thank my supervisor Prof. Mathias O. Senge for his advice, motivating and guiding me throughout my Ph. D. studies. I would also like to express gratitude to Prof. Werner J. Blau for the consultations on my project. Many thanks to Dr. Jun Wang for his assistance in the laboratory work, fruitful discussions which helped me to develop a wider perception of the studied subject, his encouragement, and all the time he devoted me. Special and warm thanks to Dr. Eimear Finnigan for all her help. Thanks to Science Foundation Ireland for the financial support.

Many thanks to technical and administrative staff from School of Chemistry, Trinity College, for their help and friendly attitude which made everyday tasks much more pleasurable. Thanks to Dr. John O'Brien and Dr. Manuel Rüther for NMR measurements, Dr. Martin Feeney for mass spectrometry measurements, Fred Cowzer, Colm Deevey and Marcus Phelan for the provision of chemicals and solvents.

Warm thanks to all of the former and current members of the Senge research group, especially to: Dr. Oliver Locos, Dr. Frances Blaikie, Dr. Sabine Horn, Dr. Aoife Ryan, Dr. Mohd Bakri Bakar, Edyta Paszko, Mia Davis and Muntaz Abu Bakar. Thanks to Marijana Fazekas and Monica Pintea for providing great compounds for open Z-scan studies. Thanks as well to the members of the Blau research group, especially to Brian Tuffy for exploring the potential of my compounds for applications in light emitting diodes.

Finally, thanks to my parents, my sister Magda, and Filip for their support.

# Contents

Declaration ..... I

Summary ..... III

Publications ..... V

Conference Abstracts ..... VI

Acknowledgements ..... IX

Abbreviations ..... XIV

Chapter 1 Introduction ..... 1

1.1 Nonlinear optics – background ..... 1

1.2 Origin of NLO effects ..... 2

1.3 NLO materials – general considerations ..... 3

1.4 Optical limiting ..... 5

1.4.1 Optical limiters ..... 5

1.4.2 Reverse saturable absorption ..... 7

1.4.3 Multiphoton absorption ..... 12

1.4.4 Free-carrier absorption ..... 15

1.4.5 Nonlinear refraction ..... 15

1.4.6 Nonlinear scattering ..... 17

1.4.7 Summary on optical limiting effects ..... 19

1.5 Experimental techniques used in NLO ..... 19

1.5.1 Z-scan ..... 21

1.6 Porphyrins ..... 24

1.6.1 Introduction to porphyrins ..... 24

1.6.2 Second order NLO properties of porphyrins ..... 26

1.6.3 Third order NLO properties of porphyrins ..... 28

1.6.4 Optical limiting properties of porphyrins ..... 31

1.6.5 Objectives and outlook ..... 39

Chapter 2 Investigation of the optical limiting properties of structurally diversified porphyrin monomers, dimers and trimers ..... 41
2.1 Introduction and outline ..... 41
2.2 Materials, experimental technique and data treatment details ..... 41
2.2.1 Materials ..... 41
2.2.2 Experimental technique ..... 43
2.2.3 Data treatment ..... 43
2.3 Results and discussion ..... 44
2.3.1 General observations and remarks ..... 44
2.3.2 Monomers ..... 48
2.3.3 Dimers ..... 54
2.3.4 Trimers ..... 57
2.4 Summary and outlook ..... 58
Chapter 3 Synthesis of novel free base and metallated 5,10-$A_2B_2$ porphyrins ..... 67
3.1 Introduction ..... 67
3.2 Review of the synthetic pathways leading to 5,10-$A_2$ and 5,10-$A_2B_2$ porphyrins 67
3.3 Metalloporphyrins ..... 71
3.4 Sonogashira coupling ..... 73
3.5 Synthesis and characterization of 5,10-$A_2B_2$ porphyrins ..... 74
3.5.1 Synthesis of 5,10-$A_2B_2$ porphyrins ..... 74
3.5.2 Identification of axial ligands with MS ..... 79
3.5.3 $^1$H NMR studies ..... 80
3.5.4 Aggregation of metalloporphyrins ..... 85
3.6 Summary ..... 89
Chapter 4 Modeling of the nonlinear absorption of 5,10-$A_2B_2$ porphyrins ..... 91
4.1 Introduction and outline ..... 91
4.2 Theoretical background ..... 91
4.3 Experimental details ..... 94

4.4 Results ..... 94
4.4.1 Ground state absorption features ..... 94
4.4.2 Nonlinear absorption responses ..... 95
4.4.3 Modeling of nonlinear absorption responses ..... 97
4.5 Discussion ..... 107
4.6 Summary ..... 112
Chapter 5 Nonlinear absorption properties of 5,10-$A_2B_2$ porphyrins – correlation of molecular structure to the nonlinear responses ..... 115
5.1 Introduction and outline ..... 115
5.2 Theoretical background ..... 115
5.3 Experimental and theoretical modeling details ..... 116
5.4 Results ..... 116
5.4.1 Ground state absorption features ..... 116
5.4.2 Nonlinear absorption responses and data fitting ..... 117
5.5 Discussion ..... 119
5.6 Summary ..... 126
Chapter 6 Solvent effect on the nonlinear absorption of 5,10-$A_2B_2$ meso substituted porphyrins. ..... 127
6.1 Introduction and outline ..... 127
6.2 Theoretical background ..... 127
6.3 Experimental and data treatment details ..... 128
6.4 Results and discussion ..... 129
6.4.1 Solvent induced nonlinear scattering ..... 133
6.4.2 Solvent effect on the nonlinear absorption ..... 135
6.5 Summary ..... 153
Chapter 7 Laser induced protonation of free base porphyrins in chloroform resulting in the enhancement of positive nonlinear absorption ..... 155
7.1 Introduction and outline ..... 155
7.2 Theoretical background ..... 155

7.3 Experimental details ..... 156
7.4 Results and discussion ..... 156
7.5 Conclusions ..... 162
Chapter 8 5,10-$A_2B_2$ porphyrins as materials for organic light emitting diodes ..... 163
Chapter 9 Conclusions and future outlook ..... 167
Chapter 10 Experimental ..... 169
10.1 Instrumentation and general considerations ..... 169
10.2 Syntheses ..... 170
Appendix ..... 183
Bibliography ..... 195

## Abbreviations

| | |
|---|---|
| 2H_Br | 5,10-dibromo-15,20-di(*p*-tolyl)porphyrin |
| 2H_CCTMS | 5,10-di(*p*-tolyl)-15,20-bis[(trimethylsilyl)ethynyl]porphyrin |
| 2H_CCTIPS | 5,10-di(*p*-tolyl)-15,20-bis[(triisopropylsilyl)ethynyl]porphyrin |
| 2H_H | 5,10-di(*p*-tolyl)porphyrin |
| $2\omega$ | second harmonic |
| Ac | acyl |
| acac | acetylacetonate |
| AF-50 | *N*,*N*-diphenyl-7-[2-(4-pyridinyl)ethenyl]-9,9-di-*n*-decyl-9*H*-fluoren-2-amine |
| Ar | aromatic |
| br | broad |
| C, $C_i$ | molar concentration |
| *c* | speed of light |
| calcd. | calculated |
| cm | centimeter |
| CN | coordination number |
| CNs | carbon nanotubes |
| CT | charge transfer |
| cw | continuous wave |
| d | doublet |
| DBU | 2,3,4,6,7,8,9,10-octahydropyrimidol[1,2-a]azepine |
| DCM | dichloromethane |
| DDQ | 2,3-dichloro-5,6-dicyano-1,4-benzoquinone |
| DFWM | degenerate four-wave mixing |
| DMF | dimethylformamide |
| *E* | laser energy |
| *E'* | strength of the electric field |
| EFISH | electric field induced second harmonic generation |
| EL | electroluminescence |
| ES | electrospray |
| ESA | excited state absorption |
| esu | electrostatic unit |
| ET | electron transfer |

| | |
|---|---|
| Et | ethyl |
| equiv. | equivalent |
| $F$ | fluence |
| $F_{RSA/SA}$ | RSA/SA turnover fluence |
| $F_{th}$ | threshold fluence |
| FRET | Förster resonance energy transfer |
| GM | Göppert-Mayer |
| GW | gigawatt |
| $h\nu$ | photon energy |
| HRMS | high resolution mass spectrometry |
| HRS | hyper-Rayleigh scattering |
| Hz | Hertz |
| $I$ | light intensity |
| $I_0$ | onfocus intensity |
| $I_i$ | saturation intensity of the ground state (i = 0) or of the excited states (i ≥ 1) |
| $I_{th}$ | threshold intensity |
| $Im\{\chi^{(3)}\}$ | imaginary part of third order susceptibility $\chi^{(3)}$ |
| InCl_Br | chloro[5,10-dibromo-15,20-di(*p*-tolyl)porphyrinato]indium(III) |
| InCl_TMS | chloro{5,10-di(*p*-tolyl)-15,20-bis[(trimethylsilyl)ethynyl] porphyrinato}idium(III) |
| IR | infrared |
| ISC | intersystem crossing |
| ITO | indium tin oxide |
| IUPAC | International Union of Pure and Applied Chemistry |
| $J$ | coupling constant measured in Hertz |
| $L$ | true optical path length through the sample |
| $L_{eff}$ | effective length of the sample |
| LC | liquid crystal |
| LD | laser desorption |
| LED | light emitting diode |
| [M] | molecular ion |
| m | multiplet |
| MALDI | matrix-assisted laser desorption/ionization |

| | |
|---|---|
| MAP | methyl-(2,4-dinitrophenyl)-aminopropanoate |
| Me | methyl |
| m.p. | melting point |
| MS | mass spectrometry |
| m/z | mass-to-charge ratio |
| $N$ | population density of electron-hole pairs |
| $n$ | refractive index |
| $N_i$ | population density of the *i*-th state (other than five level Jablonski models) |
| $N_{m_i}$ | population density of the *i*-th state *m* (five level Jablonski model) |
| $N_T$ | total population density |
| $n_0$ | linear refractive index |
| NBS | *N*-bromosuccinimide |
| Nd:YAG | neodymium-doped yttrium aluminium garnet; $Nd:Y_3A_{l5}O_{12}$ |
| NIR | near-infrared |
| NLA | nonlinear absorption |
| NLO | nonlinear optics |
| NLR | nonlinear refraction |
| NLS | nonlinear scattering |
| nm | nanometer |
| NMR | nuclear magnetic resonance |
| NPP | *N*-[4-nitrophenyl-(*L*)-prolinol] |
| ns | nanosecond |
| OL | optical limiting |
| OLED | organic light emitting diode |
| $P$ | electric polarization induced in the medium |
| $p$ | molecular electric polarization induced in the medium |
| Pb_Br | [5,10-dibromo-15,20-di(*p*-tolyl)porphyrinato]lead(II) |
| Pb_CCTMS | {5,10-di(*p*-tolyl)-15,20-bis[(trimethylsilyl)ethynyl]porphyrinato}lead(II) |
| Pd_Br | [5,10-dibromo-15,20-di(*p*-tolyl)porphyrinato]palladium(II) |
| Pd_CCTMS | {5,10-di(*p*-tolyl)-15,20-bis[(trimethylsilyl)ethynyl]porphyrinato}palladium(II) |
| PDT | photodynamic therapy |

| | |
|---|---|
| PFO | poly(9,9-dioctyluorenyl-2,7-diyl) |
| Ph | phenyl |
| PhOLED | phosphorescent light emitting diode |
| PL | photoluminescence |
| POM | 3-methyl-4-nitropyridine-1-oxide |
| ppm | parts per million |
| ps | picosecond |
| Pt_Br | [5,10-Dibromo-15,20-di(*p*-tolyl)porphyrinato]platinum(II) |
| q | quartet |
| $R$ | curvature radius of the phase front |
| $R_f$ | retention factor |
| $Re\{\chi^{(3)}\}$ | real part of third order susceptibility $\chi^{(3)}$ |
| RLi | organolithium reagent |
| RSA | reverse saturable absorption |
| RT | room temperature |
| s | singlet |
| $S_0$ | ground singlet state |
| $S_1$, $S_2$ | excited singlet state |
| SA | saturable absorption |
| $SnCl_2$_Br | dichloro[5,10-dibromo-15,20-di(*p*-tolyl)porphyrinato]tin(IV) |
| $SnCl_2$_CCTMS | dichloro{5,10-di(*p*-tolyl)-15,20-bis[(trimethylsilyl)ethynyl]porphyrinato}tin(IV) |
| t | triplet |
| $t$ | time |
| $T_1$, $T_2$ | excited triplet states |
| $T_{Norm.}$ | normalized transmission |
| TBP | tetrabenzoporphyrin |
| TEA | triethyl amine |
| TFA | trifluoroacetic acid |
| TGH | third harmonic generation |
| THF | tetrahydrofuran |
| TIPS | triisopropylsilyl |
| TLC | thin layer chromatography |
| TMS | trimethylsilyl |
| TOF | time of flight |

| | |
|---|---|
| TPA | two-photon absorption |
| TPP | 5,10,15,20-tetraphenylporphyrin |
| UV | ultraviolet |
| vis | visible |
| v/v | volume to volume |
| w/v | weight to volume |
| $Z$ | position along Z-axis |
| $Z_0$ | diffraction length |
| $Z_M$ | metal charge |
| $Z'$ | distance along the direction of beam propagation |
| Zn_Br | [5,10-dibromo-15,20-di(*p*-tolyl)porphyrinato]zinc(II) |
| Zn_CCTMS | {5,10-di(*p*-tolyl)-15,20-bis[(trimethylsilyl)ethynyl]porphyrinato}zinc(II) |
| $\alpha$ | absorption coefficient |
| $\alpha'$ | linear polarizability |
| $\beta'$ | first (quadratic) hyperpolarizability |
| $\beta_{eff}$ | effective nonlinear absorption coefficient |
| $\beta_{TPA}$ | two-photon absorption coefficient |
| $\gamma'$ | second (cubic) hyperpolarizability |
| $\delta$ | chemical shift measured in parts per million (ppm) |
| $\Delta\phi$ | nonlinearly-induced phase shift |
| $\varepsilon$ | molar absorption coefficient |
| $\varepsilon_0$ | permittivity of free space |
| $\theta$ | beam divergence |
| $\kappa_i, \kappa$ | ratio of the excited state absorption cross-section (of i-th state) to that of the ground state |
| $\lambda$ | wavelength measured in nanometre (nm) |
| $\lambda_{max}$ | maximum of the Soret band |
| $\mu$ | permanent dipole moment |
| $\mu_0$ | permeability of free space |
| $\mu$J | microjoule |
| $\mu$s | microsecond |
| $\sigma$ | free-carrier absorption cross-section |
| $\sigma_{ex}^{S}$ | singlet excited state absorption cross-section |

| | |
|---|---|
| $\sigma_{ex}^{T}$ | triplet excited state absorption cross-section |
| $\sigma_{gr}$ | ground state absorption cross-section |
| $\sigma_i$ | absorption cross-section of i-th state |
| $\sigma_{TPA}$ | two-photon absorption cross-section |
| $\tau$ | pulse width |
| $\tau_{ISC}$ | intersystem crossing time |
| $\tau_{S_1}$ | lifetime of singlet excited state $S_1$ |
| $\tau_{S_2}$ | lifetime of singlet excited state $S_2$ |
| $\tau_{T_1}$ | lifetime of singlet excited state $T_1$ |
| $\tau_{T_2}$ | lifetime of singlet excited state $T_2$ |
| $\chi^{(1)}, \chi^{(2)}, \chi^{(3)}$ | linear, second and third order susceptibility |
| $\psi_{S_1-T_1}$ | intersystem crossing quantum yield |
| $\omega$ | light frequency |
| $\omega'$ | beam waist radius |
| $\omega_0$ | beam waist radius at the focus |

# Chapter 1 **Introduction**

## 1.1 Nonlinear optics – background

Nonlinear optics (NLO) is a branch of optics which explores different phenomena that arise due to modification of the optical properties of matter by the presence of light.[1] Usually high light intensities are needed to provoke such phenomena. In very general terms light-matter interaction in NLO media, under sufficient light intensities, provides light with different frequency or spatiotemporal characteristics. The main goal of NLO is to understand the underlying mechanisms of such phenomena and to make them controllable so that they can be used in optical information and imaging processing, laser technologies, diagnostics, *etc.*

The history of NLO began long ago in 1875 with the observation made by Kerr of an electric field induced change in the refractive index of $CS_2$, which was directly proportional to the square of the strength of the applied electric field.[2] Nevertheless, it was almost a century after this observation before this branch of optics began to emerge. This was coupled directly with the discovery of the laser by Maiman in 1960.[3] Lasers gave access to high light intensities, which upon interaction with matter, resulted in new and interesting optical phenomena. The second harmonic generation of ruby lasers with quartz crystals, discovered by Franken in 1961, is usually recognized as the beginning of the new NLO era.[4, 5] Much progress has been achieved on experimental, theoretical and conceptual levels since this discovery, and the momentum of NLO is continuously increasing. New NLO phenomena such as sum-frequency generation, optical rectification, stimulated Raman scattering, self-focusing, four-wave mixing, just to mention a few, were soon discovered. Different classes of inorganic and organic materials were studied and identified as NLO active, with a lot of emphasis being put on the latter materials nowadays. Advances in new techniques for the fabrication and growth of artificial materials were made. Many efforts have been made to comprehend how structural features impact NLO

properties in order to obtain materials with enhanced NLO properties. These efforts are bearing fruits in applied aspects of NLO, though low nonlinearities are still often a hindrance in the implementation of the NLO materials into devices. Further developments in the field will inevitably be coupled with progress in material science. It is believed that the full potential of NLO is yet to be revealed, and may revolutionize information and imaging processing. Areas of great NLO applications include telecommunication, data storage, computers, and display technologies. NLO based techniques and technologies have already been implemented into science, medicine, industry, entertainment, military, and security, and will certainly expand into other areas of human activity in the future.[6-11]

## 1.2 Origin of NLO effects

Upon irradiation with an electromagnetic field a material becomes polarized. This results from the interaction of an oscillating electric field with a material's dipole moment. Upon low light irradiation electric dipoles oscillate harmonically with the applied field. This behavior is described by conventional linear optics. In this case, electric polarization, $P$, induced in the medium is simply assumed to be linearly proportional to the electric strength $E'$ of an applied optical wave according to:

$$P = \chi^{(1)}E' \qquad \textbf{1-1}$$

where $\chi^{(1)}$ is the linear susceptibility of a given medium representing its linear response, *i.e.* linear absorption and refractive index. Under high intensity light irradiation sources, when the electric field strength acquires values comparable to the interatomic electric fields ($10^5$ – $10^8$ V/m), the linear approximation is no longer obeyed. Oscillations of the electronic dipoles can no longer follow harmonically the oscillations of the applied field. This induces polarization in the material, which in turn, can act as a new source that is capable of emitting secondary electromagnetic waves. Here, the mathematical characterization of an NLO medium can be presented in the following manner, where the induced electric polarization in the material is expressed as a power series according to:

$$P = \chi^{(1)}E' + \chi^{(2)}E'E' + \chi^{(3)}E'E'E' + \ldots \qquad \textbf{1-2}$$

where $\chi^{(2)}$ and $\chi^{(3)}$ are second and third order susceptibilities, respectively. At the molecular level, the equation takes the form:

$$p = \alpha'E' + \beta'E'E' + \gamma'E'E'E' + \ldots \qquad \textbf{1-3}$$

where $\alpha'$, $\beta'$, $\gamma'$ are: linear polarizability, the first (quadratic) and second (cubic) hyperpolarizabilities respectively. Different distinctive effects arise through second and third order terms, referred to as second and third order NLO processes. The characteristic feature of NLO processes due to second order susceptibility is that they always change the frequency of light (an exception is Pockels effect, also called an electro-optics effect) and for this reason they are often used for the generation of new frequencies. Third order effects are far more diversified and may be used either to change the frequency of the light or its spaciotemporal characteristics. In contrast to second order effects, third order effects are dependent on light frequency. An example of a second order process is the second-harmonic generation or sum frequency generation. Third harmonic generation, optical phase conjugation, intensity-dependent absorption and refraction are examples of third order NLO effects. All of these NLO phenomena find applications in devices for frequency conversion, optical switching and limiting, optical logic circuits, *etc.*

It should be stated that nonlinear susceptibilities are in general tensor quantities, which define the dependence of the NLO properties on the symmetry of the molecular system. Only noncentrosymmetric systems can provide second order NLO effects whereas third order processes are allowed for all molecular systems. For that reason, liquids, gases and amorphous solids do not exhibit second order NLO processes.

It is important to emphasize that the power series expansion expressed above (**1-2** and **1-3**) does not converge for many NLO phenomena. In this case the relationship between a material's response and the applied electric field must be expressed using different procedures. This refers to different NLO effects that arise at resonant or close to resonant frequencies, though it can also refer to NLO effects at nonresonant frequencies, *e.g.*, when the applied field strength is high enough to induce photoionization in the material. Examples of resonant NLO effects involve saturable absorption, reverse saturable absorption, free-carrier absorption and refraction, and they find applications in devices for pulse shaping, mode locking and optical switching and limiting. Most of these effects will be detailed in the following parts of this thesis with regard to their application in optical limiting (OL).

## 1.3 NLO materials – general considerations

NLO research initially focused on inorganic materials. With the demonstration of strong second order NLO effects arising in donor-acceptor substituted aromatic compounds by

Davydov *et al.*[12] and third order effects in polydiacetylenes by Sauteret *et al.* in the 1970's,[13] organic materials quickly garnered much of the attention. The advent of optical fibers in telecommunication in the late 1970's initiated even more research into organic NLO materials.[14]

Up to now different classes of inorganic and organic materials were proven to be NLO active. Besides high nonlinearities, NLO materials must meet other requirements which are associated with their function in a device and fabrication process *i.e.* its integration with other device components. In these terms organic materials often outpace inorganic materials. Organic compounds offer great flexibility as a wide range of structures is accessible through chemical manipulation. This enables the tailoring of a material's NLO and secondary properties such as solubility, thermal stability, transparency, *etc.* Besides their good processability and better integration with other device components, they exhibit very fast and high NLO effects. The advantages of inorganic materials lie in their environmental and mechanical strength and good performance at high and low temperatures. They are commercially used as second order materials for frequency conversion and it is expected that they will be difficult to replace by organic equivalents.[7]

NLO materials can be classified according to the order of nonlinearity they exhibit as second and third order NLO materials. The principal feature that was identified to influence second order nonlinearity was charge asymmetry within a single unit, as electron delocalization over several identical units is essential for third order effects. Additionally, third order effects can arise through cascading second order processes. As mentioned before second order effects arise only in noncentrosymmetric media; for third order effects there is no such requirement.

Highly diverse materials were found to exhibit NLO effects. Second order NLO materials include inorganic crystals such as β-$BaB_2O_4$, $KH_2PO_4$, $LiNbO_3$; heteropolar semiconductors like GaAs, CdS; various organic and organometallic materials especially donor-acceptor aromatics, stilbenes, diarylacetylenes, diacetylenes, biaryls with varied donor and acceptor groups (*e.g.* MAP (methyl-(2,4-dinitrophenyl)-aminopropanoate), POM (3-methyl-4-nitropyridine-1-oxide), NPP (*N*-[4-nitrophenyl-(*L*)-prolinol])), urea, amino acids, metal-pyridine or –bipyridine complexes *etc.*; disordered media including poled polymers, glasses in particular fused silica and many others. Some promising classes of materials for third order applications include: covalent semiconductors such as Ge or GaAs, composite materials *i.e.* semiconductor and metal nanocrystals in glasses, linear

conjugated polymers with polydiacetylenes being the most studied, organic dyes like porphyrins, phthalocyanines, rhodamine, azo dyes and their derivatives, organometallics *e.g.* poly(silanes), as well as noncentrosymmetric media with large second order susceptibilities for cascading third order effects.[6]

It should be highlighted that the key structural feature of effective and fast nonlinearities in organic materials is the presence of a conjugated π-electron system. Mobile, weakly bound π-electrons respond quickly to the applied electric field. The introduction of donor and acceptor end groups which enhance asymmetric polarizability of such π-electron systems was demonstrated to increase the effectiveness of such processes – especially those of second order.

## 1.4 Optical limiting

Optical limiting (OL) is a research area of applied NLO. It explores different NLO effects which can be used to protect human eyes and sensitive optical sensors against accidental exposure to laser light. The importance of OL is connected to expanding applications of laser technology in many areas of medicine, research, industry and every-day use devices. Lasers are also of great interest for military purposes not only for use in different detecting and designating devices but also as a weapon itself. Whatever their application, lasers pose a great threat to human eyes and other sensitive optical sensors. Human eyes can be damaged by light pulses with an energy as low as 1 μJ. Thus, the application of laser technologies must be combined with the use of protection methods against hazards posed by the intense radiation. It should be noted that lasers operating over a broad range of visible spectra and tunable lasers are becoming widely used. Meanwhile new laser technologies are being developed. In these terms, passive filters can no longer provide complete eye protection and there is an increasing need for new solutions. At the moment, OL is recognized as the most promising protection method and is expected to provide devices of great potential use for the broadband protection against wavelength-agile lasers.[15, 16]

### 1.4.1 Optical limiters

An optical limiter is a device that strongly attenuates high fluence/intensity light while exhibiting high transmittance to low fluence/intensity ambient light. Thus the function of the sensitive optical sensor at low light fluence/intensity is not affected and once high light fluence/intensity is reached the sensor is protected. The response of an ideal optical limiter

might be represented with an OL curve plotted as input fluence/intensity *versus* output fluence/intensity as shown in Figure 1. The transmitted light fluence/intensity increases linearly with the input up to a certain fluence/intensity threshold value ($F_{th}/I_{th}$). Once this value is exceeded, the output remains constant, irrespective of the input. High transmission at low inputs, which grants unaffected detection sensitivity, along with low threshold value is an indicator of a good optical limiter. Besides protection of sensors optical limiters can find some other applications *e.g.* pulse shaping or power regulation.

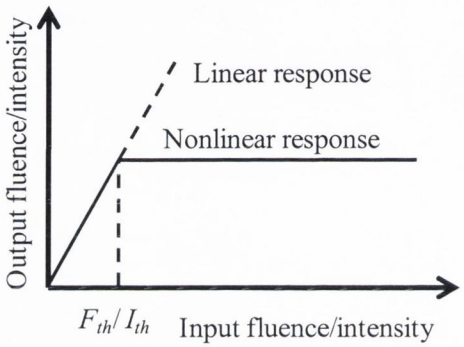



**Figure 1** Response of an ideal optical limiter.

In general optical limiters fall into two categories: passive and active devices. In active devices a photodetector first senses the level of the input light and then this information is used to control an aperture keeping the output light at the desired level. In passive devices sensing and light attenuation roles are due to NLO material itself. Passive devices are therefore far less complex. Additionally, their response times are much faster, which makes them suitable for pulsed lasers (of ns or shorter duration). From now only passive methods will be considered.

The first passive optical limiting behavior based on the laser-induced thermal lens effect exhibited by nitrobenzene was experimentally demonstrated in 1967.[17] Since then, much progress has been made in the field. Different nonlinear mechanisms have been identified as useful for OL and various materials have been recognized as promising for OL ranging from semi-conductors,[18] liquid crystals[19] and gas plasmas,[20] to different dyes.[21-23] In general, mechanisms giving rise to OL effects can be classified into two groups: energy spreading and energy absorbance. The former mechanism changes spatial energy distribution of the light after passage through the NLO medium. Self-focusing, self-defocusing, and induced scattering are examples of such NLO effects. For energy absorbing mechanisms, the functioning of the device relies on the fact that for certain materials the transmission decreases as light fluence/intensity increases. Reverse saturable

absorption (RSA) and multiphoton absorption processes, especially two-photon absorption (TPA) processes are the most important mechanisms of this type.

NLO effects that give rise to OL can also be classified differently, *i.e.* as resonant and nonresonant, which were discussed briefly in the general consideration about the origin of different NLO effects (p. 2). The most widely applied nonresonant NLO effects arise through third order susceptibility $\chi^{(3)}$, especially through its imaginary part which is associated with TPA, but also through its real part which is associated with the Kerr effect. As mentioned before, for resonant effects such as RSA, free-carrier absorption and refraction, equation **1-2**, expressing induced electric polarization as a power series of the electric field strength, does not converge. For these processes other procedures are used to describe the relationship between a material's response to the applied electric field. Nonresonant processes depend on instantaneous intensity in the medium, they involve transition to virtual levels and are thus rapid; resonant processes depend on the energy density deposited in the medium and are in principle fluence dependent, they involve transitions to real electronic levels and consequently their response times are limited by the lifetime of the excitation. Damage to eyes and sensors is usually fluence dependent and thus fluence limiting is preferable in this case. The disadvantage of resonant nonlinearities that give rise to OL effects compared to nonresonant processes is that they operate frequently at a narrower bandwidth. Additionally instantaneous nonresonant processes usually need high intensities and typically are effective against short optical pulses.

### 1.4.2 Reverse saturable absorption

RSA was discovered by Guilinia and Hess for the first time in vat dyes when they were exploring different saturable absorption (SA) materials for mode locking applications.[24] A material's absorption decreases with the input fluence when a material exhibits SA, for RSA the opposite happens, hence the nomenclature. Harter *et al.* proposed and demonstrated the applicability of RSA for the use in OL and pulse shaping devices.[25]

RSA arises through sequential absorption of photons. It is representative to use a standard five-level Jablonski energy diagram[26] to explain the RSA mechanism (Figure 2).

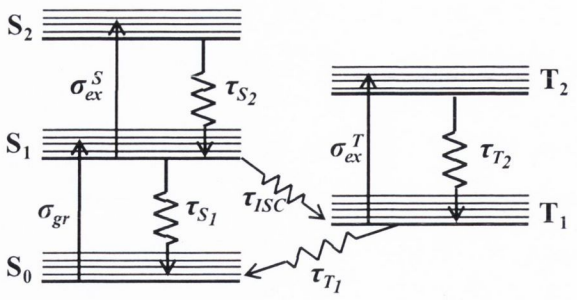



**Figure 2** Five-level energy diagram. Solid lines represent absorption, jagged lines decay paths. $S_0$, $S_1$ and $S_2$ are singlet states, $T_1$, $T_2$ are triplet states. $\sigma_{gr}$ refers to ground state absorption cross-section, $\sigma_{ex}^{S}$ and $\sigma_{ex}^{T}$ represent singlet and triplet excited state absorption cross-sections respectively, $\tau_{S_1}$ and $\tau_{T_1}$ represent the first singlet and triplet excited state lifetimes, $\tau_{ISC}$ refers to intersystem crossing time, and $\tau_{S_2}$ and $\tau_{T_2}$ refers to decay times from higher excited singlet and triplet states.

The behavior of an aromatic organic compound upon irradiation with light is considered now. Such a behavior will depend on how a material's photophysical characteristics correspond to the pulse duration of the applied laser. Typically, a molecule exists in its ground state $S_0$. After initial excitation the first excited singlet state $S_1$ is populated. Typically the lifetime of this state is of the order of ns. Thus, once a ps pulsed laser is used, the population of the first excited state can be accumulated during the pulse width, promoting absorption to higher excited singlet states. Provided the cross-section of the excited singlet states $\sigma_{ex}^{S}$ is larger than that of the ground state $\sigma_{gr}$, the material will exhibit RSA, otherwise SA will be detected. The decay time from the higher excited state $S_2$ - $\tau_{S_2}$ - is usually of the order of ps or less – thus no significant accumulation of population in this state should occur. Once a laser of longer pulse duration (ns) is used, intersystem crossing (ISC) from the first excited singlet $S_1$ state to a triplet $T_1$ state becomes possible, since the lifetime of this transition $\tau_{ISC}$ is of the order of ns or less. Even though this kind of transition is forbidden from a quantum mechanical point of view as it involves spin multiplicity change, it can be made highly efficient through the introduction of atoms with a heavy atomic number (heavy atom effect). Mixing of the electron spin of the heavy atom with the molecular orbital, *i.e.* spin-orbit coupling can considerably enhance the population of the $T_1$ state. The population build-up in triplet state $T_1$, which is in general a long-lived state, promotes absorption to the higher excited triplet state $T_2$. RSA will be observed if the absorption cross-section of the triplet state $\sigma_{ex}^{T}$ is higher than that of the ground state $\sigma_{gr}$. The relaxation time $\tau_{T_2}$ from $T_2$ to $T_1$ is usually very rapid, similar to that from $S_2$ to $S_1$ state. RSA might of course arise simultaneously from the absorption arising from singlet and triplet states upon certain conditions. If the lifetime of an absorptive state, $S_1$ or $T_1$, is

not long enough in comparison to the pulse duration, the efficiency of the OL effect will be weaker. If the lifetime of the excited state is much shorter than the laser pulse, the limiting becomes intensity rather than fluence dependent.[27]

In reference to the above model, a promising RSA material for OL applications should have the following characteristics: (1) high ratio of the excited to ground state absorption cross-section $\kappa = \sigma_{ex}/\sigma_{gr}$; (2) longer than pulse duration lifetime of the absorbing singlet or triplet excited state, so that the population in that state does not decay to any other state during the pulse width; (3) efficient and quick generation of the population of highly absorbing excited state (if $T_1$ is the highly absorbing state - high quantum yield for triplet states $\psi_{S_1-T_1}$ and rapid ISC); (4) rapid relaxation from higher excited states, which usually absorb weakly and thus which significant population would lead to saturation of the response; (5) and finally sufficiently high linear absorption which will grant significant population in the excited state. It is desirable that all these characteristics are maintained over a broad range of bandwidths. It should be highlighted that much interest is focused on the search for RSA absorbers with strong excited state absorption (ESA) arising from triplet states. The lifetime of these states reaches microseconds and this enables fabrication of OL devices that are capable of attenuating effectively long laser pulses. Moreover, an optical material must be highly soluble as high concentrations of material are required to prevent saturation of the fluence. As intermolecular interactions deteriorate RSA efficiency, they must be suppressed. Additionally, a good candidate should be transparent over a broad spectral bandwidth and be resistant to damage.[28]

In order to evaluate how the transmission of a material varies with input, the following set of equations (rate and propagation equations), which describes the behavior of the five-level system presented above must be solved numerically:

$$\frac{\partial N_{S_0}}{\partial t} = -\frac{\sigma_{gr} N_{S_0} I}{h\nu} + \frac{N_{S_1}}{\tau_{S_1}} + \frac{N_{T_1}}{\tau_{T_1}} \qquad \textbf{1-4}$$

$$\frac{\partial N_{S_1}}{\partial t} = \frac{\sigma_{gr} N_{S_0} I}{h\nu} - \frac{\sigma_{ex}^{S} N_{S_1} I}{h\nu} + \frac{N_{S_1}}{\tau_{S_1}} + \frac{N_{S_1}}{\tau_{ISC}} \qquad \textbf{1-5}$$

$$\frac{\partial N_{S_2}}{\partial t} = \frac{\sigma_{ex}^{S} N_{S_1} I}{h\nu} - \frac{N_{S_2}}{\tau_{S_2}} \qquad \textbf{1-6}$$

$$\frac{\partial N_{T_1}}{\partial t} = -\frac{\sigma_{ex}^{T} N_{T_1} I}{h\nu} - \frac{N_{T_1}}{\tau_{T_1}} + \frac{N_{S_1}}{\tau_{ISC}} + \frac{N_{T_2}}{\tau_{T_2}} \quad \textbf{1-7}$$

$$\frac{\partial N_{T_2}}{\partial t} = \frac{\sigma_{ex}^{T} N_{T_1} I}{h\nu} - \frac{N_{T_2}}{\tau_{T_2}} \quad \textbf{1-8}$$

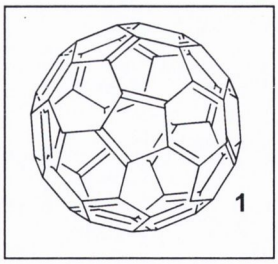
$$N_T = N_{S_0} + N_{S_1} + N_{S_2} + N_{T_1} + N_{T_2} \quad \textbf{1-9}$$

$$\frac{\partial I}{\partial z'} = -\sigma_{gr} N_{S_0} I - \sigma_{ex}^{S} N_{S_1} I - \sigma_{ex}^{T} N_{T_1} I \quad \textbf{1-10}$$

where $h\nu$ is the energy per photon, $I$ is the intensity of the pulse, $z'$ is the distance along the direction of beam propagation, $t$ – time, $N_{m_i}$ is the population density of the $i$-th state $m$, $N_T$ – total number of molecules. Stimulated emission has been neglected. In many cases this system of equations may be simplified. Since the lifetimes of higher excited singlet and triplet states are very short, population of states $N_{S_2}$ and $N_{T_2}$ might often be set to zero as there will be no population build-up in these states. This is especially valid when longer laser pulses of the order of ns are used. Further simplifications can be made when ISC is efficient and fast; in this case it might be assumed that after excitation the population is immediately transferred to the $T_1$ state, which reduces the model to a three-level system.[27] Although it also happens that the standard five-level system is not sufficient to explain the detected behavior; in this case the model has to be expanded further on. Models comprising up to seven levels have been reported.[29]

Having in mind the requirements for an efficient RSA material, one realizes that there are not too many compounds which meet these criteria. Phthalocyanines, porphyrins, fullerenes, their derivatives and few others are recognized as the most promising candidates for OL applications.[30] Most of the RSA characterization of these materials were carried out in solution. It was also demonstrated that OL efficiency is not independent on the nature of the solvent used.[31, 32] There are many reports on guest-host films, sol-gel materials and polymers.[33, 34] A brief introduction to the most promising groups of OL materials exhibiting RSA is given below.

Fullerenes: Buckmisterfullerene ($C_{60}$ **1**) is an intensively investigated benchmark RSA material. RSA in this material ranges from visible to near-infrared (NIR). The ESA arising from $S_1$ and $T_1$ has peaks at ~550 and ~740 nm respectively. A weak ground state absorption band, in the visible range, extends from 450 to 650 nm. The lifetime of the $T_1$ state was ~40 μs.[35] ISC to $T_1$ is fast and efficient ($\tau_{ISC}$ = 600±100 ps).[36] The ratio of the absorption cross-sections $\kappa = \sigma_{ex}^{S}/\sigma_{gr}$ and $\kappa = \sigma_{ex}^{T}/\sigma_{gr}$ at 532 nm were estimated to be ~5 and ~3 respectively[37]; in the range between 620 and 810 nm Kohlman *et al.* reported that $\sigma_{ex}^{T} > \sigma_{ex}^{S}$.[38] Although $\sigma_{ex}^{T}/\sigma_{ex}^{S}$ was found to increase with the wavelength, reduction in the ground state absorption made limiting weaker in longer wavelength range. The damage threshold for ns pulses is typically 5-10 μJ/cm$^2$. Different derivatives of $C_{60}$ including polymers were prepared and studied for their OL properties. The main motivation for this was to enhance nonlinear absorption (NLA) in the IR region and to improve the solubility of $C_{60}$. This aim was achieved for certain $C_{60}$ derivatives with side groups.[39, 40] Yet $C_{60}$ polymers were not promising materials as they exhibited higher limiting thresholds and weaker NLA than $C_{60}$.[36] Higher fullerenes such as $C_{70}$, $C_{76}$, $C_{78}$ and $C_{84}$ were also tested, though these were found to exhibit weaker OL than $C_{60}$.[41, 42]




Macrocyclic dyes: Porphyrins and phthalocyanines are planar aromatic compounds with large delocalized π-electron systems spread over a macrocyclic ring. The porphyrin backbone is composed of four pyrrole rings connected by unsaturated methine bridges. Phthalocyanines are composed of four *N*-fused isoindole units (Figure 3). Chemical synthesis gives access to a large range of possible structures for these aromatic compounds through introduction of various groups at peripheral positions of the ring or *via* the introduction of different metals into the central core of the macrocycle. This provides a means to alter their ground and ESA properties. The ultraviolet-visible (UV-vis) absorption spectra of these macrocycles are characterized by two distinctive features, the Soret-band and Q-bands at longer wavelengths. RSA is observed in the absorption valley between these two characteristic bands, which covers the visible to NIR spectral range. In contrast to porphyrins, phthalocyanines have a more intense Q-band, which could provide linear

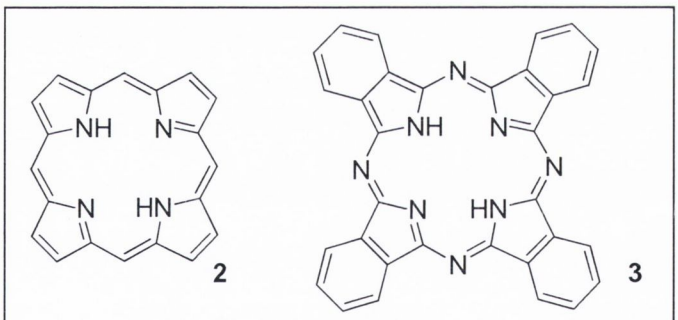



**Figure 3** The porphyrin **2** and phthalocyanine **3** framework.

limiting of the light in the longer wavelength range.[30] Naphthalocyanine (benzo-fused phthalocyanines) exhibit spectra much more shifted towards the infrared (IR), with a spectral window in the red and yellow regions.

It is desirable that promising RSA dyes have narrow ground state absorption features to provide a wide spectral window for RSA. Thus, it is no surprise that the most promising candidates are highly symmetric compounds.[37] Macrocyles were demonstrated to be effective against both subnanosecond and ns pulsed or even continuous wave (cw) lasers.[27] Most studies reported were carried out at the second harmonic of Nd:YAG laser of 532 nm; the ratios of the excited state absorption cross-sections to that of the ground state $\kappa = \sigma_{ex}^{S}/\sigma_{gr}$ and $\kappa = \sigma_{ex}^{T}/\sigma_{gr}$ at this wavelength varied from numbers slightly above unity to being on the order of 40 – 50 for different compounds.[27, 43] A very effective way of enhancing OL performance of macrocyclic dyes, broadly investigated, is to introduce heavy atom or paramagnetic metals ions into the macrocyclic core.[44, 45] Next to studies on simple molecules, there is a large body of reports on more complex macrocyclic-based compounds, such as macrocyclic oligomers,[46] rare-earth sandwich type derivatives,[47] or macrocycle-based dyads (*e.g.*, porphyrin+fullerene,[48] porphyrin+viologen[49]) displaying charge-transfer processes. A more detailed review on the OL properties of porphyrins and their derivatives will be given below.

Other organic and organometallic compounds: Indanthrene, its derivatives and oligomers were found to exhibit RSA at 532 nm, though only in ns pulse regime; under ps pulses SA was observed.[23] However, their OL performance was inferior to that of $C_{60}$. Several metal clusters were explored in ns time regime at 532 nm. The involvement of metal-ligand charge transfer to ESA was found to enhance the OL efficiency of the compounds studied. A disadvantage of these compounds is their poor photostability. This was overcome by structure modifications but this was not coupled with any superior OL efficiency.[37]

### 1.4.3 Multiphoton absorption

A k-photon absorption is an instantaneous process which arises at 1/k of the resonant frequency; its rate of absorption is proportional to $I^k$. TPA is an example of the lowest multiphoton absorption process and further considerations will be limited to this special case. TPA was observed for the first time by Kaiser and Garrett in 1961 in $Eu^{2+}$:$CaF_2$[50] although it was predicted theoretically long before in 1931 by Maria Göeppert-Mayer.[51] The mechanism of TPA can be thought of in the terms of a simplified three-level RSA model (Figure 4) where the lifetime of the intermediate virtual state populated after

absorption of the first photon approaches zero, and the absorption arising from the ground state is extremely low. Absorption of the second photon takes an electron from virtual, intermediate to final state, which results in TPA.

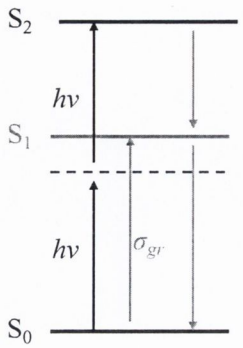



**Figure 4** Illustration of the TPA process, dashed line represents virtual level, solid line – real electronic levels.

The attenuation of light in TPA medium is governed by the following propagation equation:

$$\frac{dI}{dz} = -\alpha_{gr} I - \beta_{TPA} I^2 \qquad \textbf{1-11}$$

where $\alpha_{gr}$ is the linear absorption coefficient and $\beta_{TPA}$ is the TPA coefficient. As mentioned before, TPA is associated with an imaginary part of third order susceptibility $Im\{\chi^{(3)}\}$, which is directly related to $\beta_{TPA}$ according to:

$$Im\{\chi^{(3)}\} = n_0^2 \varepsilon_0 c \lambda \beta_{TPA}/(2\pi) \qquad \textbf{1-12}$$

where $n_0$ is the linear refractive index, $\varepsilon_0$ is the permittivity of free space, $c$ is the speed of light and $\lambda$ is the wavelength.

The solution to the propagation equation **1-11** for low linear absorption ($\alpha_{gr} = 0$) takes the following form:

$$I(L) = \frac{\mathrm{I}}{(1 + \mathrm{I}\beta_{TPA} L)} \qquad \textbf{1-13}$$

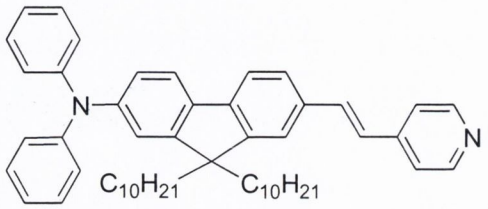
where $L$ is the length of the optical pathway. It is clear that the output intensity decreases with input, a behavior that is desirable for OL applications, and that the strength of this reduction depends on $\beta_{TPA}$, $L$ and $I$. As $\beta_{TPA}$ does not reach very high values in most of the available materials, high input intensities are needed in order to achieve a significant

reduction in transmission from a sample of reasonable length. Consequently, since intensity is essentially fluence divided by pulse duration, short pulses are required to achieve OL with TPA for fluences that might be harmful for optical sensors. Accordingly, TPA based OL is mainly suitable to protect against ultrafast pulses (pico- and femtosecond) though recent progress in materials science has begun to provide materials that are effective against longer pulses, being in the order of ns. TPA based OL in reference to RSA based OL is attractive for low visual losses. In combination with a rapid response time TPA is more suitable for other applications such as optical stabilization and reshaping.[10, 37]

Research into TPA materials attracts a lot of attention. Apart from the application of TPA in optical limiting, stabilization and reshaping, this process has potential for 3D-microfabrication and multiphoton microscopy.

Semiconductors were the earliest materials studied in TPA,[52, 53] and they exhibit relatively high $\beta_{TPA}$. They are still promising materials for IR range sensor protection even though they have considerable residual linear losses in this region. They are not suitable for the visible range as they are not transparent to visible light. HgCdTe, InAs, InSb are examples of some promising semiconductors for IR sensor protection.[18, 54]

A significant body of research has been conducted on organic materials exhibiting TPA. These studies enabled to establish key structural features of an effective TPA material. Usually it is composed of a framework for mobile π-electrons with electron donor/acceptor groups on the terminal sites with or without donors/acceptors in the middle of the conjugated framework. Such structures provide symmetric charge displacement upon excitation and this enhances TPA. Derivatives of diphenyl, stilbene, fluorene, dihyrophenanthrene, anthracene, pyrrole, squaraine, thiophene, triphenylamine, porphyrin, paracyclophanes and multi-annulene systems among other different classes of materials have been invesitgated.[55] An example of some promising organic TPA material for OL applications is AF-50 (**4**) which is effective in the visible range against pulses with a duration of up to ns.[56]




**4**

It should be mentioned that some materials may exhibit other nonlinearities associated with TPA, *i.e.* TPA-induced free-carrier absorption (as in semiconductors) and refraction, which can contribute to the OL effect.

### 1.4.4 Free-carrier absorption

Free-carrier absorption is a process which arises mainly in semiconductors since these materials have relatively low energy band gaps, which facilitates the generation of free-carriers. Such carriers can be generated by absorption of one or two photons (through TPA). Subsequent absorption of another photon gives rise to free-carrier absorption. Similarly to RSA, free-carrier absorption is an accumulative process, *i.e.* it depends on the build-up of the carrier population within the band. The attenuation equation for free-carrier absorption is as follows:

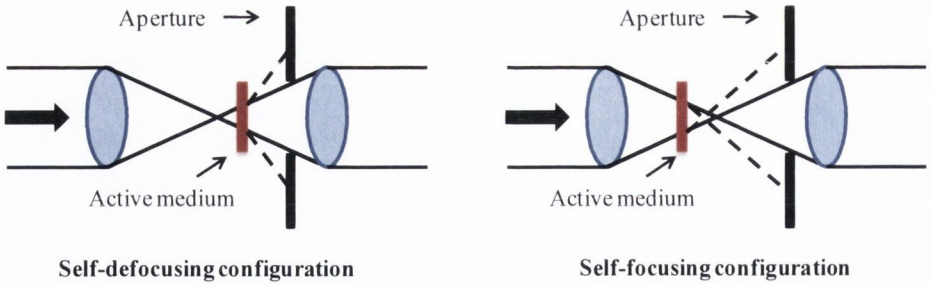
$$\frac{\partial I}{\partial z'} = -\alpha_{gr} I - \sigma N I \qquad \textbf{1-14}$$

where $\sigma$ stands for the total (electron and hole) free carrier absorption cross-section and $N$ for the population density of electron-hole pairs, which depends on intensity and thus brings in nonlinearity. An analytical approximation of the solution for the above equation can only be done for short pulse durations compared to the times associated with recombination and diffusion of the charges, and when taking no account of other absorptive and refractive nonlinear processes which are often active. Otherwise the equation must be solved numerically.

Free-carrier absorption usually contributes to the OL in semiconductors and it is important to consider this process in the precise modeling of the response. However its contribution is usually less significant than that arising through nonlinear refraction (NLR) (regardless of whether the carriers were generated through single or two photon transitions).[37]

### 1.4.5 Nonlinear refraction

NLR can be defined as a change in the refractive index or the spatial distribution of the refractive index of a medium due to the presence of optical waves. If the change is positive self-focusing occurs otherwise self-defocusing takes place. Depending on, which of these two processes occur, different optical configuration used in optical limiters are implied (Figure 5).




**Self-defocusing configuration** **Self-focusing configuration**

**Figure 5** Typical configuration of optical limiter based on self-defocusing and –focusing.

A converging lens focuses incident radiation in order to activate the device at low incident intensity. Upon activation, a spatially nonuniform refractive index arising through a nonuniform (intensity) profile of the beam, starts to act as a lens – positive or negative - refracting light away from the sensor. On one hand the enhancement of the light intensity through self-focusing might lead to catastrophic damage to the nonlinear medium; on the other hand it may lead to activation of the device at lower input. Self-defocusing has an advantage in practical devices in these terms as it provides self-protecting mechanism for the active material.

NLR can originate from electronic nonlinearity of the material, *i.e.* through the Kerr effect, which is an instantaneous process. The change in the refractive index $\Delta n$, in this case, is proportional to the applied intensity according to:

$$\Delta n = \gamma' I \qquad \textbf{1-15}$$

where $\gamma'$ is correlated with the real part of third order susceptibility $Re\{\chi^{(3)}\}$ through the following relation:

$$\gamma' = \left(\frac{\mu_0}{\epsilon_0}\right)^{1/2} \frac{3Re\{\chi^{(3)}\}}{4n_0^2} \qquad \textbf{1-16}$$

with $\mu_0$ being permeability of free space.

Usually the instantaneous electronic nonlinear index change is not high enough to lead to significant OL. More important refractive index changes arise through accumulative processes, which are characterized by a much slower temporal response.[57] Such processes occur in RSA dyes through population build-up in the excited states or in semiconductors where the populations of free-carriers can become significant through linear absorption or TPA. It is possible that both instantaneous and accumulative NLR will occur together, *e.g.*, for TPA semiconductors (however, the latter process will dominate). The refractive index

of the material in the excited state differs from that in the ground state. Thus, once significant population build-up in the excited state arises, a material's refractive properties change. Besides this, another source of refractive index change can be derived from the absorbed energy which causes material heating and subsequent expansion of the material itself or the host. Thermal expansion is especially high for different liquids which exhibit defocusing.[17] Thermal effects that arise in solids usually result in self-focusing, which can be problematic and lead to material damage. The thermally-induced change in the refractive index can become significant for pulses of the order of a few ns and alone may lead to effective OL. In many materials, it is often the case that the refractive index changes due to excited state population build-up dominates for the fluence being close to the limiting threshold value; at much higher fluences, above the limiting threshold, the change in the refractive index is due to thermal effects. Note that significant thermally-induced refractive index changes can arise at high intensities through impurities or external particles with non-zero residual absorption.[27, 41]

An interesting group of materials useful for OL, which acts through laser field-induced change in the refractive index, is liquid crystals (LC).[58] The origin of the refractive index change in these materials arises from laser field induced reorientation of the molecules. The disadvantage of OL based on this effect is a slow response time; the realignment process takes milliseconds to seconds. A significant advantage of LC is their high transparency along the entire visible spectrum.

### 1.4.6 Nonlinear scattering

Nonlinear scattering (NLS) arises when interaction of light with medium generates scattering centers which could be either physical particles or interfaces between excited and non-excited molecules. Once such centers are created, the transmission of medium at a given solid angle decreases. Optical limiters based on NLS usually rely on liquid media since processes that give rise to OL in such media are often reversible in contrast to those in solids which usually lead to material decomposition. Even if decomposition occurs in the liquid medium, the illuminated volume might be easily refreshed by circulation or diffusion.

The angular distribution of the intensity of the scattered light depends on the size of the scattering centers. For molecules smaller than the incident wavelength or non-absorbing particles, *i.e.* for Rayleigh scatterers, the scattered radiation is symmetric with respect to forward and backward directions. For molecules larger than the wavelength, *i.e.* Mie

scatterers, the distribution in these directions is asymmetric with more light being transferred in the forward directions. This makes the latter process less effective. Additionally, the percentage of the light scattered forward in Mie scattering increases with the size of scattering centre (Figure 6).

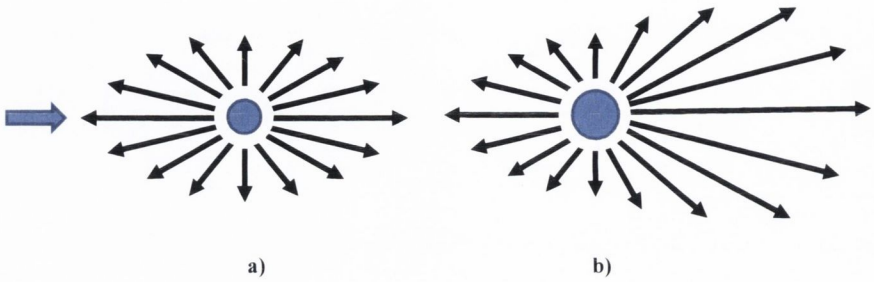



**Figure 6** Schematic representation of angular redistribution of the intensity of the scattered light for a) Rayleigh and b) Mie scatterers.

A number of methods can lead to the creation of light induced scattering centers. One way to generate such centers is to use small absorbing particles such as carbon black[59], carbon nanotubes[15, 60] or clusters[58] in solutions. When exposed to light such particles will heat rapidly, ionize and form microplasmas, which will grow quickly and scatter the light strongly. Additionally for liquid media, when the local boiling point is exceeded, the vaporisation of the liquid will lead to the formation of microbubbles which are very effective scattering centres.[61] In this case it was demonstrated that the process is solvent dependent. When the size of scattering particles approaches the wavelength, less effective Mie scattering occurs. Another disadvantage of this way of creating scattering centers is that it destroys the particles; yet, this can be overcome simply by suspension flowing. The other limitation is response time, which makes this light attenuation method suitable for ns pulsed laser sources and not adequate for ps or shorter pulses. The idea is to use NLS based on this mechanism in tandem with NLA, where the former mechanism will provide protection to high intensities, since the threshold for plasma formation is higher than that for NLA.[57] Additionally, it was demonstrated that laser-induced NLS can arise in RSA limiters based on organic materials if complete dissolution of the materials was not achieved.[62]

Another means of creating scattering centers is to induce, by light, a change in the refractive index difference on the interface of two materials - usually glass in various forms (small particles, a rough surface, highly porous glass, regular array of holes in glass) and a liquid with large refractive nonlinearity.[63] The index of the glass is matched with that of

the fluid, so that the composite material is transparent to low intensity light. At high intensities the refractive index matching is lost through liquid nonlinearity, which leads to scattering. Heating of the liquid is achieved by addition of small amount of absorber dye. NLS based on such a mechanism depends on the thermal change in the refractive index. It can be a complementary effect to NLA and NLR, which altogether would provide a hybrid OL.

### 1.4.7 Summary on optical limiting effects

As presented above, it is clear that different mechanisms can contribute to the OL effect. In order to precisely model the response one must be aware of different mechanisms that can counteract. Experimental conditions such as wavelength, pulse duration, and intensity of the laser used, as well as the features of the material under investigation as its state, purity, homogeneity, *etc.* must be considered when modeling the OL response.

## 1.5 Experimental techniques used in NLO

Emphasis is put on the open *Z*-scan technique which was used to measure the OL response of the porphyrins under investigation. In the case of second order effects, more attention will be put on the most common techniques used for organic rather than inorganic materials.

As far as second order nonlinearities are concerned, different techniques have been developed which are useful for the measurement of bulk material or molecular coefficients. These are either absolute or relative techniques. For the latter, different inorganic materials are used as standard reference materials. Since bulk optical properties of organic crystals are determined by the individual molecular units, techniques for the measurement of molecular coefficients are widely applied to these materials. For these measurements a dissolved sample of an NLO active material is usually used. Many techniques for bulk material characterization require material in the form of single crystals, which make these techniques more difficult and time consuming. Others are carried out on powders or thin films. The most widely applied techniques for characterization of molecular parameters involve electric field induced second harmonic generation (EFISH) and Hyper-Rayleigh scattering (HRS).

The EFISH technique is suitable for dipolar molecules. It enables the deduction of the first hyperpolarisability $\beta'$ of an NLO active compound in solution. Strong electric fields applied on the molecules with a permanent dipole moment $\mu$ cause their reorientation,

which "breaks" the centrosymmetry of the solution hindering the second order effect. The technique is well established for the characterization of organic compounds. Nevertheless, it has some limitations. A molecule must possess a permanent dipole moment and it cannot ionize. In addition, the technique is complex.[64]

HRS is a newly developed technique. Here, the first hyperpolarizability is determined by measuring the second harmonic ($2\omega$) scattered light intensity as a function of concentration, when a solution of an NLO active compound is irradiated by light (at frequency $\omega$). The second harmonic scatter light intensity depends on first hyperpolarizability $\beta'$ of the solute molecules. The technique does not require an external field and consequently may be used to characterize nonpolar and ionic samples, which is a big advantage over EFISH. The disadvantages of these techniques are: the scattered second harmonic is weak thus requires sensitive detection; the high intensities needed require focusing and the detection system which is highly sensitive to the focal position; additionally, high intensities might provoke other undesired processes.[64]

A large number of techniques are used to determine characteristics (magnitude, response time and spectrum) of third order non-resonant and resonant nonlinearities. These are either absolute or relative techniques, similar to those used for second order nonlinearities. Standard techniques used to characterize third order nonlinearities include: third harmonic generation (TGH), excite-probe techniques, degenerate four-wave mixing (DFWM), interferometric techniques and *Z*–scan. Different nonlinear responses often coexist under certain experimental conditions, thus, different measurements are usually required at varied irradiance, pulse width, *etc.* to fully understand the underlying mechanisms. Instantaneous nonresonant nonlinearities should be independent of pulse width. Those at close to or resonant wavelengths of slower response, will change as the pulse width approaches the response time.

THG characterizes the pure electronic nonresonant third order susceptibility $\chi^{(3)}$ in centrosymmetric media. The major disadvantage of this technique is associated with the fact that all media are third order active and thus glass or even air surrounding the sample or cell generate third harmonic which will interfere with the signal. Different techniques were developed to overcome this problem. For organic molecules NIR laser sources are usually used. They provide responses in the visible to near UV to facilitate detection and avoid the strong UV absorption which is typical for such materials.[64]

Time-resolved pump-probe techniques enable the study of the temporal dynamics in NLA.

In its most common implementation, a strong pump pulse excites the sample and changes its optical properties. Then a weak probe pulse interrogates the excitation region and detects changes. By appropriately advancing and delaying the probe pulse, the temporal response is mapped out. The disadvantage of these techniques is complex data analysis, as pump-probe experimental methods are sensitive to any and all changes in the transmission. Instead of two beams three beam interactions can be used in DFWM as discussed below.[65]

In DFWM, three coherent waves are incident on a nonlinear medium. As a result a fourth wave of the same frequency (the phase conjugate) is generated, which can be easily distinguished by spatial separation from the interacting beams. The strength of the phase conjugate wave is correlated to the third order susceptibility $\chi^{(3)}$. The objective of the experiment is to measure either the intensity or reflectance of that beam. For nonresonant conditions, phase conjugation is due to the Kerr effect. For weakly absorbing samples (when the wavelength used is in the material's absorption tail or absorbing impurities are present) the linear absorption has to be taken into account. Additionally, the thermal effect might also contribute at these conditions, which complicates the analysis. When absorption becomes substantial the material is not Kerr-like and $\chi^{(3)}$ could be due to a population redistribution. This can be deduced from data analysis. Besides $\chi^{(3)}$, time dependence of the nonlinearity as well as other material parameters, can sometimes be measured using DFWM. Likewise, samples can be provided in a variety of forms. A disadvantage is that the technique will not differentiate between the real and imaginary parts of $\chi^{(3)}$, *i.e.*, will not differentiate between the Kerr effect and TPA; consequently, supplementary measurements must be carried out to extract these parts.[64]

Different interferometric methods have been developed to characterize the nonlinear index of refraction. They are based on the interference of at least two beams, where one of them experiences an intensity dependent phase delay due to propagation through a NLO medium. Precise alignment is crucial in these techniques.[65]

### 1.5.1 Z-scan

The *Z*-scan technique, which was developed by Sheik-Bahae *et al.*, has gained broad acceptance and provides high sensitivity combined with an ease of measurement and simplicity of interpretation.[66] The technique is designed to measure both NLA and NLR in open- and close-aperture configurations, referred as open- and close-aperture *Z*-scan respectively. Samples in different forms can be studied using this technique, which is another advantage. A disadvantage of the technique is that it is sensitive to all nonlinear

mechanisms giving rise to the change of the refractive index and/or absorption coefficient.[64]

During the experiment, the sample is moved gradually along a focused, most commonly Gaussian beam, thereby it is subjected to a range of intensities as the beam waist radius varies with the position. The detector in the far field measures the transmittance (through the aperture in case of close *Z*-scan technique) of the sample as a function of its position *Z*, *i.e.* intensity. As NLA and NLR are intensity-dependent processes, an NLO active material will induce changes to the measured signal.

The typical output in an open *Z*-scan experiment is a valley or peak with the minimum or maximum about the focal point where intensity is the highest. A valley will be observed when positive change to absorption coefficient occurs($\Delta\alpha > 0$), *i.e.*, for TPA or RSA processes. For negative changes($\Delta\alpha < 0$), as in the case of SA, a peak will be observed. Normalization of the data is obtained by dividing data by far field linear transmission which thus is set to unity. In closed *Z*-scan experiments, the typical output for the sample exhibiting positive change in the refractive index ($\Delta n > 0$), *i.e.* self-focusing, is valley and peak reversed about the focal point. In the region before focus the sample moves the focus closer to the sample due to self-focusing which results in a greater far field divergence and consequently reduced transmittance passing through the aperture. As sample accesses the range after focus, self-focusing reduces the far field divergence which results in larger aperture transmittance. The opposite will happen for a sample exhibiting self-defocusing ($\Delta n < 0$) (Figure 7).

For a specific type of nonlinearity, a *Z*-scan response can be modeled for a given beam shape and sample's thickness. Under certain assumptions and approximations simple analytical, yet precise, expressions for data fitting can be obtained which enable the derivatization of parameters characterizing NLA or NLR quickly. Most commonly Gaussian beams are used. A major simplification is obtained when the nonlinear sample is "thin" so that neither diffraction nor NLR will affect the beam profile. A sample is considered thin when its length $L$ is smaller than Rayleigh range of the beam in the air $Z_0$ (Figure 8).

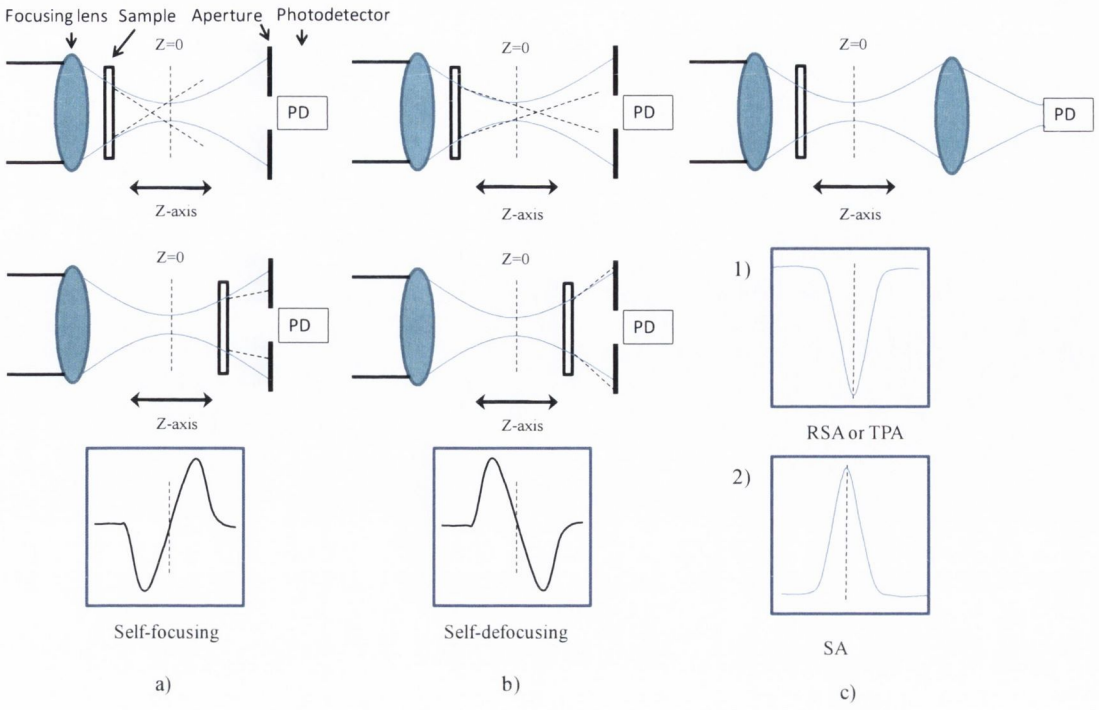
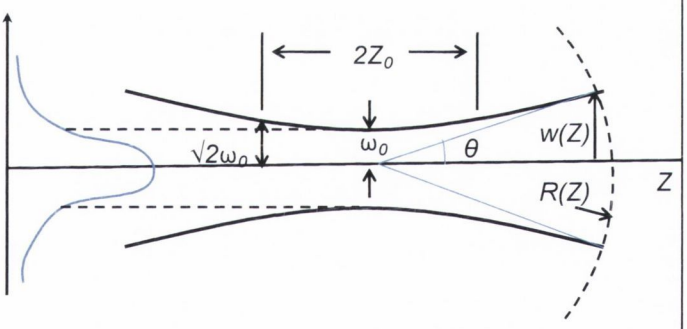



**Figure 7** Closed *Z*-scan set-up along with an illustration of experimental data for sample exhibiting a) self-focusing b) self-defocusing c) open *Z*-scan set up with an illustration of experimental data for a sample exhibiting 1) RSA or TPA 2) SA.




$$\omega(Z) = \omega_0\sqrt{1 + (Z/Z_0)^2}$$

$$Z_0 = \frac{\pi\omega_0^2}{\lambda}$$

$$R(Z) = Z[1 + (Z/Z_0)^2]$$

$$\theta = \omega_0/z_0 = \frac{\lambda}{\pi\,\omega_0}$$

**Figure 8** Illustration of Gaussian beam, $\omega(Z)$ is a beam waist radius at distance $Z$, $\omega_0$ is minimal beam waist radius (beam spot radius at the focus), $Z_0$ is confocal parameter of Rayleigh length (distance from the minimum beam waist radius where the beam area is twice the minimum area), $R(Z)$ is a curvature radius of the phasefront at a distance $Z$, $\theta$ is the beam divergence.

The propagation equations for a given NLR or NLA process can generally be presented in the following way, respectively:

$$\frac{d\Delta\phi}{dz'} = \frac{2\pi}{\lambda}\Delta n(I) \qquad \textbf{1-17}$$

$$\frac{dI}{dz'} = -\alpha(I)I \qquad \textbf{1-18}$$

where $\Delta\phi$ is nonlinearly-induced phase shift and $\alpha$ - absorption coefficient. Solution of these equations gives the amplitude and phase of the beam exiting the sample. Knowing this, the field distribution at the far-field can be calculated for a given beam shape.[67] These treatments can lead to simple analytical relations. It was demonstrated that for a material exhibiting NLA, the relation for the normalized transmission as function of position along the $Z$-axis $T_{Norm}(Z)$ takes the following form (Gaussian beam, "thin" sample approximation).[68, 69]

$$T_{Norm}(Z) = \frac{ln\,[1 + q_o(Z)]}{q_o(Z)} \qquad \textbf{1-19}$$

where:

$$q_o(Z) = \frac{\beta_{eff} I_0 L_{eff}}{1 + \left(\frac{Z}{Z_0}\right)^2} \qquad \textbf{1-20}$$

with $\beta_{eff}$ standing for effective nonlinear absorption coeffiecient, $L_{eff}$ for the effective length of the sample:

$$L_{eff} = \frac{1 - exp\,(-\alpha_{gr} L)}{\alpha_{gr}} \qquad \textbf{1-21}$$

Provided that third order effects are the only contribution to the nonlinear response, $\beta_{eff}$ is correlated to an imaginary part of third order susceptibility $Im\{\chi^{(3)}\}$ according to:

$$Im\{\chi^{(3)}\} = \frac{n_0^2 \varepsilon_0 c \lambda \beta_{eff}}{2\pi} \qquad \textbf{1-22}$$

## 1.6 Porphyrins

### 1.6.1 Introduction to porphyrins

Porphyrins are a class of naturally occurring compounds which play a crucial role in many biological processes. Hemes, chlorophyll or vitamin $B_{12}$ are classes of pigments representative of this basic structure.[70]

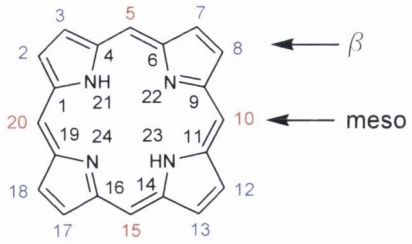



**Figure 9** The IUPAC systematic numeration of the porphyrin macrocycle with the meso (5, 10, 15, 20) and β (2, 3, 7, 8, 12, 13, 17, 18) positions indicated.

An often used abbreviated nomenclature for meso substitued compounds, associates groups at meso positions (Figure 9) with letters: A, B, C; *e.g.*, a compound with equivalent substituents at 5- and 15-meso position and different substituents at the remaining meso positions will be named as 5,15-$A_2BC$.[71] Organic synthesis offers a wide range of different derivatives that can be obtained through total synthesis or by substitution with various groups at the β and/or meso positions.[71, 72] In these terms complex porphyrin oligomers and hybrid materials bound *via* various linkers can be obtained as well. Additional derivatization involves incorporation of metal atoms into the central cavity. Further possible structural modification refers to introduction of different axial ligands to the metal in the central core which opens the door to complex supramolecular structures. In these terms porphyrins are very flexible compounds, whose properties can be fine-tuned by structural modifications. They are widely studied compounds due to their interesting photo- and electro-chemical/physical as well as binding properties. They are versatile materials with potential applications ranging from solar cells, light emitting diodes (LEDs), various sensors and receptors, catalysts, photosensitisers for cancer treatment (photodynamic therapy PDT) to NLO-based devices. These topics were broadly presented in volumes of The Porphyrin Handbook and the Handbook of Porphyrin Science.[73-77]

Due to the large size of their delocalized conjugated π-electron system, which is spread throughout the macrocyclic ring porphyrins are of great interest for NLO applications. They exhibit high second $\chi^{(2)}$ and third order $\chi^{(3)}$susceptibilities and are considered as promising candidates for optical components in photonic devices and in molecular luminescence probes in multi-photon laser scanning microscopy which is used in biological investigations and in medicine.[43, 78] In the following parts a short literature review on NLO properties of these macrocyles will be given with much emphasis put on the research trends in the field of OL.

### 1.6.2 Second order NLO properties of porphyrins

The molecular symmetry in porphyrins must be "destroyed" so that the material can exhibit second order NLO processes. One possibility of breaking the symmetry is the synthesis of so called "push-pull" molecules, *i.e.*, porphyrins with asymmetrically placed electron-donating and electron-accepting groups on its periphery. Such structures cause fluctuations in the electron density in the conjugated π-system and have reduced molecular symmetry. The effect of the quantity, mutual placement and strength of electron-donating and electron-accepting groups was studied in different compounds using mainly EFISH and HRS techniques. Theoretical studies were carried out as well in this respect. Different asymmetric push-pull compounds, which were studied for their second order nonlinearities can be classified as meso-tetraarylporphyrins of $A_2B_2$- or $A_3B$-type, 5,15-$A_2BC$ porphyrins where at least one substituent (B and/or C) is introduced *via* an ethynyl linker, porphyrins with substituents at one of the β position connected with a porphyrin through single or conjugated linkers and expanded porphyrin systems. Figure 10 shows some of the promising representatives of these groups.[43, 78]

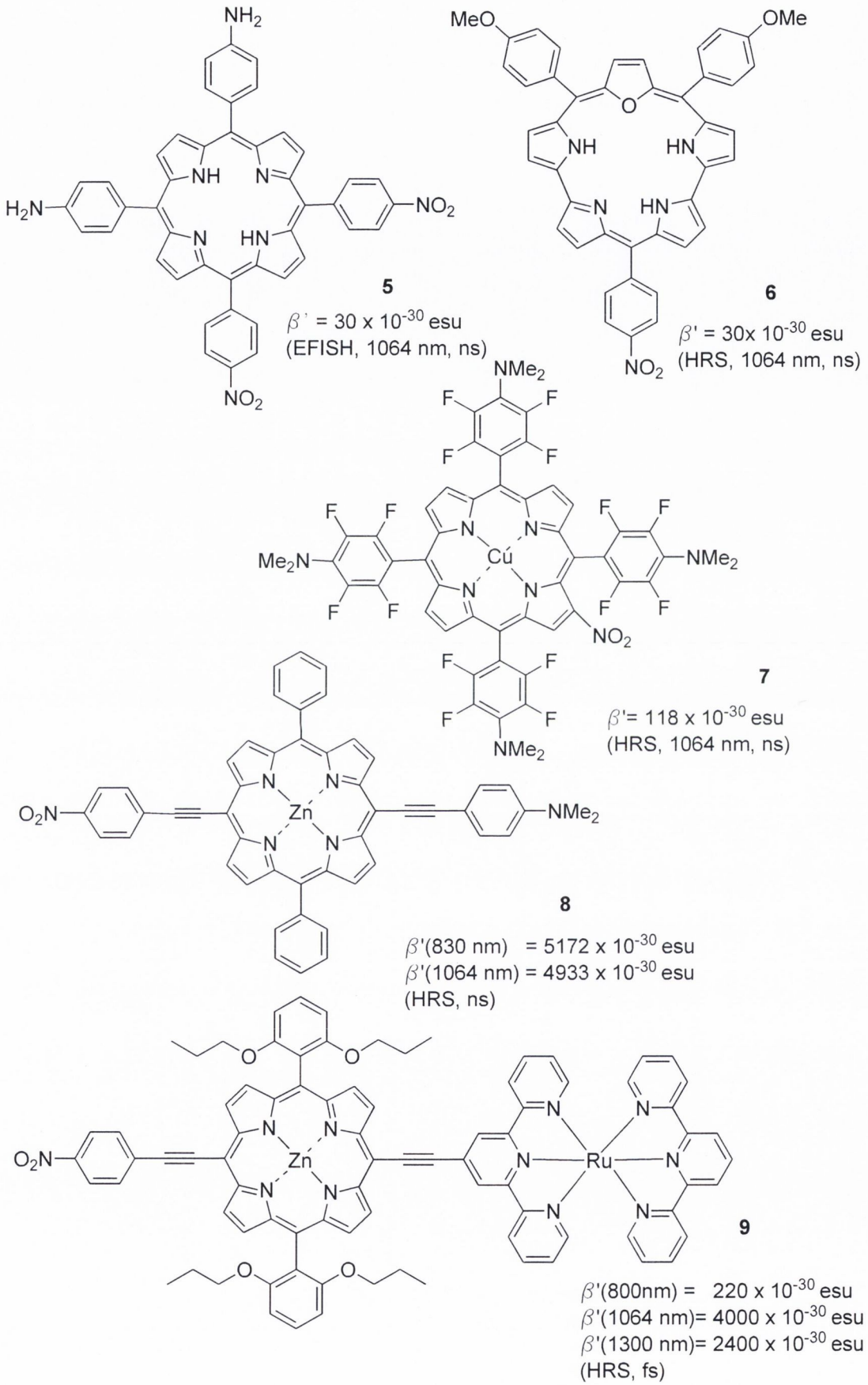



**Figure 10** Examples of second order NLO active porphyrin derivatives.

Studies carried out on asymmetric meso-tetraarylporphyrins (*e.g.*, compound **5**), which were the first compounds investigated, revealed that high nonlinearities do not arise in these compounds.[79] This is due to the dihedral angle that is formed between the porphyrin macrocycle and the aryl substituent plane, which limits the potential donor-acceptor coupling. Theoretical studies showed that the response would be enhanced when the angle is minimized *e.g.* by the introduction of π-electron spacer groups such as alkenyl or alkynyl moieties between the phenyl groups and the porphyrin core. Replacement of the phenyl rings in tetraphenylporphyrin by electron excessive or deficient heteroaromatic rings such as pyrrole or tetrazine and modification of the electron-donating or -withdrawing sites of the porphyrin itself were demonstrated to be yet another possible means to tune the properties of porphyrins for NLO.[80]

Porphyrin **8** is a very efficient second order compound with arylethynyl substituents; its first hyperpolarizability $\beta'$ of 5000 X $10^{-30}$ esu is still one of the largest measured for organic chromophores. Here the donor and acceptor groups are coplanar.[81] Compounds of similar structure, *i.e.* 5,15-$A_2BC$ porphyrins with one or two arylethynyl substituents (B or B and C) were also demonstrated to exhibit high first hyperpolarizabilities. This showed that structures with extended conjugation are very effective for the generation of second order NLO responses.[82]

Another example of a very successful compound is the terpyridine appended ethynyl porphyrin **9**. Studies revealed that terpyridine can act as an efficient and flexible acceptor group. Very high first hyperpolarizability $\beta'$ at telecommunications wavelengths were reported for this compound.[83, 84]

Theoretical and experimental studies showed that the introduction of electron-donating and electron-accepting groups at the meso positions was more effective then at the β positions.[85] No exceptional first hyperpolarizability $\beta'$ was reported for β substituted push-pull compounds (*e.g.* compound **7**).[86]

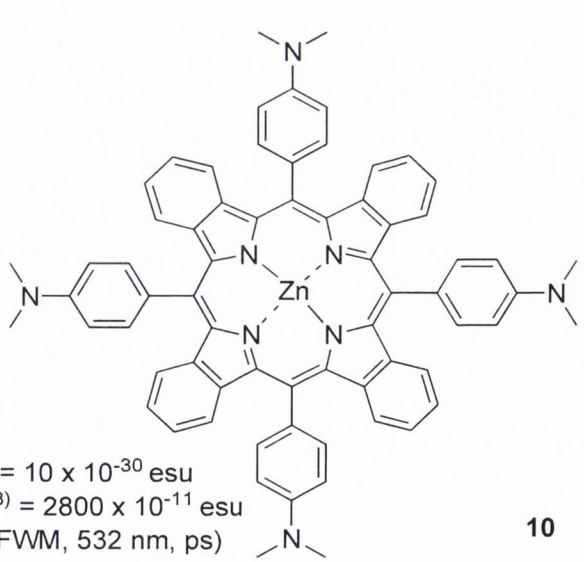
Other systems studied include expanded tetrapyrroles such as push-pull corroles (**6**), porphyrin salts and sandwich type complexes, amongst others.[87-89]

### 1.6.3 Third order NLO properties of porphyrins

Third order nonlinearities have no symmetry limitations. Thus, for most porphyrins they are the lowest allowed order of nonlinearity. Porphyrins and phthalocyanines are recognized as very promising groups of compounds that exhibit fast and high third order

responses for photonic applications. Note that porphyrin derivatives in proteins exhibit third order nonlinearities as well, which is promising for the development of new methods for their investigation and new methods for medical therapy and diagnosis.[78] Most studies were carried out with THG, DFWM and *Z*-scan. One must be cautious when comparing results obtained with different techniques. A meaningful comparison can only be done when the same technique is used, at the same wavelength, and with the same laser pulse duration.

Meso-tetraarylporphyrins and meso substituted tetrabenzoporphyrins (TBPs) are the most widely and the earliest studied compounds (Figure 11). TBPs generally provide a stronger NLO response than tetraarylporphyrins, with third order susceptibilities $\chi^{(3)}$ being on the order of $10^{-8}$ and $10^{-11}$ esu, respectively.[90-92] The effect of the metal ions in the central core and axial ligands was studied in tetraarylporphyrins revealing that such structural modifications might be used to tune their third order nonlinearities, though no drastic changes were observed.[93] An exception in the case of tetratolylporphyrin (TTP) derivatives were phosphorus P(V) complexes with azoarene axial groups, *e.g.* compound **11**. These compounds exhibited much higher second hyperpolarizabilities $\gamma'$ in comparison to other P(V) complexes with other axial ligands or in comparison to complexes with other metal ions (and ligands).[94] This effect was associated with the introduction of a charge transfer state. The introduction of electron-donating or –accepting groups also improves third order nonlinearities in the compounds discussed above [95]



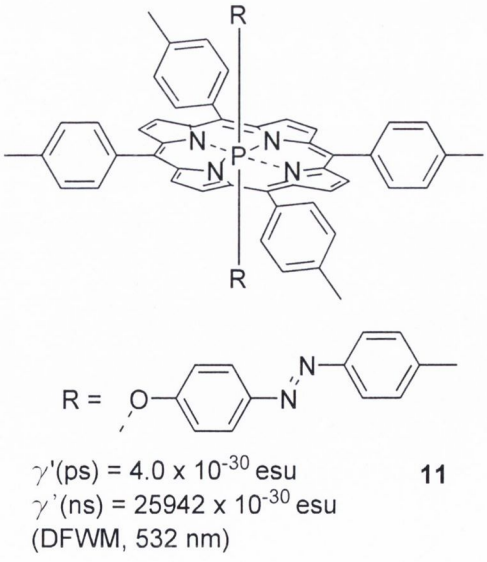
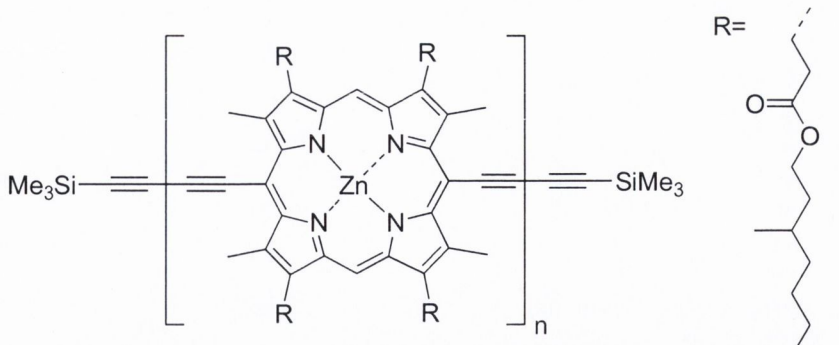




**Figure 11** Illustration of promising third order NLO compounds: Zn(II) complex of tetra-substituted TBP **10** and P(V) complex of TPP **11**.

Reasonably high second hyperpolarizabilities $\gamma'$ were reported for different expanded porphyrins.[96, 97] These systems are very amenable to structural modification. This provides a means to tune their linear and NLO properties, *e.g.*, through incorporation of metal ions into the ring or nonpyrrole units into the expanded structure.

Some studies suggest that the third order response is correlated to distortion of the porphyrin ring. For example, the dication of a dendritic porphyrin was reported to have 2-3 fold higher second hyperpolarizability $\gamma'$ than its analogous free base compound. This was associated with the distortion of the macrocyle in its protonated form.[98] Nevertheless, dendritic branches should, to some extent, counteract the out-of-plane distortion.[99] A similar trend was observed for TPP and its dication.[95] On the other hand, systematic studies carried out with basket-handle porphyrins (porphyrins with conformational constraints exerted by chains linking β or meso positions) on the conformation effect on the NLO properties, revealed that the third order susceptibility $\chi^{(3)}$ decreases with increasing macrocyclic nonplanarity. In comparison to planar compounds, $\chi^{(3)}$ of basket-handle porphyrins was 2 to 3 times smaller. This was attributed to the hindered π-delocalization in nonplanar systems.[100]

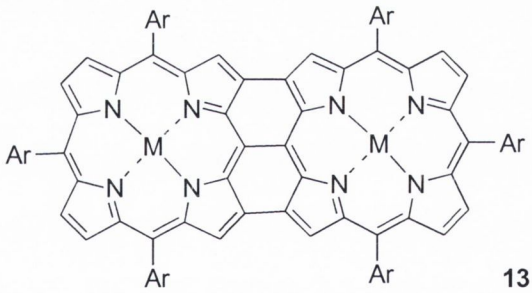
Meso-meso linked porphyrin oligomers and polymers (*e.g.*, structure **12** in Figure 12) are a powerful group of compounds exhibiting relatively high third order nonlinearities. Studies on different conjugated polymers showed that the response is enhanced in reference to monomeric compound and that it is possible to enhance the response further by varying the metal ion in the central core.[101-103] Theoretical and experimental studies on oligomers revealed that the nonlinear susceptibility per macrocyle increased by two orders of magnitude upon going from monomer to dimer and that the molecular susceptibility per chromophore showed a linear dependence with the addition of subsequent macrocyclic units up to the pentamer.[104]




**12**

**Figure 12** Promising meso-meso linked polymer for third order applications.

Theoretical studies were carried out on triply bonded meso-meso, β-β and β-β fused porphyrin arrays (compound **13**). Calculations showed that these systems should exhibit very good nonlinear efficiencies, higher then doubly bonded meso-β linked arrays, and that the nonlinearity enhancement should evolve with the number of macrocyle units in the array.[105] Comparative analyses on similar arrays showed that optical nonlinearity increases with the number of monomeric units but becomes saturated at about 3-4 units. This indicates that π-electrons do not move too much beyond the neighboring units.[106]




**13**

Interesting third order NLO properties were reported for 2D or 3D systems in which porphyrin macrocycles were not bound by covalent bonds, but self-aggregation. Examples of such systems include aggregates formed when meso groups in one oligomer coordinate to the metal in the central core of another porphyrin unit[103], aggregates formed through self-aggregation of cationic or anionic porphyrins (*e.g. J*-aggregates)[107, 108] or heterodimers formed from two different porphyrins metallated with the same metal ion[108].

## 1.6.4 Optical limiting properties of porphyrins

In 1985 Blau *et al.* first reported RSA in a series of TPP derivatives under ps laser irradiation at 532 nm.[109] Since then, much attention has been focused on the elaboration of

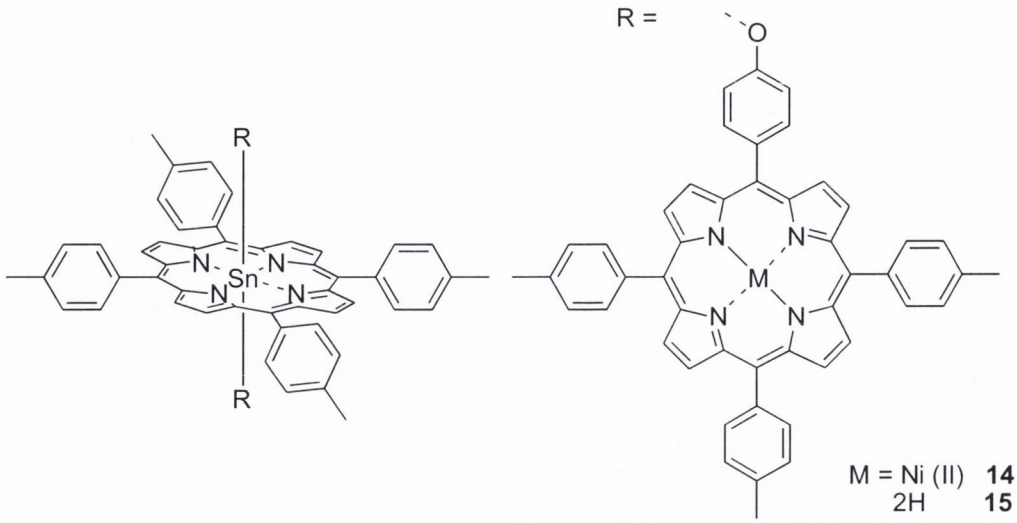
porphyrins with enhanced RSA for use in broadband optical limiters.[28, 44, 110] Besides their great design potential, which enables tuning the OL properties, it is their good chemical- and photostability which renders them interesting candidates for this application. Moreover, the ground state electronic absorption in these compounds is mostly confined to a few narrow regions: the Soret (~400 nm) and the Q-band region (~600 nm). This allows high transmission in the spectral range between these characteristic bands where RSA occurs. Compared to other materials porphyrins have the advantage of a larger ground state absorption cross-section $\sigma_{gr}$ in the visible region which can lead to saturation of the triplet state at lower fluences. Consequently, this results in a lower limiting threshold, which is especially desired in eye protecting devices.[27] The earliest and most widely studied compounds were highly symmetric $A_4$-type porphyrins. High symmetry ensures narrow ground state absorption features and is an important characteristic of efficient broadband optical limiters.

Studies on a broad range of porphyrins revealed that these materials have strong ESA and a long excited lifetime $\tau_{T_1}$. The OL properties of porphyrins depend strongly on the molecular structure. However, the rules that govern these relationships are not fully understood yet. A comparison of the results obtained by different authors requires great vigilance as different techniques, various experimental conditions, as well as diverse parameters are used to describe quantitatively OL action.[111] This makes the establishment of design rules even more complex. The paragraph below presents some consistent trends observed by various authors, as well as several more important findings.

The effect of the metal on the OL properties of various porphyrins has been investigated by many authors and compared with the response recorded for the analogous free base compounds. The presence of metal atoms in the central cavity of the porphyrin ring influences both ground and excited state features (*i.e.* $\tau_{ISC}$, $\psi_{S_1-T_1}$, Soret and Q-bands shifts and absorbance, number of Q-bands) and thus offers a convenient tool to tune their OL response. Generally, the introduction of closed shell metals (*e.g.*, Zn(II), Cd(II), Pb(II), Ga(III)) results in an enhancement of RSA through the heavy atom effect. An increase in the ISC rate in such metallated compounds, leads to higher quantum yields for the triplet states $\psi_{S_1-T_1}$ and thus to a larger number of molecules in the excited state. The presence of open shell diamagnetic (Ni(II)) or paramagnetic (Cu(II), Co(II)) metals was found to weaken NLA as a result of a decrease in the excited state lifetime.[28, 44, 110] Some systematic studies carried out on group III and IV metal complexes of 5,10,15,20-

tetra[(triisopropylsilyl)ethynyl]porphyrin revealed that the excited to the ground state absorption cross-sections ratio $\kappa$ increased when moving towards heavier members of each group,[44] with In(III), Tl(III) and Pb(II) complexes offering the highest $\kappa$ in the range 45-48. However, the effect of the metal does not necessarily follow the same trends for other series of compounds.[112]

Another way of tuning the OL properties of porphyrins involves coordinating different axial ligands to the metal in the central core. An additional role of such ligands is to hinder aggregation, which is often a problem for planar macrocycles and deteriorates RSA. For example, the use of azoarene as axial ligands in P(V)TTP (compound **11**) to induce charge transfer (CT) state, resulted in faster ISC from CT to the triplet state. Consequently this enhanced NLA and lowered the OL threshold by a factor of 2, compared to the $P(V)(OH)_2$ derivative with no CT state. Other studies showed that the OL efficiency of the $P(V)Cl_2$ complex is much better in comparison to the $P(V)(OH)_2$ derivative, with faster ISC and a 30-fold lower limiting threshold. The latter result illustrates that the heavy atom effect might arise through the axial ligand.[113, 114] Axial coordination can be used to build up porphyrin arrays. An interesting behavior in the ps regime was reported for an "axial-bonding" type porphyrin arrays based on a Sn(IV)TTP scaffold. In these arrays, the axial ligands, Zn(II) or Ni(II) porphyrin units, coordinated to tin through the meso group (compound **14**).[115] The arrays with metal-metal interactions between porphyrin units exhibited RSA at lower intensities, which turned to SA upon further increase in intensity to turn to RSA again at even higher intensities. This behavior was associated with excited state absorption (ESA) in lower fluence domain, which saturated due to long lifetime of higher excited states, and the TPA process dominating at higher intensities. No such behavior was observed for arrays with free base axially coordinating porphyrin units (*e.g.* for compound **15**).




Bromide on one of the β position was found to impact OL in the same way as closed shell metals in central core. It increased the quantum yield for triplet states $\psi_{S_1-T_1}$ to virtual unity.[116] (2,3,7,8,12,13,17,18-octabromo-5,10,15,20-tetraphenylporphyrinato)zinc(II) was also reported as a very efficient OL material.[68]

As far as the effect of the meso substituents on the OL efficiency of porphyrins is concerned, substitution of the meso hydrogen atoms with conjugating groups such as phenyl, alkenyl or alkynyl usually produce a red shift in the optical absorption bands and must therefore change their linear and nonlinear optical properties.[117] The spectral range for effective RSA is altered in this way. McEwan *et al.* reported that meso substituents have little effect on the intersystem crossing time $\tau_{ISC}$.[28] Some authors highlight the influence of the electron-donating or -withdrawing character of the meso substituents on the OL response. *E.g.*, it was reported that substitution of the phenyl group in tetra-meso substituted porphyrin by an electron-donating group produces an increase in electrical polarizability while the opposite effect was observed for electron-withdrawing groups.[118] Among different compounds studied, [5,10,15,20-tetra(4-methoxyphenyl)tetrabenzoporphyrino]lead(II),[68] metal complexes of 5,10,15,20-tetra[(triisopropylsilyl)ethynyl]porphyrin[44] and 5,10,15,20-tetra[(trimethylsilyl)ethynyl)]porphyrin[28] were reported as the most promising candidates for OL (Figure 13).

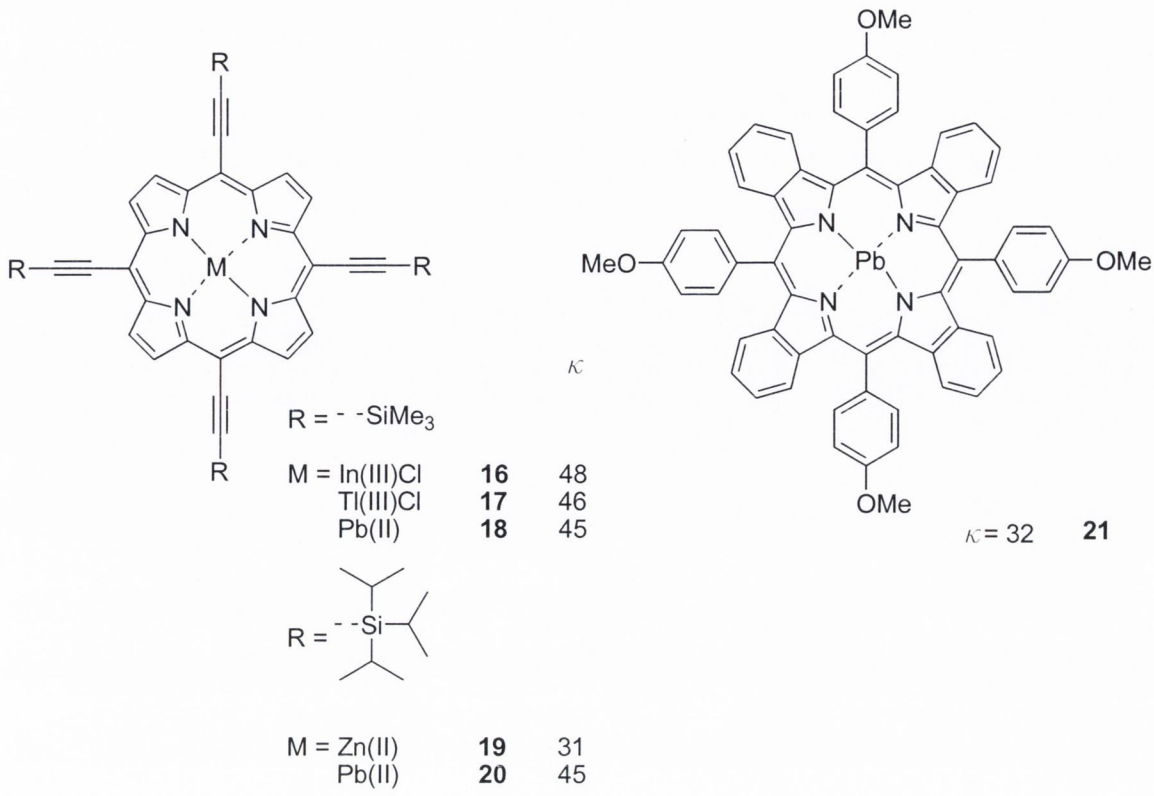



**Figure 13** Exited to ground state absorption cross-section ratio $\kappa = \sigma_{ex}^{T}/\sigma_{gr}$ for the most promising RSA compounds.

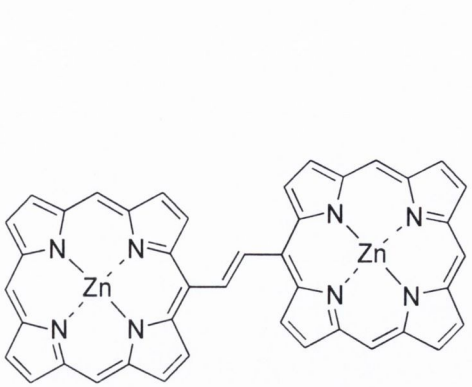
Some important conclusions on how structural features impact material parameters that describe RSA, were made by McEwan *et al.* The authors carried out systematic studies on a series of metallated tetra-meso substituted porphyrins using pump-probe experimental set-up at 532 nm and with a white light (to measure wavelength dependence of NLA).[28] The authors suggested a correlation between the proximity of the Soret-band to the measurement wavelength (of 532 nm) and the strength of the OL; *i.e.*, the closer the experimental wavelength to the Soret-band maximum, the stronger the OL effect. This pattern correlated, though not for all compounds, to the pattern observed for the singlet and triplet excited state absorption cross-sections, which were higher at experimental wavelength for the compounds whose Soret band was closer to 532 nm. Pump-probe experiments with white light revealed that: 1) both the singlet and triplet excited states absorption spectra have a single dominant feature that is much broader than the ground state bands; 2) the excited state absorption peak is much smaller than the Soret band peak; 3) the peak in the excited state absorption is located close to the Soret band peak but is shifted to a slightly longer wavelength depending on the molecular structure; and 4) the triplet state absorption is narrower and stronger at its peak than the singlet excited state absorption and consequently, its cross-section increases more rapidly than for the singlet

state in moving from the Q-band to the Soret band.

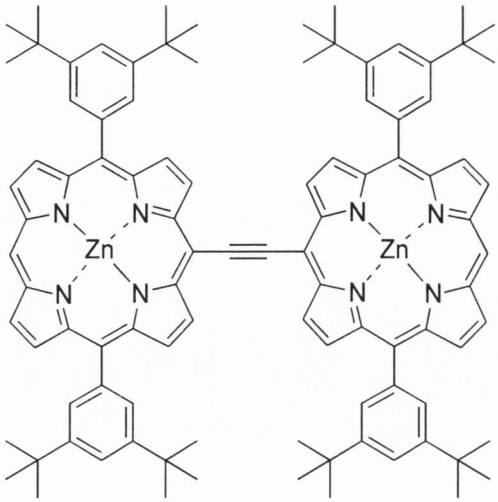
The conformation of the ring influences the OL. Macrocycle nonplanarity shortens the ISC time and triplet lifetime.[28] While it is favorable for the solubility of the compounds it broadens the linear absorption features. In general, factors that increase the ISC rate also decrease the triplet lifetime. Thus, some compromise must be achieved while tuning OL properties to ensure that the material is still effective against long duration pulses.

Next to the widely studied $A_4$ compounds, there are only separate reports on porphyrins with other substitution patterns such as 5,15-$A_2B_2$[119-121], 5,15-$A_2BC$[119] or 5,10-$A_2B_2$[122]. Interesting, though undesirable for OL applications, a RSA/SA switch was observed for the latter compounds by Senge *et al.*[122] The origin of this behavior, which arose in ns regime at 532 nm, was not understood. Interestingly, for 5,15-$A_2B_2$ or 5,15-$A_2BC$ substitution patterns, only RSA behavior was detected. This indicates that regiochemical arrangement of the substituents is an important factor.

Apart from monomers, there are few reports on meso-meso linked porphyrin oligomers and polymers. Comparative studies carried out at 532 nm in ps regime on a monomer, dimer and polymer with meso-meso butadiyne linker **12** revealed that the monomer had the largest figure of merit, mainly due to its lower linear transmission at the excitation wavelength.[46] The authors suggested that broadband measurements are necessary to establish how the properties evolve with the wavelength. Apparently ground state absorption features were affected when going from monomer to dimer and polymer, with the spectral window being red shifted for homologues with a higher number of porphyrin units. Broadband analysis carried out on a meso-meso *E*-vinylene-linked porphyrin dimer **22** showed that triplet excited state absorption reaches its maximum around 900 nm. This makes it a suitable RSA material for NIR range as there is good overlap of the excited state and ground state spectra.[123] For a similar meso-meso ethynyl-linked dimer **23**, the triplet excited state absorption was found to peak beyond 1000 nm, where there is essentially no ground state absorption thus making this material unsuitable for RSA based OL.



22



23

Reports on RSA derivatives such as basket-handle porphyrins,[124] expanded porphyrin-like complexes,[125] porphyrazines (porphyrin analogues where the meso-C atoms are substituted by nitrogen),[126] supramolecular aggregates[127] or porphyrin dyads (*i.e.*, porphyrin-viologen dyad with photoinduced intramolecular CT)[49] can also be found in the literature.

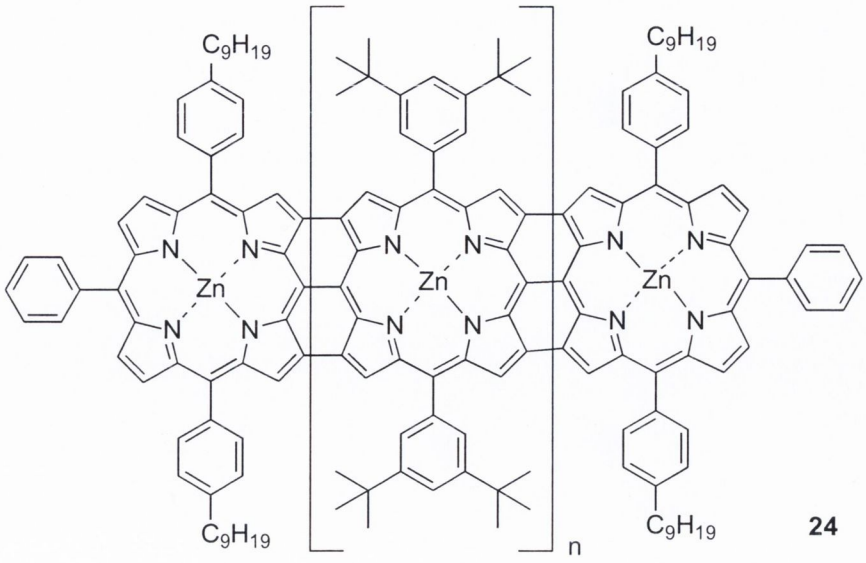
A few reports described hybrid materials where a porphyrin was covalently or noncovalently bound with $C_{60}$, graphene or carbon nanotubes (CNs), which alone act as OL materials. In $C_{60}$ and graphene OL action arises through the same mechanism as in porphyrins, *i.e.* RSA, while the dominating NLO effect giving rise to transmission reduction with intensity in CNs is NLS. Studies on hybrid materials demonstrated that their OL action is affected by photo-induced charge or energy transfer between hybrid components. An enhancement in OL properties was reported in graphene and CNs hybrids with covalently bound porphyrins,[128-130] in donor-acceptor ionic complexes formed with a positively charged porphyrin derivative and negatively charged graphene oxide,[131] in porphyrin-CNs composites,[132] and in noncovalently bound $C_{60}$-porphyrin hybrids.[48] However, covalently bound $C_{60}$-porphyrin systems such as dyads[133] or oligomers[134] were reported to exhibit lower OL efficiencies than $C_{60}$ or its unbound components. With regard to oligomers these lowered OL properties were associated with the delayed formation of the triplet state due to the intermediate CT state.

TPA is another mechanism which is useful for OL application. The wavelength range where this phenomenon arises is different from that where RSA occurs. But alike as RSA, it might be altered through molecular modification. There is a large body of work on TPA properties of porphyrins and their derivatives, ranging from simple, highly symmetric $A_4$ compounds[103] to porphyrin polymers or arrays.[103, 135, 136] In general, conjugation and

formation of extensive delocalized systems play an important role in forming cubic nonlinearities and this is reflected by the TPA properties in porphyrin systems. The TPA cross-section $\sigma_{TPA}$, the parameter used for comparison, reaches values up to hundreds of GM for simply symmetric $A_4$ compounds,[103] whereas for expanded porphyrins,[137] porphyrin oligomers, polymers[138] or arrays[136] it is usually one or two orders of magnitude higher.

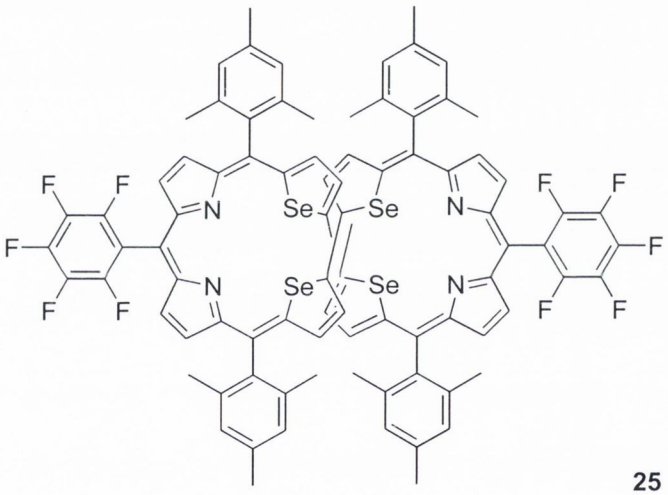
For monomeric porphyrins the TPA properties can be enhanced through incorporation of electron-donating or electron-accepting groups.[139] Theoretical studies carried out on $A_2BC$ and $A_2B_2$ compounds with various donor or acceptor groups predicted TPA cross-sections $\sigma_{TPA}$ of up to a few thousands of GM.[140, 141] Other studies on porphyrin-based donor-acceptor systems predicted an increase in $\sigma_{TPA}$ upon formation of *J*-type aggregation of up to 70 times compared to the monomer.[142] An increase in $\sigma_{TPA}$ was also predicted theoretically for porphyrin dimers and arrays.[143] Doubly meso-β or triply meso-meso, β-β, β-β linked porphyrin arrays were predicted to exhibit higher $\sigma_{TPA}$ than singly meso-meso linked analogues.[144]

These theoretical predictions were validated experimentally. Meso-meso butadiyne linked oligomers showed high $\sigma_{TPA}$ that increased with the number of porphyrin units in the oligomers (**12**). Upon formation of double-strand conjugated cross-linking of metal centers in oligomers with bipyridine to form ladder-type arrays, the TPA cross-sections $\sigma_{TPA}$ was improved further to reach 115,000 GM.[138, 143] High $\sigma_{TPA}$ were reported for other supramolecular structures[145] and meso-meso linked dimers.[146] The directly linked and fused systems also exhibit interesting TPA properties that often increased with the length of the molecular tapes, with $\sigma_{TPA}$ reaching several thousands of GM (compound **24**).[136] A clear correlation between the degree of π-conjugation and TPA was shown using meso directly-linked oligoporphyrins with different dihedral angles between porphyrin planes.[147] Apart from effective conjugation, an increase in the number of π-electrons in the conjugation pathway enhances TPA. TPA cross-sections of the order of 90,000 GM were reported for expanded porphyrin systems (compound **25**).[137]




24

n = 0-4




25

## 1.6.5 Objectives and outlook

As illustrated above most of the OL studies were carried out on highly symmetric $A_4$ type porphyrins. Still little is known about the influence of the regiochemical rearrangement of different meso substituents on the OL performance of porphyrins. Our aim was to investigate and understand these relations.

In the first part of the studies, NLA properties of a compound library comprising porphyrin monomers, dimers and trimers in different substitution patterns were investigated. This enabled to establish some consistent design rules.

In further studies more attention was focused on porphyrins in a specific meso substitution pattern *i.e.* 5,10-$A_2B_2$ porphyrins. These porphyrins exhibited distinct NLA response in reference to porphyrins in other substitution patterns. Theoretical modeling enabled to

understand the underlying photophysical mechanism of the unique NLA response. As solvent was observed to affect the NLA responses of 5,10-$A_2B_2$ porphyrins, systematic studies were carried out on the effect of the solvent on the OL performance of these porphyrins.

# Chapter 2 Investigation of the optical limiting properties of structurally diversified porphyrin monomers, dimers and trimers

## 2.1 Introduction and outline

Although much progress has been made in studying the OL properties of macrocyclic dyes, the rational design of molecules with enhanced OL efficiencies is still not accessible. Design rules established so far provide good guidance for improving the optical properties but do not answer all questions concerning the relationship between a molecular structure and its OL properties.

Most of the past studies were focused on highly symmetrical systems. Such structures narrow the ground state absorption features which are desirable for broadband optical limiters.[21, 27, 117, 148] However, it would be also interesting to investigate the influence of the regiochemical rearrangement of various substituents on the OL properties of RSA macrocyclic dyes. Besides broadband OL application, macrocyclic dyes are considered as suitable candidates for green light limiting, too. This chapter discusses NLA results obtained for structurally diversified porphyrin monomers, dimers and trimers and shows how structural features impact OL performance of these compounds.

## 2.2 Materials, experimental technique and data treatment details

### 2.2.1 Materials

The NLA properties of a range of structurally diversified meso substituted porphyrin monomers, dimers and trimers (**26-64**) were studied (Figure 14). Structural details of the compounds **26-64** are summarized in Table 1 (p. 62). The compounds were kindly provided by Senge research group.

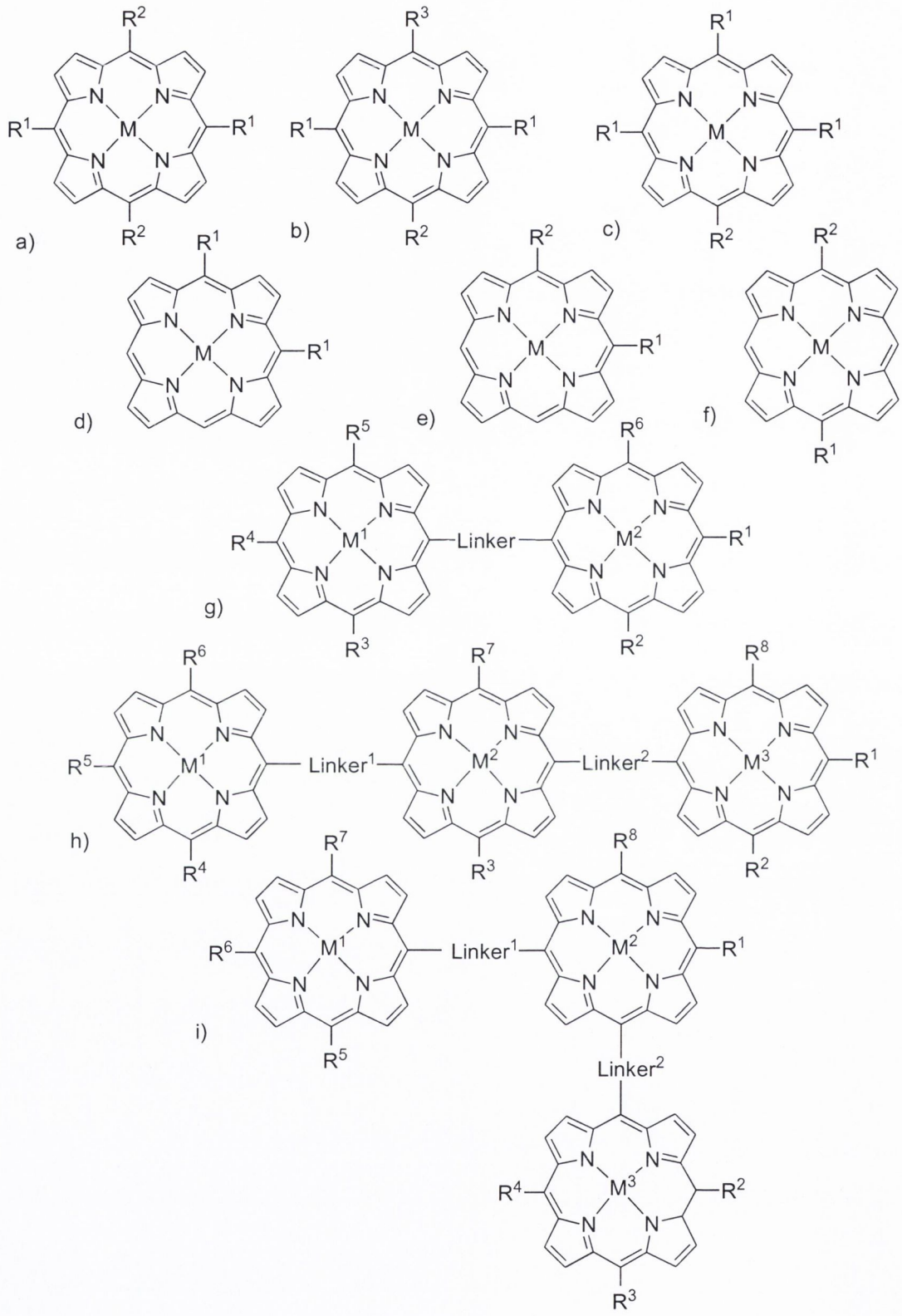



**Figure 14** The substitution patterns of the examined monomers: a) 5,15-$A_2B_2$ b) 5,15-$A_2BC$ c) $A_3B$ d) 5,10-$A_2$ e) 5,10-AB f) 5,15-AB g) dimer h) linear trimer i) L-shaped trimer. M, $M^i$ stands for metal.

### 2.2.2 Experimental technique

The characterization of the NLA properties of the compounds studied was carried out using the open aperture Z-scan technique with a 6 ns pulsed laser operating at 532 nm. Technical details of the experimental set-up can be found in the experimental section. Several measurements were carried out for each sample. The incident energy of the laser was gradually increased in each of the following measurements, with an average step of about 20 μJ starting from 35 to around 350 μJ. Additionally, the linear transmission in the far field was measured for each sample, which was recalculated to linear absorption coefficient $\alpha_{gr}$ from Beer's law. The samples were prepared by dissolving the porphyrin in DMF, at 0.01 $g.L^{-1}$ followed by gentle agitation for about 30 min in a low power sonic bath. All measurements were performed in a quartz cell with a 10 mm path length. Additionally, some measurements were carried out with more concentrated samples (concentrations up to 0.1 $g.L^{-1}$) and/or with different path lengths (1 or 5 mm).

### 2.2.3 Data treatment

The experimental data for the samples exhibiting RSA were fitted using the method of least-square regression with the equation for the normalized transmission as a function of the sample position $Z$ Eq. **1-19**. The beam waist radius $\omega_0$ ($\omega_0 = \sqrt{Z_0\lambda/\pi}$ see Figure 8) and the effective nonlinear absorption coefficient $\beta_{eff}$ were treated as free parameters in the fit. The imaginary third order optical susceptibility $Im\{\chi^{(3)}\}$ was calculated according to the Eq. **1-22**.

In order to compare OL action of different compounds, plots of normalized transmission *versus* incident pulse energy density (fluence) were produced. Alternatively, the data were presented as input fluence *versus* output fluence (output fluence = normalized transmission × input fluence × linear transmission). Some of these plots will be presented below.

On-focus intensity $I_0$ was calculated from $I_0 = E/(\pi^{\frac{3}{2}}\tau{\omega_0}^2)$ where $E$ is laser energy and $\tau$ is pulse length. Input fluence at distance $Z$ from the focus (along Z-axis) was calculated frdfrom $F(Z) = E/\{\pi{\omega_0}^2\left[1+\left(\frac{Z}{Z_0}\right)^2\right]\}$.

# 2.3 Results and discussion

## 2.3.1 General observations and remarks

For most of the compounds a reduction in the transmission about the focus was observed, which was attributed to RSA. This reduction was found to increase for the subsequent measurements carried out at increasing input laser energy (Figure 15).

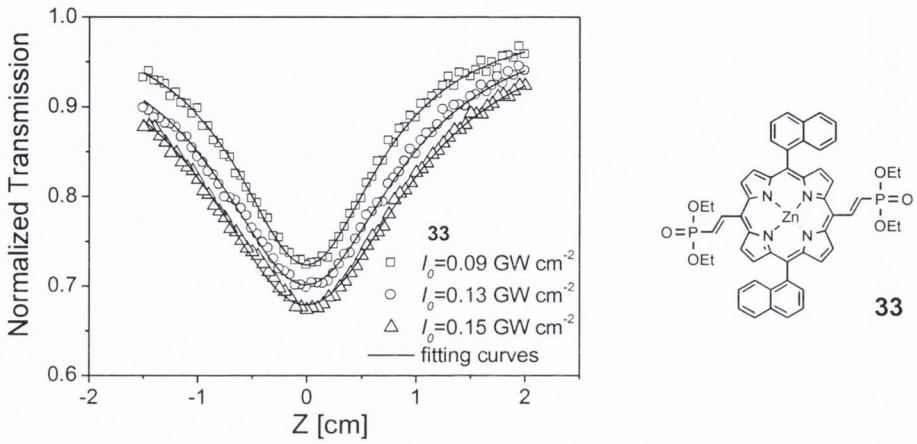



**Figure 15** Typical open aperture Z-scan data set with the normalized transmission plotted *versus* sample position *Z* for the subsequent experiments carried out at increasing input laser energy for compound **33**. $I_0$ is the laser intensity at the focus, which was recalculated for the subsequent experiments.

The magnitude of the reduction upon similar on-focus intensity $I_0$ was found to vary for different compounds indicating that the structural features impact the OL action of the porphyrins (an example in Figure 16).

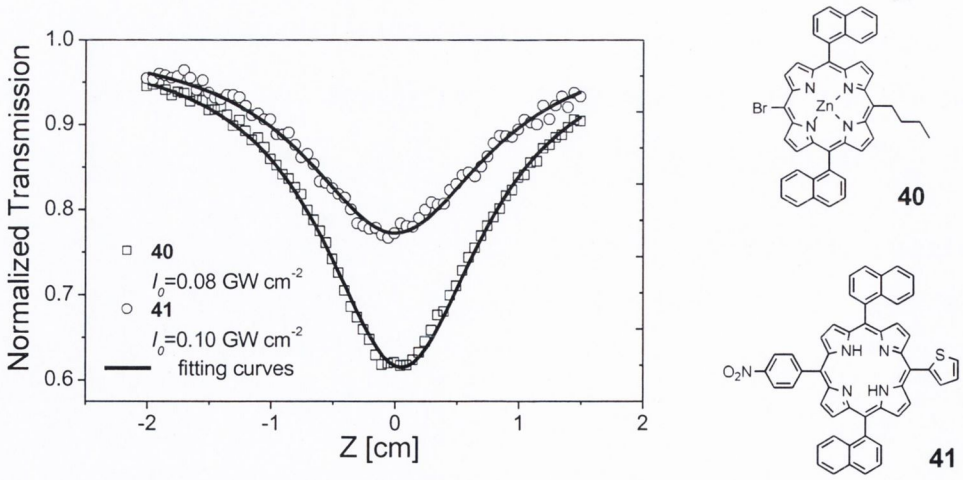



**Figure 16** Open Z-scan data for compounds **40** and **41**.

Some instability in the measured response was observed for higher incident laser energy experiments for all of the compounds exhibiting RSA. The instability was asymmetric with respect to the focal position and occurred after the sample passed the focal area. The magnitude of the instability was observed to increase in the subsequent experiments carried out at increasing laser energy. The instability appeared at different input energies for different compounds. The magnitude of the increase progressed differently for different compounds. An example of the evolution of the instability in the subsequent experiments carried at increasing input energy for two different compounds is presented in Figure 17. It should be noted that for different concentrations the instability occurred at similar on-focus intensities $I_0$. A similar type of instability was reported in literature before and was associated with thermal effects.[132]

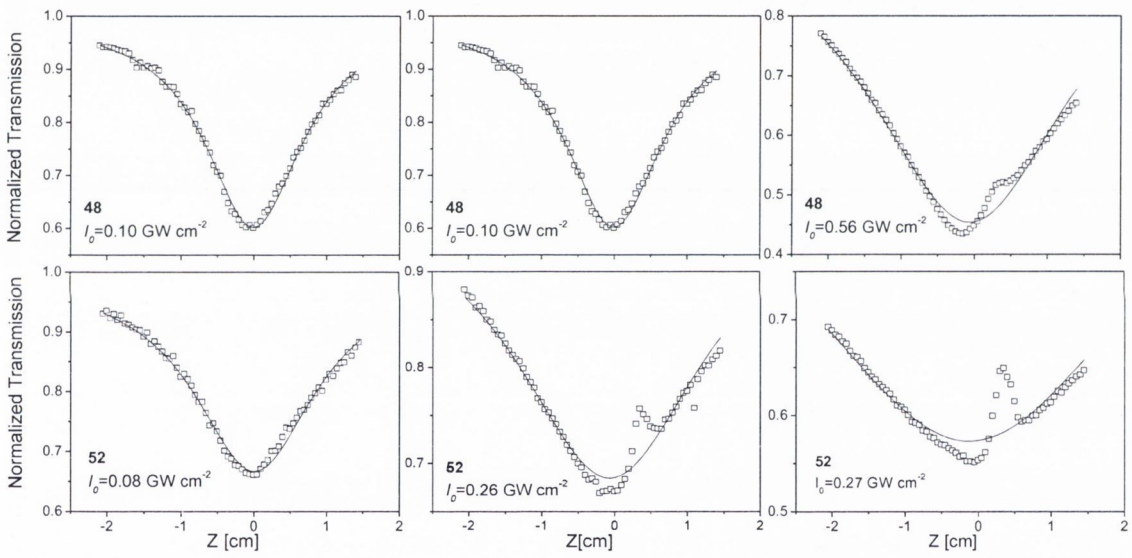



**Figure 17** Open Z-scan signal quality at various on-focus intensities for the compounds **48** (upper) and **52** (lower). Instability occurring after passage through the focal area becomes apparent at different on-focus intensities $I_0$ for the two compounds showed. The magnitude of the instability depends on compound and laser input energy.

Data containing the instability were excluded from further analysis. For the rest of the data, fitting parameters $\omega_0$ and $\beta_{eff}$ were found to increase and decrease, respectively, slowly with the on-focus intensity (Figure 18). Average values of these two parameters are presented in Table 1. The range of the on-focus intensities over which average values of $\omega_0$ and $\beta_{eff}$ were calculated is also included in this table. A decrease in $\beta_{eff}$ with intensity was reported before for phthalocyanines and was associated with higher order nonlinearities which contributed to the effective third order effects.[111]

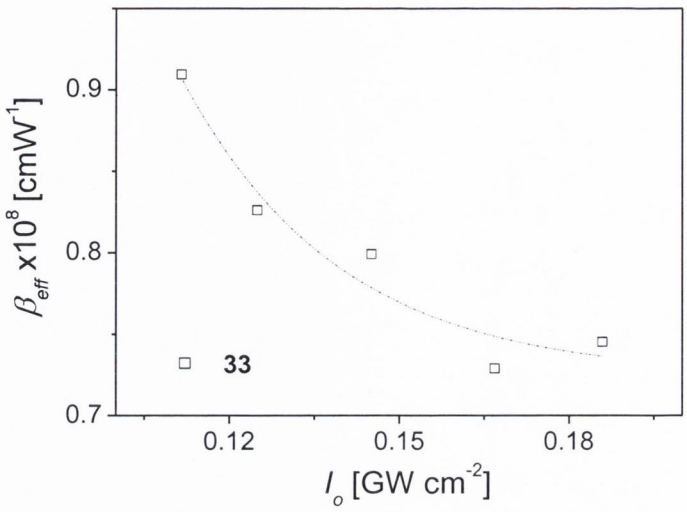



**Figure 18** Variation of the nonlinear absorption coefficient $\beta_{eff}$ with the on-focus intensity $I_0$ for compound **33**. The dotted line is intended as a guide for the eye.

It was found that $\beta_{eff}$ depends linearly on the concentration, which implies that the number of molecules in the excited state is proportional to the sample's concentration in the examined range of concentrations (Figure 19). Additionally, it indicates indirectly that aggregation does not occur in the examined range of concentrations.

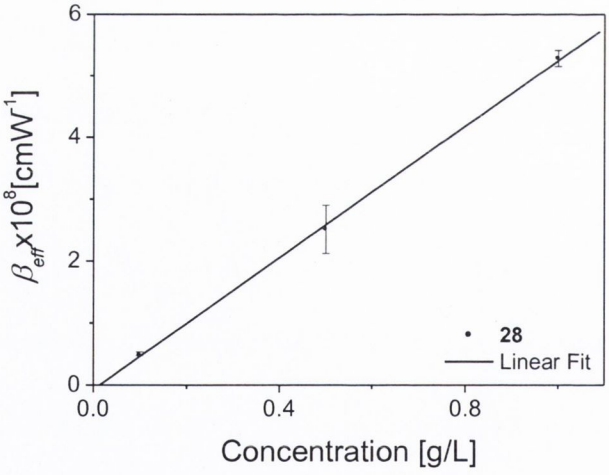



**Figure 19** Variation of the non-linear absorption coefficient $\beta_{eff}$ with the concentration for compound **28**.

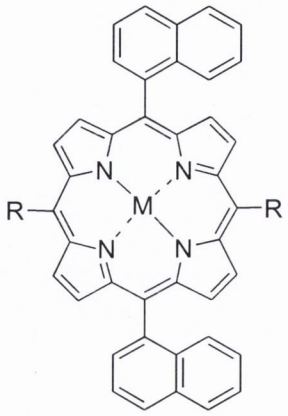
$\beta_{eff}$ of a reference compound - fullerene $C_{60}$ was deduced from the measurements under the same experimental conditions as applied for the porphyrins. $\beta_{eff}$ of $C_{60}$ was found to be lower by one order of magnitude in comparison to $\beta_{eff}$ of the porphyrins studied.

Briefly, in the following parts, the effect of the meso substituents on NLA in porphyrin monomers in 5,15-$A_2B_2$ and 5,15-$A_2BC$ substitution patterns is studied. In the case of

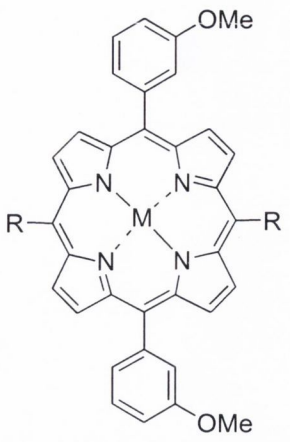
porphyrin dimers and trimers, the influence of both the meso substituents and the type of the linker bridging the porphyrin units on the nonlinear response is explored. The comparison of the OL action of different compounds is carried out in terms of nonlinear absorption coefficient $\beta_{eff}$.

## 2.3.2 Monomers

### 5,15-$A_2B_2$

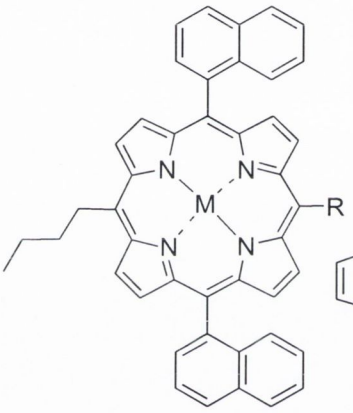


**26** R = 2-benzothiophenyl M = 2H
**27** R = 4-CN-$C_6H_4$ M = 2H
**28** R = 1-Me-indol-5-yl M = 2H
**29** R = 4-MeOOC-$C_6H_4$ M = 2H
**30** R = 3-thiophenyl M = 2H
**31** R = $C_6H_5$-ethenyl M = 2H
**32** R = 3-$NO_2$-$C_6H_4$-ethenyl M = Zn(II)
**33** R = $PO(OEt)_2$-ethenyl M = Zn(II)
**34** R = $C_6H_5$-ethynyl M = 2H

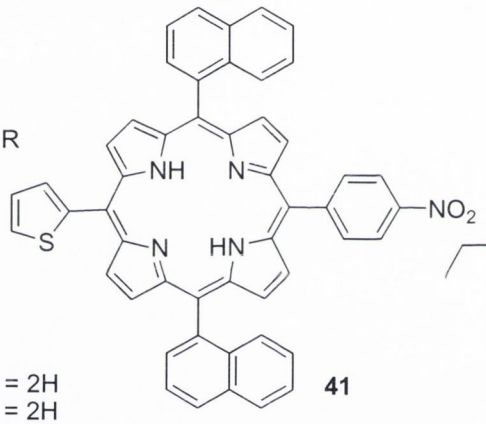


**35** R = 4-CN-$C_6H_4$ M = 2H
**36** R = TMS-ethynyl M = Zn(II)

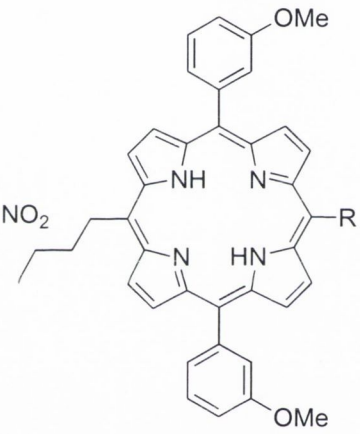
### 5,15-$A_2BC$



**37** R = 4-CN-$C_6H_4$ M = 2H
**38** R = 4-MeOOC-$C_6H_4$ M = 2H
**39** R = 4-$NO_2$-$C_6H_4$ M = 2H
**40** R = Br M = Zn(II)

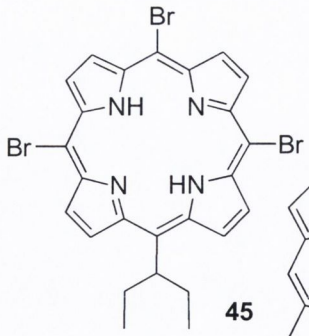


**41**



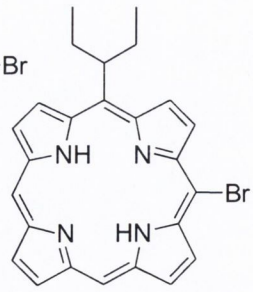
**42** R = 4-CN-$C_6H_4$
**43** R = 4-$NO_2$-$C_6H_4$
**44** R = 3,4,5-$(MeO)_3$-$C_6H_2$

### $A_3B$



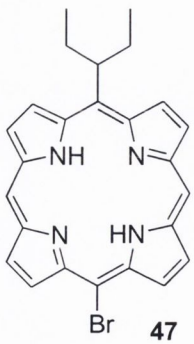
**45**

### 5,10-AB



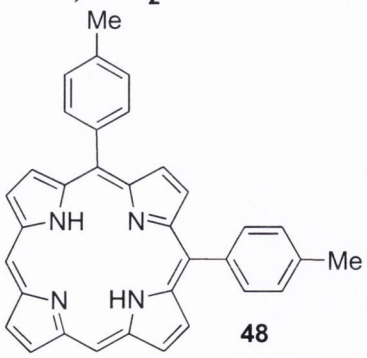
**46**

### 5,15-AB



**47**

### 5,10-$A_2$



**48**

The OL response of monomers varied between compounds with different meso substituents and substitution patterns. Some general trends in the OL behavior could be observed.

Free base 5,15-$A_2B_2$ porphyrins with 1-naphthyl as the first substituent and with the other one being linked to the porphyrin directly *via* a single bond are considered (compounds **26-30**). The following trend in $\beta_{eff}$ was observed with regard to the second substituent: 4-CN-$C_6H_4$ ~ 4-MeOOC-$C_6H_4$ > 3-thiophenyl > 2-benzothiophenyl > 1-Me-indol-5-yl (**27** ~ **29** > **30** > **26**). This tendency reveals that ESA is enhanced for the compounds with strong electron-withdrawing groups. This finding is not in agreement with studies carried out by Bergkamp *et al.* The authors reported a decrease in electrical polarizability upon substitution of phenyl residues with electron-withdrawing groups. They also observed an enhancement when electron-donating groups replaced phenyl.[118]

The response of either free base or metallated compounds, again with 1-naphthyl as the first substituent and with the second substituent connected to a porphyrin *via* a conjugated linker (**31-34**), is enhanced in comparison to the previously discussed porphyrins with the meso substituents linked to the porphyrin directly *via* a single bond (**26-30**). However, this rule does not apply to compound **33**, which might be a result of the particular electronic character of the $PO(OEt)_2$ group. The linear absorption coefficient $\alpha_{gr}$ (Table 1) for this compound was remarkably low in comparison to other compounds. Low linear absorption in the ground state hinders population build-up in the excited state, which consequently lowers RSA.

The Soret band maxima are red-shifted for the compounds with conjugated linkers (**26-30**) in comparison to those with substituents connected to the porphyrin macrocycle by a single bond (**31-34**) (see $\lambda_{max}$ in Table 1). Consequently, the experimental wavelength of 532 nm is closer to the Soret band for the compounds with conjugated linkers, which exhibited better OL properties. McEwan *et al.* suggested a correlation between the proximity of the Soret band maximum to the measurement wavelength (of 532 nm) and the strength of the OL. *i.e.*, the closer the experimental wavelength to the Soret band maximum, the stronger the OL effect.[28] Evidently, 5,15-$A_2B_2$ monomers with 1-naphthyl substituent (**26-34**) follow the same trend as reported.

The Zn(II) complex of a 5,15-$A_2B_2$ porphyrin with 3-MeO-$C_6H_4$ and TMS-ethynyl groups as substituents **36** was identified as the most promising among all of the compounds

measured (**26-64**) with the highest value of $\beta_{eff}$ = 5.3 × $10^{-8}$ cm.$W^{-1}$. At the same time, the linear absorption coefficient $\alpha_{gr}$ for this compound was found to be relatively low. High transparency at low light intensities governed by ground state absorption, combined with high NLA at higher light intensities, renders this compound especially interesting for OL applications. An investigation of the NLO response over a broader range of wavelengths of the UV-vis region would determine whether the compound is of interest for broadband OL applications. As previously shown in the introduction, metal complexes of meso tetraalkynylporphyrins with TMS-ethynyl and TIPS-ethynyl groups, as well as [5,10,15,20-tetra(4-methoxyphenyl)tetrabenzoporphyrinato]zinc(II) were reported in the literature as very promising for OL applications (Figure 13).[28, 44] Note that compound **36** contains the structural features of these compounds.

The values of $\beta_{eff}$ for 5,15-$A_2B_2$ compounds where A = 4-CN-$C_6H_4$ residues, and B = 1-naphthyl **27** or 3-MeO-$C_6H_4$ **35**, were found to be of the same order. However, the linear absorption coefficient for the compound with 3-MeO-$C_6H_4$ **35** was found to be smaller than that with 1-naphthyl (compound **27**). That makes the previous compound a more promising candidate for green light limiting.

The 5,15-$A_2B_2$ compounds **27** and **29** are structurally related to the 5,15-$A_2BC$ compounds **37** and **38,** respectively. The $\beta_{eff}$ values of both of 5,15-$A_2BC$ compounds are remarkably lower than those of the 5,15-$A_2B_2$ compounds. A consistent trend could be observed for both substitution patterns: compounds **29** and **38** with 4-MeOOC-$C_6H_4$ have a slightly higher $\beta_{eff}$ value than compounds **27** and **37** with 4-CN-$C_6H_4$, respectively.

The OL efficiency of compound **40**, with A = 1-naphthyl and B = *n*-$C_4H_9$, is enhanced in comparison to other 5,15-$A_2BC$ compounds (**37-39**). It may either be the presence of the Zn(II) in the central core or the bromine atom at the meso position acting through a heavy atom effect which renders this compounds more promising in comparison to others of similar structure. The heavy atom effect produces an increase in the ISC rate which results in a higher quantum yield of the triplet states.[110]

The response of 5,15-$A_2BC$ compounds, **42** and **43**, where A = 3-MeO-$C_6H_4$ is notably enhanced in comparison to the analogous compounds with two 1-naphthyl groups, **37** and **39**, respectively (Figure 20).

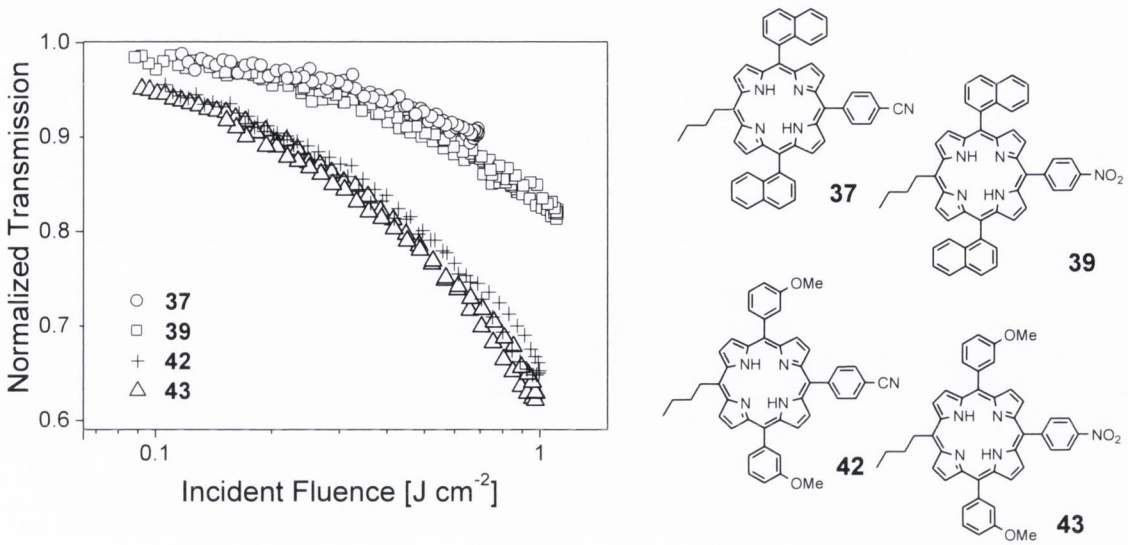



**Figure 20** OL curves plotted as normalized transmission *versus* incident fluence for compounds **37**, **39**, **42** and **43**.

Once again, compounds substituted with an electron-donating methoxy group have improved OL properties. The $\beta_{eff}$ values of both **42** and **43** are in the same range as $\beta_{eff}$ values of the 5,15-$A_2B_2$ compounds with substituents connected to the porphyrin *via* conjugated linkers (**31**, **32**, **34**, **35**).

McEwan *et al.* found that the OL performance of [5,10,15,20-tetra(*p*-tolyl)porphyrinato]zinc(II) was enhanced compared to (5,10,15,20-tetraphenylporphyrinato)zinc(II), although both compounds have similar molecular structures and exhibited similar ground state electronic absorption features. On the basis of this finding the authors suggested a new approach for the design of the OL materials. Rather than directly modifying the meso or β positions, which usually results in red-shifted Soret and Q-bands and consequently in a reduced overall transmission in the visible range, they proposed to incorporate functional groups at the *para* position of the meso phenyl rings. In further studies, they found that incorporation of a TMS-ethynyl group at the *para* position of the phenyl ring did not change the ground state absorption significantly but strongly improved NLA.[110]

5,15-$A_2$BC compounds **37-39** are structurally related. The only difference is the substituent at the *para*-position of the phenyl ring at one of the meso positions. The ground state absorption spectra of compounds **37-39** are similar but their OL performance slightly differs in accordance with McEwan *et al.*'s observations (Figure 21). We conclude that structural features that do not contribute to the ground state absorption do have an

influence on the excited state absorption. Similar observations were made for compounds **42** and **43**. It should be emphasized that the effect of the *para*–phenyl modification on the ESA is quite strong for a relatively minor chemical modification.

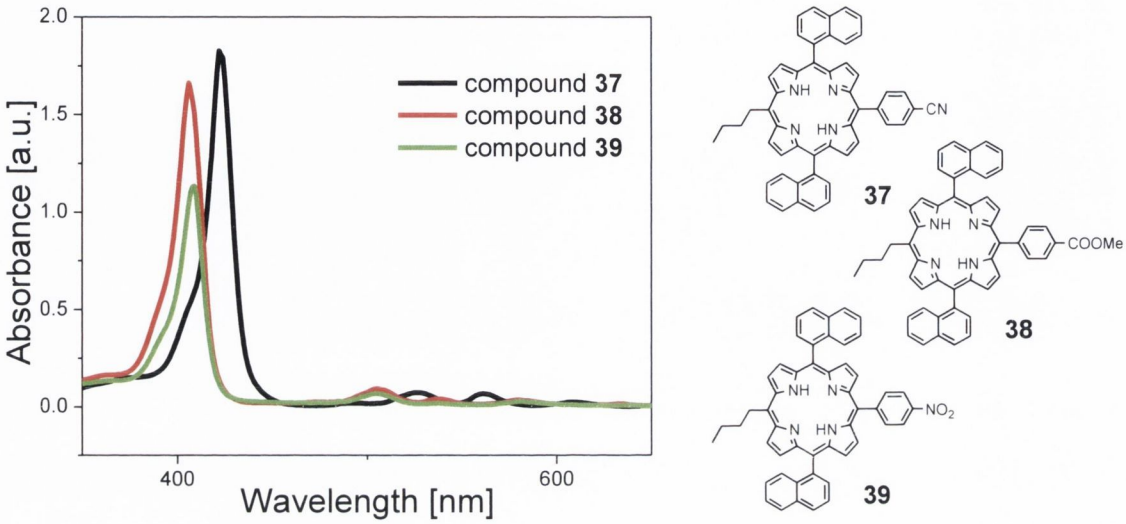



**Figure 21** The ground state absorption spectra of compounds **37**, **38** and **39** in $CH_2Cl_2$.

An interesting behavior was observed for the brominated compounds **45-47**. Upon low laser energy irradiation the 5,15-AB compound **47** with one bromine atom, exhibited an increase in transmission with input intensity - SA. When the laser energy was increased a switch from SA to RSA was observed in the focal area (Figure 22). A similar effect, but with a less pronounced RSA response, was found for compound **45** with three bromine atoms. Moreover, the RSA switch for this compound occurred at higher laser intensities. Surprisingly, the 5,10-AB compound **46** with only one bromine atom did not follow this pattern and exhibited a weak RSA over the whole intensity range studied. Thus, the regiochemical rearrangement of one bromine atom from the 10 to the 15 meso position changed the character of the NLA response. In order to understand the different characteristics of these compounds, it is necessary to analyze their ground state absorption spectra close to the experimental wavelength of 532 nm (Figure 23).

The experimental wavelength of 532 nm is close to the Q-band maxima for compounds **45** and **47** and further apart from the Q-band maximum for compound **46**. The SA behavior was previously reported for porphyrins in the Q-band absorption region.[149] Generally, SA arises at wavelength regions of high linear absorption. To our knowledge, the SA/RSA switch has not been reported for porphyrins before; only for some other materials.[150, 151] Broader considerations on the SA/RSA switch will be discussed in further parts of this thesis.

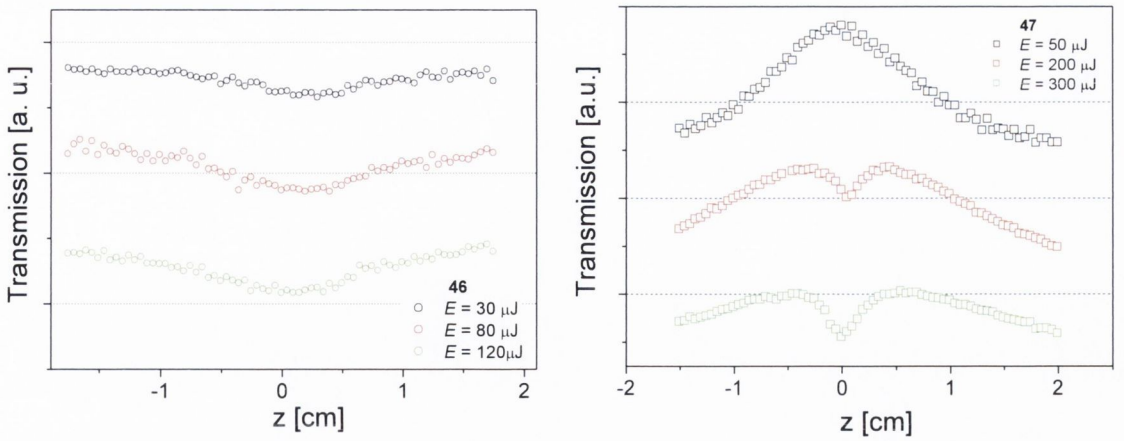



**Figure 22** Z-scan data for three measurements with increasing laser energy for compounds **46** and **47**.

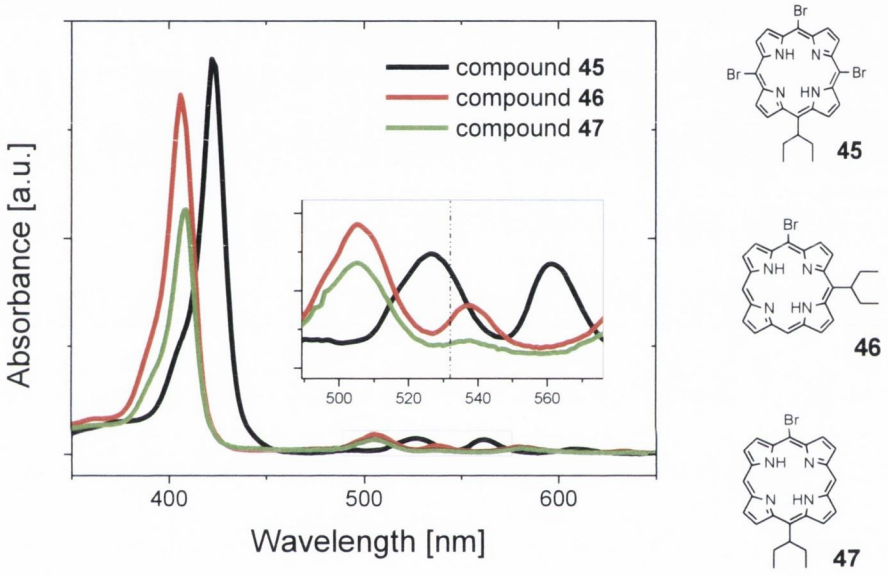
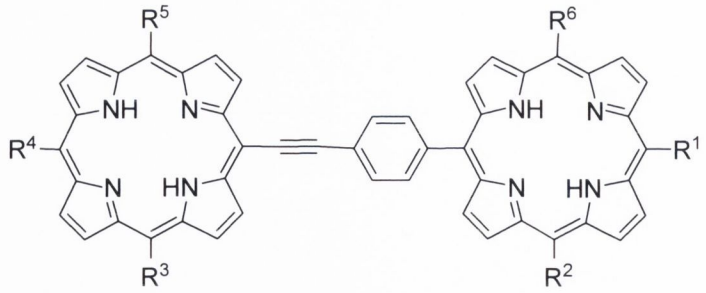
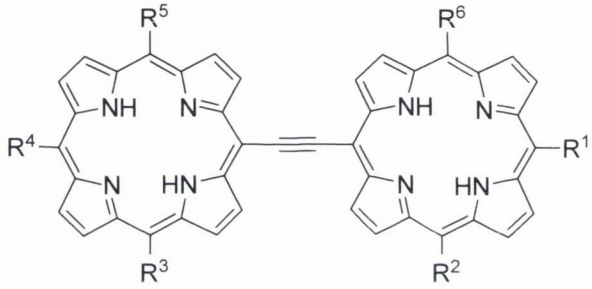



**Figure 23** Ground state absorption spectra for the brominated compounds **45-47** in $CH_2Cl_2$. Dotted line is at 532 nm.

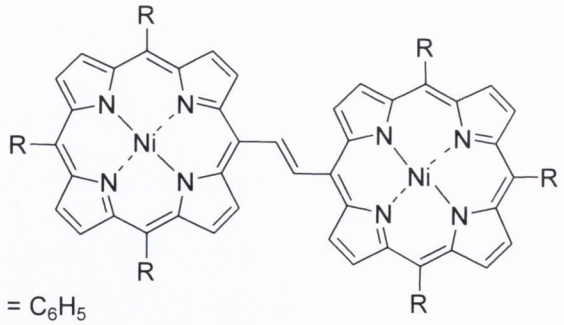
### 2.3.3 Dimers



**49** $R^1 = R^4 = H$; $R^2 = R^3 = R^5 = R^6 = C_6H_5$
**50** $R^1 = 4\text{-}NO_2\text{-}C_6H_4$; $R^2 = R^3 = R^5 = R^6 = C_6H_5$; $R^4 = n\text{-}C_4H_9$
**51** $R^1 = H$; $R^2 = R^3 = R^5 = R^6 = C_6H_5$; $R^4 = 4\text{-}NO_2\text{-}C_6H_4$
**52** $R^1 = R^3 = R^5 = H$; $R^2 = R^6 = C_6H_5$; $R^4 = 1$-ethylpropyl
**53** $R^1 = H$; $R^2 = R^6 = C_6H_5$; $R^3 = R^5 = 1$-naphthyl; $R^4 = n\text{-}C_4H_9$
**54** $R^1 = 4\text{-}NO_2\text{-}C_6H_4$; $R^2 = R^6 = C_6H_5$; $R^3 = R^5 = 1$-naphthyl; $R^4 = n\text{-}C_4H_9$



**55** $R^1 = 3\text{-}NO_2\text{-}C_6H_4$; $R^2 = n\text{-}C_6H_{13}$; $R^3 = R^5 = H$; $R^4 = 1$-ethylpropyl; $R^6 = 3,4,5\text{-}(MeO)_3\text{-}C_6H_2$
**56** $R^1 = R^3 = R^4 = H$; $R^2 = R^6 = C_6H_5$; $R^5 = 1$-ethylpropyl
**57** $R^1 = R^3 = R^5 = H$; $R^2 = R^6 = C_6H_5$; $R^4 = 1$-ethylpropyl
**58** $R^1 = 4\text{-}NO_2\text{-}C_6H_4$; $R^2 = R^6 = C_6H_5$; $R^3 = R^5 = 1$-naphthyl; $R^4 = n\text{-}C_4H_9$



**59** $R = C_6H_5$

With regard to OL efficiency of dimers, most of the compounds had relatively high $\beta_{eff}$ values, though not exceeding those of the previously discussed monomers. Therefore, no significant increase in the response was observed upon addition of another porphyrin unit. OL studies carried out on porphyrin polymers by Su *et al.* revealed that the relative transmittance at the same input fluence decreases upon addition of porphyrin units. The

monomer was found to exhibit the largest ratio of the excited to ground state absorption cross-sections $\kappa$.[152]

It was observed that the linker combining porphyrin units in dimers had an influence on the position of the Soret band maximum. An acetylene linker (**55-58**) induced a red shift in the Soret band in comparison to *p*-phenylacetylene (**49-54**). No consistent trend in the effect of the linker on the ESA could be established. With regard to the responses of structurally related dimers **52** and **57**, the dimer with a *p*-phenylacetylene linker **52** exhibited slightly lower $\beta_{eff}$ than the acetylene linked system **57**. The opposite effect was observed for **54** and **58**. Compound **58** with an acetylene linker had a lower $\beta_{eff}$ value than the analogous compound **54** with a *p*-phenylacetylene linker. This indicates that the meso substituents have a stronger effect on the ESA than the linker in the dimers studied.

Compounds **56** and **57** are structurally related in that they have the same substituents appended to the porphyrins and the same linker units. The crucial difference is the position of the 1-ethylpropyl group. Compound **56** with an 1-ethylpropyl group at the meso position 15 with respect to the linker had a slightly higher $\beta_{eff}$ value than compound **57** with the same group situated at position 10. Again, this illustrates that regiochemical positioning of meso substituents provides a tool for tailoring the OL efficiency.

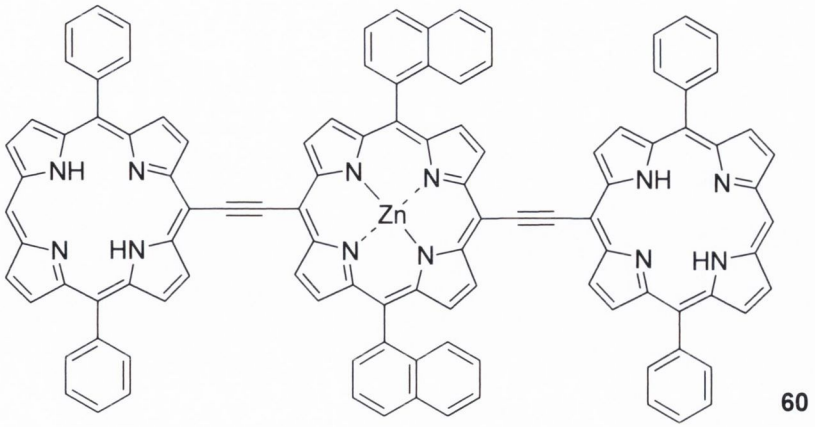
Some consistent trend in the effect of the replacement of the meso hydrogen atom with 4-$NO_2$-$C_6H_4$ groups could be observed for the *p*-phenylacetylene linked dimers. Dimers **49** and **53** with a hydrogen atom had higher $\beta_{eff}$ than analogous dimers with a 4-$NO_2$-$C_6H_4$ group at the equivalent positions (compounds **51** and **54**, respectively). For both pairs of compounds the meso position 15 with respect to the linker was altered. For the first pair of compounds hydrogen **49** and 4-$NO_2$-$C_6H_4$ **51** were situated at the meso position of the porphyrin unit directly adjacent to the phenyl unit in the linker. For the other pair (**53** and **54**) the groups were situated on the porphyrin unit adjacent to the acetylene unit of the linker.

Dimer **50** with a *p*-phenylacetylene linker and dimer **55** with an acetylene linker had the highest $\beta_{eff}$ values among all of the dimers and monomers except for the most promising monomer **36**. Based on the results obtained for other dimers which had similar meso substituents and linkers, it is difficult to establish which structural features lead to the enhancement of the OL efficiency in **50** and **55**. The observed enhancement in the OL performance of compounds **50** and **55** indicates that NLA in dimers is very susceptible to

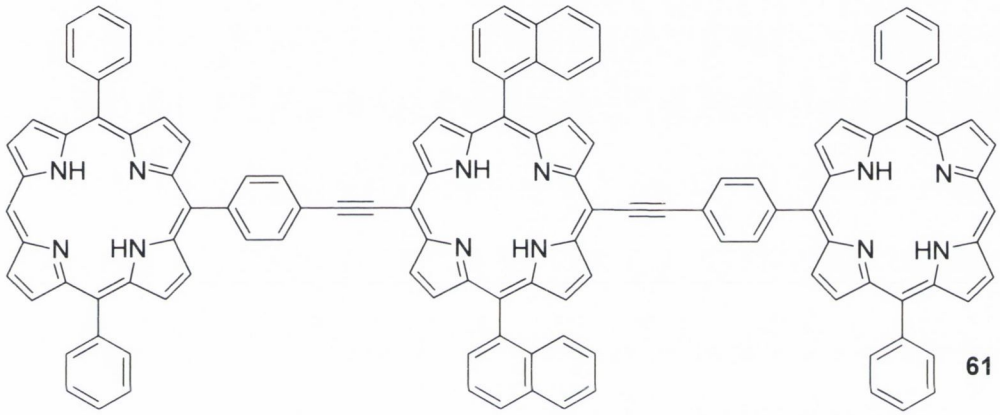
structural modifications. For example, replacement of two phenyl groups on one of the porphyrin units in **50** by two 1-naphthyl groups gives **54**, with much lower $\beta_{eff}$. Potentially, the different response of these compounds is related to different macrocyclic conformations.

No RSA response was detected for dimer **59**, which is probably due to the Ni ions present in both porphyrin units. Ni is an open shell diamagnetic metal which was found to weaken ESA *via* a decrease in the excited state lifetime in both porphyrins and related compounds like phthalocyanines.[27, 28]

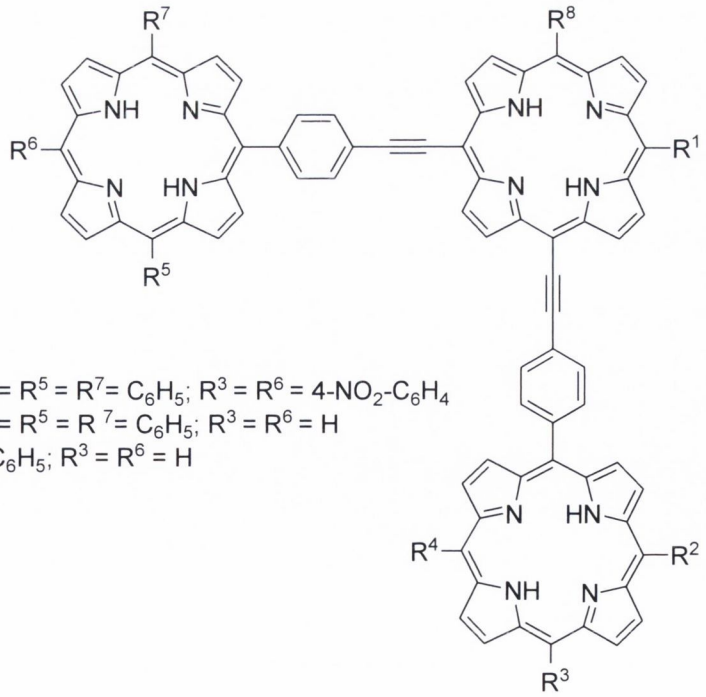
## 2.3.4 Trimers




**60**




**61**




**62** $R^1 = R^8 = 4\text{-Me-}C_6H_4$; $R^2 = R^4 = R^5 = R^7 = C_6H_5$; $R^3 = R^6 = 4\text{-}NO_2\text{-}C_6H_4$
**63** $R^1 = R^8 = 4\text{-Me-}C_6H_4$; $R^2 = R^4 = R^5 = R^7 = C_6H_5$; $R^3 = R^6 = H$
**64** $R^1 = R^2 = R^4 = R^5 = R^7 = R^8 = C_6H_5$; $R^3 = R^6 = H$

Linear trimers (**60** and **61**) were not successful candidates for OL under the experimental conditions applied. Structural features such as a 3-MeO-$C_6H_4$ residue or Zn(II) in the central core of the porphyrin, which were previously demonstrated to enhance OL performance, did not yield any increase in OL when incorporated into the structure of trimer **60**. However, the responses of the L-shaped compounds **62** and **63** were strongly enhanced compared to linear trimers (Figure 24), with $\beta_{eff}$ reaching the values of the best dimers **50** and **55**.

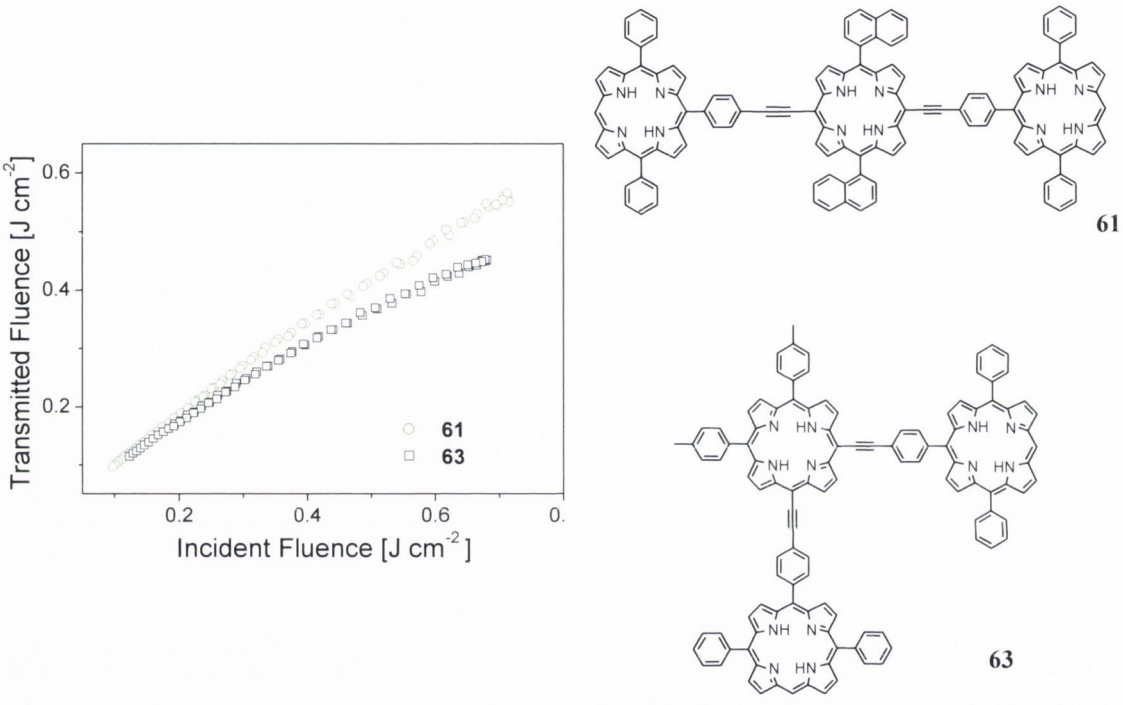



**Figure 24** OL curves plotted as transmitted fluence *versus* incident fluence for the linear trimer **61** and the L-shaped trimer **63**.

The beam waist radius was found to be larger for dimers and trimers when compared with the beam waist radius for monomers. The additional defocusing is desirable as it reduces the energy density *via* spatial dispersion of the incident pulse. In terms of practical applications in an OL device it would help to keep the incident energy density below the damage threshold of the material.[111]

## 2.4 Summary and outlook

The OL properties of structurally diverse porphyrin monomers, dimers and trimers were investigated. Initial trends concerning the dependence of the structural features on the ESA could be established. Variation of structural features such as meso substituents and linkers,

in the case of porphyrin oligomers, influences both the ground and excited state absorption. It was also shown that NLA response is not only susceptible to the character of meso groups but their regiochemical rearrangement.

For 5,15-$A_2B_2$ monomers an enhancement in RSA was observed when the meso substituent possessed some strong electron-withdrawing groups. The response was enhanced further when the substituent was linked to a porphyrin ring through a conjugated unit. Incorporation of metals into the porphyrin ring was found to enhance the response as well. Compound **36** with TMS-ethynyl and 3-MeO-$C_6H_4$ meso groups and Zn(II) in the central core was found to be the most promising compound among all of the examined compounds.

5,15-$A_2BC$ compounds, with substituent A being a 3-MeO-$C_6H_4$ group, were found to have improved OL properties in comparison to those with A = 1-naphthyl. Replacement of one 4-MeOOC-$C_6H_4$ or 4-CN-$C_6H_4$ group in 5,15-$A_2B_2$ compounds with one *n*-$C_4H_9$ group leading to the analogous 5,15-$A_2BC$ compounds lowered the efficiency of the RSA. The OL responses of structurally related 5,15-$A_2BC$ compounds with different substituents at *para*-positions were slightly different, while the ground state absorption spectra of these compounds were very similar. Thus, the structural features that do not contribute to the ground state absorption features do have an influence on the excited state absorption.

Interesting NLA responses were observed for brominated compounds with 5,15-AB and $A_3B$ substitution patterns. These compounds exhibited SA at lower input energy experiments. SA is typically observed when a region of high linear absorption is interrogated. The experimental wavelength used was within the Q-band absorption region for the brominated compounds. Notably, at higher input energy a valley within the SA peak in the close focal regime could be seen. To our knowledge, this response has not been observed for porphyrins before.

On average, dimers provided higher $\beta_{eff}$ than monomers. It was observed that meso substituents had a stronger effect on NLA than linker units for the dimers studied. L-shaped trimers were found to exhibit relatively strong RSA, while linear trimers showed weak RSA. The beam waist radius for trimers and dimers was higher than for monomers, which implies additional defocusing of the beam. This is a desirable characteristic for OL applications.

The linear absorption coefficient $\alpha_{gr}$ was plotted *versus* nonlinear absorption coefficient $\beta_{eff}$ for the examined compounds (Figure 25). $\beta_{eff}$ tends to increase with $\alpha_{gr}$. An outstanding point refers to compound **36**.

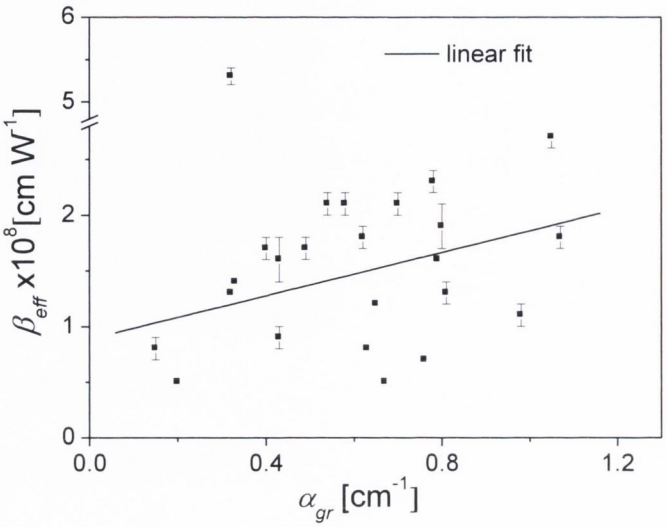



**Figure 25** Nonlinear absorption coefficient $\beta_{eff}$ plotted *versus* linear absorption coefficient $\alpha_{gr}$.

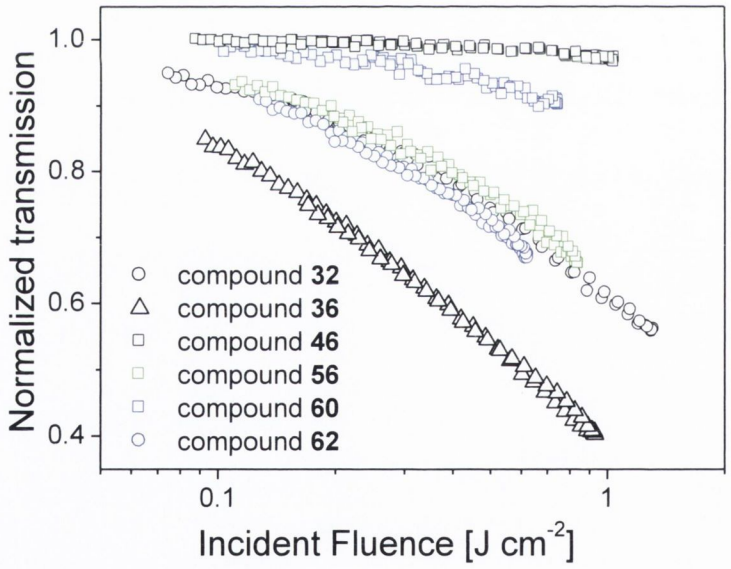



**Figure 26** Optical limiting curves plotted as normalized transmission *versus* incident fluence for the chosen compounds; monomers – black; dimer –green, trimers – blue.

Figure 26 summarizes and compares the OL action of selected compounds from three groups studied: monomers, dimers and trimers. Clearly, compound **36** emerges as the most promising candidate for applications in OL. The NLA responses recorded for the other monomers are between those presented for compounds **36** and **46**. On average dimers

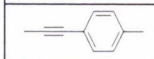
provided good OL performance that was comparable to that of stronger NLA monomers. Linear trimers were highly inefficient NLA. L-shaped trimers provided good OL properties comparable to those of dimers and stronger NLA monomers.

Concluding, the results obtained reveal that the OL properties of porphyrins can be fine-tuned by chemical modifications of the porphyrin ring *via* incorporation of different meso substituents, insertion of metal ions into the central cavity or by binding together multiple porphyrin units with different linkers. The effect of meso substituents on NLA in different porphyrin systems was highlighted and showed that the regiochemical arrangement of substituents provides yet another effective route to the modification of the OL performance of porphyrins.

**Table 1** Linear and nonlinear optical parameters of porphyrin monomers, dimers and trimers. $R^n$ – meso susbtituents; M, $M^n$ – metal in the central cavity of the porphyrin ring; No. – compound's number; $\alpha_{gr}$ – linear absorption coefficient; $\lambda_{max}$ – Soret band maximum; $I_0$ – on-focus intensity; $\beta_{eff}$ – effective nonlinear absorption coefficient; $Im\{\chi^{(3)}\}$– imaginary part of the third order susceptibility $\chi^{(3)}$; $\omega_0$ – beam waist radius at the focus.

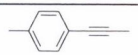
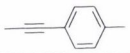
| ***Monomers*** | | | | | | | | | | | |
|---|---|---|---|---|---|---|---|---|---|---|---|
| | | | | *No.* | $\alpha_{gr}$ [$cm^{-1}$] | $\lambda_{max}$ [nm] | $I_0$ [GW $cm^{-2}$] | $\beta_{eff}$ $\times 10^8$ [$cmW^{-1}$] | $Im\{\chi^{(3)}\}$ $\times 10^{12}$ [esu] | $\omega_0$ [μm] |
| **5,15-$A_2B_2$** | | | | | | | | | | |
| $R^1$ | $R^2$ | | M | | | | | | | |
| 1-naphthyl | 2-benzothiophenyl | | 2H | **26** | 0.98 | 420 | 0.09-0.14 | 1.1±0.1 | 3.7±0.5 | 35.8±0.5 |
| 1-naphthyl | 4-CN-$C_6H_4$ | | 2H | **27** | 0.79 | 422 | 0.11-0.12 | 1.6±0.0 | 5.6±0.0 | 32.4±0.4 |
| 1-naphthyl | 1-Me-indol-5-yl | | 2H | **28** | 0.67 | 427 | 0.08-0.10 | 0.5±0.0 | 1.7±0.0 | 38.1±1.1 |
| 1-naphthyl | 4-MeOOC-$C_6H_4$ | | 2H | **29** | 0.49 | 421 | 0.08-0.12 | 1.7±0.1 | 5.8±0.3 | 35.8±0.7 |
| 1-naphthyl | 3-thiophenyl | | 2H | **30** | 0.65 | 422 | 0.08-0.09 | 1.2±0.0 | 4.0±0.0 | 37.9±0.5 |
| 1-naphthyl | $C_6H_5$-ethenyl | | 2H | **31** | 0.78 | 437 | 0.08-0.10 | 2.3±0.1 | 7.9±0.5 | 35.0±0.0 |
| 1-naphthyl | 3-$NO_2$-$C_6H_4$-ethenyl | | Zn(II) | **32** | 0.58 | 439 | 0.12-0.21 | 2.1±0.1 | 7.1±0.3 | 30.3±0.6 |
| 1-naphthyl | $PO(OEt)_2$-ethenyl | | Zn(II) | **33** | 0.15 | 437 | 0.09-0.19 | 0.8±0.1 | 3.2±0.3 | 37.6±2.7 |
| 1-naphthyl | $C_6H_5$-ethynyl | | 2H | **34** | 0.54 | 445 | 0.10-0.14 | 2.1±0.1 | 7.3±0.4 | 35.2±0.7 |
| 3-MeO-$C_6H_4$ | 4-CN-$C_6H_4$ | | 2H | **35** | 0.43 | 420 | 0.08-0.12 | 1.6±0.2 | 5.5±0.5 | 35.9±1.6 |
| 3-MeO-$C_6H_4$ | TMS-ethynyl | | Zn(II) | **36** | 0.32 | 449 | 0.09-0.11 | 5.3±0.1 | 18.0±0.0 | 34.3±0.0 |
| **5,15-$A_2BC$** | | | | | | | | | | |
| $R^1$ | $R^2$ | $R^3$ | | | | | | | | |
| 1-naphthyl | *n*-$C_4H_9$ | 4-CN-$C_6H_4$ | 2H | **37** | 0.20 | 422 | 0.07-0.08 | 0.5±0.0 | 1.5±0.1 | 43.0±2.3 |
| 1-naphthyl | *n*-$C_4H_9$ | 4-MeOOC-$C_6H_4$ | 2H | **38** | 0.76 | 422 | 0.12-0.21 | 0.7±0.0 | 2.3±0.2 | 34.6±2.4 |
| 1-naphthyl | *n*-$C_4H_9$ | 4-$NO_2$-$C_6H_4$ | 2H | **39** | 0.63 | 423 | 0.08-0.10 | 0.8±0.0 | 2.7±0.1 | 37.0±1.7 |
| 1-naphthyl | *n*-$C_4H_9$ | Br | Zn(II) | **40** | 0.62 | 425 | 0.10-0.20 | 1.8±0.1 | 6.1±0.4 | 33.5±1.3 |
| 1-naphthyl | 2-thiophenyl | 4-$NO_2$-$C_6H_4$ | 2H | **41** | 0.43 | 423 | 0.08-0.09 | 0.9±0.1 | 3.1±0.2 | 39.6±3.5 |
| 3-MeO-$C_6H_4$ | *n*-$C_4H_9$ | 4-CN-$C_6H_4$ | 2H | **42** | 0.70 | 419 | 0.09-0.18 | 2.1±0.1 | 7.1±0.4 | 35.1±1.5 |
| 3-MeO-$C_6H_4$ | *n*-$C_4H_9$ | 4-$NO_2$-$C_6H_4$ | 2H | **43** | 0.80 | 420 | 0.09-0.17 | 1.9±0.2 | 6.5±0.5 | 36.3±1.7 |
| 4-MeOOC-$C_6H_4$ | *n*-$C_4H_9$ | 3,4,5-$(MeO)_3$-$C_6H_2$ | 2H | **44** | 0.32 | 420 | 0.07-0.10 | 1.3±0.0 | 4.3±0.1 | 38.6±0.0 |
| **$A_3B$** | | | | | | | | | | |
| $R^1$ | $R^2$ | | M | | | | | | | |
| Br | 1-ethylpropyl | | 2H | **45** | 0.25 | 422 | - | - | - | - |

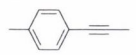
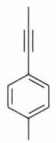
| ***Monomers*** | | | | | | | | | |
|---|---|---|---|---|---|---|---|---|---|
| | | | *No.* | $\alpha_{gr}$ [$cm^{-1}$] | $\lambda_{max}$ [nm] | $I_0$ [GW $cm^{-2}$] | $\beta_{eff}$ $\times 10^8$ [$cmW^{-1}$] | $Im\{\chi^{(3)}\}$ $\times 10^{12}$ [esu] | $\omega_0$ [μm] |
| $R^1$ | $R^2$ | M | | | | | | | |
| **5,10-AB** | | | | | | | | | |
| Br | 1-ethylpropyl | 2H | **46** | 0.50 | 409 | 0.10-0.12 | 0.1±0.0 | 0.3±0.0 | 33.8±0.1 |
| **5,15-AB** | | | | | | | | | |
| Br | 1-ethylpropyl | 2H | **47** | 0.53 | 406 | - | - | - | - |
| **5,10-$A_2$** | | | | | | | | | |
| | | | | | | | | | |
| 4-Me-$C_6H_4$ | | 2H | **48** | 0.73 | 405 | 0.10-0.20 | 1.9±0.1 | 6.5±0.4 | 33.4±0.1 |

| ***Dimers*** | | | | | | | | | |
|---|---|---|---|---|---|---|---|---|---|
| Linker | $R^n$ | $M^n$ | *No.* | $\alpha_{gr}$ [$cm^{-1}$] | $\lambda_{max}$ [nm] | $I_0$ [GW $cm^{-2}$] | $\beta_{eff}$ $\times 10^8$ [$cmW^{-1}$] | $Im\{\chi^{(3)}\}$ $\times 10^{12}$ [esu] | $\omega_0$ [μm] |
|  | $R^1 = R^4 = H$<br>$R^2 = R^3 = R^5 = R^6 = C_6H_5$ | $M^1 = M^2 = 2H$ | **49** | 0.62 | 432 | 0.05-0.06 | 1.8±0.1 | 6.1±0.4 | 47.7±3.4 |
| | $R^1$ = 4-$NO_2$-$C_6H_4$<br>$R^2 = R^3 = R^5 = R^6 = C_6H_5$<br>$R^4$ = *n*-$C_4H_9$ | $M^1 = M^2 = 2H$ | **50** | 1.05 | 435 | 0.07-0.10 | 2.7±0.1 | 9.0±0.0 | 38.8±0.9 |
| | $R^1 = H$<br>$R^2 = R^3 = R^5 = R^6 = C_6H_5$<br>$R^4$ = 4-$NO_2$-$C_6H_4$ | $M^1 = M^2 = 2H$ | **51** | 0.33 | 437 | 0.04 | 1.4±0.0 | 4.7±0.0 | 51.8±0.0 |
| | $R^1 = R^3 = R^5 = H$<br>$R^2 = R^6 = C_6H_5$<br>$R^4$ =1-ethylpropyl | $M^1 = M^2 = 2H$ | **52** | 0.40 | 425 | 0.05-0.06 | 1.7±0.1 | 5.7±0.3 | 46.4±2.9 |
| | $R^1 = H$<br>$R^2 = R^6 = C_6H_5$<br>$R^3 = R^5$ =1-naphthyl<br>$R^4$= *n*-$C_4H_9$ | $M^1 = M^2 = 2H$ | **53** | 1.07 | 439 | 0.07-0.11 | 1.8±0.1 | 6.1±0.5 | 38.8±0.9 |
| | $R^1$ = 4-$NO_2$-$C_6H_4$<br>$R^2 = R^6 = C_6H_5$ | $M^1 = M^2 = 2H$ | **54** | 0.81 | 439 | 0.09-0.10 | 1.3±0.1 | 4.6±0.2 | 44.2±1.0 |

| ***Dimers*** | | | | | | | | | |
|---|---|---|---|---|---|---|---|---|---|
| Linker | $R^n$ | $M^n$ | *No.* | $\alpha_{gr}$ [$cm^{-1}$] | $\lambda_{max}$ [nm] | $I_0$ [GW $cm^{-2}$] | $\beta_{eff}$ $\times 10^8$ [$cmW^{-1}$] | $Im\{\chi^{(3)}\}$ $\times 10^{12}$ [esu] | $\omega_0$ [μm] |
| | $R^3 = R^5$ = 1-naphthyl<br>$R^4$ = *n*-$C_4H_9$ | | | | | | | | |
|  | $R^1$ = 3-$NO_2$-$C_6H_4$<br>$R^2$ = *n*-$C_6H_{13}$<br>$R^3 = R^5$ = H<br>$R^4$ = 1-ethylpropyl<br>$R^6$ = 3,4,5-$(MeO)_3$-$C_6H_2$ | $M^1 = M^2$ = 2H | **55** | 3.03 | 467 | 0.06-0.10 | 2.6±0.2 | 8.8±0.7 | 45.1±1.9 |
| | $R^1 = R^3 = R^4$ = H<br>$R^2 = R^6 = C_6H_5$<br>$R^5$ = 1-ethylpropyl | $M^1 = M^2$ = 2H | **56** | 0.55 | 465 | 0.08-0.15 | 1.6±0.2 | 5.4±0.8 | 39.0±1.2 |
| | $R^1 = R^3 = R^5$ = H<br>$R^2 = R^6 = C_6H_5$<br>$R^4$ = 1-ethylpropyl | $M^1 = M^2$ = 2H | **57** | 0.63 | 464 | 0.10-0.14 | 1.9±0.1 | 6.4±0.5 | 36.8±1.3 |
| | $R^1$ = 4-$NO_2$-$C_6H_4$<br>$R^2 = R^6 = C_6H_5$<br>$R^3 = R^5$= 1-naphthyl<br>$R^4$ = *n*-$C_4H_9$ | $M^1 = M^2$ = 2H | **58** | 0.28 | 473 | 0.04-0.05 | 0.7±0.0 | 2.5±0.1 | 55.2±3.2 |
|  | $R^1 = R^2 = R^3 = R^4 = R^5 = R^6 = C_6H_5$ | $M^1 = M^2$ = Ni(II) | **59** | - | - | - | - | - | - |

| ***Linear Trimers*** | | | | | | | | | |
|---|---|---|---|---|---|---|---|---|---|
| Linkers | $R^n$ | $M^n$ | *No.* | $\alpha_{gr}$ [$cm^{-1}$] | $\lambda_{max}$ [nm] | $I_0$ [GW $cm^{-2}$] | $\beta_{eff}$ $\times 10^8$ [$cmW^{-1}$] | $Im\{\chi^{(3)}\}$ $\times 10^{12}$ [esu] | $\omega_0$ [μm] |
| $L^1 = L^2$=  | $R^1 = R^5$ = H<br>$R^2 = R^4 = R^6 = R^8$ = 3-MeO-$C_6H_4$<br>$R^3 = R^7$ = 1-naphthyl | $M^1 = M^3$ = 2H<br>$M^2$ = Zn(II) | **60** | 0.60 | 411 | 0.07-0.08 | 0.4±0.0 | 1.4±0.1 | 40.9±2.1 |

| ***Linear Trimers*** | | | | | | | | | |
|---|---|---|---|---|---|---|---|---|---|
| Linkers | $R^n$ | $M^n$ | *No.* | $\alpha_{gr}$ [$cm^{-1}$] | $\lambda_{max}$ [nm] | $I_0$ [GW $cm^{-2}$] | $\beta_{eff}$ $\times 10^8$ [$cmW^{-1}$] | $Im\{\chi^{(3)}\}$ $\times 10^{12}$ [esu] | $\omega_0$ [μm] |
| $L^1$=  $L^2$=  | $R^1 = R^5 = H$<br>$R^2 = R^4 = R^6 = R^8 = C_6H_5$<br>$R^3 = R^7$ = 1-naphthyl | $M^1 = M^2 = M^3$ = 2H | **61** | 0.45 | 413 | 0.07-0.08 | 1.1±0.0 | 3.8±0.0 | 40.8±2.1 |

| ***L-shaped Trimers*** ($M^1 = M^2 = M^3$ = 2H) | | | | | | | | |
|---|---|---|---|---|---|---|---|---|
| Linkers | $R^n$ | *No.* | $\alpha_{gr}$ [$cm^{-1}$] | $\lambda_{max}$ [nm] | $I_0$ [GW $cm^{-2}$] | $\beta_{eff}$ $\times 10^8$ [$cmW^{-1}$] | $Im\{\chi^{(3)}\}$ $\times 10^{12}$ [esu] | $\omega_0$ [μm] |
| $L^1$=  $L^2$=  | $R^1 = R^8$ = 4-Me-$C_6H_4$<br>$R^2 = R^4 = R^5 = R^7 = C_6H_5$<br>$R^3 = R^6$ = 4-$NO_2$-$C_6H_4$ | **62** | 0.67 | 420 | 0.06 | 2.4±0.2 | 8.1±0.6 | 43.4±1.8 |
| | $R^1 = R^8$ = 4-Me-$C_6H_4$<br>$R^2 = R^4 = R^5 = R^7 = C_6H_5$<br>$R^3 = R^6 = H$ | **63** | 1.02 | 413 | 0.06-0.09 | 2.6±0.2 | 9.0±0.6 | 40.1±0.2 |
| | $R^1 = R^2 = R^4 = R^5 = R^7 = R^8 = C_6H_5$<br>$R^3 = R^6 = H$ | **64** | 0.19 | 412 | 0.05-0.06 | 0.8±0.0 | 2.7±0.1 | 54.1±9.8 |

# Chapter 3 Synthesis of novel free base and metallated 5,10-$A_2B_2$ porphyrins

## 3.1 Introduction

5,10-$A_2B_2$ meso substituted porphyrins are relatively underexplored in comparison to other porphyrin monomers with different substitution patterns. Still little is known about their linear and nonlinear optical properties. In the previous chapter the impact of the chemical arrangement of the substituents on the NLA properties of porphyrins was demonstrated. Taking this into account, a group of 5,10-$A_2B_2$ porphyrins was synthesized and their NLA properties were explored.

## 3.2 Review of the synthetic pathways leading to 5,10-$A_2$ and 5,10-$A_2B_2$ porphyrins

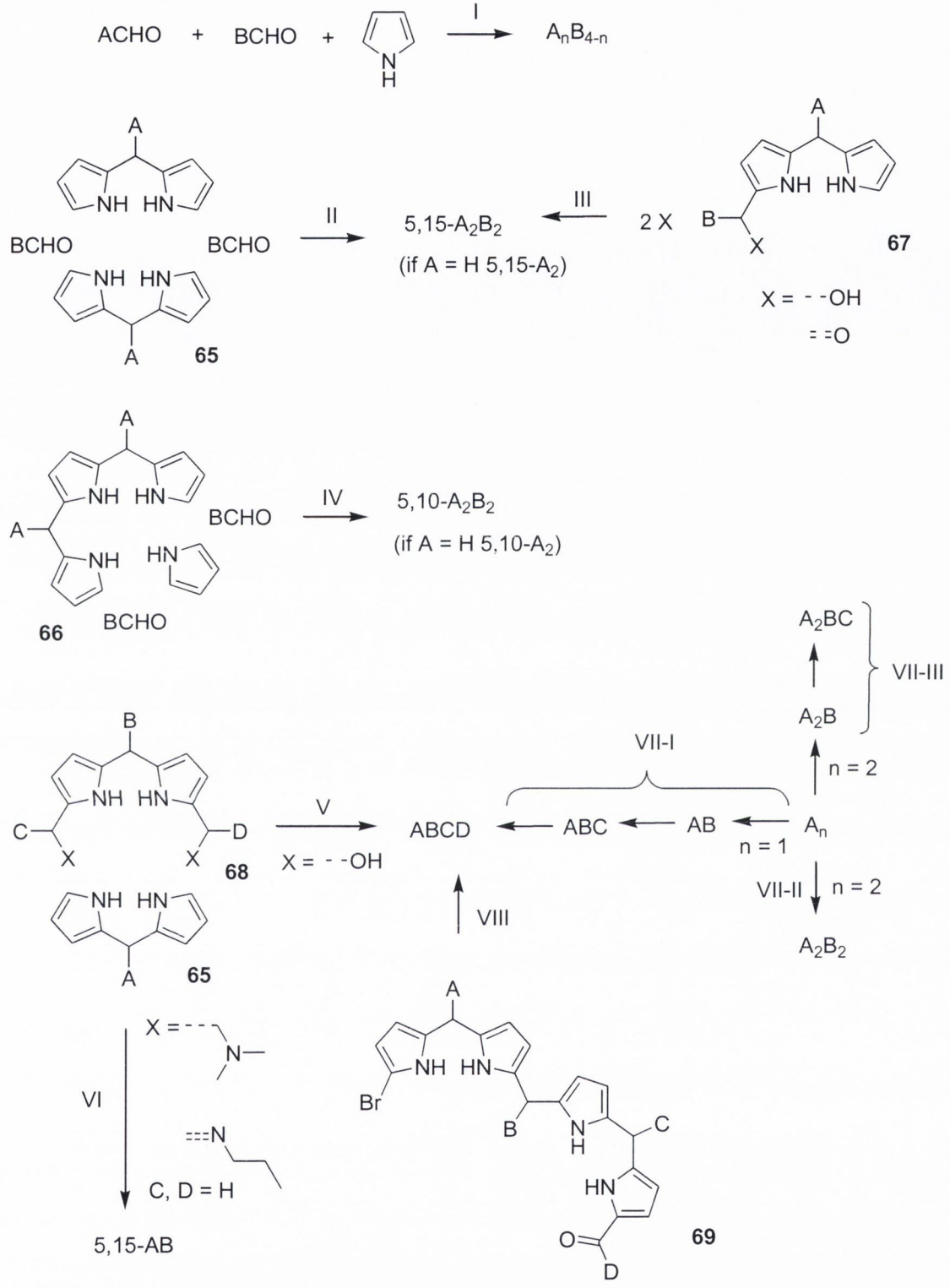
Meso substituted porphyrins do not occur in nature. They can only be prepared synthetically, which offers a great spectrum of possible structures (2.2.1). Porphyrins with four equivalent meso substituents are easily accessible in a one-flask reaction of pyrrole with a corresponding aldehyde.[153-155] However, many applications necessitate molecules with an unsymmetrically substituted porphyrin ring. These include push-pull molecules for NLO applications,[43] amphiphilic porphyrins for photodynamic therapy,[156] and donor-acceptor systems for electron-transfer studies.[157] Different pathways have been developed to obtain porphyrins with different numbers of meso substituents in the desired substitution pattern (Scheme 1). They can generally be classified into three groups: (i) condensation reactions, (ii) total synthesis based on the "porphyrins *via* bilanes" route and (iii) functionalization of preformed porphyrins.

Condensation reactions between pyrrole and two or more aldehydes yield a mixture of different porphyrins, the separation of which can be troublesome (I).[74] More advanced methods involve preparation of substituted or unsubstituted dipyrromethanes **65** or tripyrranes **66** which then react with the appropriate reagents, *i.e.* an aldehyde, or an

aldehyde and pyrrole, respectively (II and IV).[158, 159] Homocoupling of different derivatives of dipyrromethanes **67** (III) or coupling of derivatives of dipyrromethanes **68** with appropriate dipyrromethanes **65** (VI) was also reported.[160-164]

Total synthesis "*via* bilanes" involves multistep preparation of bilanes **69** which are then subjected to cyclization and oxidation to give the desired product (VIII).[165]

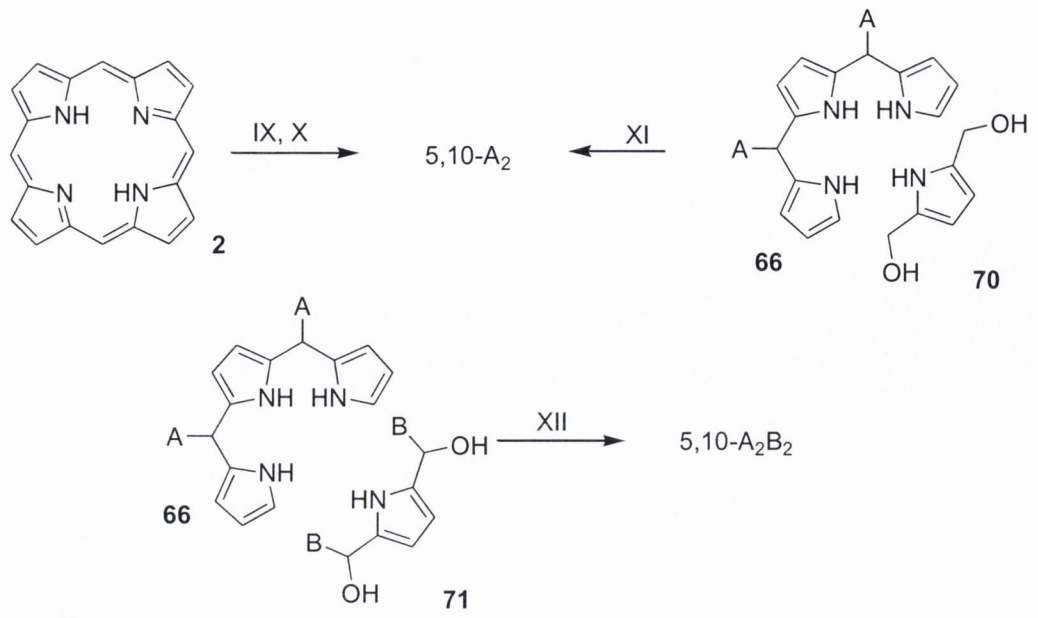
Finally, the step-wise functionalization of a preformed porphyrin ($A_n$), most commonly using C-C coupling and organolithium reactions, is a very versatile method for the preparation of compounds with different substituents in different substation patterns (*e.g.* VII-I, VII-II, VII-III).[166]




**Scheme 1** Examples of synthetic routes leading to different substitution patterns of porphyrins. I , II, III (X = OH), V: (1) acid catalyst (2) DDQ; III X = O: $MgBr_2$, DBU, toluene or KOH, $Pd(CH_3CN)_2Cl_2$, EtOH; IV: (1) TFA, $CH_2Cl_2$ (2) DDQ; VI X = $N(CH_3)_2$: (1) EtOH, $Zn(OAc)_2$, reflux (2) DDQ; X = $N(CH)_2CH_3$: EtOH, $Zn(OAc)_2$, reflux; VII-I, V-III, V-III: *e.g.* step one: bromination (NBS, $CHCl_3$, 0°C); step two: Sonogashira coupling (alkyne, $NEt_3$, CuI, $Pd(PPh_3)_2Cl_2$, THF) / Suzuki coupling ($RB(OH)_2$, $Pd(PPh_3)_4$, $K_3PO_4$, THF) / Heck coupling (olefin, NaOAc, $Pd(OAc)_2$, $PPh_3$, DMF, reflux); VIII: $MgBr_2$, DBU, toluene, 115°C.

The first method reported for the synthesis of a 5,10-$A_2$ porphyrin involved dinitration of porphine **2** with nitric acid at 0 °C (Scheme 2 IX).[167] The product was obtained in 56% yield, however, the compound was not characterized. It was not until the last decade that more attention was given to 5,10-$A_2$ and 5,10-$A_2B_2$ porphyrins. Some isolated reports on the synthesis of 5,10-$A_2$ porphyrins *via* different condensation methods can be found in literature. For example, Sugiura reported the synthesis of 5,10-bis(3,5-di-*tert*-butylphenyl)porphyrin in 3% yield by condensing 3,5-di-*tert*-butylphenylbenzaldehyde, pyrrole and tripyrrane (general route IV).[168] Brinas and Bruckner synthesized 5,10-diphenylporphyrin *via* the acid catalyzed condensation of dicarbinol-dipyrromethane with dipyrromethane in 10-20% yield in 5 steps (general route V, A = C, B = D = H).[169] Ryppa and Hatcher carried out broader studies on 5,10-$A_2$ porphyrins.[159] In their studies, different aryl- and alkyl-substituted 5,10-$A_2$ porphyrins were synthesized *via* TFA catalyzed condensation of tripyranne with appropriate aldehydes with yields up to 11% (general route IV). Apart from the desired 5,10-$A_2$ porphyrin, a monosubstituted porphyrin byproduct was obtained. Formation of the monosubstituted product was explained by acid catalyzed scrambling. Ryppa and Hatcher also prepared alkyl- and aryl- 5,10-$A_2$ porphyrins treating porphine with the appropriate concentration of an organolithium reagent (X). Although this method was shown to be more efficient than the TFA catalyzed condensation, it was more technically demanding. An interesting approach was introduced by Goncalves who synthesized 5,10-dipyridylporphyrin *via* the TFA catalyzed condensation of a substituted tripyrrane **66** with 2,5-bis(hydroxymethylpyrrole) **70** (XI).[170]

5,10-$A_2B_2$ porphyrins can be accessed through the statistical condensation of two aldehydes and pyrrole (I). However, this method requires extensive chromatographic separation. A more rational approach proposed by Heo and Lee, involved the TFA catalyzed reaction of tripyranne with pyrrole-dicarbinol **71** (XII).[171] Lindsey proposed a pathway whereby preformed diacyl dipyrromethanes were reduced to the corresponding dicarbinols and condensed with dipyrromethanes to afford 5,10-$A_2B_2$ porphyrins up to gram scale (V, B = D, A = C).[160] A significant approach which gives access to numerous different 5,10-$A_2B_2$ porphyrins was demonstrated by Senge *et al.* It involved the functionalization of a preformed 5,10-$A_2$ precursor with organolithium or C-C coupling reactions (VII-II).[172] Lastly, the "bilane strategy" developed by Lindsey can give access to 5,10-$A_2B_2$ porphyrins, however, this route was not yet studied broadly (VIII, A = B, C = D).[173]




**Scheme 2** Synthetic routes leading to 5,10-$A_2$ and 5,10-$A_2B_2$ porphyrins. IX: $HNO_3$, 0°C X: (1) RLi, THF (2) $H_2O$, DDQ; XI, XII: (1) TFA, $CH_2Cl_2$ (2) DDQ.

It is worth mentioning that 5,10-$A_2B_2$ porphyrins are interesting candidates for applications in NLO and for ET studies which require a strong dipolar moment. A 5,10-$A_2B_2$ push-pull system requires introduction of only two substituents instead of three in 5,15-$A_2$BC porphyrins which are commonly applied for these studies (Figure 27).

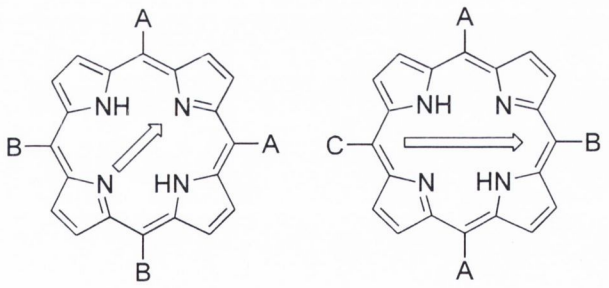



**Figure 27** Orientation of the intramolecular dipole moment in 5,10-$A_2B_2$ and 5,15-$A_2$BC porphyrins.

## 3.3 Metalloporphyrins

Metalloporphyrins are porphyrin derivatives in which at least one lone electron pair from the central nitrogen atoms is shared with a metal ion which acts as a Lewis acid. Usually, a metal ion not only coordinates to the two lone pairs on the central nitrogen atoms, but furthermore replaces the two hydrogen atoms on the pyrrole nitrogen atoms; thus, two more lone pairs are donated from the porphinato ligand to the valence shell of the metal ion.[174]

If the metal has a positive charge $Z_M > 2$, the porphyrin complex gains charge electro-neutrality by coordination of anions to the central metal. If the coordination number of the metal CN > Z+2 the metal completes its coordination sphere by further complexing with neutral donor molecules (*e.g.*, water).

Depending on the metal and the number of ligands, porphyrins can exhibit different geometries. Metals can be more or less coplanar with the porphyrin ring. The more ligands in the molecule and the larger the metal, the more possible configurations of these ligands with respect to the plane of the porphyrin system can theoretically exist.

With regard to the metals which were the subject of our interest, according to literature Pt(II) and Pd(II) complexes form square planar geometry (Figure 28 a). Zn(II) complexes form square planar geometry or if neutral ligands (typically: pyridine, water, methanol) are coordinated - square pyramidal geometry (Figure 28 b). In(III) complexes also form square pyramidal geometry yet the central metal is situated above the mean plane of the four pyrrole nitrogens (Figure 28 e).[175] In Pb(II) complexes, the central metal is situated outside the plane of the macrocycle and the Pb(II) complexes form out-of-plane coordination with the metal at the apex of a square pyramid (Figure 28 d).[176] Tin(IV) complexes typically form distorted octahedral complexes (Figure 28 c).[177]

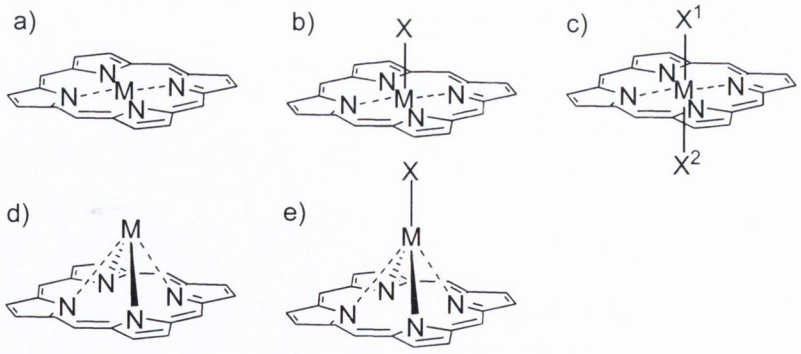



**Figure 28** Structural types of porphyrin complexes.

Almost all metals form complexes with porphyrins. Various methods were developed in order to incorporate these metals into the porphyrin core which can be distinguished by the type of 'metal carrier' or solvent used, *i.e.* acetate method, acetylacetonate method or DMF method.

## 3.4 Sonogashira coupling

Sonogashira coupling is a palladium catalyzed reaction which allows the formation of C-C bonds between terminal alkynes and aryl halides.[178] Bis(triphenylphosphine)palladium dichloride [$Pd(PPh_3)_2Cl_2$] is used as a catalyst in this reaction. The reaction is carried out in the presence of an aliphatic amine and CuI co-catalyst. Sonogashira coupling is widely applied in porphyrin chemistry to obtain various β- or meso-alkenyl-substituted porphyrins or to bridge porphyrin units to form oligomers.[179-181] The proposed mechanism of Sonogashira coupling is shown in Figure 29. Two catalytic cycles are distinguished: for palladium (A) and for copper (B).

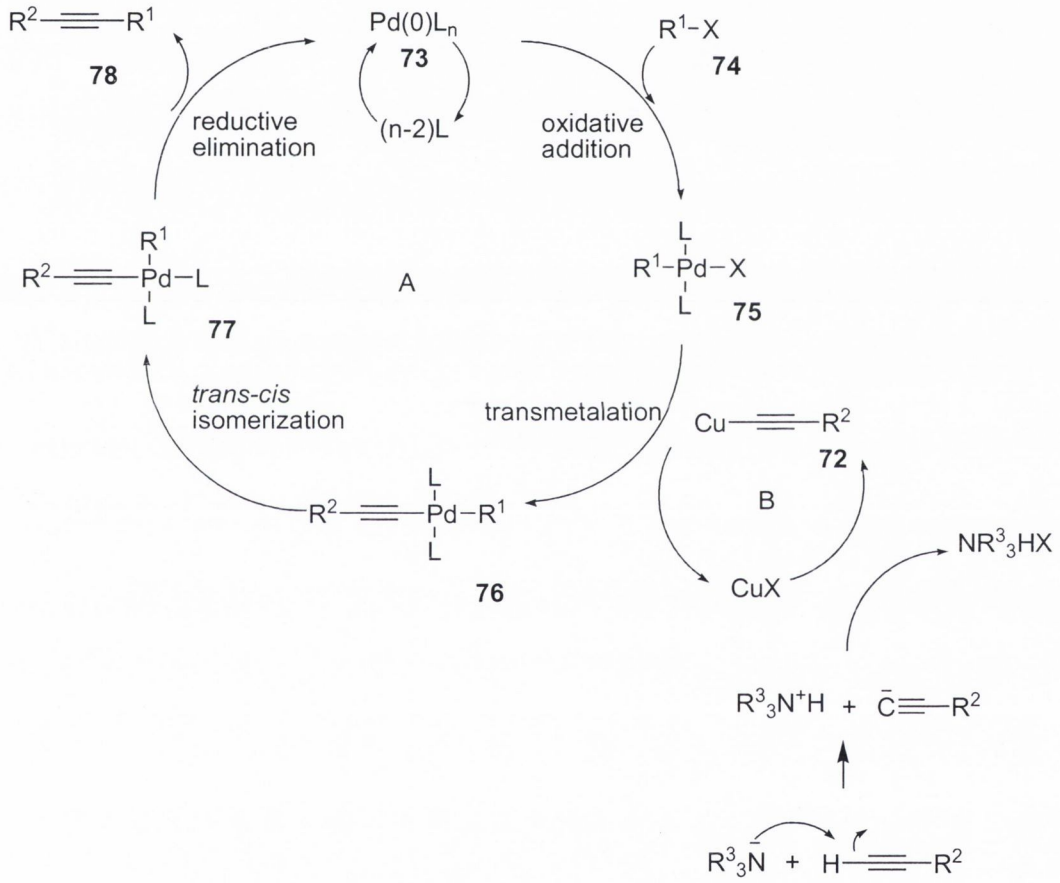



**Figure 29** Mechanism of Sonogashira coupling.

The copper cycle (B) generates an alkynyl cuprate **72** which takes part in the palladium cycle.

In the palladium cycle (A), the palladium catalyst $Pd(0)L_n$ **73** reacts in a rate limiting oxidative addition with the halide **74** to produce a Pd(II) intermediate complex **75**. Then

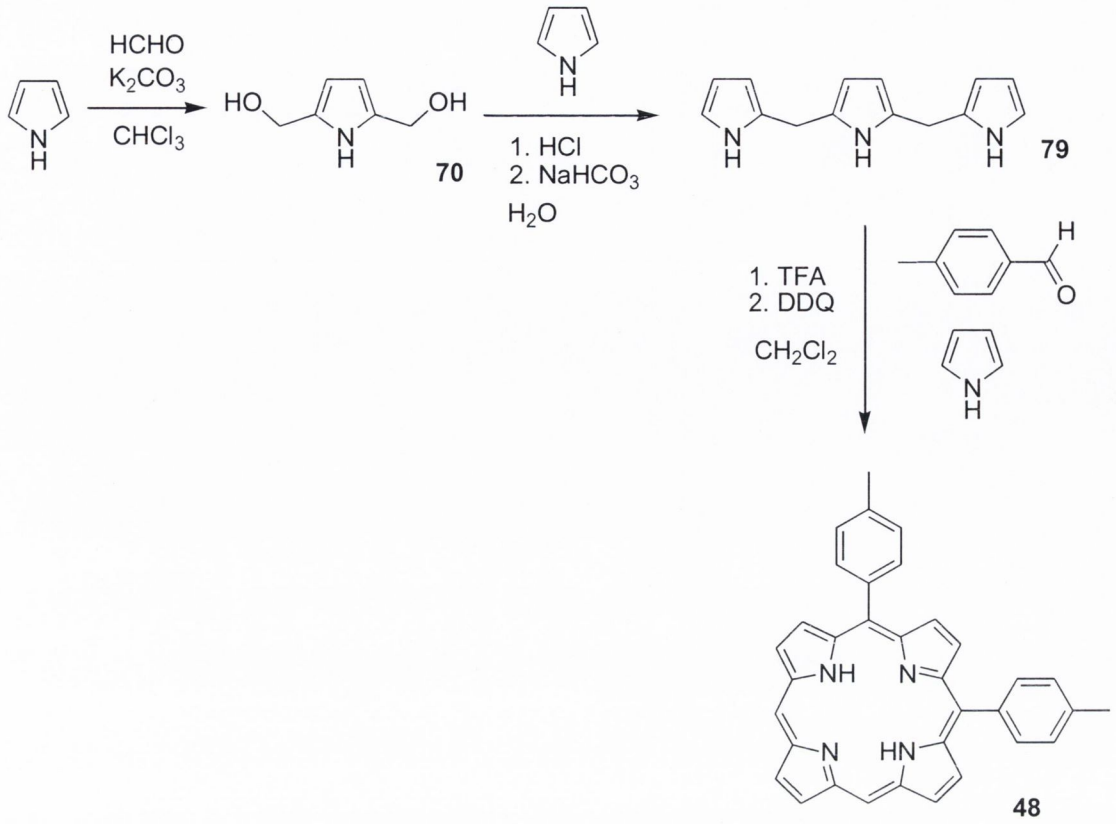
the complex **75** reacts in transmetallation with copper acetylide **72** which is formed in the copper cycle, to give complex **76**. CuX is expelled at this stage. The next step involves *trans-cis* isomerization of the ligands. Initially *trans* oriented ligands in **76** are coverted to *cis* orientation in complex **77**. The final product **78** is released in a reductive elimination from **77**, with the regeneration of the palladium catalyst.

The reaction medium must be typically basic to neutralize the hydrogen halide which is formed as a byproduct, therefore, alkylamines such as triethylamine or diethylamine are often used as solvents. As Pd(0) complexes are unstable in air, deoxygeneated conditions are required for Sonogoshaira coupling reactions.

## 3.5 Synthesis and characterization of 5,10-$A_2B_2$ porphyrins

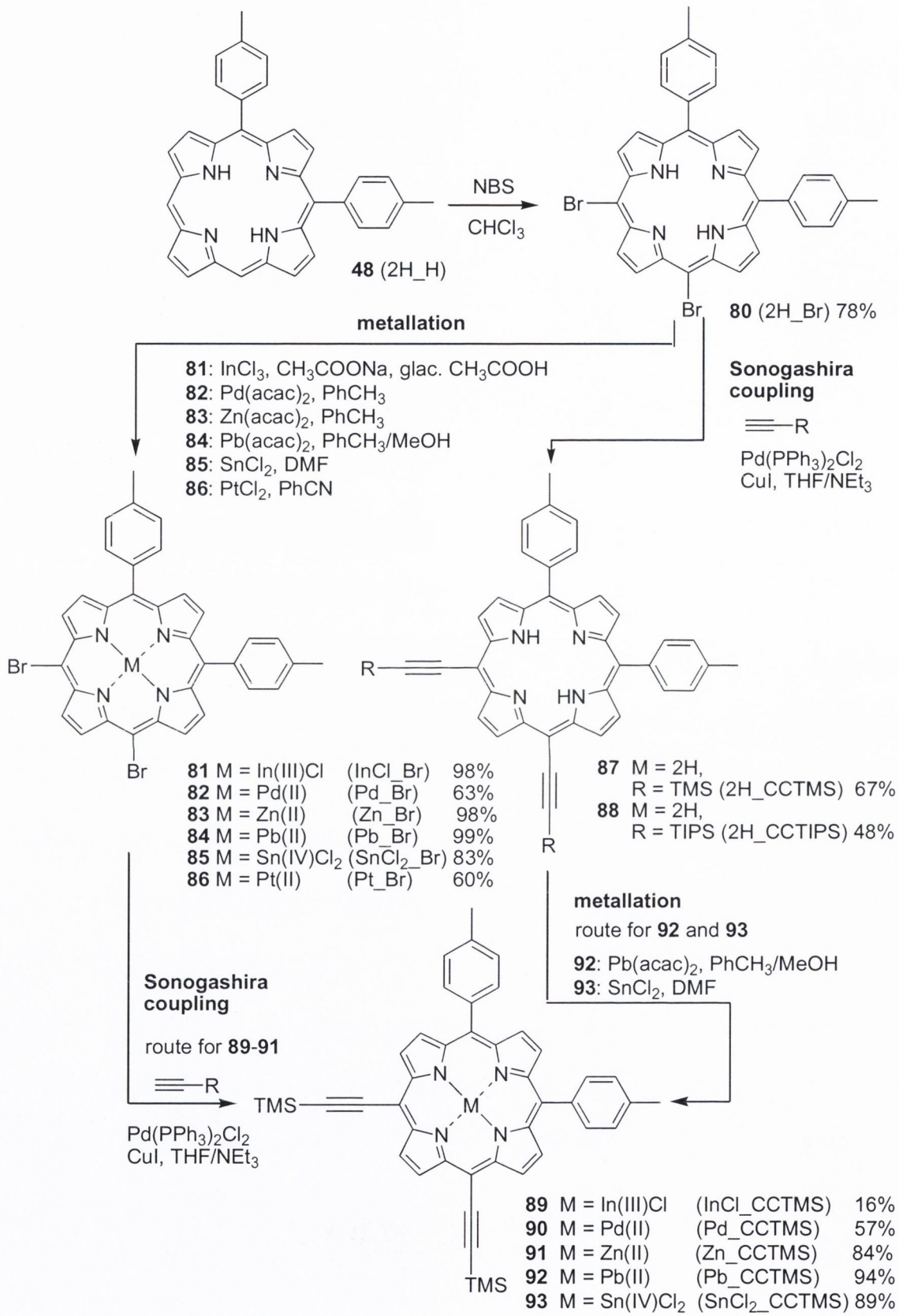
### 3.5.1 Synthesis of 5,10-$A_2B_2$ porphyrins

Two series of free base and metallated 5,10-$A_2B_2$ porphyrins **80-93**, both bearing tolyl as substituent A and bromide or TMS-/TIPS-ethynyl as the other meso substituent, were synthesized from a 5,10-$A_2$ precursor (5,10-di(*p*-tolyl)porphyrin **48**). 5,10-Di(*p*-tolyl)porphyrin **48** was obtained in the TFA catalyzed condensation of tripyrrane **79** with pyrrole and aldehyde in yields of 8-10% (Scheme 3).[159] Tripyrrane was synthesized from pyrrole and 2,5-bis(hydroxymethylpyrrole) **70**.[182] The latter compound was obtained from pyrrole as previously reported (Scheme 3).[183] The TFA catalyzed condensation of tripyrrane with pyrrole and aldehyde was sensitive to concentration. The use of half the amount of the solvent compared to that reported in literature, resulted in a lower yield of 4%. This finding is in agreement with the previous reports.[184] The use of $BF_3{\cdot}O(C_2H_5)_2$ instead of TFA, in the condensation reaction did not improve the yield of the 5,10-$A_2$ product (3.5%).




**Scheme 3** Synthesis of 5,10-$A_2$ precursor **48**.

The synthetic route to two series of 5,10-$A_2B_2$ porphyrins, brominated and TMS-/TIPS-ethynyl-substituted, is presented in Scheme 4. Note, that the abbreviated compound names shown in Scheme 4 will be used in further parts of this thesis.




**Scheme 4** Synthetic route to brominated and TMS-/TIPS-ethynyl 5,10-$A_2B_2$ porphyrins.

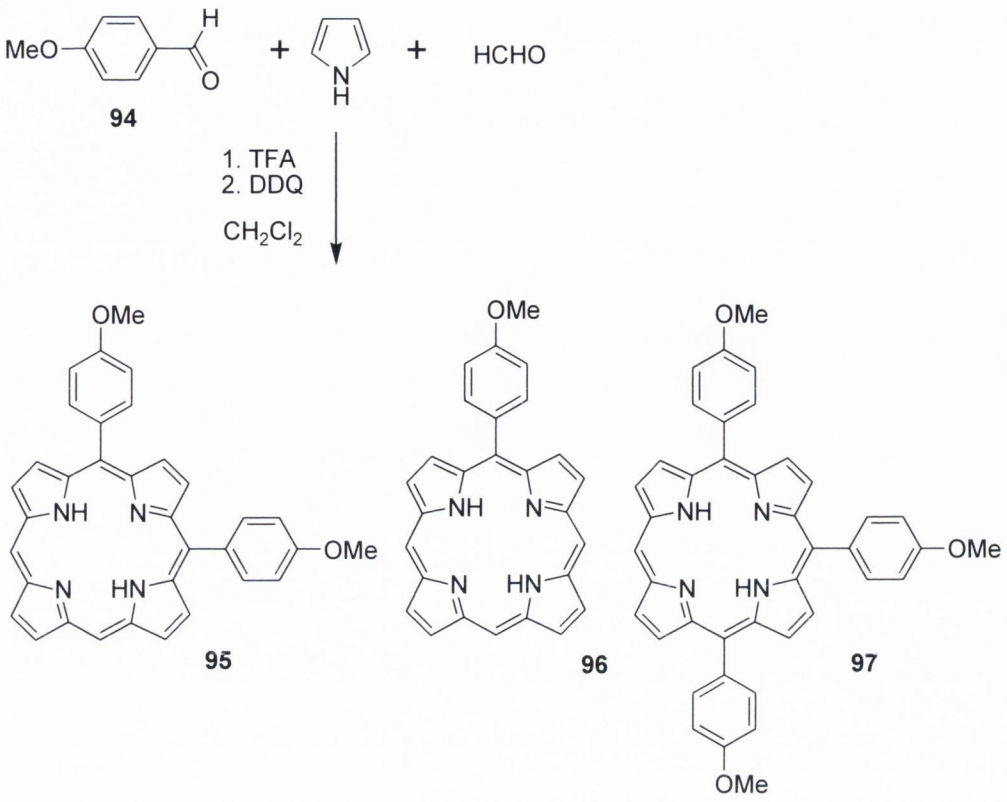
Therien *et al.* showed that treatment of a chloroform solution of 5,15-diphenylporphyrin with NBS at 0 °C resulted in the introduction of bromide at the free meso positions.[185] This procedure was successfully applied to the 5,10-$A_2$ precursor **48** to obtain the product **80** in good yield (78%). The same reaction carried out at room temperature also gave the desired product in a similar yield (83%).

Metallation of free base bromoporphyrin **80** with different metal carriers: $InCl_3$, $Pd(acac)_2$, $Zn(acac)_2$, $Pb(acac)_2$, $SnCl_2$, and $PtCl_2$ according to reported procedures[174, 186-189] gave brominated metal complexes **81-86** in good yields. As far as metallation with metal acetylacetonates is concerned, reaction of **80** with $Pd(acac)_2$ (1.1 eq.) or $Zn(acac)_2$ (5 eq.) in refluxing toluene gave metal complexes **82** and **83**, after 5 h and 2 h respectively; with regards to $Pb(acac)_2$ (16 eq.) the complete metallation of the starting material **80** to give complex **84** was achieved after 30 min at room temperature. Note, that the use of $Pt(acac)_2$ (heated under reflux in toluene) to metallate free base bromoporphyrin **80** did not yield the desired product **86**. **86** was obtained in harsher reaction conditions, *i.e.* upon stirring **80** with $PtCl_2$ (3 eq.) in benzonitrile at 170 °C for 12 h. Metal chlorides were also successfully used to obtain In(III) and Sn(IV) complexes **80** and **85**, after after 24 h reaction of **80** with $InCl_3$ and sodium acetate in refluxing glacial acetic acid, and after 1.5 h reaction of **80** with $SnCl_2$ in refluxing DMF. It should be mentioned that the reaction with $SnCl_2$ was performed in an ambient atmosphere. Such conditions trigger the oxidation of Sn(II) to Sn(IV). It has to be noted that Sn(II) is an uncommon oxidation state in porphyrin complexes.[177] The alternative procedure with $Zn(OAc)_2$ as the metal carrier was used to obtain **83** as well, yet this resulted in a lower yield (70% compared to 98% for $Zn(acac)_2$).

Free base and metallated porphyrins **80** and **81-83** subjected to Sonogashira coupling with TMS-acetylene provided compounds **87** and **89-91**. Similar coupling reactions of **80** with TIPS-acetylene yielded compound **88**. Depending on the central metal, yields varied from 16% to 85%. The lowest yield was obtained for the indium complex **89**. For this compound total consumption of the starting material did not occur during 24 h contrary to other compounds for which the starting material was consumed within 12 h. The Sonogashira reaction was also carried out using lead starting material **84**. The sample taken from this reaction, initially green, changed to purple when it was developed on silica or aluminum oxide TLC plate. Also, the retention factors of the compounds on a TLC plate corresponded to those of free base compounds **80** and **87**. The presence of the latter two compounds was not identified in the reaction sample by UV-vis absorption. These observations suggested that demetallation of the starting material **84** and of the desired

product **92** occurred on silica and aluminum oxide. Pb(II) porphyrin complexes have indeed been reported as very unstable complexes.[190] Similarly to the In(III) complex **81**, Sonogashira coupling of Pb(II) bromoporphyrin **84** with TMS-acetylene, did not proceed to total conversion to the complex **84** over 24 h. Purification by column chromatography gave the free base compound **87** in the amount which when recalculated gave 24% yield for the conversion of lead starting material **84** into TMS-ethynyl substituted lead complex **92**. Complex **92** was then obtained by direct metallation of free base **87** with $Pb(acac)_2$ (in the same way as it was achieved for bromoporphyrin **84**). A similar approach was used to obtain tin complex **93**, *i.e.* free base **87** was subjected to metallation with $SnCl_2$ (similar to bromoporphyrin **85**). The platinum complex with TMS-ethynyl substituents could not be obtained following either of the routes presented above. Increasing the temperature to 60 °C and changing the solvent to DMF in the Sonogashira coupling reaction, did not afford the desired platinum complex, whereas reaction of **87** with $Pt(acac)_2$ or $PtCl_2$ led to decomposition of the starting material.

Finally, the mixed condensation reaction (Scheme 5) was explored in order to obtain 5,10-di(*p*-methoxyphenyl)porphyrin **95**. The following ratio of starting materials was used: paraformaldehyde : pyrrole: *p*-anisaldehyde (**94**) 1.5: 3 :1. Apart from the desired product **95** (1.9%), two byproducts were obtained: mono- and tri-substituted porphyrins **96** (1.1%) and **97** (2.8%) respectively. Theoretically six different products can be formed in mixed condensation conditions when two aldehydes A-CHO and B-CHO are used: $A_4$, $A_3B$, 5,10-$A_2B_2$, 5,15-$A_2B_2$, $AB_3$, and $B_4$. In reality, however, the reactivity of aldehydes governs the formation and the yield of the porphyrins in the specific substitution pattern.[191]




**Scheme 5** Mixed condensation reaction.

### 3.5.2 Identification of axial ligands with MS

Mass spectrometry (MS) enabled identification of the chloride axial ligands in Sn(IV) and In(III) complexes (Figure 30). Peaks, which were in agreement with the calculated isotopic patterns[192] could be seen in the region corresponding to molecular ion [M] and [M-Cl] for InCl_Br and to [M] for InCl_CCTMS. With regard to Sn(IV) complexes, similar peaks corresponding to [M] and [M-Cl] could also be detected for both compounds $SnCl_2$_Br and $SnCl_2$_CCTMS. However, only low abundant [M] were observed. This is in agreement with previous reports. Typically, molecular ions are not detected for Sn(IV) complexes and peaks corresponding to molecular ion diminished by one axial ligand are most abundant in the MS spectra for these complexes.[193, 194] It should be noted, that [M-2Cl] could be seen in the spectrum of $SnCl_2$_Br, yet it was not detected for $SnCl_2$_CCTMS. Peaks at mass to charge ratio m/z ~817 in the MS spectrum of $SnCl_2$_CCTMS could indicate the contamination with hydroxo complexes (SnOHCl_CCTMS or $Sn(OH)_2$_CCTMS).

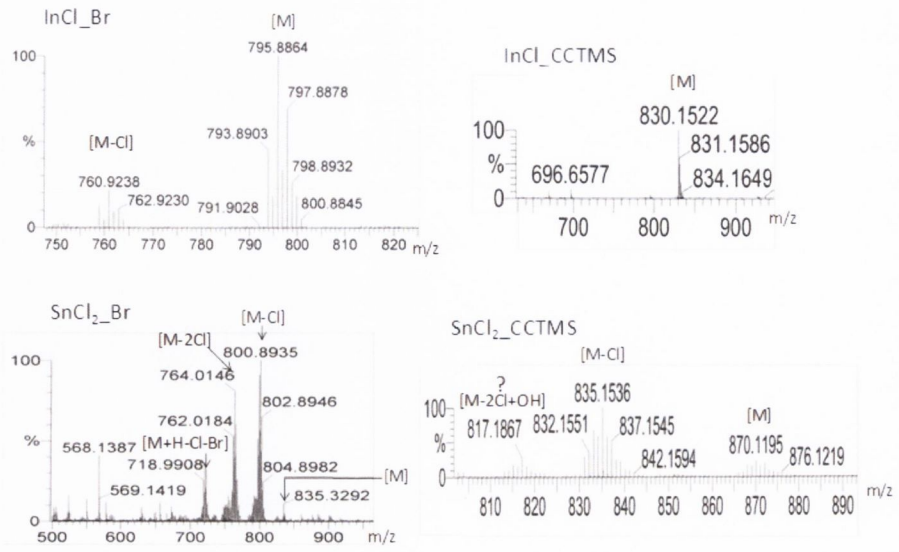



**Figure 30** Identification of axial ligands with MS for InCl_Br, InCl_CCTMS, $SnCl_2$_Br and $SnCl_2$_CCTMS.

## 3.5.3 $^1$H NMR studies

$^1$H NMR signals of a porphyrin depend on the distance and orientation of the protons with respect to the π-electron of the porphyrin ring system.[195] Protons that are above or inside the ring (the protons on the inner nitrogen atoms N-protons) are shielded from the external magnetic field and so their signals are shifted to higher field. Protons that are outside the ring (β- and meso-protons) are deshielded and thus their signals are shifted to lower field.

The symmetry of a porphyrin can be identified based on the pattern of the $^1$H NMR β-proton signals. 5,10-$A_2$ and 5,10-$A_2B_2$ porphyrins have a $C_2$ symmetry, where the $C_2$ axis is diagonally bisecting the opposing pyrrole units (Figure 31).[159] Thus the characteristic β-proton signal pattern shows two doublets and two singlets. Non-equivalent β-protons of a given pyrrole unit (H2/H3 and H12/H13) give doublets while equivalent ones (H7/H8 and H17/H18) give singlets.

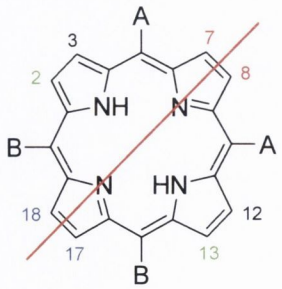



**Figure 31** Symmetry of a 5,10-$A_2B_2$ porphyrin with indicated equivalent β-protons (same color).

The characteristic $^1$H NMR β-proton signals pattern for 5,10-$A_2$ and 5,10-$A_2B_2$ porphyrin (2H_H, 2H_Br and 2H_CCTMS) is shown in Figure 32 (upper panel). The chemical shifts for β-proton signals do not vary significantly between 2H_Br and 2H_CCTMS. As far as 2H_H is concerned, both singlets and both doublets are situated closer to each other than for the other compounds. The singlet in the low field (> 10 ppm) in the spectra of 2H_H corresponds to the two meso-protons.

Introduction of bromide atoms at the two meso position in 2H_H to form 2H_Br resulted in the downfield shift of inner N-protons signals from -3.32 ppm to -2.77 ppm (Figure 32 lower panel). The signal was shifted even further into the low field region (-2.11 ppm) upon introduction of the TMS-ethynyl groups (2H_CCTMS). This finding agrees with previous reports which showed that the N-protons signals undergo low-field shifts with increasing number of meso substituents.[196]

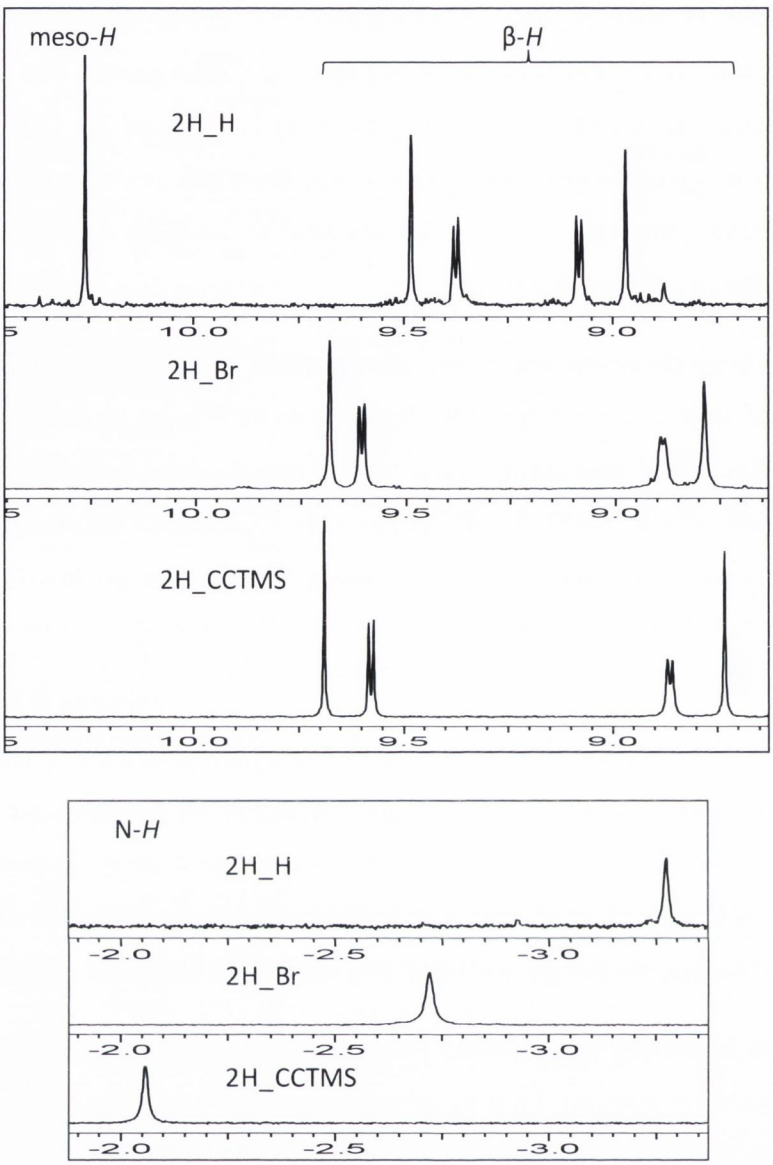



**Figure 32** $^{1}$H NMR signals of 2H_H, 2H_Br and 2H_CCTMS: β-protons and meso-protons (upper) and N-protons (lower) in $CDCl_3$.

The central metal has an effect on the $^{1}$H NMR of the two series of compounds (brominated and TMS-ethynyl substituted, Figure 33 and Figure 34). In comparison to free base compounds, metal complexes show no high field signals for N-protons. The low field spectra of Pd(II) and Zn(II) complexes of the two series of compounds were very similar to those of the respective free base compounds (2H_Br and 2H_CCMTS). The β-protons signals of other metal complexes of the two series of compounds were observed to shift downfield compared to the signals of the respective free base compounds. Consistently in both series of compounds, the chemical shifts increased in the following order with regard to the central metal: Pb(II) < In(III) < Sn(IV). Contrary to Zn(II) and Pd(II) complexes, the

signals of the aromatic protons of the tolyl group were affected by the central metal for Pb(II), Sn(IV) and In(III) complexes compared to similar signals of the free base compounds. Consistently for both Sn(IV) complexes, the respective signals were shifted downfield. For In(III) complexes, four doublets instead of just two doublets which were observed for other compounds appeared. For Pb(II) complexes, only broad signals could be observed in the respective spectral region. A similar effect was reported before for Pb(II) complexes with aryl meso groups. A lead atom can be situated off centre from the mean plane of the porphyrin ring and thus the meso aryl ring can be sufficiently crowded to make rotation slow on the NMR time scale.[189]

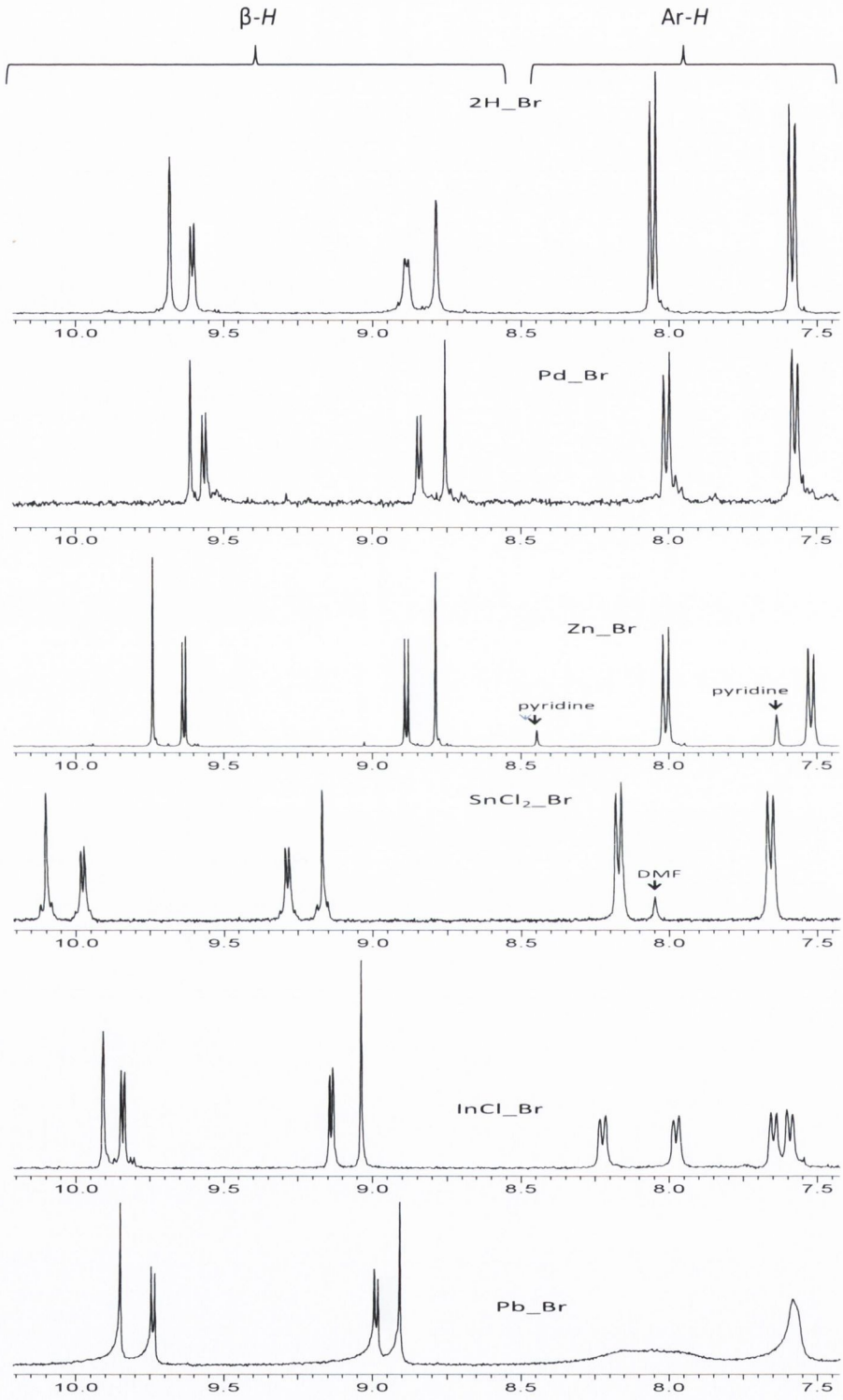



**Figure 33** Comparison of the lower field region of $^{1}$H NMR spectra for brominated porphyrins in $CDCl_3$.

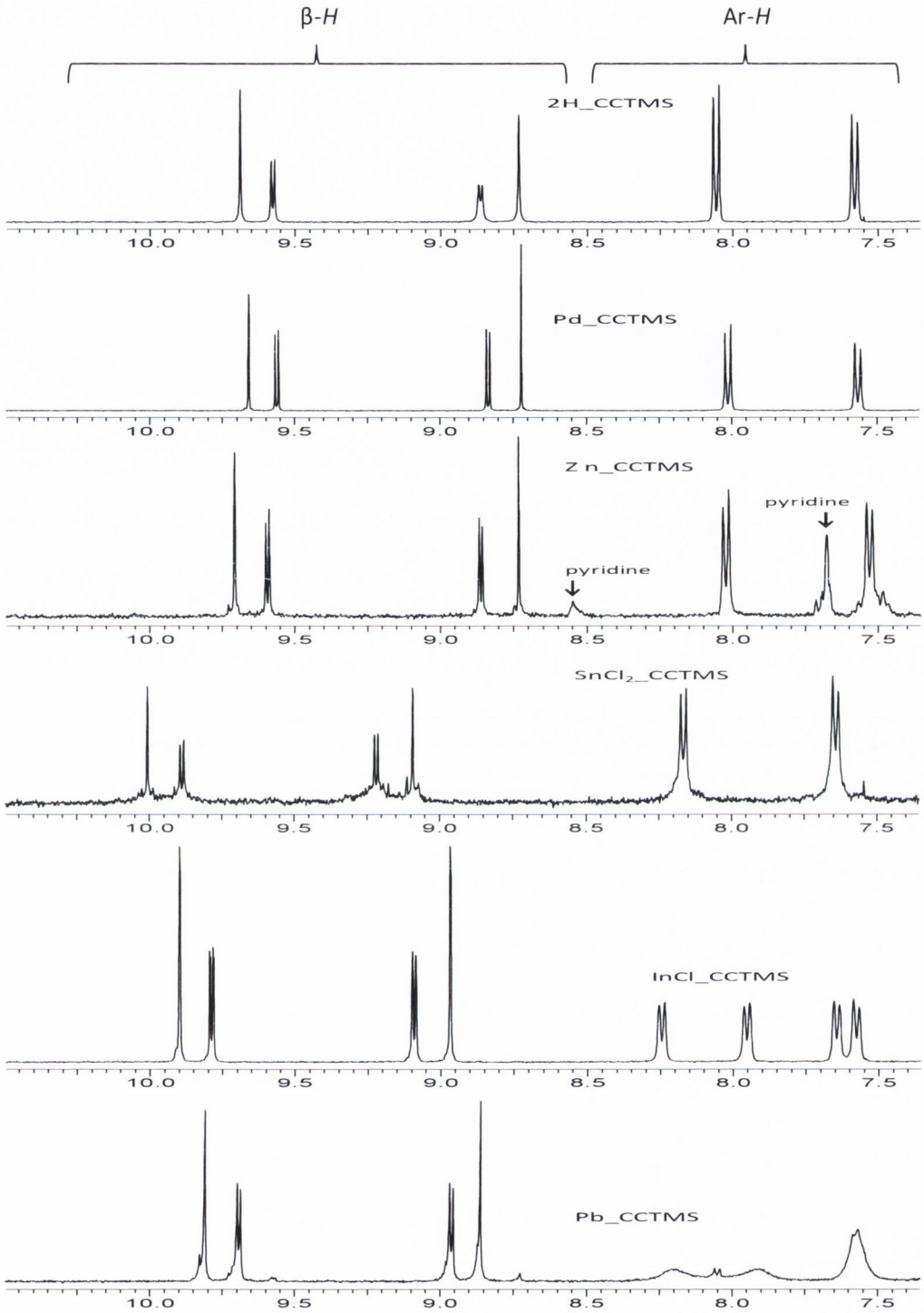



**Figure 34** Comparison of the lower field region of the $^{1}H$ NMR spectra of TMS-ethynyl substituted porphyrins in $CDCl_3$.

### 3.5.4 Aggregation of metalloporphyrins

The $^{1}H$ NMR spectra of Pd_Br and Pt_Br in $CDCl_3$ were sensitive to concentration (Figure 35). This was attributed to π-π aggregation which is a well known phenomenon for metalloporphyrins.[197, 198] $^{1}H$ NMR studies on metalloporphyrins reported in literature

demonstrated that the strength of aggregation is dependent on the interaction of the metal ion with the porphyrin π-system. The aggregation was enhanced by the presence of electron-withdrawing substituents on the porphyrin periphery.

Changes in the β-protons signals for Pd_Br were observed upon dilution and over time. More significant changes occurred for β-protons signals in the lower field region (> 9.4), whereas β-protons signals in the higher field region (< 9.0) were less affected. Changes observed for the β-proton signals in the lower field region are discussed below. The most concentrated sample ($C_0 = 2.6 \times 10^{-3}$ M) exhibited a doublet overlapping with a singlet which after 6 days changed to a broad signal at a similar chemical shift. A ten-fold diluted sample ($C_1 = 2.6 \times 10^{-4}$ M) exhibited a singlet and a doublet which appeared in the lower field region in comparison to the signal of the more concentrated sample. The doublet and singlet shifted into the higher field region over two days. The sample which was further diluted ten-fold ($C_2 = 2.6 \times 10^{-5}$ M) also exhibited a singlet and a doublet which were slightly shifted towards the lower field region in comparison to the respective signals of the more concentrated sample ($C_1 = 2.6 \times 10^{-4}$ M). No changes in the signals of the most diluted sample occurred up to four days.

The area of the peaks corresponding to lower field β-proton signals for Pd_Br, divided by molar concentration of the freshly prepared samples ($t_0$), were plotted against molar concentration (Figure 35 lower panel). Clearly the ratio decreased with concentration, which was associated with aggregation.

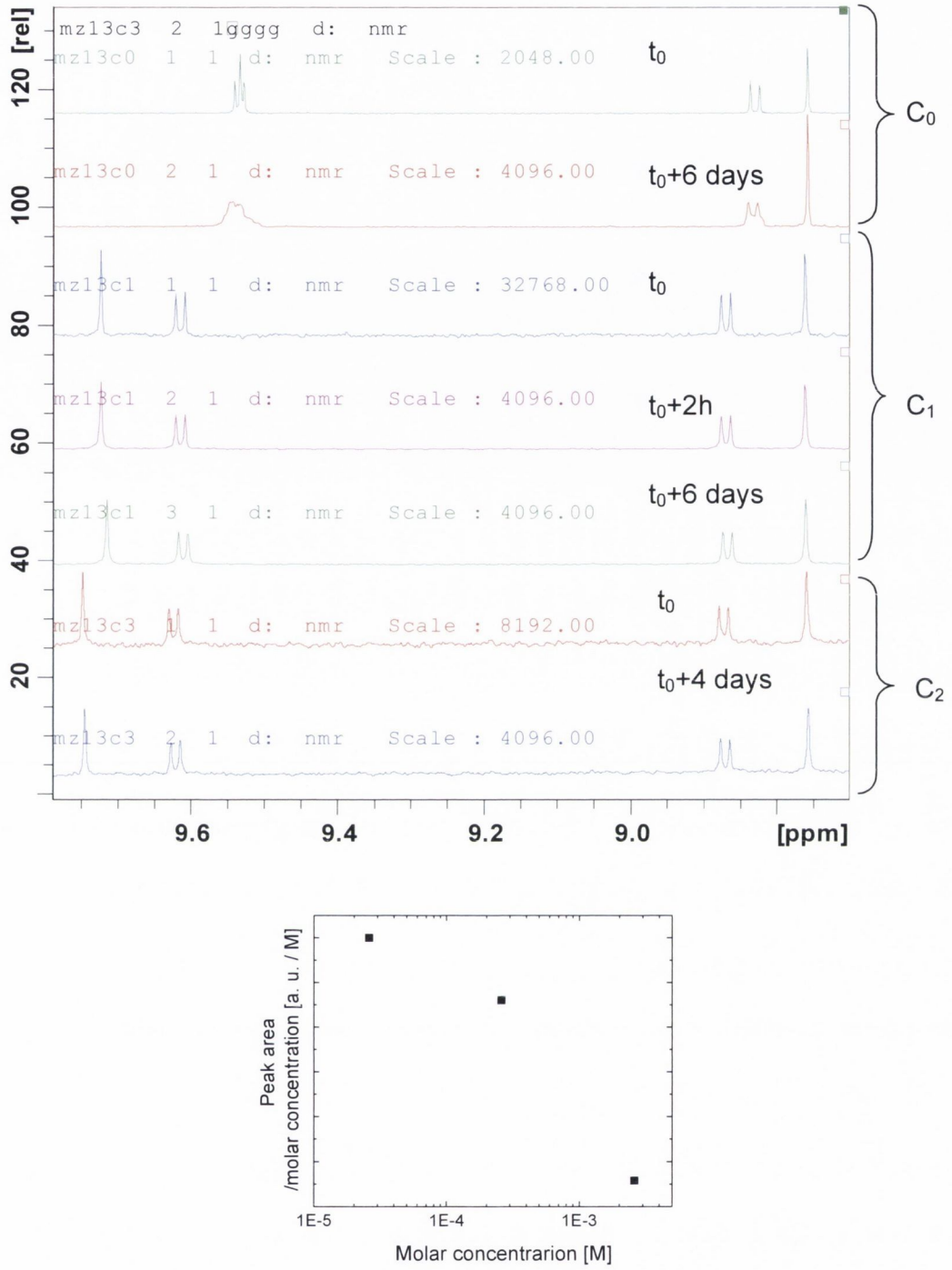



**Figure 35** Upper panel: low field region of $^1$H NMR spectrum showing changes in the β-proton signals of Pd_Br upon dilution and over time. $C_0 = 2.6 \times 10^{-3}$ M, $C_1 = 2.6 \times 10^{-4}$ M and $C_2 = 2.6 \times 10^{-5}$ M in $CDCl_3$. Lower panel: ratio of the area of the lower field β-proton signals and molar concentration plotter *versus* molar concentration for freshly prepared samples ($t_0$).

Changes in the lower field β-protons signals were also observed for Pt_Br (Figure 36). Consistent with the studies on Pd_Br, the signals for Pt_Br shifted downfield upon dilution. It can be seen from Figure 36 that the mutual position of the doublet and the singlet changes upon dilution from the lower field doublet and the higher field singlet to

the singlet overlapping with the doublet, and finally to the lower field singlet and the higher field doublet.

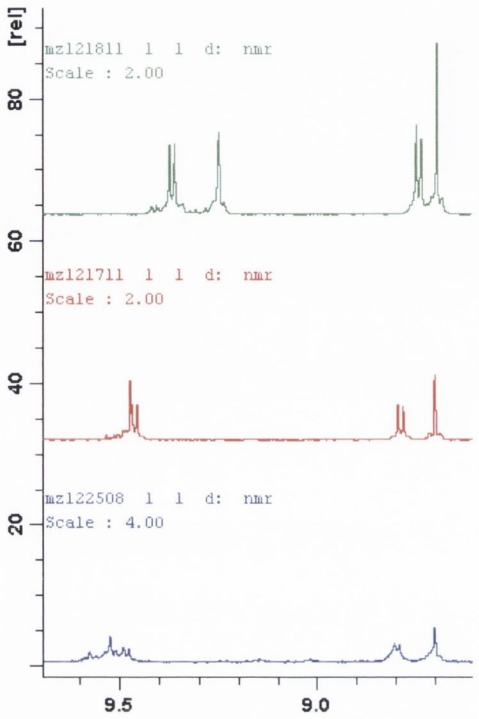



**Figure 36** Low field region of $^{1}$H NMR spectrum showing changes in β-protons signals of Pt_Br upon dilution (upper to lower spectrum) in $CDCl_3$.

The aggregation properties of Pd_Br were studied further with UV-vis absorption spectroscopy. Porphyrins exhibit two characteristic bands in their UV-vis spectra: an intense Soret band (around 400 nm) and less intense Q-bands (500-650 nm). Aggregation can induce changes to the positions of the absorbances and their intensities.[199-201] Broadening of absorbances is also indicative of aggregation. The UV-vis absorption spectra of Pd_Br were recorded in the $10^{-3}$ - $10^{-6}$ M concentration range in chloroform, DMF and toluene (Figure 37). No changes in the extinction coefficient, ε, of the Q-band with concentration were observed in toluene. However, such changes was observed in DMF (up to $2.5 \times 10^{-4}$ M) and in chloroform (up to $2.5 \times 10^{-5}$ M) which indicated that aggregation occurred in these solvents.

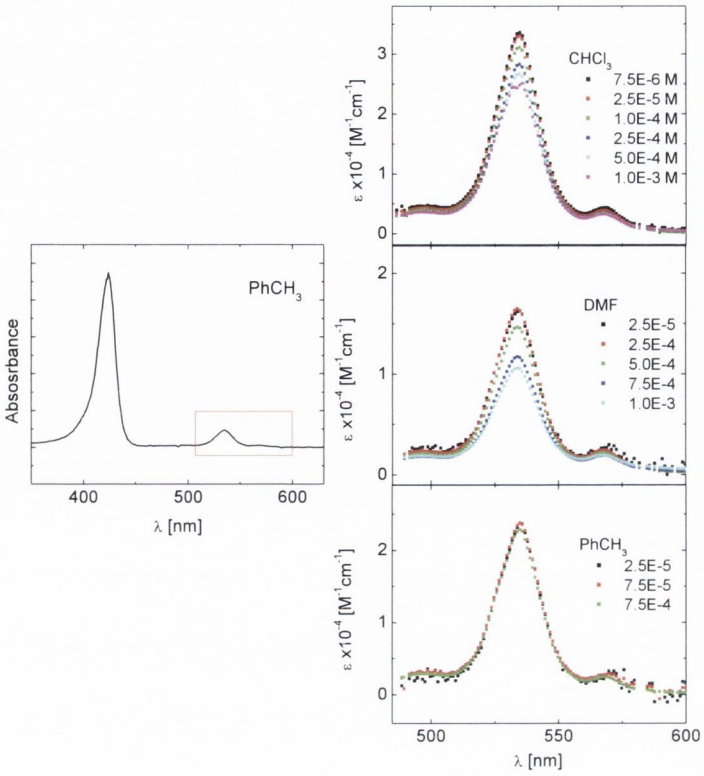



**Figure 37** UV-vis absorption spectrum of Pd_Br in toluene (left); Q-band spectra range (molar extinction coefficient ε *versus* wavelength λ) of Pd_Br at different concentrations in chloroform, DMF and toluene (right, upper to lower graph).

## 3.6 Summary

Two series of novel, free base and metallated 5,10-$A_2B_2$ porphyrins, both bearing tolyl as substituent A and bromide or TMS-ethynyl as the other meso group, were synthesized following standard procedures reported in literature. The starting material: 5,10-di-(*p*-tolyl)porphyrin was subjected to bromination with NBS, and to further metallation with different metal carriers, to yield a brominated series of metalloporphyrins in good yields. Bromoporphyrins were then coupled with TMS-acetylene in a Sonogashira coupling reaction to obtain the other series of compounds. Alternatively, metallation of TMS-ethynyl substituted free base was applied to obtain some metal complexes of the TMS-ethynyl series.

The $^1$H NMR signals of β- and aromatic protons of the tolyl group were affected by Sn(IV), In(III) and Pb(II) for the two series of compounds in similar way. Free base porphyrins, and both Zn(II) and Pd(II) complexes showed very similar $^1$H NMR signals for β- and aromatic protons of the tolyl group.

Chloroform was found to be an aggregating solvent for Pd(II) and Pt(II) bromoporphyrins. Changes in $^{1}H$ NMR were observed for these compounds upon dilution and over time. Further studies on the aggregating properties of the palladium complex with UV-vis technique showed that this compound also forms aggregates in DMF.

# Chapter 4 Modeling of the nonlinear absorption of 5,10-$A_2B_2$ porphyrins

## 4.1 Introduction and outline

The NLA properties of free base and metallated 5,10-$A_2B_2$ porphyrins, the synthesis of which was presented in the previous chapter, were studied with the open Z-scan technique at 532 nm in the ns regime over a broad range of input fluence. The NLA responses were found to be dependent on structural features and solvent. In most cases the character of the response differed from that typically observed for other porphyrins under similar experimental conditions (*i.e.* RSA), suggesting unique photophysical properties. A series of models was considered in order to understand the NLA responses. Although the character of the responses varied between compounds and solvents it was found that one model best fits all of the recorded responses. Thus, a four-level model with simultaneous two-photon absorption arising from the higher excited state is proposed (1+1+2 photon absorption). Modeling studies that were performed on a few chosen compounds are presented in this chapter.

## 4.2 Theoretical background

Typically a five-level Jablonski model (Figure 2, p. 8),[26] is used to explain the behavior of a material under illumination with light which was broadly discussed in the introduction. Often the five-level model can be simplified when fitting NLA responses. Once subnanosecond pulses are used, ISC from $S_1$ to $T_1$ can often be neglected since the lifetime of this transition is typically on the order of ns in organic dyes. Under ns pulses, provided that ISC is fast and efficient, absorption arising from $S_1$ is often ignored. Usually

populations of higher excited states can be neglected since their lifetimes are very short (~ps or less).[27]

However, especially at higher input intensities, the model often needs to be modified further in order to be able to reproduce the recorded responses. A contribution of higher excited states or multiphoton absorptive processes, which in general necessitates higher inputs to evolve, might change the character of NLA inducing switches from a transmission drop to an increase or *vice versa* (RSA to SA or SA to RSA respectively). Different models were proposed in literature to explain switches in NLA behavior. RSA switching to SA was observed for different materials in the ps regime.* Si *et al.* demonstrated by means of a six-level model (ground, three singlet and two triplet states) that in the ps regime the main contribution to the NLA response in texaphyrin comes from singlet states and that RSA converts to SA when the accumulation of population in the second excited state depletes the number of molecules contributing to the absorption processes.[202] Swatton *et al.* reported a RSA/SA switch in the ps regime for 1,1',3,3,3',3'-hexamethylindotricarbocyanine iodide and explained it in terms of a four singlet manifold where the absorption cross-section of the highest excited state was lower than that of the lower lying excited state.[203] Przhonska *et al.* suggested that the RSA/SA switch arises in polymethine dyes in the ps regime due to a fast reabsorption process from $S_1$ to $S_2$ (three-level model composed of singlet states) or due to photoinduced transformation of the polymethine molecule into some new configuration or species that is non-absorbent at the experimental wavelength.[204] Theoretical studies carried out by Deng *et al.* demonstrated that a RSA/SA switch will occur when the cross-section of the higher excited state is lower than that of the lower excited state (four-level manifold), but only when a certain value of input fluence is surpassed.[205] An RSA/SA switch at high fluence due to weak ESA arising from the higher excited states was observed in the ps regime in azorene-appended phosphorus(V) tetratolylporphyrins.[113] The Senge research group has previously reported a RSA/SA switch for 5,10-$A_2B_2$ porphyrins in the ns regime but could not fully explain the mechanism of the recorded behaviour.[122] It should be pointed out that such a behavior is uncommon for ns pulses. The opposite behavior, *i.e.* a SA response switching to RSA, has been observed both in the ns and ps regime for different materials. The weak transmission drop within SA observed in [5,10,15,20-tetra(*p*-methoxyphenyl)tetrabenzo-porphyrinato]zinc(II) in the ns regime was attributed to the absorptive processes arising from triplet state $T_1$, which brought the population of that state to the higher excited states,

* RSA is understood here as transmission drop.

while SA was associated with saturation of the $T_1$ state.[206] A similar model was found to be insufficient to explain the SA/RSA switch in the ns regime in subphthalocyanines, where RSA was attributed to absorptive processes arising from even higher excited triplet states (five-level model: ground, singlet and three triplet excited states).[207] The SA/RSA behavior detected in linear polymers in the ns regime was explained by means of a four-level manifold and attributed to the fact that the absorption cross-section of the first excited state is smaller than that of the ground state and that of the second excited state.[151] In red dyes under ns pulses a transmission drop within the SA peak was attributable to TPA.[208] In ruthenium and osmium complexes of modified terpyridines the transmission drop within the SA peak arose from TPA of the solvent in the ps time regime. In the same study osmium complexes also showed SA/RSA in the ns regime and this was associated with absorptive processes arising from metal to ligand CT states.[209] The SA/RSA behavior detected in Rhodamine B at the edge of the absorption band in the ps regime was attributed to TPA and was associated with aggregation.[210] A RSA/SA/RSA switch was observed for an 'axial-bonding' type hybrid porphyrin by Kiran *et al.* in the ps regime. This complex behavior was due to saturation of the ESA followed by TPA.[115]

It can be concluded that switches in the NLA response with input intensity involves complex photophysics. Likewise, simple models are often insufficient to explain responses which do not exhibit any switches, especially when higher input intensities are applied. McKerns introduced a seven-level model (ground, three singlet and three triplet states) in order to explain the NLA behavior of an expanded porphyrin cadmium complex, which exhibited a transmission drop with intensity.[211] Dini *et al.* proposed a model with TPA arising from the higher excited triplet state $T_2$ and another model with TPA arising from the $S_1$ state in order to explain a similar behavior in hemiporphyrazine derivatives.[212] O'Flaherty *et al.* observed that the nonlinear absorption coefficient decreases with intensity for phthalocyanines suggesting a contribution of higher than third order absorptive processes to the overall NLA measured.[111] A similar deviation in the nonlinear absorption coefficient for phthalocyanines was also reported by Venkatram *et al.*[213]

The distinct pattern, *i.e.* RSA/SA switch in the ns regime observed before for meso substituted 5,10-$A_2B_2$ porphyrins, prompted us to investigate this class of compounds in more detail. Note, that related compounds with similar substituents though in a 5,15-$A_2B_2$ substitution pattern did not reveal any switch to SA at higher inputs.[122] Likewise, no RSA/SA switch was reported for broadly studied 5,10,15,20-tetrasubstituted porphyrin compounds which can be found in the literature.[21, 43] This clearly demonstrates that 5,10-

$A_2B_2$ compounds exhibit distinct photophysical properties. Interestingly, the present studies on 5,10-$A_2B_2$ compounds provide further details on noteworthy NLA behavior. The character of these responses was found to depend on structural features and the solvent used. Different models were considered in order to explain the observed phenomena and, as outlined below, the most successful model for all response types involved a four-level manifold where one-photon ESA was followed by instantaneous TPA arising from higher excited states. This suggests that despite varied structural features and conditions all 5,10-$A_2B_2$ compounds studied have similar excited state structures.

## 4.3 Experimental details

NLA of 5,10-$A_2B_2$ porphyrins (Pd_Br, Zn_Br, Zn_CCTMS and 2H_CCTMS) were measured with open Z-scan following the procedure introduced in 2.2.2. Samples were prepared by dissolving the porphyrin in spectroscopic grade toluene or DMF at a concentration of $2.5 \times 10^{-4}$ M, followed by gentle agitation for about 1 hour in a low power sonic bath. Additionally for compound Pd_Br, studies were performed using more dilute samples, at a concentration of $2.5 \times 10^{-5}$ M. Samples were freshly prepared prior to experiments. All measurements were performed in a quartz cell with a 1 mm path length.

## 4.4 Results

### 4.4.1 Ground state absorption features

The ground state absorption spectra of porphyrins exhibit two characteristic features – a high energy Soret and low energy Q bands (Figure 38). The Soret band maxima of the two compounds 2H_CCTMS and Zn_CCTMS with TMS-ethynyl groups are red-shifted in reference to brominated compounds Zn_Br and Pd_Br, which is expected for compounds with an extended conjugated system. The Q-bands were observed in similar wavelength ranges for all compounds and the experimental wavelength of 532 nm is situated in their close proximity. An exception is compound Pd_Br, for which a Q-band maximum is equal to 532 nm. The number of Q-bands of the metallated porphyrins Zn_Br, Pd_Br and Zn_CCTMS is reduced to two in reference to free-base compound 2H_CCTMS with four Q-bands. Reduction in the number of Q-bands is commonly observed upon metallation due to an increase in the symmetry of the porphyrin core.[70]

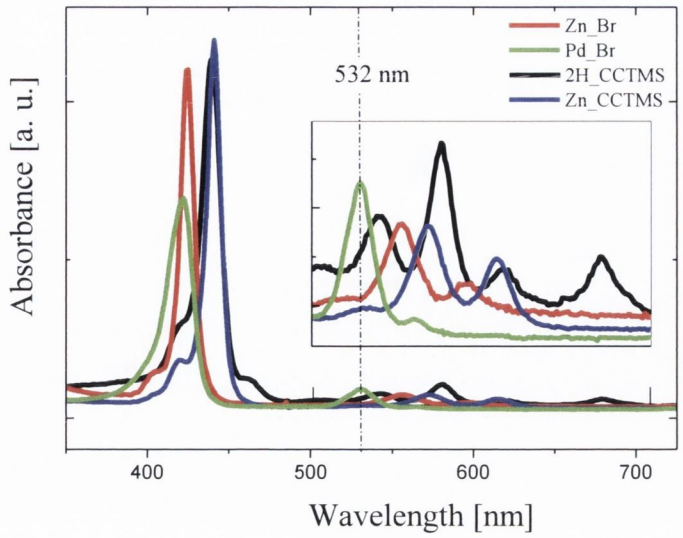



**Figure 38** Ground state absorption spectra of Zn_Br, Pd_Br, 2H_CCTMS and Zn_CCTMS in $CH_2Cl_2$. Inset shows the Q-band area.

### 4.4.2 Nonlinear absorption responses

We first carried out open Z-scan studies on Zn_Br, Pd_Br, 2H_CCTMS and Zn_CCTMS in toluene (Figure 39 upper row). An interesting NLA was observed for 2H_CCTMS, for which at higher input laser energy experiments two distinctive parts became apparent in the Z-scan trace. A steep drop in transmission could be seen in close focal area, whereas further away from the focus the transmission drop was gentler. This type of behavior is referred to as an RSA/RSA switch. Zn_Br provided a response profile similar to 2H_CCTMS, however, with a much smoother transition between the two parts. The character of the Z-scan response recorded for Zn_CCTMS was much broader compared to the previous compounds, with no distinctive parts in Z-scan trace. Pd_Br with high linear absorption at the experimental wavelength exhibited an increase in transmission followed by a decrease closer to the focal regime, which switched again to an increase even closer to the focal regime. This response is referred to as a SA/RSA/SA switch. However, symmetric reproducible responses for this compound could only be obtained at very low input energies. Once the input energy was increased the Z-scan response became asymmetric, indicating a degenerative process. High linear absorption, as exhibited by this compound, should enhance such processes. Clearly, none of the responses observed in toluene exhibited the characteristic RSA/SA switch which was previously observed for 5,10-$A_2B_2$ compounds in DMF. As the solvent is known to affect the NLA properties of RSA materials further studies were carried out in DMF.[31, 32] DMF was a poor solvent for compounds Pd_Br and 2H_CCTMS in comparison with toluene, whereas for compounds

Zn_Br and Zn_CCTMS it provided good solubility. It is known that DMF coordinates to zinc ions. Since both compounds Zn_Br and Zn_CCTMS bear zinc in the central core, their good solubility in DMF can be associated with the coordination of the solvent molecules to the metal in the central core. Much higher input energies could be applied in Z-scan experiments in DMF than in toluene. Good quality, symmetric and reproducible data were obtained in DMF at high input energies. In contrast, at similar inputs some asymmetric features in the Z-scan trace especially in the focal regime were observed in toluene, implying a degenerative process. The evolutions of the responses recorded in DMF for all porphyrins studied are presented in Figure 39 (lower row). Clearly, the solvent affected the character of the response. The RSA/RSA character of 2H_CCTMS in toluene changed to RSA/weak SA/RSA/SA. For Zn_Br and Zn_CCTMS a switching from RSA to SA in the focal regime in the experiments carried out at higher input energies was observed. A SA/RSA/SA type response was detected for Pd_Br in DMF, as it was in toluene. However, the SA/RSA/SA Z-scan trace profile became apparent only in experiments at higher input energies in DMF, which were inaccessible for toluene. At lower inputs only SA was detected in DMF which evolved to SA/RSA when the input was increased and finally to SA/RSA/SA at even higher inputs.

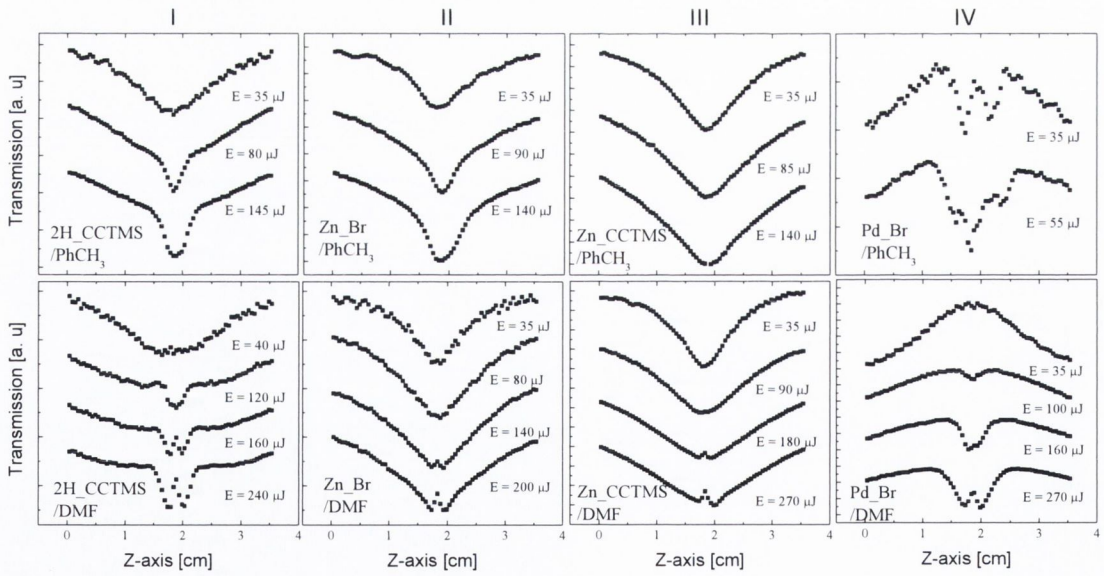



**Figure 39** Each box illustrates the evolution of the Z-scan response for the following experiments carried out at increasing input energy for a given compound. Each column shows results for one compound: column I - 2H_CCTMS, column II - Zn_Br, column III - Zn_CCTMS and column IV - Pd_Br. Upper row shows experiments carried out in toluene, lower row - in DMF.

### 4.4.3 Modeling of nonlinear absorption responses

RSA arises in porphyrins in the spectral window between the Soret and Q-bands.[117] The transmission drop with intensity observed for Zn_Br, 2H_CCTMS and Zn_CCTMS was attributed to such a process. It should dominate at lower fluences before higher excited states become populated. The SA character of the response observed for Pd_Br indicated that the cross-section of the excited state was smaller than that of the ground state. In order to explain subsequent switches following RSA or SA behavior, additional processes have to be considered.

The following assumptions were made in modeling the NLA responses. We assumed that the triplet state $T_1$ is quickly and efficiently populated through ISC. Typically $\tau_{ISC}$ is on the order of ns or shorter for porphyrins and is shorter for compounds with heavy atoms in the central core or the molecular periphery (such as halogen atoms). Introduction of heavy metal atoms not only improves the ISC rate but also enhances the yield of triplet state formation.[28, 214] Therefore, the assumption that the triplet state $T_1$ is quickly and efficiently populated through ISC should be valid, especially for metallated and brominated compounds, under the ns pulsed laser used in the studies. Based on this assumption the contribution of the absorption arising from $S_1$ state to the measured response can be neglected under ns pulses. Instantaneous TPA arising from the ground state can be ignored at the experimental wavelength and under ns pulse duration. Concerning the latter statement, different approaches were described by various groups in the literature, which either consider or neglect the contribution of instantaneous TPA arising from the ground state at close to resonant wavelength range in the ns regime.[28, 206, 213] A steady-state approximation which assumes that the population of electronic states does not vary within the pulse width ($dN_i/dt = 0$) was applied. The steady-state approximation is valid when the pulse width is much longer than relaxation times. Different authors demonstrated that such an assumption approximated dynamic models well. Gao *et al.* proved that such an approximation is valid while modeling the SA/RSA type of behavior of a linear polymer in the ns regime with a four-level mode.[151] O'Flaherty *et al.* showed that a steady-state model approximated well the NLA response of phthalocyanines in the ns regime.[111] They also demonstrated that the five-level Jablonski model can be simplified with a three-level model provided that ISC is fast and efficient. According to the three-level model, NLA is entirely due to $T_1$-$T_2$ ESA transitions. Effectively, such a model is equivalent to model **A** presented in Figure 40, where the lifetime of state $N_1$ is actually the lifetime of state $S_1$ and the absorption arising from the state $N_1$ is attributed to $T_1$-$T_2$ transitions. We considered

different models by addition of subsequent higher excited states (Figure 40). The populations of the highest excited state were neglected for each of these models.

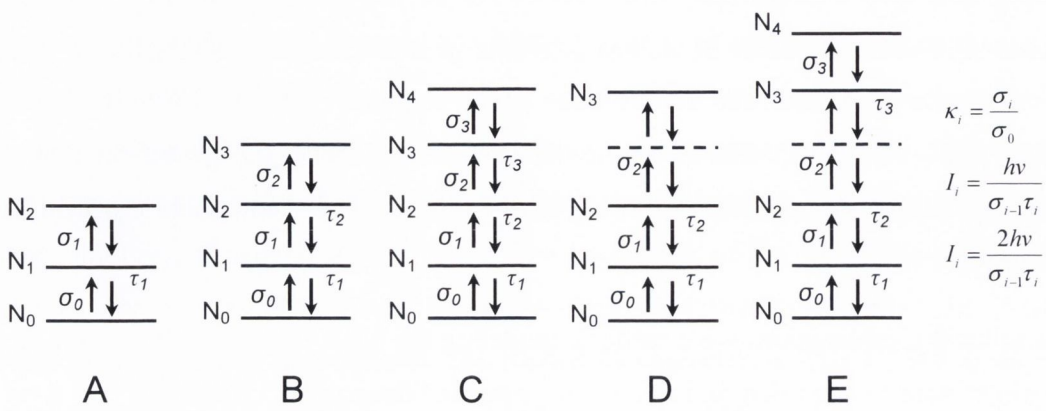



**Figure 40** Schematic illustration of different models A-E considered in modeling studies along with the definition of fitting parameters $\kappa_i$ and $I_i$. $N_i$ stands for the population densities corresponding to $i$-th electronic state $\sigma_i$ stands for the cross-sections of the ground (i = 0) and excited states (i ≥ 1), $\tau_i$ for the lifetime of $i$-th state. $\kappa_i$ is the ratio of the excited state absorption cross-section $\sigma_i$ to that of the ground state $\sigma_0$. $I_i$ is saturation intensities of one- or two-photon absorption processes.

Rate equations and the expression for the absorption coefficient as a function of input intensity $\alpha(I)$ obtained from analytical solutions of these equations are presented below for models **A-E**.

$N_T$ is the total population density and $\alpha_{gr}$ is the linear absorption coefficient. The latter two parameters are correlated according to:

$$\alpha_{gr} = N_T \sigma_0 \qquad \textbf{4-1}$$

The populations of the highest excited states are neglected in all models. The steady-state approximation is applied, *i.e.* $dN_i/dt = 0$.

Model **A**

$$\frac{dN_0}{dt} = -\frac{N_0 \sigma_0 I}{h\nu} + \frac{N_1}{\tau_1} \qquad \textbf{4-2}$$

$$\frac{dN_1}{dt} = \frac{N_0 \sigma_0 I}{h\nu} - \frac{N_1}{\tau_1} \qquad \textbf{4-3}$$

$$\frac{dI}{dz'} = -\sigma_0 N_0 I - \sigma_1 N_1 I \qquad \textbf{4-4}$$

$$N_T = N_0 + N_1 \qquad \textbf{4-5}$$

Defining:

$$I_1 = \frac{h\nu}{\sigma_0 \tau_1} \quad \textbf{4-6}$$

$$\kappa_1 = \frac{\sigma_1}{\sigma_0} \quad \textbf{4-7}$$

and after some formula rearrangements, the expression for $\alpha(I)$ takes the following form:

$$\alpha(I) = \alpha_{gr} \frac{1 + \kappa_1 \frac{I}{I_1}}{1 + \frac{I}{I_1}} \quad \textbf{4-8}$$

Model **B**[150, 151, 205]

Eq. **4-2**.

$$\frac{dN_1}{dt} = \frac{N_0 \sigma_0 I}{h\nu} - \frac{N_1}{\tau_1} - \frac{N_1 \sigma_1 I}{h\nu} + \frac{N_2}{\tau_2} \quad \textbf{4-9}$$

$$\frac{dN_2}{dt} = \frac{N_1 \sigma_1 I}{h\nu} - \frac{N_2}{\tau_2} \quad \textbf{4-10}$$

$$\frac{dI}{dz'} = -\sigma_0 N_0 I - \sigma_1 N_1 I - \sigma_2 N_2 I \quad \textbf{4-11}$$

$$N_T = N_0 + N_1 + N_2 \quad \textbf{4-12}$$

Defining:

$$I_2 = \frac{h\nu}{\sigma_1 \tau_2} \quad \textbf{4-13}$$

$$\kappa_2 = \frac{\sigma_2}{\sigma_0} \quad \textbf{4-14}$$

$I_1$ and $\kappa_1$ as defined before according to Eq. **4-6** and Eq. **4-7**, respectively. After some formula rearrangements, the expression for $\alpha(I)$ takes the following form:

$$\alpha(I) = \alpha_{gr} \frac{1 + \kappa_1 \frac{I}{I_1} + \kappa_2 \frac{I^2}{I_1 I_2}}{1 + \frac{I}{I_1} + \frac{I^2}{I_1 I_2}} \quad \textbf{4-15}$$

Model **C**

Eq. **4-2**, Eq. **4-9**.

$$\frac{dN_2}{dt} = \frac{N_1 \sigma_1 I}{h\nu} - \frac{N_2}{\tau_2} - \frac{N_2 \sigma_2 I}{h\nu} + \frac{N_3}{\tau_3} \quad \textbf{4-16}$$

$$\frac{dN_3}{dt} = \frac{N_2 \sigma_2 I}{h\nu} - \frac{N_3}{\tau_3} \quad \textbf{4-17}$$

$$\frac{dI}{dz'} = -\sigma_0 N_0 I - \sigma_1 N_1 I - \sigma_2 N_2 I - \sigma_3 N_3 I \quad \textbf{4-18}$$

$$N_T = N_0 + N_1 + N_2 + N_3 \quad \textbf{4-19}$$

Defining:

$$I_3 = \frac{h\nu}{\sigma_2 \tau_3} \quad \textbf{4-20}$$

$$\kappa_3 = \frac{\sigma_3}{\sigma_0} \quad \textbf{4-21}$$

$I_1$, $I_2$, $\kappa_1$ and $\kappa_2$ as defined before according to Eq. **4-6**, Eq. **4-13**, Eq. **4-7** and Eq. **4-14**, respectively. After some formula rearrangements, the expression for $\alpha(I)$ takes the following form:

$$\alpha(I) = \alpha_{gr} \frac{1 + \kappa_1 \frac{I}{I_1} + \kappa_2 \frac{I^2}{I_1 I_2} + \kappa_3 \frac{I^3}{I_1 I_2 I_3}}{1 + \frac{I}{I_1} + \frac{I^2}{I_1 I_2} + \frac{I^3}{I_1 I_2 I_3}} \quad \textbf{4-22}$$

Model **D**

Eq. **4-2**, Eq. **4-9**, Eq. **4-10** and Eq. **4-12**.

$$\frac{dI}{dz'} = -\sigma_0 N_0 I - \sigma_1 N_1 I - \sigma_2 N_2 I^2 \quad \textbf{4-23}$$

$I_1$, $I_2$, $\kappa_1$ and $\kappa_2$ as defined before according to Eq. **4-6**, Eq. **4-13**, Eq. **4-7** and Eq. **4-14**, respectively. After some formula rearrangements, the expression for $\alpha(I)$ takes the following form:

$$\alpha(I) = \alpha_{gr} \frac{1 + \kappa_1 \frac{I}{I_1} + \kappa_2 \frac{I^3}{I_1 I_2}}{1 + \frac{I}{I_1} + \frac{I^2}{I_1 I_2}} \quad \textbf{4-24}$$

Model **E**

Eq. **4-2**, Eq. **4-9** and Eq. **4-19**.

$$\frac{dN_2}{dt} = \frac{N_1 \sigma_1 I}{h\nu} - \frac{N_2}{\tau_2} - \frac{N_2 \sigma_2 I^2}{2h\nu} + \frac{N_3}{\tau_3} \quad \textbf{4-25}$$

$$\frac{dN_3}{dt} = \frac{N_2 \sigma_2 I^2}{2h\nu} - \frac{N_3}{\tau_3} \quad \textbf{4-26}$$

$$\frac{dI}{dz'} = -\sigma_0 N_0 I - \sigma_1 N_1 I - \sigma_2 N_2 I^2 - \sigma_3 N_3 I \quad \textbf{4-27}$$

Defining:

$$I_3 = \frac{2h\nu}{\sigma_2 \tau_3} \quad \textbf{4-28}$$

$$\kappa_3 = \frac{\sigma_3}{\sigma_0} \quad \textbf{4-29}$$

$I_1$, $I_2$, $\kappa_1$ and $\kappa_2$ as defined before according to Eq. **4-6**, Eq. **4-13**, Eq. **4-7** and Eq. **4-14**, respectively. After some formula rearrangements, the expression for $\alpha(I)$ takes the following form:

$$\alpha(I) = \alpha_{gr} \frac{1 + \kappa_1 \frac{I}{I_1} + \kappa_2 \frac{I^3}{I_1 I_2} + \kappa_3 \frac{I^4}{I_1 I_2 I_3}}{1 + \frac{I}{I_1} + \frac{I^2}{I_1 I_2} + \frac{I^4}{I_1 I_2 I_3}} \quad \textbf{4-30}$$

The expressions $\alpha(I)$ (Eq. **4-8**, Eq. **4-15**, Eq. **4-22**, Eq. **4-24**, Eq. **4-30**) were implemented to the propagation equation (Eq. **1-18**) used to fit the recorded responses using Mathematica software. For each position along the Z-axis the expressions were integrated over $z'$ from 0 to $L$, where $L$ is the sample thickness, and divided by input intensity recalculated according to[215]:

$$I(Z) = \frac{2E}{\pi^{\frac{3}{2}} \tau {\omega_0}^2 \left[1 + \left(\frac{Z}{Z_0}\right)^2\right]} \quad \textbf{4-31}$$

where $E$ stands for pulse energy and $\tau$ for pulse width. The beam radius $\omega_0$ = 18-24 μm. In order to obtain normalized transmission values, the integrated expressions were subsequently divided by a far field linear transmission, which was measured. Curve fits were carried out with free-floating parameters. The quality of the fit was evaluated by sight first. Then, to obtain a more precise fit, the parameters were adjusted further by means of minimizing the least square error.

First, attention was focused on the NLA response of 2H_CCTMS. As illustrated in Figure 41, model **A** provided good fitting only for the experiments recorded at low input energies. For experiments at higher input energies, where RSA/RSA switching became apparent, the fitting curve followed only the part of the curve furthest from the focus well. This suggests that the response arising at lower fluences would proceed through a sequential absorption of two photons. Model **B**, created by adding another higher excited state, could not reproduce the steep drop in transmission appearing in the focal area in higher input energy experiments. Moreover, fitting of the "less steep" part of the curve was less precise in comparison to the previous model (data not shown). This reinforced the assumption that

absorption in the lower fluence regime arises through sequential absorption of two photons. Interestingly, fitting based on the five-level model **C** was far more improved and could reproduce the characteristic RSA/RSA shape. Meanwhile, it was observed that the RSA/RSA switch is reproduced best when $\kappa_2 = 0$. Only for experiments at higher input energies did the response predicted by the model slightly diverge from the experimental data, *i.e.* reaching slightly lower transmission values than those actually recorded. $\kappa_2 = 0$ means that absorption arising from state $N_2$ is insignificant. This is the absorption arising from state $N_3$ which grants good fitting of the "steep" part of the curve in the close focal regime. The absorption arising from state $N_2$ and $N_3$ are associated with terms in the numerator of the expression for the absorption coefficient (Eq. **4-22**), depending upon second and third power of intensity respectively. Since the second power term is insignificant and the third power term grants good fitting of the response in the close focal regime, yet another model **D** with the expression for the absorption coefficient with no second but only third order term in the numerator was proposed (Eq. **4-24**). The population of the state $N_2$ is transferred into a higher level state in a one step TPA in model **D** instead of two sequential one-photon absorption processes as in model **C**. A similar model with TPA arising from the $T_2$ excited state was previously proposed for a hemiporphyrazine derivative.[212] Such a four-level model, model **D,** provided a similar fitting quality to that observed for model **C** with a slight divergence from the experimental data at higher input energies. This could suggest the saturation of higher excited states. The fitting at higher inputs was improved when the population of state $N_3$ was taken into account in the total population (model **E**). At the same time absorption arising from the $N_3$ state was set to 0 *i.e.* $\kappa_3 = 0$. In reference to theoretical studies on NLA switches cited before, it can be predicted that at even higher fluences, if those were accessible, switching to SA should be observed, since $\kappa_3 = 0 < 1$ and $\kappa_2 > 0$.[205]

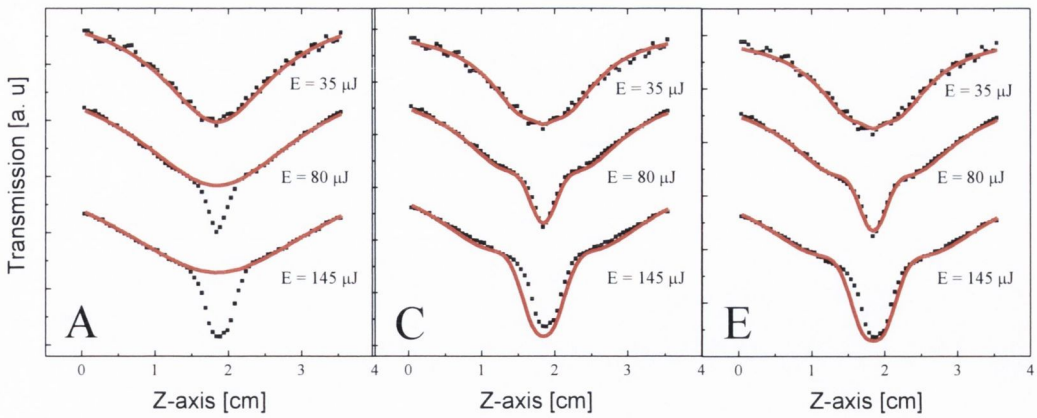



**Figure 41** Comparison of the fitting curves (red lines) obtained with models **A**, **C** and **E** for the experiments carried out at increasing input energy for compound 2H_CCTMS in toluene. The following set of parameters were used in the fittings: model **A**: $I_1$ = 0.14 GW cm$^{-2}$, $\kappa_1$ = 1.65; model **C**: $I_1$ = 0.13 GW cm$^{-2}$, $I_2$ = 0.4 GW cm$^{-2}$, $I_3$ = 1.7 GW cm$^{-2}$, $\kappa_1$ = 2.3, $\kappa_2$ = 0, $\kappa_3$ = 6.3; model **E**: $I_1$ = 0.45 GW cm$^{-2}$, $I_2$ = 0.1 GW cm$^{-2}$, $I_3$ = 2.05 GW$^2$ cm$^{-4}$, $\kappa_1$ = 4.4, $\kappa_2$ = 2.8 cm$^2$ GW$^{-1}$, $\kappa_3$ = 0. ■ represents experimental data.

Similar observations were made when modeling the response for compound Zn_Br. A five-level model with subsequent one-photon absorptive processes **C** could reproduce the response as well as a four-level model with a two-photon absorption process arising from the excited state **D**. The term with parameter $\kappa_2$ in the expression for the absorption coefficient Eq. **4-22** describing model **C** had much less effect on the fit quality than the remaining terms and could be neglected. Analogous to previous studies, both models **C** and **D** predicted a larger transmission drop than was actually observed in experiments carried out at higher input energies. This deviation was more pronounced for compound Zn_Br compared to 2H_CCTMS. The fitting was improved when the population of state $N_3$ (model **E**) was taken into account (Figure 42). Clearly, the population of state $N_3$ can not be neglected. Yet absorption arising from this state is negligible. The best fit was obtained when $\kappa_3 = 0$.

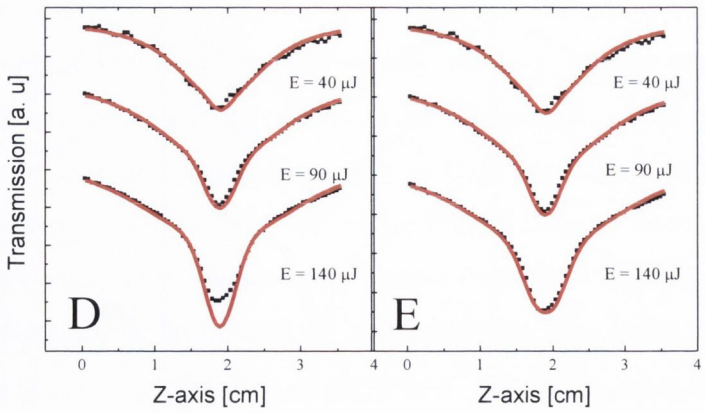



**Figure 42** Comparison of the fitting curves (red lines) obtained with models **D** and **E** for the experiments carried out at increasing input energy for compound Zn_Br in toluene. The following set of parameters were used in the fittings: model **D**: $I_1$ = 0.29 GW cm$^{-2}$, $I_2$ = 0.2 GW cm$^{-2}$, $\kappa_1$ = 5.3, $\kappa_2$ = 4.2 cm$^2$ GW$^{-1}$; model **E**: $I_1$ = 0.3 GW cm$^{-2}$, $I_2$ = 0.16 GW cm$^{-2}$, $I_3$ = 2.2 GW$^2$ cm$^{-4}$, $\kappa_1$ = 5.4, $\kappa_2$ = 5.6 cm$^2$ GW$^{-1}$, $\kappa_3$ = 0. ■ represents experimental data.

Next, the response of compound Zn_CCTMS which exhibited a much broader Z-scan trace (Figure 43) was analyzed. Both three- and four-level models with sequential absorption of two and three photons **A** and **B**, respectively, provided comparable good quality fits for the low and moderate input energy data but no longer followed the response at higher input energies. Evidently, model **E** with TPA arising from the excited state provided the best fit for the results at both low and high inputs. Absorptive processes arising from the state $N_3$ (*i.e.* $\kappa_3$ = 0) were neglected as before.

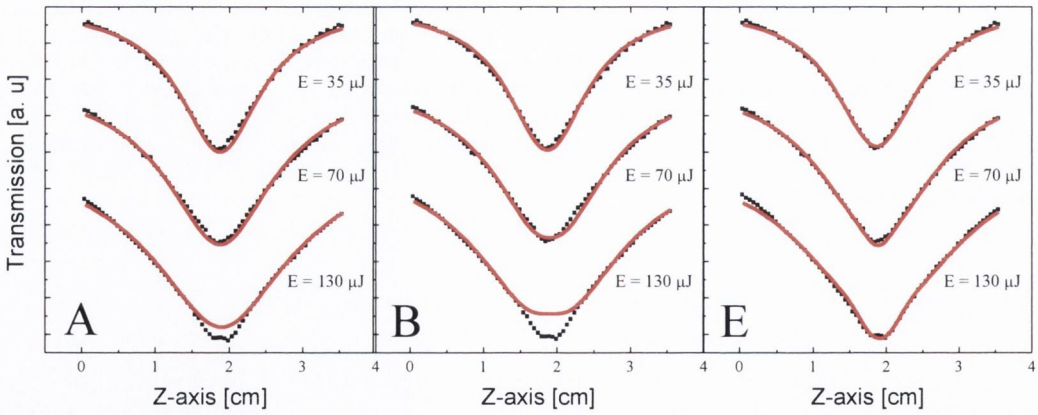



**Figure 43** Comparison of the fitting curves (red lines) obtained with models **A**, **B** and **E** for the experiments carried out at increasing input energy for compound Zn_CCTMS in toluene. The following set of parameters were used in the fittings: model **A**: $I_1$ = 0.12 GW cm$^{-2}$, $\kappa_1$ = 4.2; model **B:** $I_1$ = 0.14 GW cm$^{-2}$, $I_2$ = 0.9 GW cm$^{-2}$, $\kappa_1$ = 4.3, $\kappa_2$ = 3.2; model **E**: $I_1$ = 0.17 GW cm$^{-2}$, $I_2$ = 0.5 GW cm$^{-2}$, $I_3$= 1.7 GW$^2$ cm$^{-4}$, $\kappa_1$ = 5.2, $\kappa_2$ = 6.5 cm$^2$ GW$^{-1}$, $\kappa_3$ = 0. ■represents experimental data.

Compound Pd_Br exhibited an interesting response, *i.e.* a SA/RSA/SA switch. As stated before, no good quality data could be obtained at moderate and higher input energies for the compound. As soon as the input energy was increased the Z-scan response became asymmetric. The two switches in the Z-scan trace suggested that at least the five-level model is needed to reproduce the response, provided that consecutive absorptive processes are considered. Models **C** and **E** were investigated in modeling the response of compound Pd_Br in toluene. Model **E** provided a better fit to the experimental data (Figure 44).

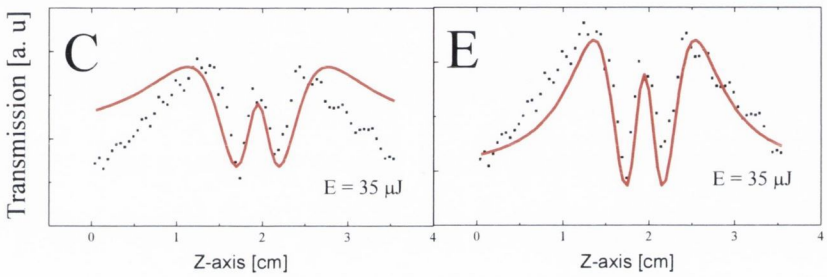



**Figure 44** Comparison of the fitting curves (red lines) obtained with models **C** and **E** for compound Pd_Br in toluene. The following set of parameters were used in the fittings: model **C**: $I_1$ = 0.1 GW cm$^{-2}$, $I_2$ = 0.08 GW cm$^{-2}$, $I_3$ = 0.4 GW cm$^{-2}$, $\kappa_1$ = 0.05, $\kappa_2$ = 2, $\kappa_3$ = 0; model **E**: $I_1$ = 0.08 GW cm$^{-2}$, $I_2$ = 0.07 GW cm$^{-2}$, $I_3$ = 0.036 GW$^2$ cm$^{-4}$, $\kappa_1$ = 0.75, $\kappa_2$ = 11.5 cm$^2$ GW$^{-1}$, $\kappa_3$ = 0. ■represents experimental data.

Similar modeling studies were carried out for the responses recorded in DMF for all compounds. Again, model **E** provided the best fitting among all of the models considered. However, once a final switch to SA in the higher fluence regime was observed, the predicted response started to deviate more and more from the recorded data for the subsequent experiments that were carried out at increasing input energy. The response predicted by the model could not reach the minimal transmission recorded for the compound. It also could not reproduce the SA peak observed experimentally in the close focal regime. (An example: compound 2H_CCTMS in Figure 45a, red line represents fitting with model **E**). Similar observations were made for all other compounds in DMF. We concentrated on the analysis of the response of compound 2H_CCTMS. It was found that the fitting quality improved when parameter $\kappa_3$ was allowed to take variable (increasing) values for the subsequent experiments at higher inputs (Figure 45a, blue line represents curves based on model **E** with varied values of parameter $\kappa_3$). This indicates that further absorptive processes arising from state $N_3$ cannot be neglected at very high input energies. Note that none of the fitting parameters varied between subsequent experiments at increasing input energy. However, as the unusual behavior of parameter $\kappa_3$ was observed for high input energy experiments, the parameter is possibly affected by

thermal effects. We re-treated data obtained for compound 2H_CCTMS in DMF at higher input energies and plotted them as normalized transmission *versus* pulse energy density (Figure 45b). It can be seen from the figure that the experimental data for the subsequent experiments does not overlap in higher fluence range. RSA/SA turnover fluence increases and the minimal transmission reaches lower values for each of the following experiments carried at increasing input energy. The same was observed for the other compounds in DMF. Such a behavior indicates that some additional processes contribute to the NLA signal at higher fluences. We associate this processes with thermally affected absorption arising from the state $N_3$.

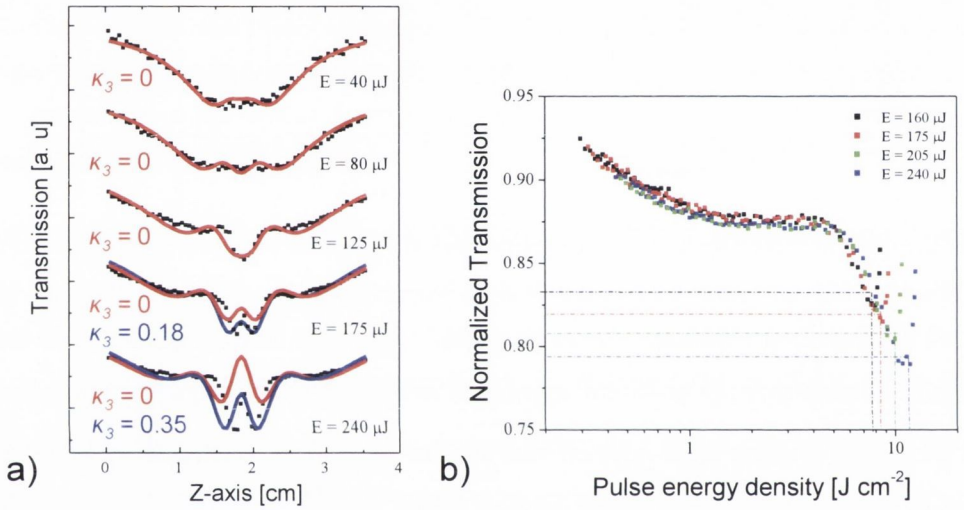



**Figure 45** a) Experimental data (■) for compound 2H_CCTMS in DMF at increasing input energy along with fitting curves. Red lines represent fitting curves obtained with model **E** while keeping all parameters constant for all of the experiments ($I_1$ = 0.48 GW cm$^{-2}$, $I_2$ = 0.14 GW cm$^{-2}$, $I_3$ = 2 GW$^2$ cm$^{-4}$, $\kappa_1$ = 3.7, $\kappa_2$ = 2 cm$^2$ GW$^{-1}$, $\kappa_3$ = 0); blue lines represent fitting curves based on the same model with varied values of parameter $\kappa_3$ for the experiments at high inputs while keeping the values of all of the other parameters constant and equal to those in the previous case. b) High input energy data plotted as normalized transmission *versus* pulse energy density.

Figure 46 shows the fitting curves obtained with model **E** for the other compounds (Zn_Br, Zn_CCTMS and Pd_Br) in DMF. Only the experimental data, for which the model provided good fit with $\kappa_3$ = 0, are presented.

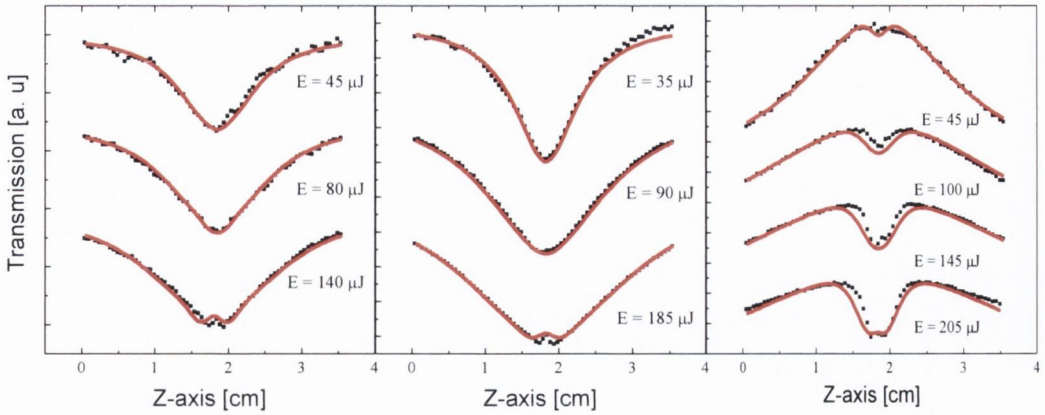



**Figure 46** Illustration of the experimental data (■) obtained at increasing input energy for compounds Zn_Br, Zn_CCTMS and Pd_Br in DMF (left to right) along with fitting curves (red lines) based on model **E**. Fitting parameters used in the modeling are summarized in Table 2.

**Table 2** Best fit parameters (model **E**) for 5,10-$A_2B_2$ porphyrins in toluene (T) and DMF (D). Parameter $\kappa_3$ = 0 in all cases.

| Por/ Solvent | $\alpha_{gr}$ [$cm^{-1}$] | $\kappa_1$ | $\kappa_2$ [$cm^2GW^{-1}$] | $I_1$ [$GWcm^{-2}$] | $I_2$ [$GWcm^{-2}$] | $I_3$ [$GW^2cm^{-4}$] |
|---|---|---|---|---|---|---|
| Zn_Br/T | 1.73 | 5.4 | 5.5 | 0.3 | 0.16 | 2.2 |
| Zn_Br/D | 1.38 | 4.7 | 3.7 | 0.38 | 0.3 | 1.65 |
| 2H_CCTMS/T | 3.96 | 4.4 | 2.8 | 0.45 | 0.1 | 2.05 |
| 2H_CCTMS/D | 3.54 | 3.7 | 2 | 0.48 | 0.14 | 2 |
| Zn_CCTMS/T | 2.3 | 5.2 | 6.5 | 0.17 | 0.5 | 1.7 |
| Zn_CCTMS/D | 1.84 | 5 | 6.4 | 0.14 | 2 | 1.5 |
| Pd_Br/T | 6.32 | 0.75 | 11.5 | 0.08 | 0.07 | 0.036 |
| Pd_Br/D | 6.72 | 0.4 | 1.1 | 0.013 | 3 | 1.8 |

## 4.5 Discussion

The diverse range of profiles of the Z-scan traces recorded for 5,10-$A_2B_2$ porphyrins could suggest different NLA processes for different compounds. However, it was shown that the five-level model **E** provided the best fit for all compounds, implying that all compounds exhibit similar excited state behavior. Best fit parameters used in modeling the recorded responses are compiled in Table 2. With the parameter $\kappa_3$ = 0 used in all fittings, the model can actually be reduced to a four-level manifold where population of the highest excited state $N_3$ is not neglected. The applicability of such a model to the NLA responses of 5,10-

$A_2B_2$ compounds reveals that their excited state structure differs from that of other meso tetrasubstituted porphyrins[21] and resembles that of a hemiporphyrazine derivative.[212] For the latter the model with instantaneous TPA from a higher excited state applied to only one compound (chloroindium hemiporphyrazine derivative), whereas it was not applicable to the related lead complex or similar compounds. As a result and in reference to the present study, it is difficult to delineate common structural features that lead to a distinct NLA mechanism.

The model was developed based on the steady state approximation. Additionally, it was assumed that ISC is fast and efficient. Such assumptions should be valid for metallated compounds however, further studies are needed to elucidate the photophysical properties of the 5,10-$A_2B_2$ compounds in more detail. This would enable validation of the mechanism. The ISC rate and the quantum yield for triplet state formation are usually lower for free base porphyrins.[28, 216] Thus, the assumptions applied in the present model might not necessarily be valid for the free base compound 2H_CCTMS. However, for the sake of simplicity, here the same model was used for the free base compound and the model did reproduce the recorded response of compound 2H_CCTMS well. Thus, it is believed that the parameters can be used for comparative studies, bearing in mind, the assumptions applied.

The character of the Z-scan traces recorded in toluene and DMF for compound Zn_CCTMS were broader compared to those for compounds Zn_Br and 2H_CCTMS. A broadening of the Z-scan wings was observed by Kimball *et al.* when investigating solvent effects on the NLA of (tetrabenzoporphyrinato)zinc(II).[31] The broadening was attributed to a contribution of a triplet excited state cross-section and a larger ISC rate. In our case we associate the broadening with an increase in $\kappa_1$ and $\kappa_2$ combined with a decrease in $I_1$. $\kappa_1$ and $\kappa_2$ increase and $I_1$ decrease for the compounds in the following order: Zn_Br, 2H_CCTMS and Zn_CCTMS. A lower $I_1$ ensures that a saturated regime of NLA is reached at lower inputs, which enhances the effective contribution of ESA to the NLA response. Likewise, ESA is enhanced by a large ISC rate.

Compound 2H_CCTMS showed a RSA/RSA response in toluene and RSA/weak SA/RSA/SA in DMF. A RSA/SA/RSA profile was reported before in the ps regime for porphyrin arrays and was attributed to saturation of ESA followed by TPA.[115] The profile of the Z-scan response of compound 2H_CCTMS in DMF is explained with similar processes. We attribute the RSA/SA observed at lower intensities to saturation of one-

photon excited state absorption. The following switch in the closer focal regime arises due to TPA from the higher excited triplet states (rather than from $S_0$ as in porphyrin arrays). The final switch to SA is associated with saturation of the two-photon absorption. The different NLA responses in the two solvents studied are associated with $\kappa_1$ and $\kappa_2$ being higher in toluene than in DMF as $I_1$, $I_2$ and $I_3$ did not vary significantly between the solvents.

The experimental data obtained for all compounds in toluene and DMF were manipulated and plotted as normalized transmission *versus* pulse energy density (Figure 47). The parameters $\kappa_1$ and $\kappa_2$, being the ratios of the higher excited states cross-sections to that of the ground state, were larger in toluene than in DMF for all compounds. This indicates the impact of the solvent on NLA parameters in agreement with previous reports.[31, 217] For all compounds with an overall drop in transmission with intensity (Zn_Br, 2H_CCTMS and Zn_CCTMS) the transmission reached a lower minimal value in toluene than in DMF. This was associated with higher values of parameters $\kappa_1$ and $\kappa_2$ in toluene. Additionally, the linear absorption at the experimental wavelength, 532 nm, was higher in toluene than in DMF for compounds Zn_Br, 2H_CCTMS and Zn_CCTMS. A higher ground state absorption would result in larger population of the excited state which should contribute to the larger transmission drop observed in toluene. Note that all compounds in DMF exhibited switching to SA at higher fluences. At such high fluences asymmetric and unreproducible Z-scan data were recorded in toluene. Except for compound Pd_Br, none of the compounds exhibited switches to SA in toluene in the fluence regime investigated. However, as discussed before, a RSA/SA switch would be expected to occur for those compounds if a higher fluence range was experimentally accessible in toluene. This behavior can be expected for $\kappa_2 > 1$ and $\kappa_3 < 1$, in reference to theoretical studies previously reported.[205]

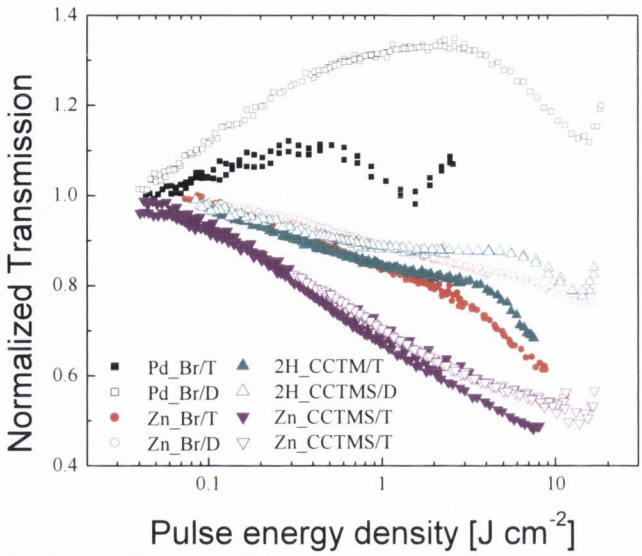



**Figure 47** Experimental data shown as normalized transmission *versus* pulse energy density for all compounds in toluene (T) and DMF (D).

Zn_CCTMS exhibited the largest transmission drop in both solvents in reference to the analogous free base compound 2H_CCTMS and the brominated zinc complex Zn_Br. This makes Zn_CCTMS most promising for application as an OL material against green laser light. The result agrees well with general trends observed for macrocyclic dyes, according to which, firstly, compounds with extended conjugation provide better OL efficiency and, secondly, metal complexes outperform free base compounds.[21] In addition, meso tetrasubstituted porphyrins with TMS-ethynyl groups were reported to be highly potential OL candidates.[28] It is in agreement also showed in 2.3.2, that a 5,15-$A_2B_2$ porphyrin with TMS-ethynyl groups provided much better OL performance than porphyrins with other substituents.[218] Thus, the present study reinforces the utility of the TMS-ethynyl group as a very useful substituent for OL porphyrins. Compound Zn_Br reached slightly lower minimal transmission than compound 2H_CCTMS in both solvents. Evidently, a combination of structural features such as heavy atoms (here bromine atoms at the meso position and the central metal compound Zn_Br) did not yield a material superior to the free base compound 2H_CCTMS with an extended conjugated system.

The minimal transmission for the most promising compound, Zn_CCTMS, reached 50%, which is above the value reported for the previously discussed hemiporphyrazine (~30% at 3 J.cm$^{-2}$) acting through a similar mechanism. We surmise that 5,10-$A_2B_2$ compounds would exhibit better OL efficiency if probed at shorter wavelengths for NLA. The experimental wavelength of 532 nm was situated in close vicinity to the Q-bands area for

the 5,10-$A_2B_2$ porphyrins studied. Both singlet and triplet excited state absorption cross-sections were reported to reach their maxima between the Soret and Q-bands for porphyrins. In the close vicinity to the Q-band area both absorption cross-sections are lower.[28] Possibly weak ESA at 532 nm lowers the overall transmission drop detected for the 5,10-$A_2B_2$ porphyrins studied.

Compound Pd_Br, for which the Q-band maximum was equal to the experimental wavelength of 532 nm, exhibited a linear absorption approximately 1.5 to 5 times higher at that wavelength compared to other compounds. Evidently, the excited state cross-section was lower than that of the ground state ($\kappa_1 < 1$) for this compound, both in toluene and in DMF, resulting in SA at lower fluences. The SA/RSA/SA character of the response developed in the two solvents. Yet, SA/RSA and RSA/SA turnover fluences and the magnitude of transmission rise and drop (likely SA and subsequent RSA before the final SA occurred) differed significantly between the two solvents. The values of the parameters (model **E**, Table 2) were very different for the two solvents for compound Pd_Br compared to the other compounds, for which the values of the parameters appeared to be of the same order of magnitude for both solvents. We attributed this to aggregation. It was demonstrated in 3.5.4 that Pd_Br aggregates in DMF for concentrations of up to $10^{-4}$ M, and concentrations of the same order were also used in Z-scan studies. No aggregation was observed previously for Pd_Br in toluene.

Generally, aggregation adds relaxation pathways, resulting in shorter lifetimes of the excited states. It also lowers the yield of triplet state formation.[219, 220] The model applied assumes that the ISC process is quick and efficient. Yet, one can deduce how a lower yield of triplet state formation impacts on the fitting parameters. A lower yield of triplet state formation will lower the population of the state $N_1$. Thus, higher intensities will be needed to populate $N_1$ efficiently so that significant one-photon ESA could arise from it. Therefore, one can expect that higher intensities will be needed to saturate the one-photon process. Additionally, shorter lifetimes of the excited states should enhance the saturation intensities. It can be observed that both $I_2$ and $I_3$ are two orders of magnitude larger in DMF than in toluene, which is attributed to aggregation in the former solvent.

The NLA responses of diluted samples of compound Pd_Br in DMF and toluene were then recorded. As illustrated in Figure 48, these samples exhibited weak and comparable SA. Note that contrary to concentrated samples, no switch from SA to RSA was detected for the diluted ones. This finding is similar to those reported in literature. Srinivas *et al.*

observed that NLA response of Rhodamine B in the ps regime changed from SA to SA/RSA when the concentration was increased, which was associated with aggregation.[210] Konstantaki *et al.* observed some similar phenomena for osmium complexes in the ns regime. Although the SA/RSA character of the response was maintained for different concentrations the threshold intensity for RSA was slightly lower at higher concentration. The RSA character of the response was attributed to charge transfer processes occurring in highly excited states.[209]

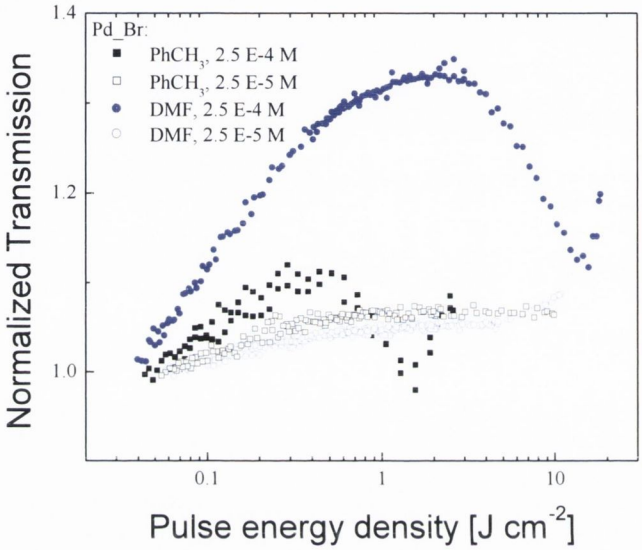



**Figure 48** Nonlinear absorption responses of compound Pd_Br recorded in toluene and DMF at different molar concentrations.

## 4.6 Summary

The NLA properties of 5,10-$A_2B_2$ porphyrins were investigated with the open Z-scan technique in toluene and DMF. The responses were found to be dependent on structural features, the solvent used and the input fluence. Although the character of the responses varied between compounds, the same model was shown to be suitable to follow the evolution of NLA with input fluence for all of the compounds. A four-level model, where one-photon ESA is followed by a simultaneous TPA process arising from the higher excited state was proposed to explain the NLA in 5,10-$A_2B_2$ porphyrins. This indicated that all 5,10-$A_2B_2$ compounds share similar excited state structures and that the specific 5,10-$A_2B_2$ regiochemical substitution pattern results in a NLA behavior distinct from that found in meso tetrasubstituted compounds, where NLA is typically explained by one-photon ESA. The steady state model approximated the NLA processes arising in 5,10-$A_2B_2$ porphyrins well. We found the stability of the signal to be dependent on the solvent;

reproducible data could be obtained at much higher intensities in DMF in comparison to toluene. For all compounds which exhibited an overall transmission drop with intensity (Zn_Br, 2H_CCTMS and Pd_CCTMS) the minimal transmission reached a lower value in toluene than in DMF. Higher ratios of the excited to ground state absorption cross-sections were obtained in toluene than in DMF. The Zn complex with TMS-ethynyl groups Zn_CCTMS tuned out to be the most promising candidate for OL application. Compound Pd_Br with strong linear absorption at the experimental wavelength exhibited a SA/RSA/SA response in both solvents. The fitting parameters differed much more between the two solvents studied compared to other compounds. This was associated with enhanced aggregation of this compound in DMF. Clearly, these initial studies on 5,10-$A_2B_2$ porphyrins reveal interesting NLA properties which will be investigated further.

# Chapter 5 Nonlinear absorption properties of 5,10-$A_2B_2$ porphyrins – correlation of molecular structure to the nonlinear responses

## 5.1 Introduction and outline

Here we focus on the comparison of the NLA responses obtained for two newly synthesized series of 5,10-$A_2B_2$ porphyrins in order to establish the correlation between structure and NLA properties. Depending on the structural features such as central metal and meso substituents, 5,10-$A_2B_2$ porphyrins generated different classes of NLA responses which resembled those presented in the preceding chapter (*i.e.* RSA, RSA/RSA, RSA/SA, SA/RSA). All responses were successfully fitted and rationalized with the four-level model developed previously (consecutive one- + one- + two-photon absorption). 5,10-$A_2B_2$ porphyrins were proven interesting candidates for OL application upon certain structural modifications. The introduction of meso substituents to the porphyrin periphery and metal ions to the porphyrin core, allowed for the OL response to be tuned. It is demonstrated that structural features must be tailored simultaneously to maximize the OL performance.

## 5.2 Theoretical background

Significant progress has been made in the improvement of the OL performance of porphyrins since the first observation of the OL effect in TPP in 1985[21, 109, 221], which was covered broadly in the introduction. Briefly, most studies investigated either the effect of substituents or of the central metal on the OL performance. The presence of a central closed shell metal atom has been demonstrated in many reports to improve NLA *via* enhancement of the ISC rate and the quantum yield for triplet states due to the heavy atom effect. Incorporation of bromine on the β or meso position was found to impact OL in the same way as closed shell metals in the central core. Likewise, the incorporation of

conjugated groups at the meso positions was shown to enhance the OL action of porphyrins.[116]

## 5.3 Experimental and theoretical modeling details

Open Z-scan studies were carried out on toluene solution of 5,10-$A_2B_2$ porphyrins **80-93** following the procedure reported in 2.2.2, using same conditions as in 4.3.

All data were fitted with the four-level model described in the preceding chapter according to procedure established in 4.4.3. Additionally, experimental data at low input energy of ~50 μJ (which corresponds to an onfocus intensity of about 0.6 GW.cm$^{-2}$) were fitted with the analytical expression for the normalized transmission as a function of the sample's position along the Z-axis Eq. **1-19** to extract the effective nonlinear absorption coefficient $\beta_{eff}$, according to the procedure reported in 2.2.3. The latter fitting was carried out for compounds which exhibited RSA character of the response in low input energy Z-scan experiments.

## 5.4 Results

For broader comparison we refer to data for the compounds presented in the preceding chapter.

### 5.4.1 Ground state absorption features

The ground state absorption spectra of free base and metallated 5,10-$A_2B_2$ porphyrins for a brominated and TMS-/TIPS-ethynyl substituted series are presented in Figure 49. The spectra of the TMS-/TIPS-ethynyl series are red-shifted compared to the bromoporphyrins. In both series, the spectra of the metal complexes are bathochromically shifted compared to the free bases. Exceptions include Pt_Br which shows a hypsochromic shift in reference to the free base 2H_Br and palladium complexes Pd_Br and Pd_CCTMS which appear at a similar wavelength to their free base analogues 2H_Br and 2H_CCTMS respectively. The behavior of Pt_Br is in agreement with previous reports on platinum porphyrins.[187] The spectra of lead complexes are even more shifted towards longer wavelengths in both series of compounds. As expected, the number of Q-bands is reduced for metallated compounds due to an increase in symmetry.[70] Except for the free base forms, the same metal complexes of both series exhibit similar Q-band characteristics. In both series of compounds, the Soret and Q-band maxima appear at similar wavelengths for the tin and indium complexes. 2H_CCTMS and 2H_CCTIPS provided very similar UV-vis spectra.

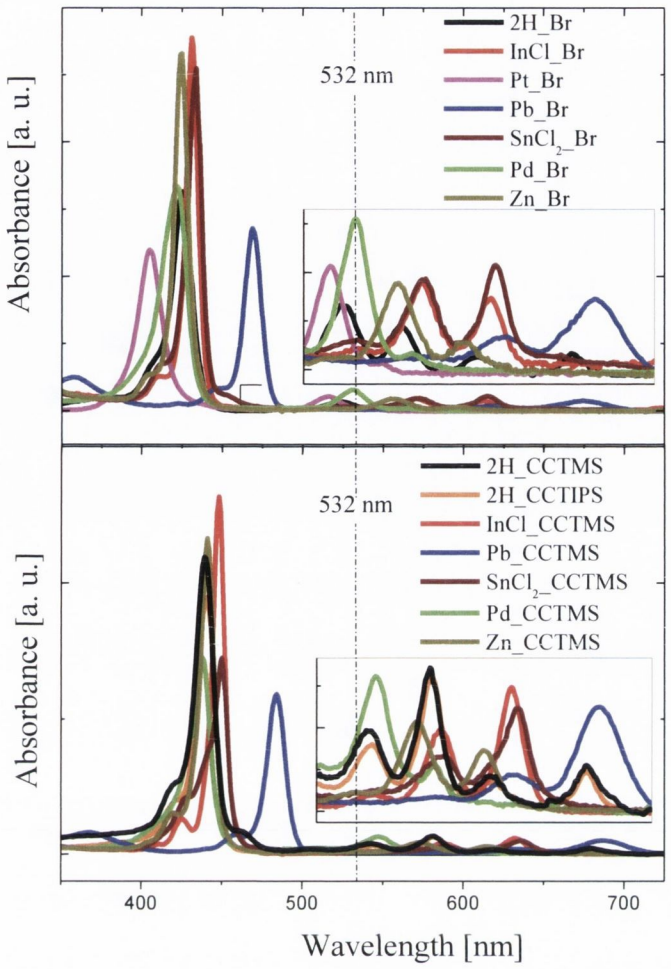



**Figure 49** Ground state absorption spectra of 5,10-$A_2B_2$ porphyrins in $CH_2Cl_2$.

### 5.4.2 Nonlinear absorption responses and data fitting

Responses recorded for 5,10-$A_2B_2$ porphyrins of the brominated and the TMS-/TIPS-ethynyl series are presented in Figure 50. These responses were successfully fitted with the four-level model described in the preceding chapter, where one photon ESA is followed by instantaneous TPA arising from higher excited states. The fitting curves generated based on the four-level model, are presented along with the OL curves in Figure 50. Best fit parameters used in the modeling of the responses are summarized in Table 3. The values of $\beta_{eff}$ derived from low input energy experimental data are given in the same table. For the experiments carried out at higher input energies, the fitting curve based on Eq. **1-19** diverged from the experimental data, to larger or lesser extent, depending on the compound (see example in Figure 51). Thus, the parameter $\beta_{eff}$ could not be derived for the higher input energy measurements.

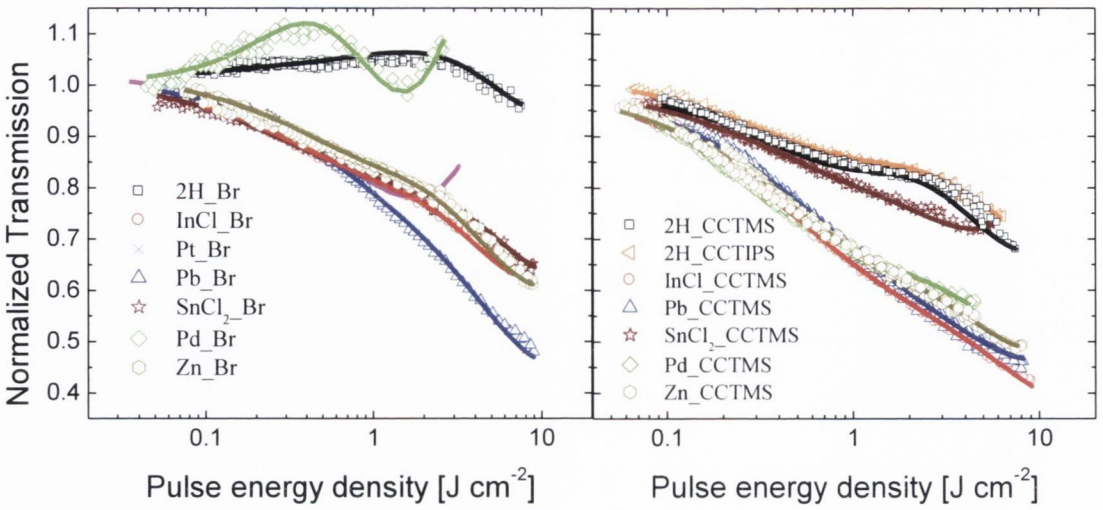



**Figure 50** Comparison of the nonlinear responses along with fitting curves generated based on the four-level model for brominated (left panel) and TMS-/TIPS-ethynyl (right panel) substituted 5,10-$A_2B_2$ porphyrins.

**Table 3** Comparison of linear and nonlinear optical parameters of 5,10-$A_2B_2$ porphyrins. $\alpha_{gr}$, $\kappa_1$, $\kappa_2$, $I_1$, $I_2$ and $I_3$ for Zn_Br, Pd_Br, Zn_CCTMS and 2H_CCTMS can be found in Table 2. $\beta_{eff}$ and $\lambda_{max}$ for these compounds equaled to: 4.8, -[†], 15.3, 8.1 [cm.W$^{-1}$] and 424, 422, 441, 439 nm, respectively.

| Comp. | $\lambda_{max}$ | $\alpha_{gr}$ [cm$^{-1}$] | $\beta_{eff}$ $\times 10^8$ [cmW$^{-1}$] | $\kappa_1$ | $\kappa_2$ [cm$^2$GW$^{-1}$] | $I_1$ [GWcm$^{-2}$] | $I_2$ [GWcm$^{-2}$] | $I_3$ [GW$^2$cm$^{-4}$] |
|---|---|---|---|---|---|---|---|---|
| 2H_Br | 423 | 3.45 | -[†] | 0.88 | 1.70 | 0.0015 | 0.90 | 1.90 |
| InCl_Br | 431 | 1.49 | 5.7 | 4.4 | 6.7 | 0.17 | 0.35 | 1.70 |
| Pt_Br | 405 | 2.58 | -[†] | 10.0 | 3.8 | 0.95 | 0.10 | 0.28 |
| Pb_Br | 470 | 1.28 | 6.2 | 6.5 | 14.0 | 0.28 | 0.90 | 1.40 |
| $SnCl_2$_Br | 434 | 2.26 | 6.7 | 2.8 | 4.6 | 0.11 | 0.68 | 1.80 |
| 2H_CCTIPS | 440 | 3.65 | 8.3 | 2.5 | 3.3 | 0.16 | 0.30 | 1.30 |
| InCl_CCTMS | 449 | 2.06 | 13.7 | 5.9 | 8.5 | 0.16 | 0.90 | 1.90 |
| Pd_CCTMS | 438 | 3.53 | 18.1 | 4.2 | 4.5 | 0.17 | 0.30 | 1.70 |
| Pb_CCTMS | 484 | 1.38 | 9.4 | 8.0 | 12.0 | 0.21 | 1.50 | 1.20 |
| $SnCl_2$_CCTMS | 450 | 1.71 | 6.4 | 3.7 | 8.4 | 0.13 | 0.50 | 0.45 |

[†] the compound did not exhibit pure RSA behavior at low input experiment and no good data fit could be obtained to derive $\beta_{eff}$.

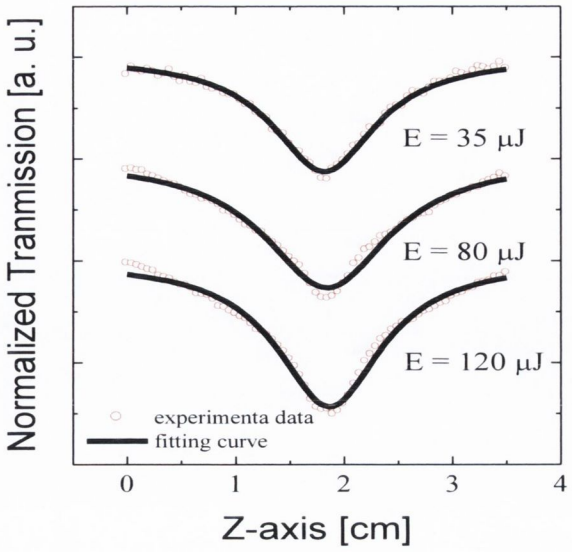



**Figure 51** Illustration of the experimental data obtained for compound $SnCl_2$_Br along with fitting curves generated with the analytical expression for the normalized transmission. The theoretical curves provided good fit to low input energy data and diverged for those at higher inputs.

## 5.5 Discussion

The effective nonlinear absorption coefficient $\beta_{eff}$ derived from low input energy open Z-scan data, was in the range of 4.8 – 18.1× $10^{-8}$ cm.$W^{-1}$ for the compounds studied. The highest values of $\beta_{eff}$ were obtained for the palladium, indium, zinc and lead complexes from the TMS-ethynyl substituted series. These compounds also exhibited the strongest transmission drop with input intensity, making them most promising for OL applications. The values of $\beta_{eff}$ obtained were comparable to those reported before for phthalocyanines and porphyrins typically being of the order of $10^{-8}$ cm.$W^{-1}$.[111, 218, 222]

All of the recorded responses, at whole range of input energies, were successfully fitted with the four-level model. This implies that the compounds studied exhibit the same excited state absorption behavior as the recently examined 5,10-$A_2B_2$ porphyrins with similar structural features. This behavior is distinct from that reported for most other macrocycles, which is typically explained with third order NLO processes.

A switch from transmission drop to an increase (RSA/SA switch) was observed for $SnCl_2$_CCTMS in the higher fluence regime (~6 J.$cm^{-2}$). A similar switch, though at lower input fluence (2 J.$cm^{-2}$) was detected for a platinum complex from the brominated series Pt_Br (Figure 50). A RSA/SA switch at comparable low input fluence was also observed for Pd_Br which exhibited an overall SA/RSA/SA character of the response. Typically, a

RSA/SA switch does not occur in the ns regime for macrocyclic dyes but has been reported to arise for different materials under ps pulses.[113, 202, 203] In these cases the RSA/SA switch in the ps regime was attributed to a contribution of poorly absorbing higher excited states to the measured NLA signal. We associated the switch with further inefficient absorptive processes arising from the $N_3$ state. The four-level model neglects further absorptive processes arising from state $N_3$, which are assumed to be negligible. The fitting parameter $I_3$ was lower for Pt_Br, Pd_Br and $SnCl_2$_CCTMS compared to other porphyrins. Since the lifetime of state $N_3$ - $\tau_3 \sim 1/(\alpha_{gr} \cdot \kappa_2 \cdot I_3)$, the ratios of the lifetimes of state $N_3$ - $\tau_3$ for compounds Pt_Br, Pd_Br and $SnCl_2$_CCTMS to the lifetimes $\tau_3$ of other porphyrins can be easily evaluated. Values in the range of 4.1 – 12.1 and 4.3 – 12.7 were obtained for Pt_Br and Pd_Br respectively; for $SnCl_2$_CCTMS, for which a switch occurred in the higher fluence regime, lower ratios of 1.7 – 5.1 were found. Longer lifetimes of higher excited states will lead to higher population of these states and this triggers further undesirable poorly absorptive processes, resulting in SA behavior for compounds Pt_Br, Pd_Br and $SnCl_2$_CCTMS.

Compound 2H_Br exhibited weak SA for fluences up to 2 $J.cm^{-2}$ to then switch to RSA in the higher fluence range. A SA/RSA switch was observed also for Pd_Br but at much lower fluence of 0.4 $J.cm^{-2}$. Typically, SA is observed at excitation wavelengths close to/at ground state absorption peaks. The experimental wavelength of 532 nm was situated in the Q-band peak regime for 2H_Br and equaled to the Q-band maximum for Pd_Br. SA/RSA has been reported before for other macrocycles in the ns regime and was attributed to the contribution of more absorptive higher excited states at higher fluences.[206, 207] The switch observed for 2H_Br and Pd_Br can be explained in a similar way. The ratios of the absorption cross-sections of the following excited states ($N_1$ and $N_2$ to ground state absorption cross-section took values $\kappa_1 < 1$ and $\kappa_2 > 1$ for both compounds. However, according to the four-level model, which provided a good fit to experimental data for 2H_Br and Pd_Br, in contrast to previous reports, RSA is due to TPA arising from higher excited states rather than to one photon ESA.

In all series of compounds, the free bases 2H_Br and 2H_CCTMS (and 2H_CCTIPS also) exhibited the weakest transmission drop in comparison to the metal complexes. (An exception is Pd_Br which transmission drop was comparable to that exhibited by 2H_Br.) This observation agrees with previous reports.[21, 44] Insertion of metals into the central core is usually an efficient way to improve the OL performance of macrocyclic dyes due to a

heavy atom effect through the enhancement of the ISC rate and the quantum yield for the triplet states.

Both 2H_CCTIPS and 2H_CCTMS showed very similar NLA responses. Thus, introduction of different alkyl groups on the silicon atom had no effect on the NLA response.

The effect of the metal on the OL efficiency was different for the two series of porphyrins. This finding is in agreement with other reports.[21] It indicates that both structural features *i.e.* the metal and the substituents must be tailored simultaneously to maximize the OL performance. Still, one report stated that the NLA response does not vary strongly between different metal complexes.[223] InCl_Br, $SnCl_2$_Br and Zn_Br exhibited very similar NLA responses, in agreement with the previous report. The lead compound Pb_Br provided the best OL efficiency amongst the bromoporphyrins. In the TMS-ethynyl series the tin complex exhibited weaker OL efficiency than the palladium compound which in turn was outperformed by the zinc, lead and indium complexes. The latter three compounds provided very similar OL curves. In conclusion, the lead complexes were consistently strong positive nonlinear absorbers within a series which is in agreement with literature.[28, 44] Indium and zinc complexes provided very similar OL curves within each series. Thus, the metal effect is less important than that exerted by substituents for these compounds.

With the exception of tin, all other complexes from the TMS-ethynyl substituted series outperformed their metal analogues from the brominated series. Even though lead brominated compound Pb_Br exhibited a comparable minimal transmission to that recorded for stronger nonlinear absorbers from the TMS-ethynyl series (Pb_CCMTS, Zn_CCTMS and InCl_CCTMS), its OL performance was suppressed in reference to those compounds over lower fluence range (Figure 50). This indicates that replacement of the heavy bromine atoms at two meso positions in 5,10-$A_2B_2$ porphyrins with conjugated groups enhances the OL efficiency. TMS- and TIPS-ethynyl tetra-substituted porphyrins, as indicate before, were previously reported as very promising materials for OL application[28, 44] and our studies confirm the potential of the TMS-ethynyl meso substituent for generating an efficient OL effect. Only few studies dealt with the effect of bromination on NLA.[119, 224] Introduction of bromine atoms at both the meso or β position was reported to enhance the ISC rate and quantum yield for triplet states up to unity.[116] (2,3,7,8,12,13,17,18-Octabromo-5,10,15,20-tetraphenylporphyrinato)zinc(II) was shown to have especially strong positive NLA with an OL efficiency comparable to the advanced

phthalocyanine [chloro(tetra-*tert*-butyl)phthalocyaninato]indium(III).[224] Compared to TMS-ethynyl substituted 5,10-$A_2B_2$ compounds the brominated porphyrins exhibited weaker OL efficiency and thus have less potential for green light OL.

Next we compare the fitting parameters obtained for different 5,10-$A_2B_2$ porphyrins. Normalized transmission at a fluence of 5 J.cm$^{-2}$ was plotted together with $\kappa_1$ and $\kappa_2$ for different compounds (Figure 52). Data for compounds Pd_Br and Pt_Br are not presented in the plots. Measurement at higher input energies (covering higher fluence range) did not provide any reproducible data for these compounds. Evidently, normalized transmission correlates to both parameters - $\kappa_1$ and $\kappa_2$. Additionally, $\kappa_1$ follows a trend similar to $\kappa_2$. The one- and two-photon excited state absorption cross-sections $\sigma_1$ and $\sigma_2$ respectively, were then recalculated from $\sigma_i = \kappa_i \sigma_0$ where $\sigma_0 = \alpha_{gr}/N_T$, and plotted for the compounds studied. Since the concentration $N_T$ was the same for all the compounds $\sigma_1 \sim \kappa_1 \alpha_{gr}$ and $\sigma_2 \sim \kappa_2 \alpha_{gr}$. The normalized transmission correlates to both $\sigma_1$ and $\sigma_2$. However, it is likely that the correlation with the latter parameters is stronger. TMS-ethynyl substituted metallated complexes exhibited higher $\sigma_2$ than brominated compounds. An exception is the lead complex Pb_Br. Except for the tin complex, TMS-ethynyl substituted porphyrins also exhibited higher $\sigma_1$ than the other compounds. Overall, there seems to be a correlation between $\sigma_1$ and $\sigma_2$ suggesting that compounds which exhibit a higher excited state absorption cross-section of one-photon process $\sigma_1$ tend to exhibit a higher excited state absorption cross-section of the consecutive two-photon process $\sigma_2$, too.

It can be seen from Figure 52 (lower panel) that $\beta_{eff}$ correlates to the one-photon excited state absorption cross-section $\sigma_1$. $\beta_{eff}$ was derived from low input energy experiments. Upon such experimental conditions, the NLA response of 5,10-$A_2B_2$ porphyrins should be dominated by one-photon ESA as demonstrated in the preceding chapter. Therefore one can expect these parameters to be correlated.

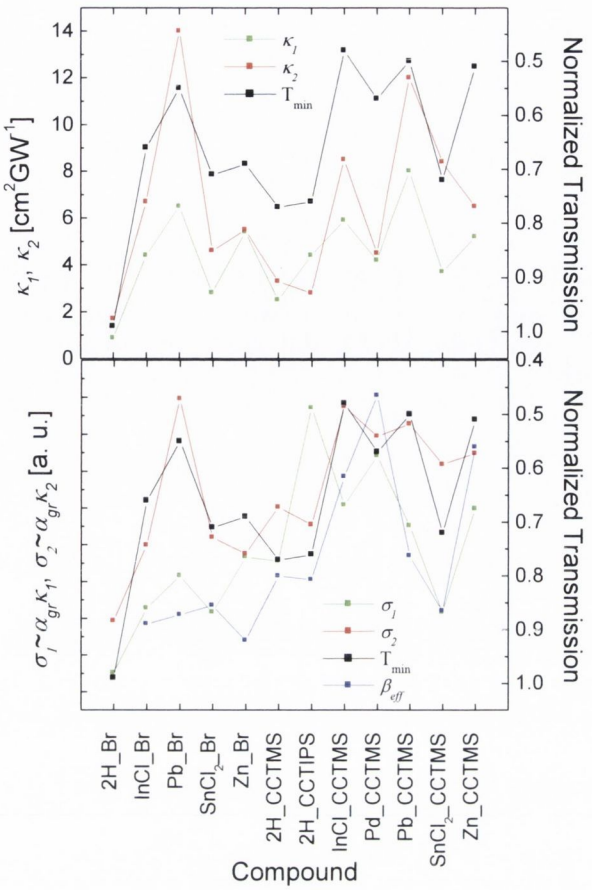



**Figure 52** Parameters $\kappa_1$ and $\kappa_2$ plotted along with normalized transmission at input fluence of 5 J.cm$^{-2}$ (top panel) and similar plot for $\sigma_1$ and $\sigma_2$ and $\beta_{eff}$ (lower panel).

Parameters $\kappa_1$, $\kappa_2$ and $\sigma_1 \sim \kappa_1 \alpha_{gr}$ and $\sigma_2 \sim \kappa_2 \alpha_{gr}$ were plotted against the linear absorption coefficient $\alpha_{gr}$ and the Soret band maximum $\lambda_{max}$ (Figure 53). Both parameters $\kappa_1$ and $\kappa_2$ increase with $\lambda_{max}$ and decrease with $\alpha_{gr}$. The opposite trend observed for $\kappa_1$ and $\kappa_2$ with respect to $\lambda_{max}$ and $\alpha_{gr}$ can be associated with a rough correlation between the latter two parameters (Figure 54). $\alpha_{gr}$ generally appears to decrease with $\lambda_{max}$. This could be understood since roughly speaking the red shift of the linear absorption spectra (*i.e.* an increase in $\lambda_{max}$) causes the experimental wavelength of 532 nm to move further apart from the Q-band region of high linear absorption. No specific trend could be observed for $\sigma_1 \sim \kappa_1 \alpha_{gr}$ and $\sigma_2 \sim \kappa_2 \alpha_{gr}$ plotted against $\alpha_{gr}$. However, part of the data plotted *versus* $\lambda_{max}$ tends to increase with increasing $\lambda_{max}$. This is in agreement with data in the literature. Broadband studies carried out by McEwan *et al.* showed the excited state absorption cross-section to reach its maximum close to the Soret band and to decrease upon moving closer to the Q-band region for porphyrins.[28] For TMS-ethynyl substituted compounds, in which the UV-vis spectra are more shifted towards longer wavelength, the

excitation wavelength of 532 nm is situated closer to the Soret band. These compounds exhibit higher values of the excited state absorption cross-sections than porphyrins from the brominated series, for which 532 nm is closer to the Q-band area. McEwan *et al.* also proposed that there is a correlation between the position of the Soret band maximum *versus* the experimental wavelength and the OL efficiency, *i.e.* the closer the Soret band is to 532 nm the stronger is the transmission drop. We noted a similar trend for structurally diverse porphyrins of the 5,15-$A_2B_2$, 5,15-$A_2BC$ series before.[218] The same observation can be applied to the 5,10-$A_2B_2$ compounds studied, *i.e.*, both $\kappa_1$ and $\kappa_2$ increase with the maximum of the Soret band.

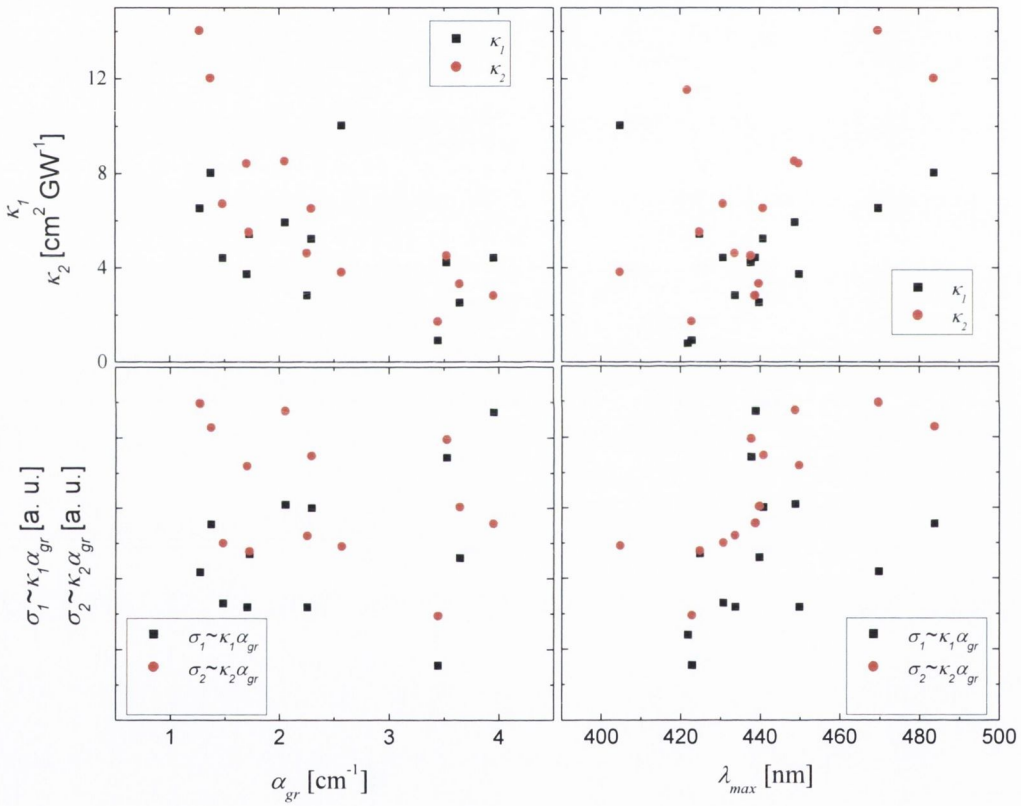



**Figure 53** Parameters $\kappa_1$ and $\kappa_2$ plotted *versus* the linear absorption coefficient $\alpha_{gr}$ (upper left) and the Soret band maxim (upper right). $\sigma_1 \sim \kappa_1 \alpha_{gr}$ and $\sigma_2 \sim \kappa_2 \alpha_{gr}$ *versus* $\alpha_{gr}$ (lower left) and *versus* $\lambda_{max}$ (lower right). Data for Pd_Br are not shown.

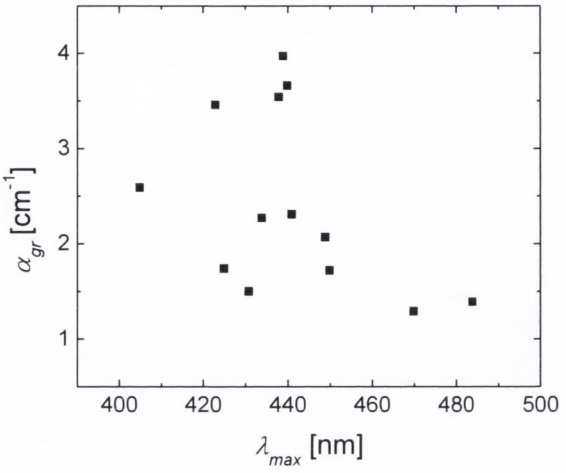



**Figure 54** Linear absorption coefficient $\alpha_{gr}$ *versus* Soret band maximum $\lambda_{max}$ for 5,10-$A_2B_2$ porphyrins. Data for compound Pd_Br is not shown.

Finally, $\kappa_1$ and $\kappa_2$ were plotted against the atomic mass of the central metal for the brominated and TMS-ethynyl substituted compounds (Figure 55). Previously, O'Flaherty *et al.* reported that although no definite correlation could be observed between the ratio of the excited to ground state absorption cross-sections $\kappa$ and the atomic mass of the central atom for metallated phthalocyanines, the parameter $\kappa$ generally appeared to increase with the atomic mass of the metal.[111] A similar trend can be observed for the 5,10-$A_2B_2$ porphyrins with regard to parameters $\kappa_1$ and $\kappa_2$. However, the correlation tends to be stronger if one analyses the variation of parameter $\kappa_1$ or $\kappa_2$ for a given series of compounds, *i.e.* brominated or TMS-ethynyl substituted compounds (exception: parameter $\kappa_2$ from the brominated series).

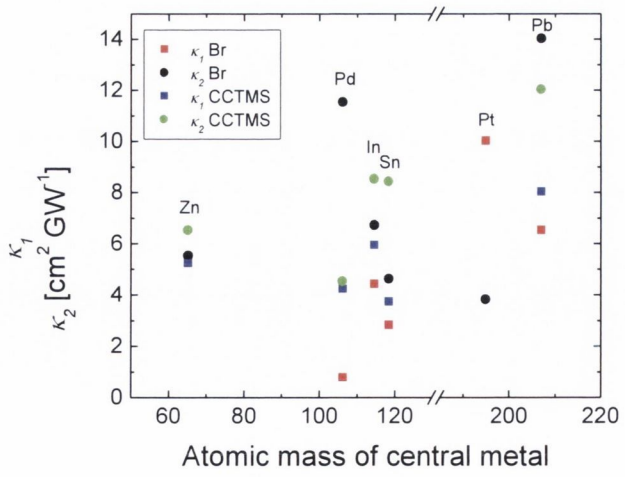



**Figure 55** The ratio of the excited to ground states absorption cross-section $\kappa_1$ and $\kappa_2$ *versus* atomic mass of the central metal.

## 5.6 Summary

Two series of 5,10-$A_2B_2$ porphyrins both bearing *p*-tolyl as substituent A and bromine or TMS-ethynyl groups as substituent B with different metals in the central core were investigated for their NLA properties with an open Z-scan technique. The NLA responses were successfully fitted with a four-level model where one photon ESA is followed by instantaneous two-photon absorption processes. Most of the compounds exhibited a transmission drop with input fluence. An undesirable response for OL applications, a RSA/SA switch, was found for the platinum complex of a bromoporphyrin at very low input fluence and at higher input for a tin complex of TMS-ethynyl substituted porphyrins. This was associated with longer lifetimes of the higher excited states triggering further weakly absorptive processes. A similar switch was also observed at low fluence for palladium bromoporphyrin which exhibited an overall SA/RSA/SA character of the response. The RSA/SA switch could be explained in the same manner as above. Besides palladium bromoporphyrin, a SA/RSA switch was detected for a free base bromoporphyrin. Both compounds exhibited high linear absorption at experimental wavelength. The TMS-ethynyl meso substituent was found to be a more promising OL group than a bromine atom at equivalent positions. Consistently, the lead complexes were found to be strong positive nonlinear absorbers in both series of compounds. Only smaller differences were found for the NLA responses of tin, indium and zinc brominated complexes and for the indium, zinc and lead porphyrins of the TMS-ethynyl substituted series. Thus, the substituent effect is stronger than the central metal effect. Excited state absorption cross-sections were found to increase with longer wavelength positions of the Soret band maxima. The ratio of the excited to ground state absorption cross-sections were found to increase with the atomic mass of the central metal.

The studies showed that modification of the porphyrin periphery has a great impact on its excited state structure. The 5,10-$A_2B_2$ regiochemical substitution pattern provides compounds with interesting NLA behavior distinct from that of meso tetrasubstituted porphyrins. The central metal significantly improves the NLA of 5,10-$A_2B_2$ porphyrins. Yet both the central metal and the meso substituents must be tailored simultaneously to maximize the OL performance.

# Chapter 6 Solvent effect on the nonlinear absorption of 5,10-$A_2B_2$ meso substituted porphyrins.

## 6.1 Introduction and outline

Here we discuss the effect of the solvent on the nonlinear absorptive properties of two series of 5,10-$A_2B_2$ porphyrins. The recorded responses, which varied between compounds and solvents, were fitted with the previously developed four-level model. For most of the compounds the positive nonlinear absorption was stronger in toluene than in DMF and chloroform. This was attributed to enhanced two-photon absorption in toluene. For DMF and chloroform the solvent effects were most likely compound specific. It was demonstrated that high saturation intensity of two-photon absorption shifted the RSA/SA turnover into higher fluence range, which is desirable for optical limiting applications. This saturation intensity of two-photon absorption varied between compounds and solvents. Additionally, nonlinear scattering contributed strongly to the open Z-scan responses for many compounds in chlorobenzene and chloroform/chlorobenzene solutions. This was associated with the photodegradation of chlorobenzene.

## 6.2 Theoretical background

Solvent – solute interactions can result in changes of the optical properties of the organic dyes. The chemical environment influences the OL efficiency of RSA dyes, however, only few reports have explored this subject until now. The solvent type can impact on the ground and excited state properties of the molecule and alteration of these properties modifies the compound's OL characteristics. For example, in a study on the solvent effect of the RSA of $C_{60}$ under ns pulsed laser, Koudoumas *et al.* demonstrated that the solvent influenced the OL efficiency *via* changes in the local field exerted on the solute or *via* solvatochromism.[32] No significant changes were reported in the OL efficiency of $C_{60}$ with the normalized transmission varying less than 10% between different solvents. Kimball *et*

*al.* reported more severe changes induced by the solvent for (tetrabenzoporphyrinato)zinc(II) with the normalized transmission varying between 20 to 80% for different solvents.[31] Such a solvent effect was only observed in the ns regime, whereas under irradiation with ps pulsed laser no changes in the OL efficiency were observed between solvents. This was attributed to that fact that under ps laser light the contribution of triplet states to the NLA response was negligible and the triplet states became accessible only under ns pulses. In the ns regime the solvent modulates the ISC rates and the threshold fluences. For (tetrabenzoporphyrinato)zinc(II) an attempt was made to simulate the solvent effect numerically, however, no good fit to the experimental data was obtained.[225] This indicates the high complexity of the solute-solvent interactions in the excited state.

The solvent can also induce additional NLO processes such as nonlinear scattering (NLS). For example, an improvement of the limiting threshold of $C_{60}$ as an RSA material in chlorobenzene compared to toluene was attributed to lasers-induced NLS in chlorobenzene.[226] Numerous attempts to incorporate RSA dyes into solid hosts such as polymer films[227] or sol-gel glasses[228, 229] have been reported. In most cases the solid state materials exhibited a better OL performance than solutions as higher densities of active molecules are achieved in the solid state resulting in stronger NLA.

Aggregation is an undesirable process for OL applications using RSA dyes.[21] It is influenced by the chemical environment and is usually enhanced in solid hosts. It minimizes the OL efficiency as it shortens the lifetime of the triplet excited states, adds additional relaxation pathways, and reduces the effective NLA. Taking this into account the choice of a chemical environment which minimizes aggregation is crucial.

## 6.3 Experimental and data treatment details

Open Z-scan studies were carried out on compounds: **48** and **80-93** in toluene, DMF, chloroform, chlorobenzene, and a 2:3 (v/v) chloroform/chlorobenzene solvent mixture, following the procedure reported in 2.2.2, using same conditions as in 4.3.

The scattered light signal was measured simultaneously to the detection of the transmitted laser irradiance in open Z-scan experiments, with the photodetector placed at 30° angle to the Z-axis.

The experimental data were fitted with the four-level model according to the previously established procedure (4.4.3).

The experimental data obtained for all compounds in DMF, chloroform and toluene at an input energy of ~50 μJ, which corresponds to an onfocus intensity of about 0.6 $GW.cm^{-2}$, was fitted according to a procedure presented in 2.2.3. This provided the effective nonlinear absorption coefficient $\beta_{eff}$. Note, that the fitting was applied for compounds which exhibited a pure RSA response character at the relevant input energy.

## 6.4 Results and discussion

Open Z-scan studies were carried out for all compounds in DMF and chlorobenzene. In the preceding chapter the NLA results in toluene were reported, which will be referred to in this chapter for comparison. It should be noted that protonation of free base compounds was observed in chloroform upon laser light irradiation. This phenomenon will be described in detail in subsequent sections of this thesis. To avoid additional effects, for now free base compounds were excluded from studies in chloroform and in a chloroform/chlorobenzene mixture (2:3 v/v).

Generally, DMF and chloroform were poorer solvents for the compounds than toluene and chlorobenzene. The range of laser input energies within which symmetric and reproducible data could be obtained varied between solvents. Higher energies (E > 125 μJ) were experimentally inaccessible for the measurements in chlorobenzene and chloroform/chlorobenzene as cell damage, induced by thermal effects, occurred. DMF provided highly symmetric and reproducible data over the broadest laser input energy range, whereas for toluene and chloroform the data quality and reproducibility were more compound dependent. An example of this effect is illustrated in Figure 56 for compound Zn_Br.

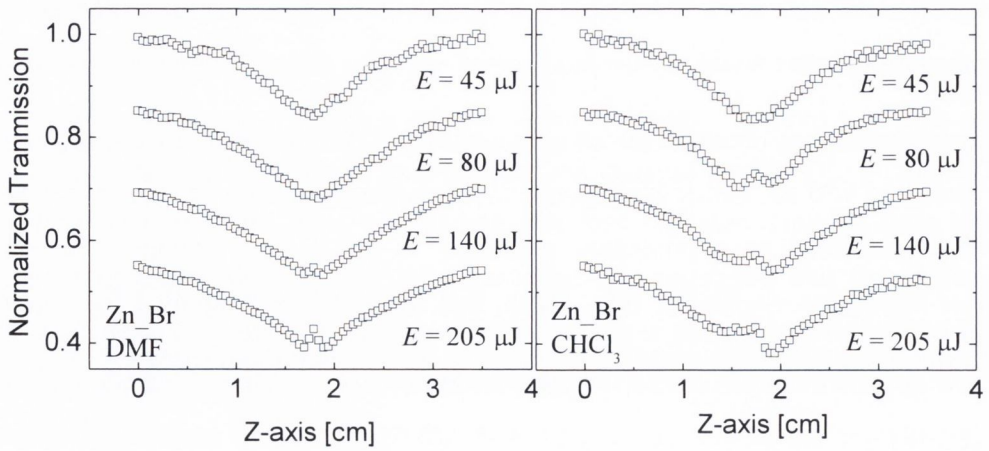
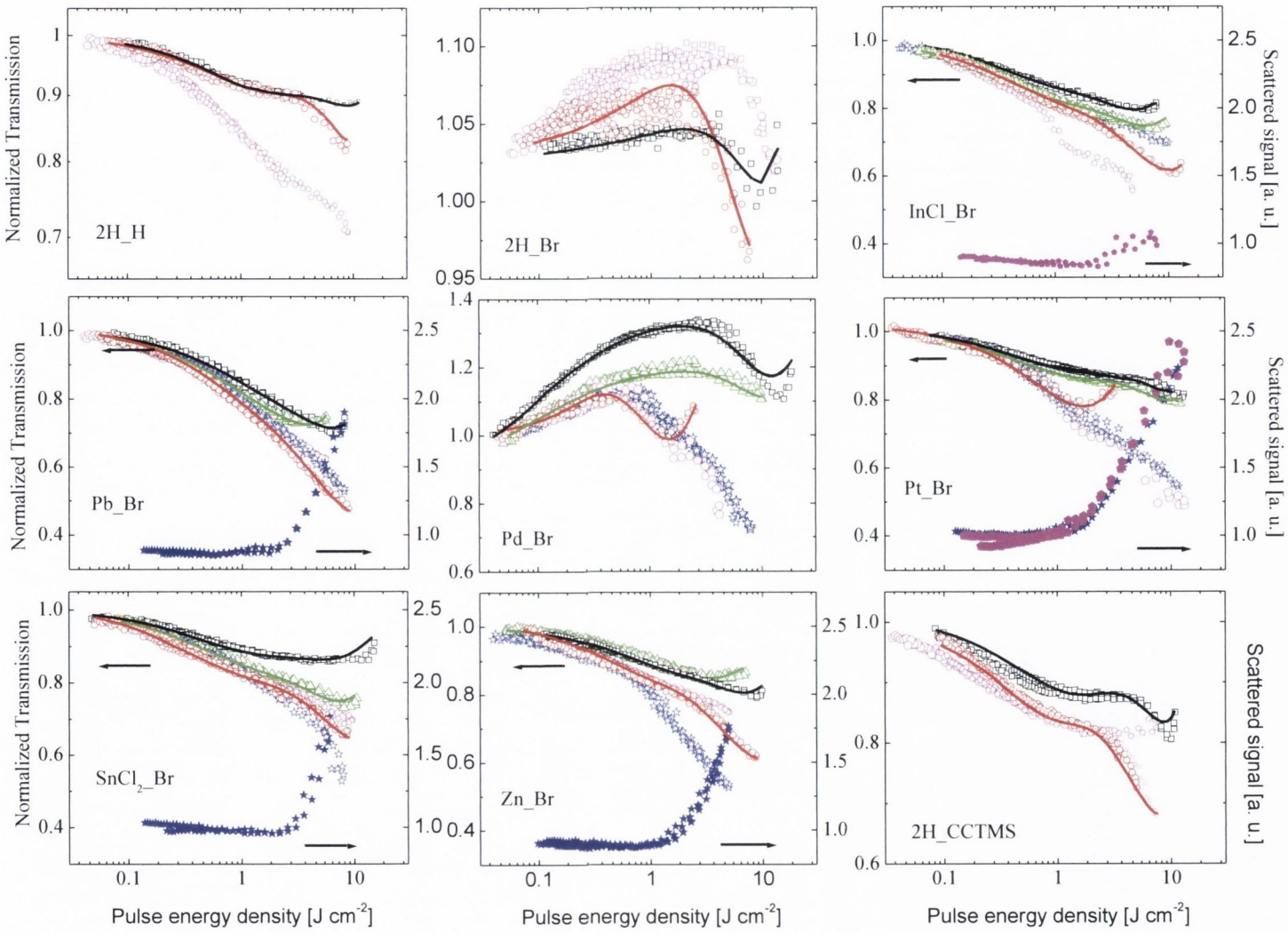



**Figure 56** Plots illustrate data obtained for compound Zn_Br in DMF and chloroform at increasing input energy. The quality of the data deteriorates with increasing input energy for studies in chloroform, while in DMF the data curve remains highly symmetric even at high input energies.

The open Z-scan responses varied between compounds and solvents studied (Figure 57). Most of the compounds exhibited a transmission drop with the input fluence, which for certain compounds in certain solvents turned over to a transmission increase in higher fluence range (RSA/SA). For some compounds a SA/RSA switch was observed, which in some experiments eventually turned over to SA again. The solvent type was found to impact the magnitude of the transmission drop/increase and the fluence at which the switches occurred. In general, the overall character of the response was maintained in different solvents for a given compound.


Normalized Transmission
Scattered signal [a. u.]
2H_H
2H_Br
InCl_Br
Pb_Br
Pd_Br
Pt_Br
SnCl2_Br
Zn_Br
2H_CCTMS
Pulse energy density [J cm-2]

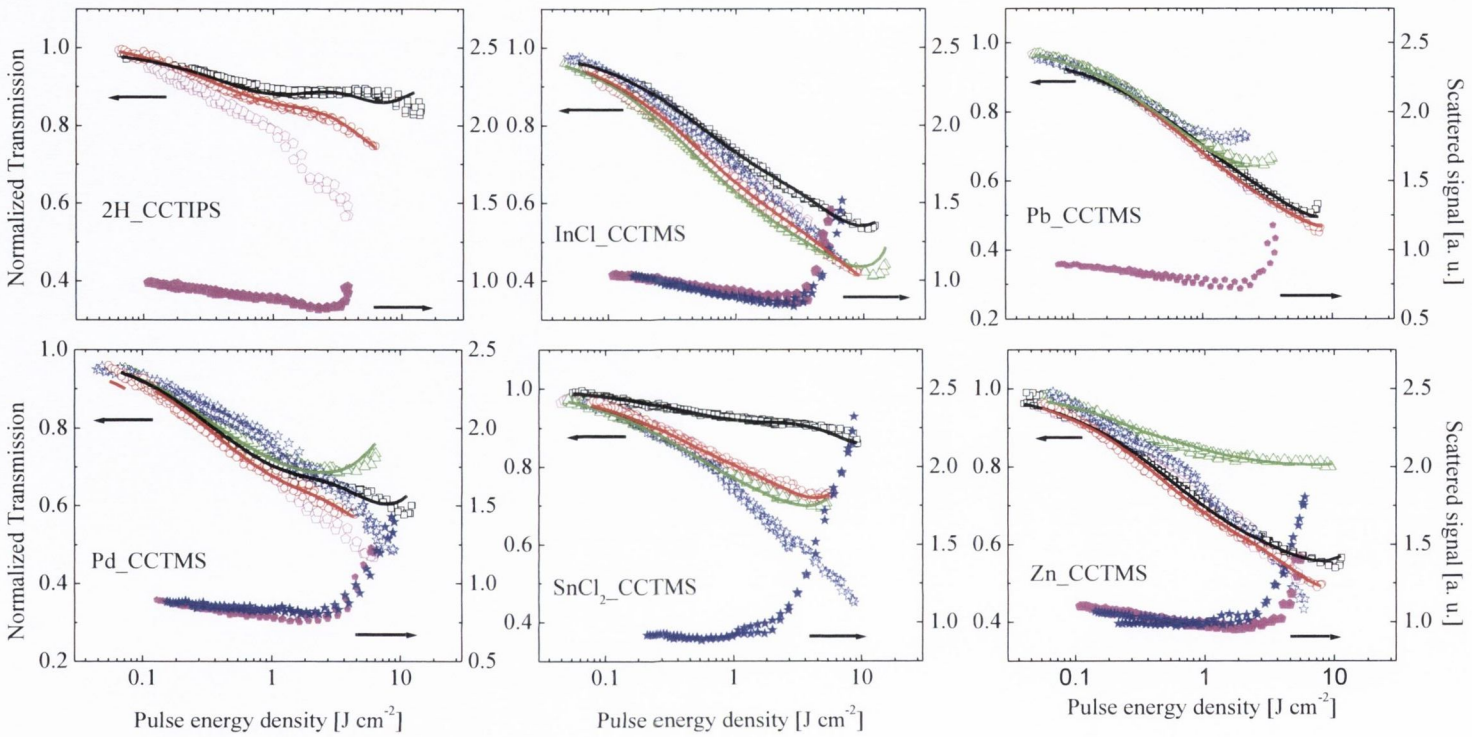



**Figure 57** NLA responses of 5,10-$A_2B_2$ compounds (empty pattern) with fitting curves (line) plotted along with scatted light signal data (filled pattern) for different solvents. One color stands for one solvent: ♦ - DMF, ♦ - toluene, ♦ - chloroform, ♦ - chloroform/chlorobenzene (2:3, v/v), ♦ - chlorobenzene.

### 6.4.1 Solvent induced nonlinear scattering

In some experiments, the NLS was found to rise at higher input energies for chloroform, toluene and DMF porphyrin solutions, which was associated with degenerative processes. Yet, this phenomenon was considerably enhanced for many porphyrins in chloroform/chlorobenzene and for a number of compounds in chlorobenzene. For these solutions the scattered light signal was detected at low and moderate input energies (40 – 100 μJ). The evolution of a NLS light signal in experiments carried out at increasing input energies, along with the corresponding measured transmission for compound Zn_Br in a chloroform/chlorobenzene solvent mixture is given in Figure 58.

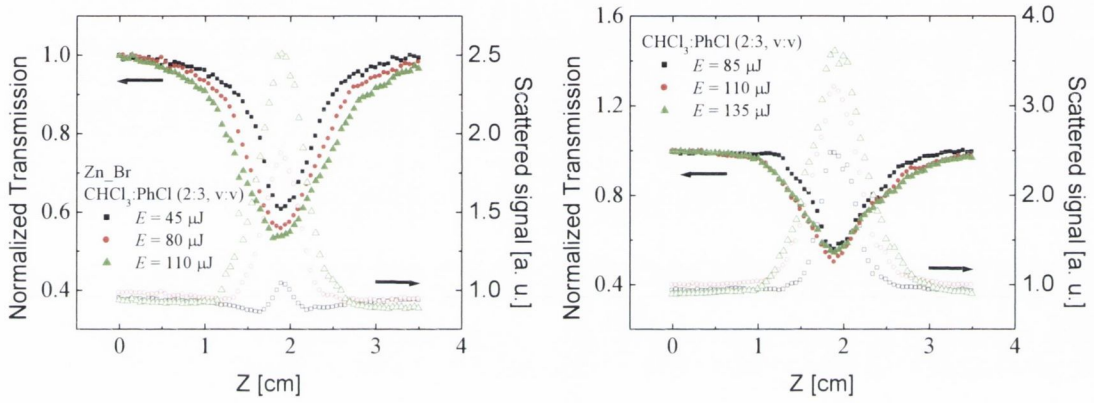



**Figure 58** Open Z-scan data with normalized transmission (filled pattern) and scattered light signal (empty pattern) plotted as a function of sample position Z for the experiments carried out at increasing input laser energy for Zn_Br in a chloroform/chlorobenzene solvent mixture (left panel). Right panel shows similar data for a neat chloroform/chlorobenzene solvent mixture.

Neat chlorobenzene, toluene, DMF or chloroform subjected to the open Z-scan experiment did not yield any NLO response. Interestingly, the drop in transmission accompanied by the detection of scattered light signal could be observed for the neat chloroform/chlorobenzene solvent mixture (Figure 58).

The NLS maxima (in the focal regime, see Figure 58) from the subsequent experiments at increasing input energies for chloroform/chlorobenzene porphyrin solutions were plotted against the input laser energy and compared with similar maxima for the neat chloroform/chlorobenzene mixture (Figure 59). For most of the chloroform/chlorobenzene porphyrin solutions, NLS signals appeared at lower input energy than for the neat chloroform/chlorobenzene solvent mixture. This indicates that the presence of the porphyrin molecules facilitate nucleation of the light scattering centers in the chloroform/chlorobenzene solvent mixture. The signals detected for all

chloroform/chlorobenzene porphyrin solutions were weaker than those detected for the neat chloroform/chlorobenzene solvent mixture, at comparable input energies. In general, the NLS maxima plotted *versus* input energy follow a similar trend for most chloroform/chlorobenzene porphyrin solutions. Therefore, it can be concluded that structural features of porphyrins have no effect on the NLS signal. NLS was previously reported for RSA materials and associated with incomplete dissolution of the material.[62] Evidently herein, the scattered light signal depends on the solvent used. Yet, as previously stated, porphyrin molecules facilitate nucleation of light scattering centers.

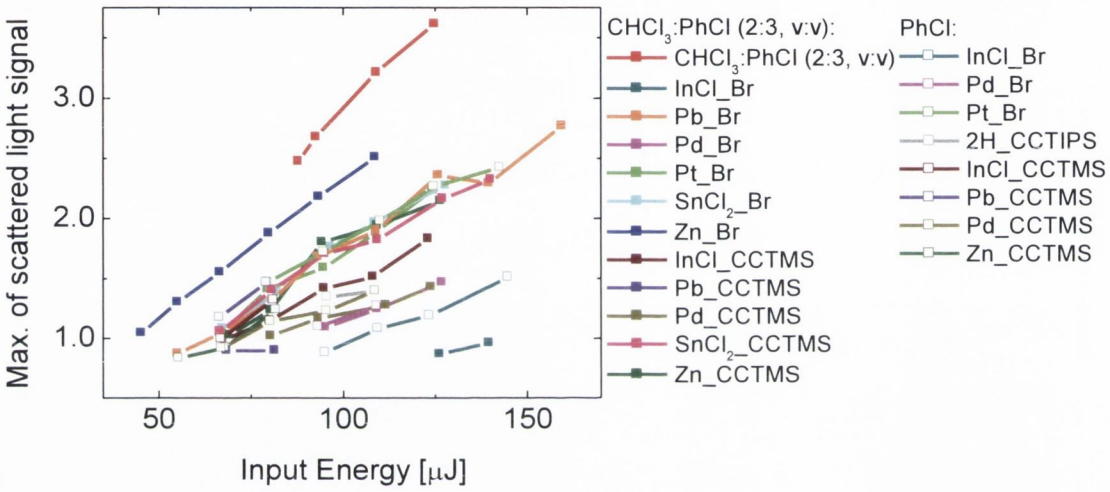



**Figure 59** Maxima of scattered light signals plotted against input energy for studies in chlorobenzene and chloroform/chlorobenzene (2:3, v/v) for different compounds. The lowest energy points correspond to lowest input energy at which the NLS signal became detectable.

A report on the OL efficiency of $C_{60}$ as an RSA material described a transmission drop to lower values in chlorobenzene compared to toluene and related this to laser-induced NLS in the former.[226] The NLS signal was also detected, in our studies, for porphyrin solutions in neat chlorobenzene, although not for all of the compounds studied (detected for: InCl_Br, Pd_Br, Pt_Br, 2H_CCTIPS, InCl_CCTMS, Pb_CCTMS, Pd_CCTMS and Zn_CCTMS). No specific trend could be established to correlate the structural features of compounds with the triggering of the scattered light signal in chlorobenzene. However, for those porphyrin solutions which exhibited NLS in chlorobenzene, scatter light signal maxima plotted *versus* input energy followed a similar trend to that of the chloroform/chlorobenzene porphyrin solutions (Figure 59). We surmise that this phenomenon has a similar origin in both solvents.

The rate of transmission drop in the higher fluence range was very similar for the chlorobenzene or chloroform/chlorobenzene porphyrin solutions, which developed scattered light signals. In the lower fluence range the OL curves for these solutions followed those recorded in toluene of the respective porphyrin. (No thermal effects of similar nature were detected in toluene). Porphyrin solutions in chlorobenzene or chloroform/chlorobenzene, which did not exhibit any, or only exhibited a weak NLS signal, showed comparable or lower OL efficiency compared to that of the respective porphyrin in toluene (Figure 57). The lowering of the OL efficiency was associated with a solvent effect. The solvent type was previously shown to influence the photophysical parameters associated with the NLA process.[31]

The OL response detected for chlorobenzene porphyrin solutions and chloroform/ chlorobenzene porphyrin solutions, which developed NLS, can be explained in the following way: in the lower fluence range (< 1 $J.cm^{-2}$) the response is dominated by NLA exhibited by the porphyrin, in the higher fluence (> 1 $J.cm^{-2}$) range the response is mostly due to NLS. The origin of the scattered light in chlorobenzene and chlorobenzene/chloroform was not investigated further, but it must derive from photochemical processes involving chlorobenzene (in which the solvent undergoes photodegradation most likely through a radical mechanism).

For a given bromoporphyrin, the OL efficiency of the chlorobenzene or chlorobenzene/chloroform solution which exhibited NLS, was higher than that of the toluene solution. For TMS-ethynyl substituted metalloporphyrins, which were in general stronger nonlinear absorbers than bromoporphyrins, the contribution of NLS to the OL effect led to comparable or slightly lower OL efficiency in chlorobenzene or chlorobenzene/chloroform solutions in comparison to toluene (Figure 57).

The above studies illustrate that secondary NLO effects associated with degenerative processes of the solvent led to strong OL behavior. Thus, these NLO effects may serve as additional protection against laser light in the higher fluence regime.

### 6.4.2 Solvent effect on the nonlinear absorption

The four-level model developed previously was successfully applied to fit the NLA responses detected in toluene, DMF and chloroform for all compounds (Figure 57). Data recorded in chlorobenzene and chloroform/chlorobenzene were excluded from the fitting due to the NLS which would affect the nonlinear absorptive parameters used for comparative studies. The best fit parameters used in the experimental data modeling are

summarized in Table 4. More data for studies in DMF and toluene can be found in previous chapters (4.4.3, 5.4.2). The values of the effective nonlinear absorption coefficients $\beta_{eff}$ derived from low input energy are also presented in Table 4. The values of $\beta_{eff}$ obtained for 5,10-$A_2B_2$ porphyrins were comparable to those reported in the literature for other porphyrins and phthalocyanines.[111, 218, 222]

**Table 4** Comparison of the linear and nonlinear optical parameters of 5,10-$A_2B_2$ porphyrins; T – toluene, D – DMF, C – chloroform.

| Compound /solvent | $\alpha_{gr}$ [$cm^{-1}$] | $\beta_{eff}$ $\times 10^8$ [$cmW^{-1}$] | $\kappa_1$ | $\kappa_2$ [$cm^2GW^{-1}$] | $I_1$ [$GWcm^{-2}$] | $I_2$ [$GWcm^{-2}$] | $I_3$ [$GW^2cm^{-4}$] |
|---|---|---|---|---|---|---|---|
| 2H_H / T | 1.58 | 2.4 | 4.5 | 2.4 | 0.47 | 0.15 | 2.90 |
| 2H_H/ D | 1.17 | 2.0 | 4.7 | 2.1 | 0.47 | 0.26 | 3.10 |
| 2H_Br/ D | 2.55 | - | 0.88 | 1.60 | 0.0015 | 2.0000 | 1.60 |
| InCl_Br/ C | 1.70 | 5.1 | 4.1 | 4.8 | 0.17 | 0.34 | 1.15 |
| InCl_Br/ D | 1.78 | 3.6 | 3.0 | 4.8 | 0.14 | 0.54 | 0.85 |
| Pb_Br/ C | 1.32 | 5.6 | 5.8 | 8.2 | 0.30 | 0.90 | 0.40 |
| Pb_Br/ D | 1.25 | 3.7 | 5.4 | 6.9 | 0.34 | 0.70 | 1.00 |
| Pd_Br/ C | 5.59 | - | 0.44 | 1.10 | 0.0011 | 3.200 | 1.50 |
| Pt_Br/ C | 2.09 | 4.2 | 3.3 | 2.4 | 0.27 | 0.35 | 2.85 |
| Pt_Br/ D | 1.77 | 3.3 | 6.0 | 3.3 | 0.65 | 0.10 | 1.00 |
| $SnCl_2$_Br/ C | 1.62 | 4.6 | 3.0 | 5.2 | 0.13 | 1.10 | 1.20 |
| $SnCl_2$_Br/ D | 1.38 | 3.3 | 2.7 | 2.6 | 0.12 | 1.20 | 1.80 |
| Zn_Br/ C | 1.86 | 3.6 | 3.8 | 3.4 | 0.43 | 0.34 | 0.80 |
| 2H_CCTIPS/ D | 2.54 | 5.8 | 3.1 | 1.8 | 0.27 | 0.26 | 2.70 |
| InCl_CCTMS/ C | 2.27 | 17.9 | 6.0 | 8.2 | 0.17 | 0.70 | 1.20 |
| InCl_CCTMS/ D | 1.44 | 8.6 | 6.0 | 8.5 | 0.17 | 0.90 | 1.60 |
| Pb_CCTMS/ C | 1.41 | 10.9 | 7.5 | 4.5 | 0.21 | 0.90 | 0.40 |
| Pb_CCTMS/ D | 1.13 | 6.9 | 8.5 | 14.0 | 0.24 | 1.60 | 1.05 |
| Pd_CCTMS/ C | 3.68 | 11.6 | 2.8 | 3.7 | 0.10 | 1.00 | 0.55 |
| Pd_CCTMS/ D | 3.53 | 16.2 | 4.1 | 3.8 | 0.18 | 0.27 | 1.50 |
| $SnCl_2$_CCTMS/ C | 2.27 | 8.1 | 4.2 | 8.5 | 0.14 | 0.60 | 0.40 |
| $SnCl_2$_CCTMS/ D | 1.56 | 3.2 | 2.2 | 1.9 | 0.14 | 0.85 | 4.50 |

| Compound /solvent | $\alpha_{gr}$ [$cm^{-1}$] | $\beta_{eff}$ $\times 10^8$ [$cmW^{-1}$] | $\kappa_1$ | $\kappa_2$ [$cm^2GW^{-1}$] | $I_1$ [$GWcm^{-2}$] | $I_2$ [$GWcm^{-2}$] | $I_3$ [$GW^2cm^{-4}$] |
|---|---|---|---|---|---|---|---|
| Zn_CCTMS/ D | 1.84 | 11.9 | 5.0 | 6.4 | 0.14 | 2.00 | 1.50 |

The following trend in the solvent effect on $\beta_{eff}$ could be observed for most compounds: $\beta_{eff}$ (DMF) < $\beta_{eff}$ (toluene) (Figure 60). As far as responses in chloroform are concerned, the values of $\beta_{eff}$ for all brominated metal complexes were consistently between those obtained in DMF and toluene. For TMS-ethynyl substituted metallated complexes $\beta_{eff}$ in chloroform did not follow any specific trend compared to other solvents: InCl_CCTMS, Pb_CCTMS and $SnCl_2$_CCTMS exhibited the highest, and Pd_CCTMS and Zn_CCTMS the lowest $\beta_{eff}$ in chloroform compared to other solvents. To summarize, the central metal impacts on the solvent effect on $\beta_{eff}$ for TMS-ethynyl substituted compounds, while for brominated porphyrins the solvent effect on $\beta_{eff}$ is the same for various central metals. It was noted that TMS-ethynyl substituted compounds tended to exhibit higher $\beta_{eff}$ than bromoporphyrins.

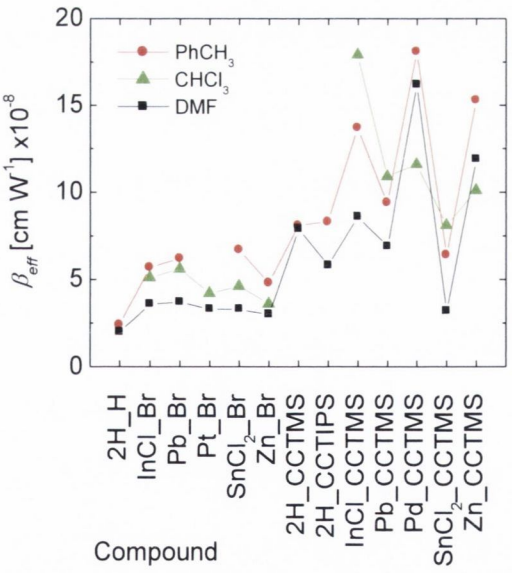



**Figure 60** $\beta_{eff}$ derived from experiments at an input energy of 50 μJ plotted for 5,10-$A_2B_2$ porphyrins in different solvents. Line to guide the eye only.

$\beta_{eff}$ proved to be a useful parameter for the comparison of the results obtained at low input laser energy. However, no good theoretical fit could be obtained for higher input energy experiments for the extraction of $\beta_{eff}$ (see Figure 51). Contrary to $\beta_{eff}$, the four-level

model fitting parameters were useful for the comparison of data obtained at the whole spectrum of accessible input energies. The model provided good fit to all data as presented in Figure 57.

According to the four-level model the NLA behavior is governed by five parameters. The relevant parameters are the ratios of the first and the second excited state absorption cross-sections to that of the ground state absorption cross-section, $\kappa_1$ and $\kappa_2$ respectively, and the saturation intensities associated with the ground, the first and the second excited states: $I_1$, $I_2$ and $I_3$ respectively. The impact of these parameters on the NLA responses was studied.

#### *6.4.2.1 Impact of the four-level model fitting parameters on the nonlinear absorption*

For OL applications it is desirable that a material exhibits a rapid transmission drop with the input and that RSA/SA conversion is inhibited up to the intensity at which the material is damaged.[205] According to a standard five-level Jablonski model, low saturation intensities of the ground state $I_1$ combined with high ratio(s) of the excited state absorption cross-section to the ground state absorption cross-section $\kappa$ are indicators of a good OL material. The same applies to the four-level model used to fit the NLA response of 5,10-$A_2B_2$ porphyrins. A low saturation intensity $I_1$ allows the saturated regime of one-photon excited state absorption to be quickly accessed with the input intensity. Analogously, a low saturation intensity $I_2$ allows the saturated regime associated with two-photon excited state absorption to be quickly accessed with the input intensity. However, contrary to $I_1$, $I_2$ does not always need to be low to maximize OL efficiency, which will be demonstrated below. High values of $I_3$ are desirable for OL. This is because the absorptive processes arising from the state $N_3$ are highly inefficient, as demonstrated in 4.4.3, and high $I_3$ will impede the contribution of these processes to NLA. Finally, high ratios of the excited to ground state absorption cross-sections $\kappa_1$ and $\kappa_2$ enhance the absorption coefficient, and therefore a transmission drop, which can be easily deduced from Eq. **4-30**.

In the next paragraphs a detailed analysis of the impact of the fitting parameters of the four-level model on the NLA responses is presented. It is illustrated how the fitting parameters of the four-level model influence RSA/SA turnover fluence $F_{RSA/SA}$ and the maximum possible absorption coefficient; *i.e.* the absorption coefficient at RSA/SA conversion fluence $\alpha(F_{RSA/SA})$. The conversion from RSA to SA or from SA to RSA will occur provided that $d\alpha(I)/dI = 0$. If $d\alpha(I)/dI$ changes with intensity - from positive to negative passing through zero of the function - an RSA/SA switch occurs, in the opposite

case a SA/RSA turnover takes place. The equation $d\alpha(I)/dI = 0$ was solved symbolically for one parameter using Mathematica software while the other four parameters were kept at constant, chosen values. Intensities were then converted to fluences. The values of the absorption coefficient at the conversion point $\alpha(F_{RSA/SA})$ were calculated and plotted *versus* the chosen parameter. Our aim was to show that the strength or even the character of the effect of the particular parameter on $\alpha(F_{RSA/SA})$ and $F_{RSA/SA}$ depends on the values of all parameters. For purposes of clarity, only the most relevant plots are shown (Figure 61, Figure 62). Plots illustrating how $\alpha$ and $d\alpha/dF$ vary with input fluence are shown in the Appendix. The values of the parameters used in these plots are the same as in A-M (Figure 61, Figure 62).

Studies on the effect of $\kappa_1$ and $\kappa_2$ on the maximum value of the absorption coefficient $\alpha(F_{RSA/SA})$ and RSA/SA turnover fluence $F_{RSA/SA}$ were carried out with $I_1$ = 0.15 GW.cm$^{-2}$, $I_2$ = 0.35 GW.cm$^{-2}$ and $I_3$ = 2.5 GW$^2$.cm$^{-4}$ (Figure 61 A, B, E) or $I_1$ = 0.15 GW.cm$^{-2}$, $I_2$ = 0.35 GW.cm$^{-2}$ and $I_3$ = 0.3 GW$^2$.cm$^{-4}$ (Figure 61 C, D). For these studies $\kappa_1$ = 4 (B, D) or $\kappa_2$ = 8 cm$^2$ GW$^{-1}$. Figure 61 (A-E) depicts an increase in $\alpha(F_{RSA/SA})$ with both $\kappa_1$ and $\kappa_2$. However, the rate of the increase is influenced by the values of other parameters. Low $I_3$ significantly weakens the dependence of $\alpha(F_{RSA/SA})$ on $\kappa_2$ (B, D) but enhances that of $\alpha(F_{RSA/SA})$ on $\kappa_1$ (A, C). It can also be seen that $F_{RSA/SA}$ increases with increasing $\kappa_2$ (B, D) but decreases or increases with increasing $\kappa_1$ (A, C, E). $F_{RSA/SA}$ increases with $\kappa_1$ only when the one-photon process strongly dominates a two-photon process. This is the case *e.g.* when $\kappa_2$ is low in comparison to $\kappa_1$ (E) or when $\kappa_2$ is high but $I_3$ is low (not shown).

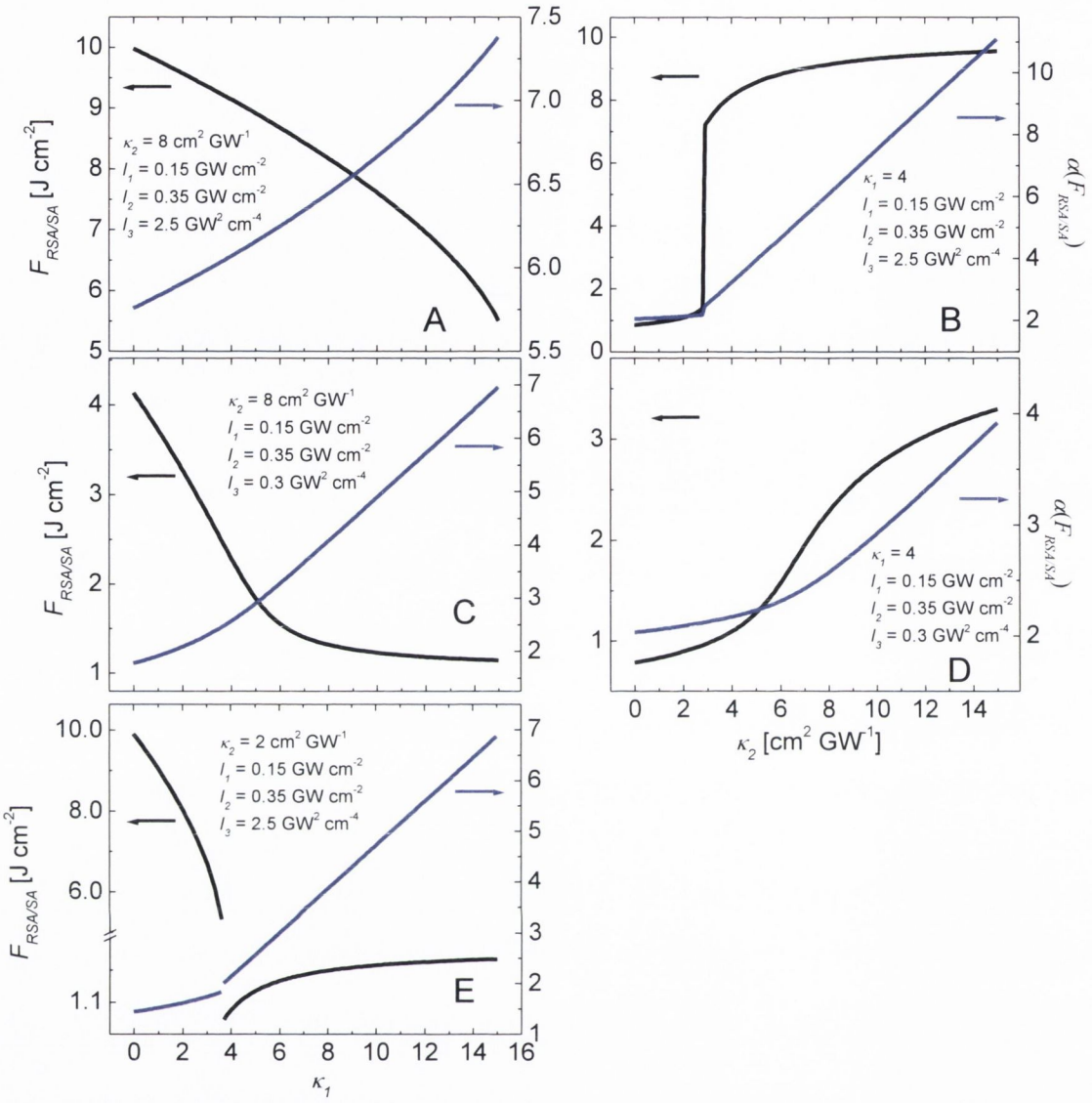



**Figure 61** RSA/SA conversion fluence $F_{RSA/SA}$ (♦) and absorption coefficient at the RSA/SA conversion fluence $\alpha(F_{RSA/SA})$ (♦) plotted *versus* $\kappa_1$ (A, C, E) and $\kappa_2$ (B, D). $\alpha_{gr}$ = 1 cm$^{-2}$, A, B, E: $I_1$ = 0.15 GW.cm$^{-2}$, $I_2$ = 0.35 GW.cm$^{-2}$, $I_3$ = 2.5 GW$^2$.cm$^{-4}$; C, D: $I_1$ = 0.15 GW.cm$^{-2}$, $I_2$ = 0.35 GW.cm$^{-2}$, $I_3$ = 0.3 GW$^2$.cm$^{-4}$, A, C: $\kappa_2$ = 8 cm$^2$.GW$^{-1}$, B, D: $\kappa_1$ = 4, E: $\kappa_2$ = 2 cm$^2$.GW$^{-1}$.

Figure 62 illustrates how $\alpha(F_{RSA/SA})$ and $F_{RSA/SA}$ depend on $I_1$, $I_2$ and $I_3$. Again, the character and strength of the effect depends on the values of all parameters. F, G and H represent the dependence of $\alpha(F_{RSA/SA})$ and $F_{RSA/SA}$ on $I_1$, $I_2$ and $I_3$, respectively, when $\kappa_1$ = 4 and $\kappa_2$ = 8 cm$^2$.GW$^{-1}$. I, J and K show the same dependencies, but for $\kappa_1$ = 8 and $\kappa_2$ = 4 cm$^2$.GW$^{-1}$. The other parameters are kept the same for the respective plots, *i.e.* $I_2$ = 0.35 GW.cm$^{-2}$ and $I_3$ = 2.5 GW$^2$.cm$^{-4}$ for F and I, $I_1$ = 0.15 GW.cm$^{-2}$ and $I_3$ = 2.5 GW$^2$.cm$^{-4}$ for G and J and $I_1$ = 0.15 GW.cm$^{-2}$ and $I_2$ = 2.5 GW.cm$^{-2}$ for H and K. L and M illustrate how a low $I_3$ ($I_3$ = 0.3 GW$^2$.cm$^{-4}$) impacts on the dependence of $\alpha(F_{RSA/SA})$ and $F_{RSA/SA}$ on $I_1$

and $I_2$. The remaining parameters for L and M are kept the same as in F and G, respectively.

With regard to the effect of $I_1$ on $F_{RSA/SA}$ and $\alpha(F_{RSA/SA})$, it can be observed that $F_{RSA/SA}$ increases and $\alpha(F_{RSA/SA})$ decreases with $I_1$ for all cases studied (F, I, L). Low $I_1$ ensures that the most efficient saturated regime of the one-photon absorption will be quickly accessed with input intensity, and thus $\alpha(F_{RSA/SA})$ decreases with $I_1$. Provided that the one-photon absorption process has a stronger contribution to the maximal transmission drop (cases I (high $\kappa_1$) and L (high $\kappa_2$ but low $I_3$)) it is important that $I_1$ is not too low as this leads to very low $F_{RSA/SA}$ which quickly ceases OL action. It can also be seen that $\alpha(F_{RSA/SA})$ and $F_{RSA/SA}$ depend on $I_1$ more in I and L than in F where the maximal transmission drop is dominated by two-photon absorption process.

The character of the effect of $I_2$ on $\alpha(F_{RSA/SA})$ and $F_{RSA/SA}$ is not consistent for the three examples studied (G, J, M). $\alpha(F_{RSA/SA})$ decreases with $I_2$ in G and increases with $I_2$ in J and M. $F_{RSA/SA}$ increases with $I_2$ in G while in J and M it decreases up to a certain value of $I_2$ but increases once that value is surpassed. Low $I_2$ ensures that a two-photon absorption process quickly accesses its most efficient saturated regime. Provided that the two-photon absorption has a stronger contribution to the maximal transmission drop than the one-photon process, *i.e.* $\kappa_2$ is high compared to $\kappa_1$, $\alpha(F_{RSA/SA})$ decreases with $I_2$ (G). Thus, in this case, low values of $I_2$ are desirable to enhance OL efficiency. In the opposite case, *i.e.*, when $\kappa_2$ is low compared to $\kappa_1$, low values of $I_2$ are not desirable for OL as the effective one-photon process is quickly saturated and the less effective two-photon process starts to contribute to the NLA at lower inputs. In this case, $\alpha(F_{RSA/SA})$ increases with $I_2$ (J). However, apart from $\kappa_1$ and $\kappa_2$, $I_3$ also impacts on the dependence of $\alpha(F_{RSA/SA})$ on $I_2$ (M). Low $I_3$ limits the effectiveness of the two-photon process and therefore the one-photon absorption process contributes more strongly to the maximal transmission drop when $\kappa_2$ is high but $I_3$ is low and thus $\alpha(F_{RSA/SA})$ increases with $I_2$ in M.

$F_{RSA/SA}$ is expected to increase with increasing saturation intensities of any of the states. This can be observed for $F_{RSA/SA}$ plotted *versus* $I_1$ and $I_3$ (F, I, L, H, K). However, a similar trend is not always followed in reference to parameter $I_2$ (J, M). This happens when a one-photon process is much more effective than a two-photon process.

$F_{RSA/SA}$ as well as $\alpha(F_{RSA/SA})$ increase with $I_3$ (H, K). Both parameters depend strongly on $I_3$ when $\kappa_1$ is low and $\kappa_2$ is high (H). In the opposite case, when $\kappa_1$ is high but $\kappa_2$ is low, $\alpha(F_{RSA/SA})$ and $F_{RSA/SA}$ do not depend strongly on $I_3$ unless a certain value of $I_3$ is reached (K). This can be explained as up to a certain value of $I_3$, the one-photon process has a greater contribution to the maximal transmission drop than the two-photon process. Therefore $I_3$ will have a weaker influence on $\alpha(F_{RSA/SA})$ and $F_{RSA/SA}$. For higher $I_3$ the contribution of the two-photon process to the maximal transmission drop becomes more significant. Thus, more dramatic changes in $\alpha(F_{RSA/SA})$ and $F_{RSA/SA}$ with $I_3$ can be expected. Note, that for both H and K, $F_{RSA/SA}$ reaches very low values for low $I_3$. Therefore low $I_3$ is highly undesirable for OL as it ceases the OL effect.

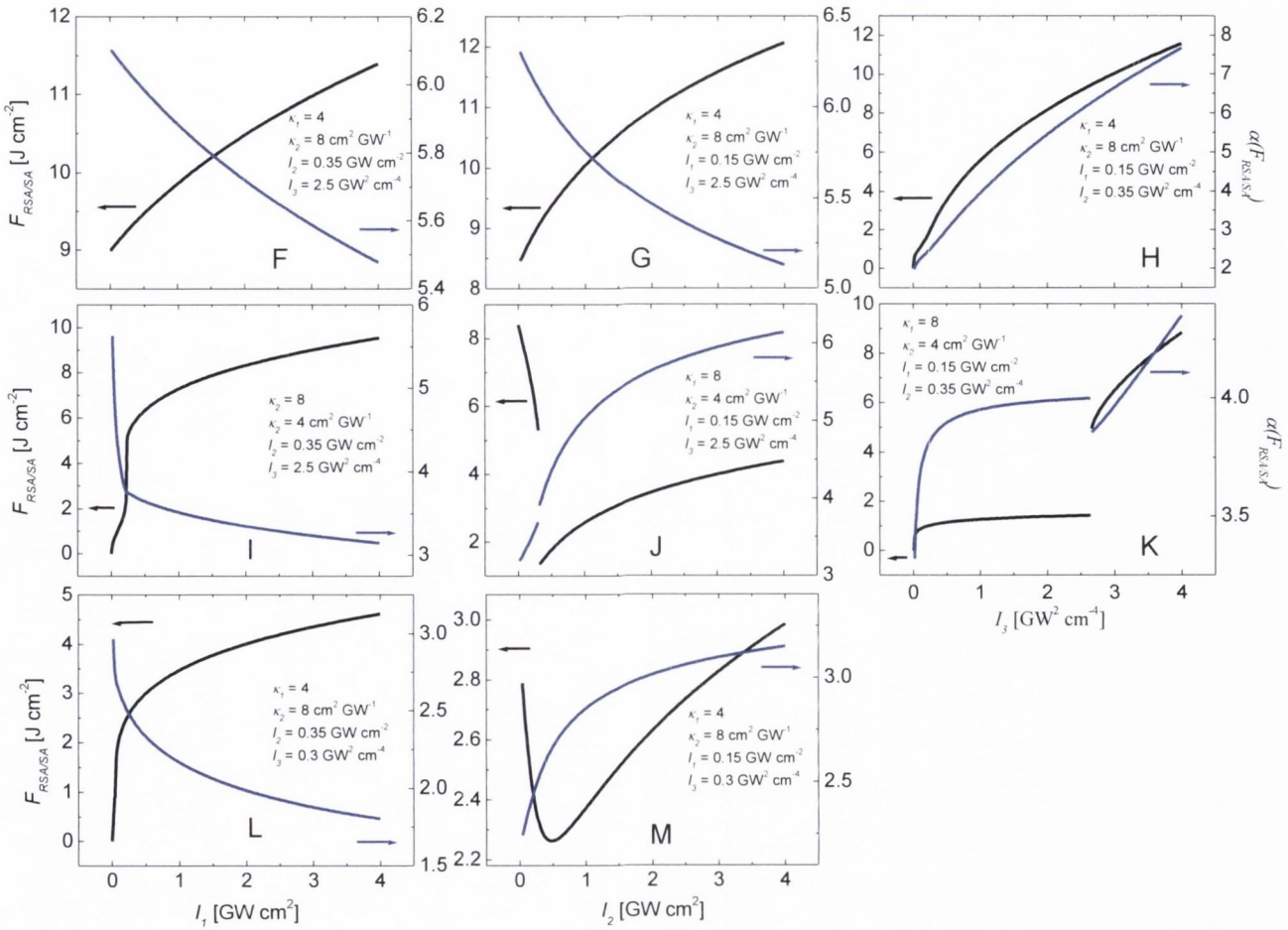



**Figure 62** RSA/SA conversion fluence $F_{RSA/SA}$ (♦) and absorption coefficient at the RSA/SA conversion fluence $\alpha(F_{RSA/SA})$ (♦) plotted *versus* $I_1$, $I_2$ and $I_3$. $\alpha_{gr}$ = 1 cm$^{-2}$ for all cases; F, G, H, L, M: $\kappa_1$ = 4, $\kappa_2$ = 8 cm$^2$.GW$^{-1}$; I, J, K: $\kappa_1$ = 8, $\kappa_2$ = 4 cm$^2$.GW$^{-1}$; F, I: $I_2$ = 0.35 GW.cm$^{-2}$, $I_3$ = 2.5 GW$^2$.cm$^{-4}$; G, J: $I_1$ = 0.15 GW.cm$^{-2}$, $I_3$ = 2.5 GW$^2$.cm$^{-4}$; H, K: $I_1$ = 0.15 GW.cm$^{-2}$, $I_2$ = 0.35 GW.cm$^{-2}$; L: $I_2$ = 0.35 GW.cm$^{-2}$, $I_3$ = 0.3 GW$^2$.cm$^{-4}$, M: $I_1$ = 0.15 GW.cm$^{-2}$, $I_3$ = 0.3 GW$^2$.cm$^{-4}$.

Deng *et al.* carried out similar theoretical studies on the influence of different parameters on the RSA/SA conversion intensity based on a three-level manifold with three consecutive one-photon absorptive processes.[205] They demonstrated that, for an RSA/SA switch to occur, the cross-section of the higher lying excited state must be lower than that of the lower lying excited state, which in turn must be larger than that of the ground state absorption cross-section. The switch occurs only when the intensity threshold is reached. The threshold decreases with increasing excited states lifetimes and increasing cross-section of the strongly absorptive state. Although a different model was used in the current studies, similar findings were obtained. The current four-level model neglects processes arising from the $N_3$ state. These processes are assumed to be unabsorptive (with an absorption cross-section $\approx 0$). As shown in 4.4.3, the population of the state $N_3$ cannot be neglected and the population buil-up of the unabsorptive state $N_3$ leads to an RSA/SA switch. $F_{RSA/SA}$ increases with increasing $I_3$ for the four-level model (Figure 62 H, K). Therefore, according to the definition of $I_3$ (**4-20**), $F_{RSA/SA}$ decreases with increasing lifetime $\tau_3$ and the absorption cross-sections $\sigma_2$ of the absorptive state (the state directly adjacent to the unabsorptive state).

### *6.4.2.2 Solvent effect on the four-level model fitting parameters*

The studies on the influence of the four-level model fitting parameters on $\alpha(F_{RSA/SA})$ and $F_{RSA/SA}$ showed that the dependence of $\alpha(F_{RSA/SA})$ and $F_{RSA/SA}$ on these parameters is complex, and that the effect of a given parameter on the NLA action must be considered in relation to the values of all other parameters. As can be seen from Figure 57, both the character of the NLA response and the fluence of the final RSA/SA turnover $F_{RSA/SA}$ (if detected) varied between solvents and compounds. In order to delineate why this was the case we compared different fitting parameters for all 5,10-$A_2B_2$ porphyrins in three solvents: toluene, DMF and chloroform. Additionally, based on the four-level model, $\alpha(F_{RSA/SA})$ and $F_{RSA/SA}$ were numerically predicted for all of the compounds in solvents studied and compared against the parameters obtained.

$\kappa_1$ and $\kappa_2$ were plotted for all compounds in the three solvents studied (Figure 63). The values of $\kappa_1$ did not vary significantly between solvents for a given compound while the values of $\kappa_2$ were more affected by the solvent. It has to be noted that, even though the solvent effect on $\kappa_2$ was compound specific, in general $\kappa_2$ followed similar trends for different solvents. The brominated compounds and the free base porphyrins (2H_H, 2H_CCTMS and 2H_CCTIPS) consistently exhibited higher $\kappa_2$ values in toluene than in DMF.

Additionally, $\kappa_2$ in chloroform for metallated bromoporphyrins exhibited values similar to those obtained in DMF. An exception to this rule was $SnCl_2$_Br, which exhibited comparable values of $\kappa_2$ in toluene and chloroform and lower values in DMF. Interestingly, the tin complex of the TMS-ethynyl substituted series $SnCl_2$_CCTMS revealed a similar behavior in the three solvents. For metallated TMS-ethynyl substituted complexes, studies in toluene provided $\kappa_2$ higher or as high as in other solvents.

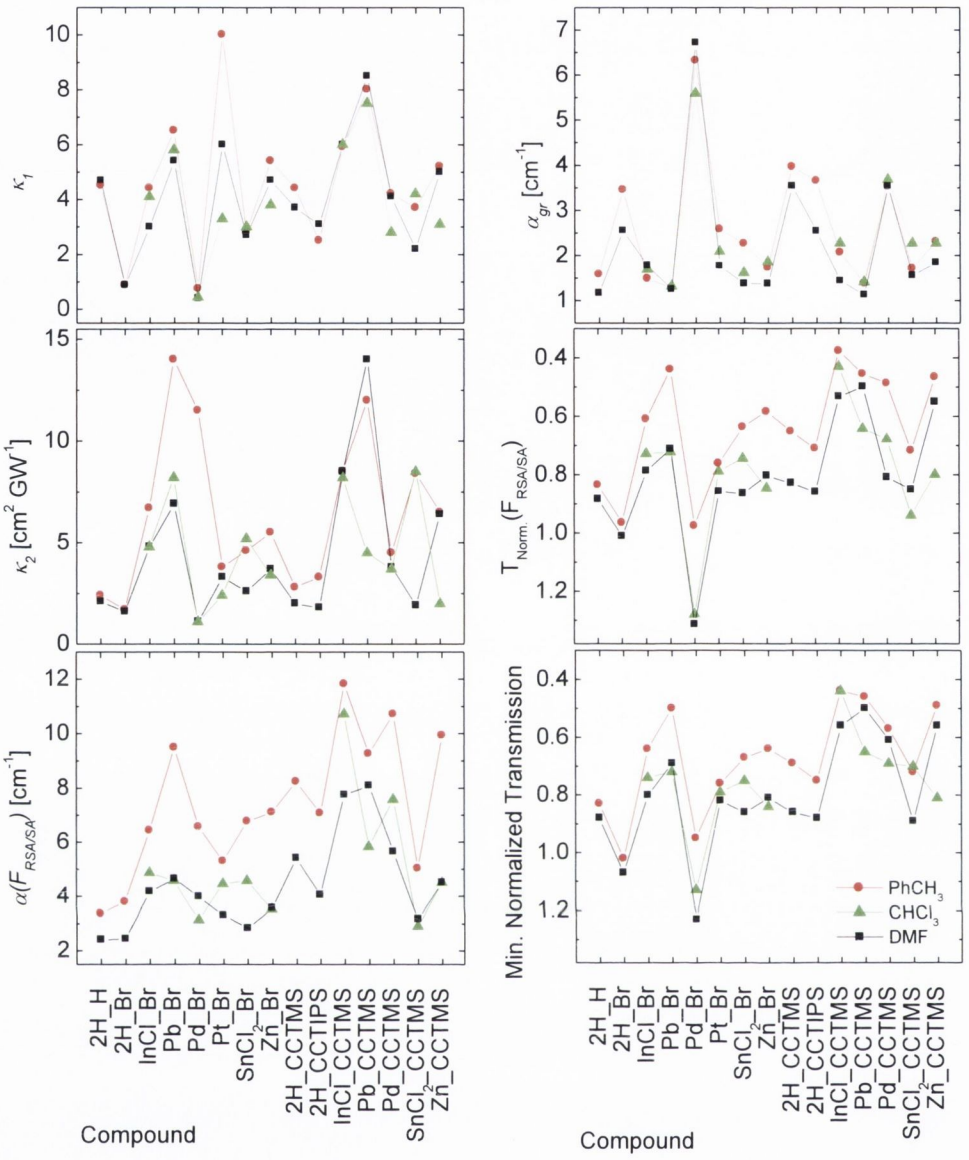



**Figure 63** Different parameter plotted for 5,10-$A_2B_2$ porphyrins in different solvents. Left column: ratios of the excited state one- and two-photon absorption cross-sections to the ground state absorption cross-section, $\kappa_1$ and $\kappa_2$ respectively, and the predicted values of absorption coefficient at RSA/SA turnover fluence $\alpha(F_{RSA/SA})$. Right column: linear absorption coefficient $\alpha_{gr}$, predicted normalized transmission at RSA/SA conversion fluence $T_{Norm.}(F_{RSA/SA})$ and the minimal normalized transmission obtained experimentally in fluence range 0 – 7 J.cm$^{-2}$.

$\alpha(F_{RSA/SA})$ was calculated for all compounds in all three solvents. The solvent trend in $\alpha(F_{RSA/SA})$ for a given compound correlated with that in $\kappa_1$ and $\kappa_2$. However, the degree of correlation varied between compounds. This can be explained with regard to the previous studies on the influence of the fitting parameters on $\alpha(F_{RSA/SA})$, which showed that all parameters must be considered simultaneously to understand the character of the

dependence of $\alpha(F_{RSA/SA})$ on a given parameter. Therefore, the values of saturation intensities must also be considered. Note, that the values of $\alpha(F_{RSA/SA})$ are much higher for studies in toluene compared to those in DMF and chloroform for the compounds examined.

To comprehend the correlation between $\alpha(F_{RSA/SA})$ and $\kappa_1$ and $\kappa_2$ further, $I_1$, $I_2$ and $I_3$ were plotted for different compounds in different solvents (Figure 64 middle row). Except for Pt_Br, $I_1$ does not vary significantly between solvents. With the exception of 2H_Br, Pd_Br and Zn_CCTMS, the solvent does not have a strong effect on $I_2$, either. However, $I_2$ tends to exhibit slightly lower values in toluene than in other solvents. No specific trend in the behavior of $I_3$ was observed for different solvents. As discussed before, low $I_2$ weakens the contribution of the one-photon process and enhances that of the two-photon process. Low $I_2$ combined with a high $\kappa_2$, obtained for many of the compounds in toluene, should therefore enhance the contribution of the two-photon process to $\alpha(F_{RSA/SA})$ in toluene compared to DMF and chloroform. Finally, $\alpha(F_{RSA/SA})$ also depends on the linear absorption coefficient $\alpha_{gr}$. No significant changes in $\alpha_{gr}$ were observed between solvents. It was, however, noted that $\alpha_{gr}$ was slightly higher in toluene, which, additionally, should increase $\alpha(F_{RSA/SA})$ in toluene.

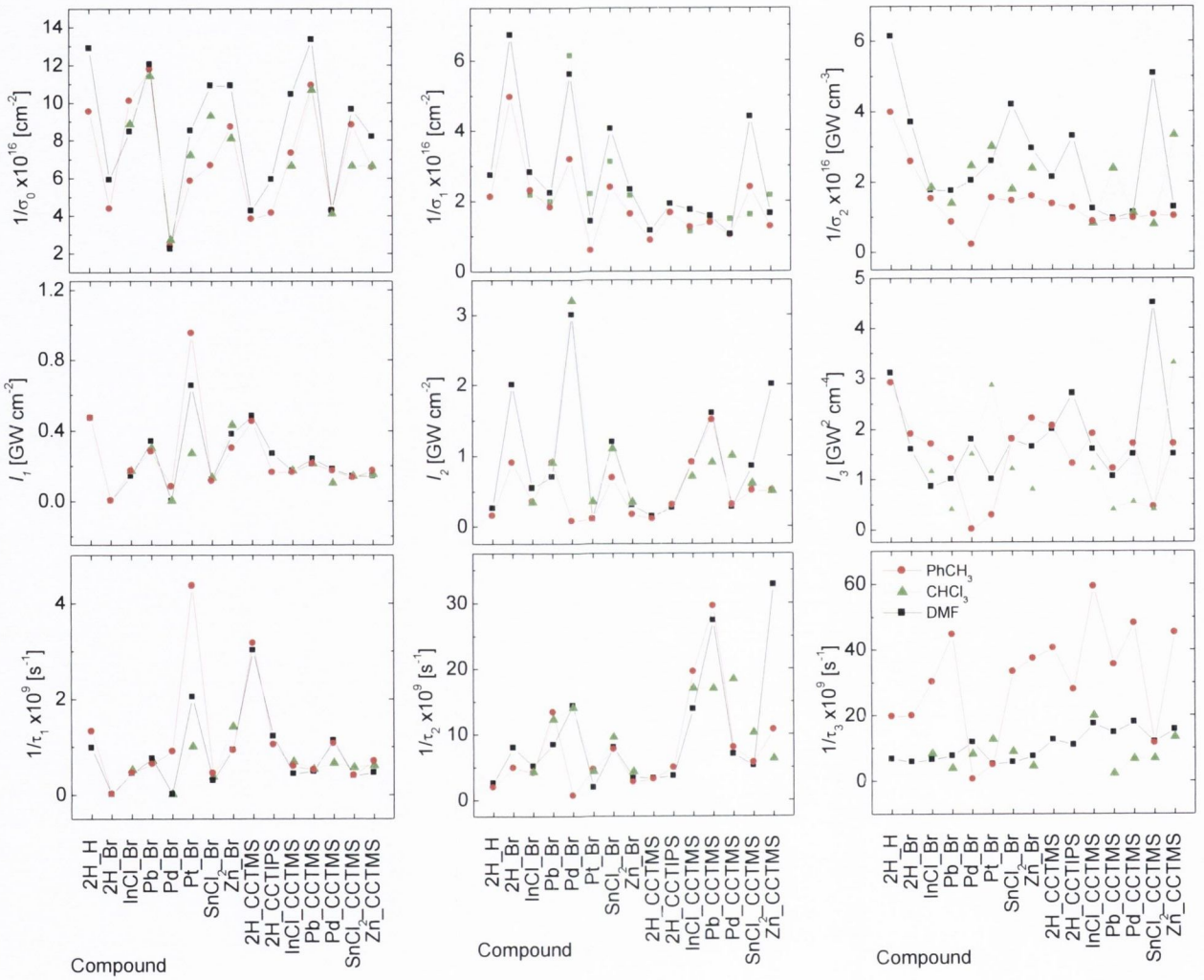



**Figure 64** Saturation intensities $I_1$, $I_2$ and $I_3$ (middle row),$1/\sigma_0$, $1/\sigma_1$ and $1/\sigma_2$ (upper row) and $1/\tau_1$, $1/\tau_2$ and $1/\tau_3$ (lower low), for 5,10-$A_2B_2$ porphyrins in different solvents.

Note, that $\alpha(F_{RSA/SA})$ is the maximal possible absorption coefficient at RSA/SA turnover fluence which varies between solvents. Therefore, in order to evaluate the OL capability of the material, $F_{RSA/SA}$ and the linear absorption coefficient $\alpha_{gr}$ must also be taken into account. Alternatively, the OL efficiency can be assessed by comparing the absorption coefficient at a chosen fluence for different compounds.

In order to do this, a fluence of 7 J.cm$^{-2}$ was chosen and the minimal values of the normalized transmission obtained for different compounds in three solvents at that fluence were plotted (for compounds which exhibited an RSA/SA switch below 7 J.cm$^{-2}$ the normalized transmission at RSA/SA conversion fluence is given) (Figure 63 Min. Normalized Transmission). Based on the values of $\alpha(F_{RSA/SA})$ the minimal possible transmission at RSA/SA conversion fluence $T_{Norm.}(F_{RSA/SA})$ were recalculated and plotted against fluence. Both plots were very similar. Therefore it can be concluded that trends observed for $\alpha(F_{RSA/SA})$ are a good approximation of trends for the absorption coefficient $\alpha(F)$ in the higher fluence range.

It can be seen from Figure 63 that most of the compounds exhibited the strongest transmission drop at the fluence of 7 J.cm$^{-2}$ (Min. normalized transmission) in toluene. Except for $SnCl_2$_Br, all brominated metal complexes exhibited a similar normalized transmission at the fluence of 7 J.cm$^{-2}$, both in DMF and in chloroform, whereas for the TMS-ethynyl substituted series the minimal transmission at the fluence of 7 J.cm$^{-2}$ did not follow any specific trend in DMF and chloroform.

As far as a solvent effect on the saturation intensities $I_1$, $I_2$ and $I_3$ is concerned, we previously showed that $I_1$ did not vary significantly between solvents. $I_2$ tended to be lower in toluene, and $I_3$ did follow any specific trend for different solvents. Since the saturation intensities are proportional to $I_i \sim 1/(\sigma_{i-1}\tau_i)$, $I_1$, $I_2$ and $I_3$ along with $1/\sigma_0$ ($\sim 1/\alpha_{gr}$), $1/\sigma_1$ ($\sim 1/(\alpha_{gr}\kappa_1)$), $1/\sigma_2$ ($\sim 1/(\alpha_{gr}\kappa_2)$), and $1/\tau_1$, $1/\tau_2$ and $1/\tau_3$ were plotted for different compounds and solvents, to see how they correlate (Figure 64). The lifetimes of the respective states were recalculated from $\tau_1 = h\nu/(I_1\sigma_0)$, $\tau_2 = h\nu/(I_2\kappa_2\sigma_0)$ and $\tau_3 = h\nu/(I_3\kappa_2\sigma_0)$, where $\sigma_0 = \alpha_{gr}/(CN_A)$, $C$ is a molar concentration and $N_A$ - Avogadro constant. Figure 64 shows that $1/\tau_1$ did not vary between solvents, whereas $1/\sigma_0$ reached only slightly higher values in DMF than in other solvents. As a result $I_1$ did not vary significantly between solvents. $1/\tau_2$ was not affected by the solvent, while $1/\sigma_1$ tended to reach higher values in DMF and chloroform than in toluene. Therefore, low $\sigma_1$ in

chloroform and DMF resulted in higher $I_2$ in these solvents. Finally, $1/\tau_3$ reached much higher values in toluene than in other solvents, but at the same time $1/\sigma_2$ tended to be lower in toluene than in other solvents. These correlations led to comparable values of $I_3$ in toluene, DMF and chloroform (Figure 64).

$\tau_1$ was found to be of the order of $10^{-10}$ s while $\tau_2$ and $\tau_3$ were one order of magnitude lower for most compounds in all solvents studied. Typically the lifetime of $\tau_1$, which is the lifetime of the first excited singlet state, is of the order of ns while lifetimes of higher excited states are of the order of picoseconds for macrocyclic dyes. This is in good agreement with the obtained results. It should be noted that Dini *et al.* proposed a very similar model for hemiporphyrazine with the TPA process arising from higher excited states.[212] Compared to our findings, they reported comparable lifetimes associated with the second excited state $\tau_2$ ~$10^{-10}$, but a shorter lifetime for the highest excited state $\tau_3$ ~$10^{-13}$. They did not, however, observe an RSA/SA switch at higher fluences which we associate with the longer lifetime $\tau_3$ detected for the 5,10-$A_2B_2$ porphyrins. Longer $\tau_3$ results in a lower saturation intensity $I_3$, which leads to RSA/SA turnover occurring at lower intensities/fluences in the examined 5,10-$A_2B_2$ porphyrins.

Finally, to study the solvent effect further, the predicted values of $F_{RSA/SA}$ were plotted (Figure 65). They appear to be in good agreement with the measured values for the compounds exhibiting RSA/SA turnover, which demonstrates the validity of the model over a broad fluence range. It can be seen that $F_{RSA/SA}$ tends to be slightly higher in toluene than in other solvents, and that $F_{RSA/SA}$ follows similar trends to those of $I_3$ in all solvents for most of the compounds. $F_{RSA/SA}$ strongly depends on $I_3$ provided that the two-photon absorption has a greater contribution than the one-photon process to the maximal transmission drop. Therefore, the observed correlation implies that the two-photon process has a greater contribution to transmission in higher fluence regime for the studied compounds.

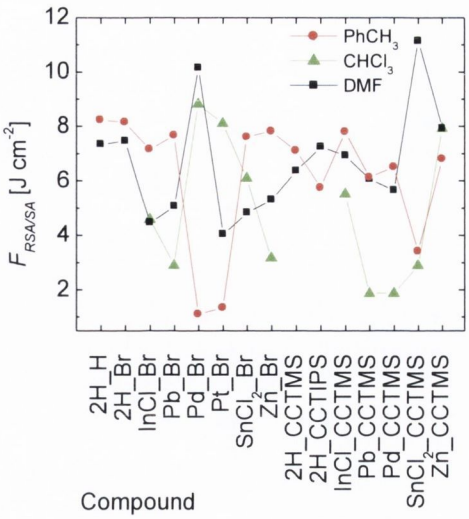



**Figure 65** Numerically predicted values of $F_{RSA/SA}$ for 5,10-$A_2B_2$ porphyrins in different solvents.

It has to be noted that an exceptionally low $F_{RSA/SA}$ was obtained for Pd_Br and Pt_Br in toluene, both compared to the same compounds in DMF and chloroform, and to the other compounds in all solvents. These two metal complexes exhibited an RSA/SA turnover at very low fluences in toluene, which can be associated with low $I_3$.

As far as responses recorded in DMF and chloroform are concerned, similarities in the solvent effect on NLA responses were observed for the complexes from the two series (brominated and TMS-ethynyl substituted macrocycles) having the same central metal. Both indium and both tin complexes (InCl_Br and InCl_CCTMS, and $SnCl_2$_Br and $SnCl_2$_CCTMS) exhibited a more rapid drop in transmission with the input fluence in chloroform than in DMF. However, the solvent effect on the fitting parameters for those compounds was not particularly strong or consistent.

The NLA curves for Pb_Br, Pb_CCTMS, Zn,_Br and Pd_CCTMS in DMF were very similar in the lower fluence regime to those in toluene for the respective compound. However, in the higher fluence range the NLA curves diverged (Figure 57) and the RSA/SA switch for these compounds occurred at lower fluence in chloroform than in DMF. For all of these compounds $I_3$ was lower in chloroform than in DMF.

In comparison to other compounds, NLA responses of $SnCl_2$_CCTMS and Zn_CCTMS varied the most between DMF and chloroform. It was noted that for these compounds $\kappa_1$ and particularly $\kappa_2$ were higher in the solvent in which a more rapid transmission drop with the input fluence was observed *i.e.* in chloroform for $SnCl_2$_CCTMS and in DMF for Zn_CCTMS.

In summary, the studies in toluene generally provided the best OL characteristics for most of the compounds analyzed. This was associated with the fact that in toluene the TPA is stronger than in the other solvents used. Conversely, for DMF and chloroform the solvent effect on the OL characteristics was more compound-specific and therefore difficult to identify.

Two compounds, 2H_Br and Pd_Br, exhibited a distinct character of the NLA response in comparison to other compounds, *i.e.* SA which switched to RSA when the input fluence was increased. Furthermore, a consecutive switch back to SA was observed in some of the measurements when the fluence was increased further. Refer to 5.5 for a broader explanation of the phenomenon.

The normalized transmission increased to a slightly higher value through SA, and the SA/RSA switch occurred at a lower fluence in toluene than in DMF for 2H_Br (Figure 57). The consecutive RSA/SA switch was detected for studies in DMF, but it did not occur in toluene within the range of fluence studied. Except for $I_2$ which was considerably lower for toluene than for DMF, the fitting parameters did not vary considerably between the two solvents. The lower $I_2$ weakens the effectiveness of the one-photon process which consequently strengthens the SA character of the response. As a result, normalized transmission reaches a higher value in toluene through SA. Lower $I_2$ also causes the faster saturation of a one-photon process, and therefore the consecutive two-photon process starts to contribute more effectively to the NLA response at lower fluences. Therefore, an SA/RSA switch occurs at lower fluence in toluene.

With regard to responses of compound Pd_Br in different solvents, an increase in the normalized transmission through SA was highest in DMF, lower in chloroform, and lowest in toluene. An SA/RSA switch occurred at comparable fluences in DMF and chloroform, and at much lower fluence in toluene. The consecutive RSA/SA turnover was detected at low fluence in toluene and at significantly higher in DMF. In chloroform, an RSA/SA switch was not detected within the studied fluence range. The values for $\kappa_2$, $I_2$ and $I_3$ were particularly different in toluene from those in DMF and chloroform. $\kappa_2$ was significantly higher and both saturation intensities $I_2$ and $I_3$ were notably lower in toluene compared to the other two solvents. As demonstrated in the preceding paragraph, high $\kappa_2$ weakens SA, while low $I_2$ strengthens it. Evidently, the effect of $I_2$ is weaker than that of $\kappa_2$ as the transmission increase through SA was the lowest in toluene. Lower $I_2$ in toluene leads to faster saturation of the ineffective one-photon process, and therefore the consecutive two-

photon process starts to contribute effectively to the NLA signal at lower inputs. This shifts the RSA/SA switch into lower a fluence regime. Furthermore, significantly higher $\kappa_2$ in toluene should additionally lower the value of the SA/RSA turnover fluence. For responses in DMF and chloroform $I_2$ and $I_3$ were more affected by the solvent than other parameters. In DMF, $I_2$ was lower and $I_3$ was higher than in chloroform. Lower $I_2$ in DMF led to stronger increase in the normalized transmission through SA. Finally, the numerically predicted fluence of RSA/SA switch $F_{RSA/SA}$ in chloroform was lower than that predicted and measured in DMF. $F_{RSA/SA}$ in both DMF and chloroform were higher than that in toluene. The trend in RSA/SA turnover fluence clearly correlates to that in $I_3$, for all three solvents studied.

Summarizing, for both 2H_Br and Pd_Br, the SA/RSA turnover occurred at the lowest fluence.

## 6.5 Summary

We carried out open Z-scan studies in the ns regime for two series of free base and metallated 5,10-$A_2B_2$ porphyrins in various solvents. The compounds exhibited different characters in the NLA responses, depending on their molecular structure. Most of the compounds exhibited a drop in transmission with input fluence (RSA) which switched to an increase (SA) in the higher fluence regime in some of the experiments. A couple of compounds exhibited SA first, which then turned to RSA, and in some of the experiments turned back to SA again in the higher fluence regime. The solvent type was found to affect the magnitude of the transmission drop or increase and the RSA/SA or SA/RSA turnover fluence. In order to understand the solvent effect better, the recorded responses were fitted with a four-level model, where a one-photon excited state absorption is followed by a two-photon process. The two-photon absorption process was enhanced in toluene in comparison to the other solvents. This was attributed to a stronger transmission drop in this solvent. The RSA/SA turnover fluence correlated to the saturation intensity of the two-photon process ($I_3$) for different compounds in all solvents studied. However, no specific solvent trend in $I_3$ was found.

For the compounds exhibiting a SA/RSA (or an SA/RSA/SA) character of the response, SA/RSA turnover occurred consistently at the lowest fluence in toluene in comparison to the other solvents.

As far as open Z-scan results in chlorobenzene and chloroform/chlorobenzene mixture solutions are concerned, NLS was found to contribute to the NLO responses for many of the compounds in higher fluence range. This phenomenon was associated with the photodegradation of chlorobenzene. For weaker nonlinear absorbers (brominated compounds), the contribution of NLS led to an enhancement of the OL efficiency. For stronger nonlinear absorbers (TMS-ethynyl substituted compounds), NLS led to a comparable OL effect to that based on NLA.

# Chapter 7 Laser induced protonation of free base porphyrins in chloroform resulting in the enhancement of positive nonlinear absorption

## 7.1 Introduction and outline

It was observed that free base porphyrins in chloroform solution irradiated with a focused laser beam, in an open Z-scan set-up, changed color from purple to green in the area where the laser penetrated the sample. As a similar phenomenon was not observed in other solvents like toluene and DMF, the effect was associated with the solvent. The effect was substantially suppressed when base was added to the porphyrin solution. We proposed that upon illumination with focused laser beam chloroform undergoes photodegradation which generates protonic species. The species react with the porphyrin to give its protonated green form. We also demonstrated that protonation efficiently improves the optical limiting performance of free base compounds.

## 7.2 Theoretical background

Nitrogen atoms in the central core of the porphyrin can be protonated under acidic conditions to form porphyrin diacids resulting in conformational changes leading to highly nonplanar structures.[230, 231] The conformational changes are manifested in variations of the photophysical properties. The ground state absorption bands are shifted bathochromically and the number of Q-bands is reduced upon protonation. Fluorescence, intersystem crossing and first excited singlet state lifetimes decrease upon protonation, as does the quantum yield for triplet state formation. Moreover, the ratio of the excited to ground state absorption cross-section increases upon protonation.[232-236] The latter change is especially desirable for application in passive optical limiting devices.

Protonation of free base porphyrins can be carried out deliberately simply by adjusting the pH of the solution. Recent reports indicate that protonation can also be achieved

unintentionally by subjecting free base porphyrins to sonification in a variety of chlorinated solvents. This phenomenon was associated with the formation of acidic products from sonolysis of the solvents, which reacted with free-base porphyrins to give their protonated form.[237] Here we report a similar phenomena arising upon subjecting free base porphyrins in chloroform solution to a focused 532 nm 6 ns pulsed laser beam. We associate this phenomenon with the photodegradation of the solvent providing acidic species which transform the free base compound to the respective protonated form.

## 7.3 Experimental details

Characterization of the nonlinear absorption of 2H_H and 2H_Br was carried out with open Z-scan technique following the general procedure reported in 2.2.2. Concentrations of porphyrin solutions used in this study were in the range of $2–3 \times 10^{-4}$ M. The cell with 1 mm path length was used in the measurements. Protonation of free base compounds was achieved upon addition of a few drops of trifluoroacetic acid (TFA). Likewise, a few drops of triethylamine (TEA) were added to prevent protonation in chloroform solution in additional experiments.

## 7.4 Results and discussion

Deliberate protonation of the chloroform solution of 2H_H and 2H_Br with TFA induced changes to the ground state absorption spectra. The number of Q-bands was reduced and the spectrum was shifted bathochromically. Addition of TFA resulted in a color change from purple to green (Figure 66). Similar red shifts of the Soret and Q-bands observed upon protonation were previously reported for porphyrins and were associated with the induction of a nonplanar deformation.[119, 230-232, 238, 239] Reduction in the number of Q-bands is typically observed upon protonation or metal insertion and arises from an increase in the symmetry of the molecule. Note that the absorption spectrum of 2H_Br, both in free base and protonated form, is red-shifted in comparison to 2H_H. This is in accordance with previous reports which showed that bromination of meso positions induces a bathochromic shift in the UV-vis absorption spectra.[116, 119]

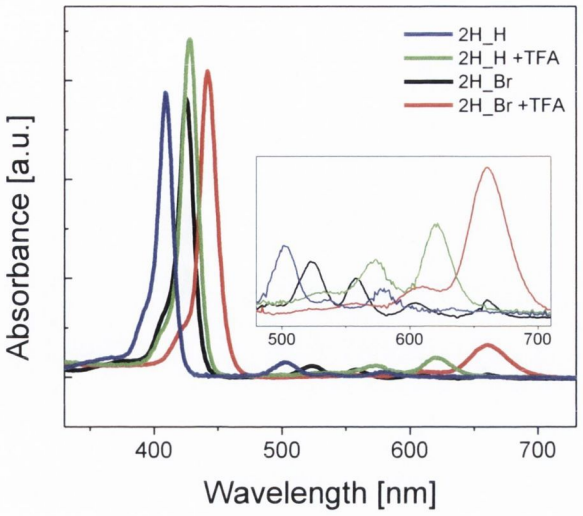



**Figure 66** UV-vis absorption spectra of 2H_H and 2H_Br in free base and protonated forms (+ TFA).

We observed that a chloroform solution of 2H_H subjected to a focused Gaussian beam in an open Z-scan experiment changed color from purple to green in the area where the laser penetrated the sample. The phenomenon was enhanced when the laser energy was increased further in subsequent experiments. The sample was shaken after each of the experiments in order to refresh the experimental volume. No such phenomenon was observed by us before for free base porphyrins in other solvents such as toluene or DMF. We consider the photoinduced protonation of free base porphyrin with chloroform acting as a proton source as a possible explanation for the observed process. Photolysis of chlorinated solvents has been widely noted in the literature and has been demonstrated to provide different species including protons through various channels depending on the solvent nature and experimental conditions used.[240, 241] Further studies will be needed to explore and unravel the exact mechanism of the observed phenomenon.

In order to prove that protonation was involved we carried out open Z-scan studies on a sample containing TEA in order to suppress protonation. Additionally, we investigated NLA of a fully protonated sample in chloroform with TFA. The formation of the green cloud was indeed inhibited in the sample with TEA, however only in experiments at lower input energies (~E < 100 μJ). When the energy was increased a green area close to the laser spot became apparent and it slowly disappeared after each experiment. This effect was less pronounced than in neat chloroform porphyrin solution. The open Z-scan data were manipulated and plotted as normalized transmission *versus* pulse energy density and are shown in Figure 67. We also present data recorded in toluene for comparison.

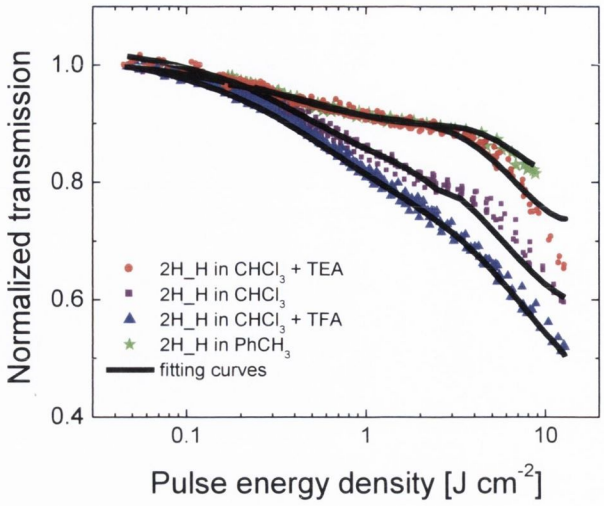



**Figure 67** Optical limiting curves plotted as normalized transmission *versus* pulse energy density for compound 2H_H under various experimental conditions.

The three different samples investigated (chloroform solution of compound 2H_H, and the same solutions with added TEA or TFA) provided different NLA responses. The transmission dropped to the lowest minimal value for the fully protonated sample while the sample with added TEA exhibited the weakest drop in transmission. The curve representing studies in pure chloroform exhibited a pattern in between the other two curves. Figure 67 shows that studies carried out in toluene, in which no color change was observed upon illumination, recovered those recorded for chloroform with added TEA over a broad fluence range. It should be noted that studies at very high input energies were inaccessible in toluene as the asymmetric profile of the Z-scan traces indicated the onset of degenerative processes. Based on these results it can be concluded that a porphyrin in its protonated form absorbs light efficiently. Secondly the addition of base inhibits the process leading to an enhancement of the OL performance in pure chloroform porphyrin solution. As protonated species are highly absorptive to laser light, their formation results in an improvement of the OL efficiency which we believe explains the response recorded for neat chloroform solutions of 2H_H. As a color change was observed for studies at higher input energies for the sample with added TEA, protonation cannot be ruled out fully for these experiments. However, as the NLA curve representing studies in chloroform with added TEA recovered the curve representing studies in toluene to fluences up to about 7 J.cm$^{-2}$, it is assumed that protonation is efficiently inhibited by the presence of TEA up to that fluence. It can be observed that two curves start to diverge in the higher fluence regime. However, it is difficult to assess if this arises due to laser induced protonation or is associated with solvent effects akin to those recently demonstrated by us to impact the

NLA response of compound 2H_H and other 5,10-$A_2B_2$ porphyrins. The curve representing studies in chloroform diverged from the curve of the sample with added TEA which inhibited protonation at very low input fluences. Thus, it can be concluded that fluences of the order of 0.3 $J.cm^{-2}$ are sufficient to trigger the effective formation of protonated species of compound 2H_H.

In the preceding chapters we demonstrated that compound 2H_H in its free base form (in toluene and DMF) and other 5,10-$A_2B_2$ porphyrins, exhibit a complex NLA behavior which can be rationalized with a four-level model . This four-level model was successfully used to fit the responses recorded in chloroform according to the previously established procedure (4.4.3). The best fit parameters used in the modeling of the responses are listed in Table 5. Results obtained for studies on compound 2H_H in toluene can be found in Table 4 (p. 159).

**Table 5** Comparison of the best fit parameters used in the modeling of the responses of compound 2H_H and 2H_Br (C – chloroform, T - toluene).

| #/ solvent | $\alpha_{gr}$ [$cm^{-1}$] | $\kappa_1$ | $\kappa_2$ [$cm^2GW^{-1}$] | $I_1$ [$GWcm^{-2}$] | $I_2$ [$GWcm^{-2}$] | $I_3$ [$GW^2cm^{-4}$] |
|---|---|---|---|---|---|---|
| 2H_H/C+TEA | 1.31 | 3.1 | 3.6 | 0.14 | 0.35 | 3.8 |
| 2H_H /C | 1.34 | 4.5 | 5.8 | 0.20 | 0.45 | 3.5 |
| 2H_H /C+TFA | 1.49 | 4.9 | 8.0 | 0.25 | 0.60 | 2.5 |
| 2H_Br/C | 2.77 | 0.85 | 4.5 | 0.03 | 0.60 | 1.8 |
| 2H_Br/T+TFA | 1.08 | 12 | 8.0 | 0.53 | 1.00 | 1.1 |

The theoretical curves diverged from the experimental data in the higher fluence regime for studies carried out in neat chloroform and solutions with added TEA. Most likely, the concentration of the protonated species varies with the input fluence within the experimental volume giving rise to the observed deviations. More complex procedures of data fitting, which would have to consider concentration variations of different species with the input fluence, possibly could provide a better fit. The theoretical curve matched well the experimental data for the fully protonated compound with TFA over the whole fluence range investigated. The applicability of the model implies that protonation does not affect the excited state structure of compound 2H_H.

It can be observed that $\kappa_1$ and $\kappa_2$, being the ratios of the excited one- and two-photon absorption- to ground state absorption cross-section, and the saturation intensities $I_1$ and $I_2$, increase for the studies carried out on the three solutions in the following order: chloroform solution with added TEA < neat chloroform solution < chloroform solution with added TFA. Meanwhile, $I_3$ decreases in the same order (Table 5). We associate the stronger transmission drop observed for the following three samples with an increase in parameters $\kappa_1$ and $\kappa_2$. The finding that protonated species exhibit a higher ratio of the excited to ground state absorption and better OL efficiency agrees with previous reports. According to our previous studies on the effect of the particular parameters on NLA performance (6.4.2.1), the trends observed for saturation intensities $I_1$, $I_2$ and $I_3$ weaken the OL performance of the protonated sample. However, clearly this effect is negligible in reference to that exerted by high $\kappa_1$ and $\kappa_2$ obtained for the protonated porphyrin. Higher $I_1$ causes the saturated regime of one-photon excited state absorption to be accessed more slowly with input fluence. A similar conclusion refers to high $I_2$ in reference to two-photon processes. Provided that $\kappa_2$ is high enough in reference to $\kappa_1$, which is the case in the present studies, high $I_2$ weakens the maximal transmission drop. This happens as a more effective two-photon process is suppressed. As far as $I_3$ is concerned, we previously found that high $I_3$ is important to prevent consecutive processes arising from state $N_3$. As these processes are highly unabsorptive their contribution lowers the transmission drop which consequently leads to RSA/SA turnover.

As protonation turned out to be an efficient means of improving the OL performance, we decided to investigate its effect on the NLA of another compound, *i.e.* porphyrin 2H_Br. The NLA response of compound 2H_Br in its protonated form (with TFA) was studied in toluene. For comparison, data of the free base form in toluene are included. Additionally, we also carried out open Z-scan studies on compound 2H_Br in neat chloroform solution (Figure 68).

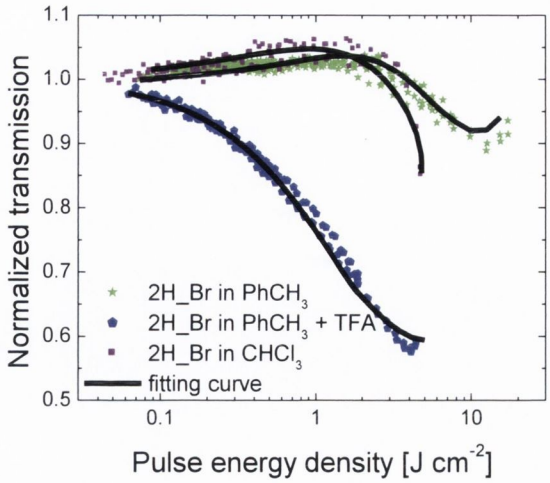



**Figure 68** Optical limiting curves plotted as normalized transmission *versus* pulse energy density for compound 2H_Br under different experimental conditions.

Compound 2H_Br is characterized by high linear absorption at the experimental wavelength of 532 nm which interrogated the compound's Q band. Provided that the absorption arising from the excited state is higher than that arising from the ground state the material exhibits SA. Such a behavior, although weakly pronounced, was detected for compound 2H_Br in toluene and chloroform up to fluences of about 2 J.cm$^{-2}$. A subsequent switch from SA to RSA could be observed for both solvents at higher fluences. Another switch in behavior, again to SA, was observed for studies in toluene at even higher fluences. Again, this NLA behavior could be modeled using our four-level model. The experimental wavelength of 532 nm was no longer in the Q-band wavelength range for the protonated form of compound 2H_Br (Figure 66). The fully protonated compound exhibited RSA/weak SA (Figure 68). The responses recorded in chloroform recovered that in toluene over a broad fluence range up to 3.5 J.cm$^{-2}$. This implies that 2H_Br has a much weaker affinity to protonation than 2H_H. Clearly, effective protonation would lead to a strong transmission drop as was observed for the dication of compound 2H_Br. It remains open whether the observed switch from SA to RSA in chloroform is associated with induced protonation or a solvent effect, which was demonstrated previously to shift SA/RSA turnover fluence. Nevertheless, different parameters follow similar changes upon protonation as those observed for compound 2H_H. $\kappa_1$, $\kappa_2$, $I_1$ and $I_2$ increased and $I_3$ decreased for a fully protonated sample in reference to the free base form. Additionally, it was observed that the fully protonated compound exhibited RSA/SA turnover at lower fluence than the free base compound which we associate with higher $I_3$ obtained for the latter form of the compound.

## 7.5 Conclusions

Protonation of free base porphyrins is a quick and easy way of enhancing their optical limiting efficiency. Special care must be taken while performing studies in chloroform solutions on free base porphyrins with focused laser beams as compounds can undergo protonation under the experimental conditions, which affects their photophysical properties.

# Chapter 8 5,10-$A_2B_2$ porphyrins as materials for organic light emitting diodes

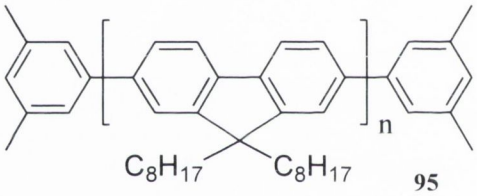
Organic light emitting diodes (OLEDs) are an emerging class of diodes that have already found commercial applications in mobile devices and TV displays. In comparison to typical LEDs whose function is based on doped silicon, OLEDs use emissive organic materials which range from small molecules, used as dopants or alone, to diverse polymers. OLEDs offer better light emitting efficiency and are therefore less power demanding than typical LEDs. This makes them a highly desirable solution for portable devices. A big disadvantage of OLEDs is their lifetime. Organic materials are liable to oxidation and other degenerative processes which decrease a materials' emitting efficiency. OLEDs potential applications are not limited to displays. They are being considered as a source of general lighting, components of the panels that can be introduced to walls or windows, and flexible paper – epaper. More advanced potential applications of OLEDs are seen in medical devices, sensors, optical communication and memory devices.

The key component of an OLED device is an emissive organic layer placed between a usually transparent anode – most commonly indium tin oxide (ITO) and a metal cathode. When a voltage is applied to the electrodes, holes and electrons are injected from anode and cathode respectively. The injected charges migrate towards each other and eventually meet and recombine to form excitons – *i.e.* an electron-hole pairs. Eventually, excitons decay releasing energy as photons or heat. The wavelength of the emitted light depends on the structural features of the emitting material.

An important group of OLEDs which attracts more and more attention is phosphorescent OLEDs – PhOLEDs. It is known from quantum mechanical statistics that material based on fluorescence can exhibit maximal efficiency of 25% with the rest of the carriers being lost as heat. A phosphorescence based emitter (PhOLEDs) can reach 100% efficiency with

all of the carriers being used in light emission. Porphyrins constitute an important and promising group of compounds for PhOLEDs.[242-244]

The potential of some of the newly synthesized 5,10-$A_2B_2$ porphyrins (2H_Br, Pd_Br, Pb_Br, Pt_Br, 2H_CCTMS, Pd_CCTMS, Pb_CCTMS) as OLED materials was investigated. The studies were entirely carried out by Brian Tuffy and are fully presented in his Master Thesis.[245] In general brominated compounds were not promising materials for OLED applications as they did not exhibit any significant photoluminescence (PL). It was proposed that bromine quenches the emission. 5,10-$A_2B_2$ metallated porphyrins with a TMS-ethynyl substituent instead of bromine were more promising compounds. A significant PL signal was measured for these compounds. The palladium complex Pd_CCTTMS was identified as the most promising compound from all of the compounds studied. Even though no electroluminescence (EL) was detected for Pd_CCTMS based diode, the compound was successfully used as dopant in poly(9, 9-dioctyluorenyl-2,7-diyl) (PFO) **95** host to exhibit strong red EL (Figure 69).




**95**

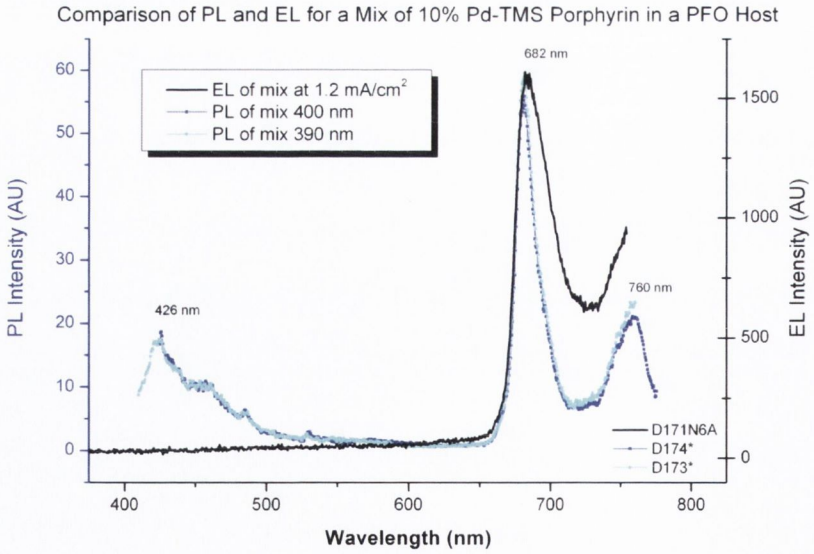



**Figure 69** EL and PL spectra of 10% Pd_CCTMS doped PFO.

Optical properties of Pd_CCTMS doped PFO were found to depend on the dopant concentration. An increase in Pd_CCTMS concentration resulted in lower emission intensity, which was attributed to aggregation. Förster resonance energy transfer (FRET) between the palladium porphyrin and the PFO host was identified. This energy transfer process, which is dependent on the overlap of the host emission spectrum with the absorption spectrum of the dopant, is desirable in OLEDs as it enhances the quantum efficiency of the device.[243, 244, 246]

Besides OL, 5,10-$A_2B_2$ porphyrins were demonstrated be interesting candidate for OLED application.

# Chapter 9 **Conclusions and future outlook**

The studies carried out on structurally structurally diversified free base and metallated meso substituted porphyrin monomers, dimers and trimers in different meso configuration patterns enabled to identify correlation between compound structure and its OL performance. It should be highlighted that most of the studies published so far concerned porphyrins with equivalent meso substituents. Besides the electronic character of the meso substituents, it was also the meso configuration pattern which impacted the NLA properties of porphyrins. These findings show that both the configuration pattern and the electronic character of the meso substituents must be tailored simultaneously to maximize the OL efficiency. With regards to this, the rational design of the porphyrin for OL use remains a challenging task.

Metallation or Sonogashira coupling reactions proceed well for 5,10-$A_2B_2$ porphyrins. The yields of these reactions were comparable to those typically reported for porphyrins in other meso substitution patterns. This indicates that the meso substitution pattern has little effect on the porphyrin's reactivity in the reactions discussed.

Depending on the structural features, 5,10-$A_2B_2$ porphyrins exhibited various types of NLA response in the open Z-scan experiments at 532 nm with 6 ns pulsed laser. These responses involved a transmission drop with intensity, which is typically observed for porphyrins and similar compounds, or more complex responses which switched from a transmission increase to a decrease (evolving with input fluence) or *vice versa*. Although the character of the responses varied between 5,10-$A_2B_2$ compounds, the modeling studies revealed that a four-level model with simultaneous two-photon absorption arising from the higher excited state (1 + 1 + 2 photon absorption) best fitted all of the responses. This suggested that 5,10-$A_2B_2$ porphyrins exhibited photophysical properties different from those of compounds in other substitution patterns. Yet, further experimental studies are needed to confirm the mechanism.

With regards to the OL performance of two series of free base and metallated 5,10-$A_2B_2$ porphyrins, the TMS-ethynyl meso substituent was found to be a more promising OL group than a bromine atom at a equivalent positions. Except for lead, the effect of the metal on the OL performance was not consistent for the two series of compounds. This showed that the effect of the substituent was significant.

It was found the solvent had an influence on the OL performance of 5,10-$A_2B_2$ porphyrins. It was showed that solvent can either induce changes to NLA and/or provoke additional OL processes like nonlinear scattering. It was also demonstrated that free base compounds can undergo protonation in chloroform solutions upon laser light, which enhances NLA. The above shows that the choice of the solvent is important in OL studies and special care must be taken when interpreting the results obtained as solvent can induce additional OL mechanisms.

All the studies covered in this thesis were carried out in solution. For device purposes the material will have to be implemented into the solid state, which necessities further studies. The other aspect that should be addressed in the future is the characterization of the OL performance of the compounds studied at different wavelengths in order to prove the broadband character of the NLA response. It is believed that OL efficiency of the compounds studied should be enhanced at longer wavelength. Additionally, full characterization of the optical properties should be carried out, especially for 5,10-$A_2B_2$ porphyrins which exhibited unique NLA response. This would enable the NLA mechanism proposed for these compounds to be confirmed and also would enhance the knowledge on this still unexplored but promising class of porphyrins.

# Chapter 10 **Experimental**

## 10.1 Instrumentation and general considerations

NMR spectra were recorder on Bruker DPX 400 (400.13 MHz for $^{1}H$ NMR, 100.62 MHz for $^{13}C$ NMR) and/or Bruker AV 600 (600.13 MHz for $^{1}H$ NMR, 150.2 MHz for $^{13}C$ NMR). Chemical shifts recorded in ppm refer to tetramethylsilane (TMS) set at 0.00 ppm. Data are reported as follows: chemical shift, multiplicity (s: singlet, d: doublet, dd: double doublet, t: triplet, br: broad, m: multiplet), coupling constant (*J* in Hz), integration and assignment. High resolution mass spectroscopy (HRMS) was carried out on a Micromass/Waters Corp. USA liquid chromatography time-of-flight (TOF) spectrometer equipped with electrospray (ES) source or a matrix-assisted laser desorption/ionization (MALDI) Q TOF Premier MS system. Melting points were measured with Stuart SMP10 melting point apparatus. Thin layer chromatography (TLC) was performed on silica gel $60F_{254}$ (Merck) precoated aluminum sheets. Chromatography on silica gel was carried out using a forced flow of the indicated solvent system on Fluka Silica Gel 60 (230-400 mesh). Tetrahydrofuran (THF) was distilled from sodium/benzophenone under argon. All commercial chemical were supplied by Aldrich and used without further purification.

Nonlinear absorption properties were investigated with open aperture Z-scan technique. The second harmonic, 532 nm, of a Q-switched Nd:YAG laser was used with a pulse repetition rate of 10 Hz. The beam was spatially filtered to remove the higher order modes and tightly focused with a 9 cm focal length lens. The schematics illustration of the experimental set-up is shown in Figure 70.

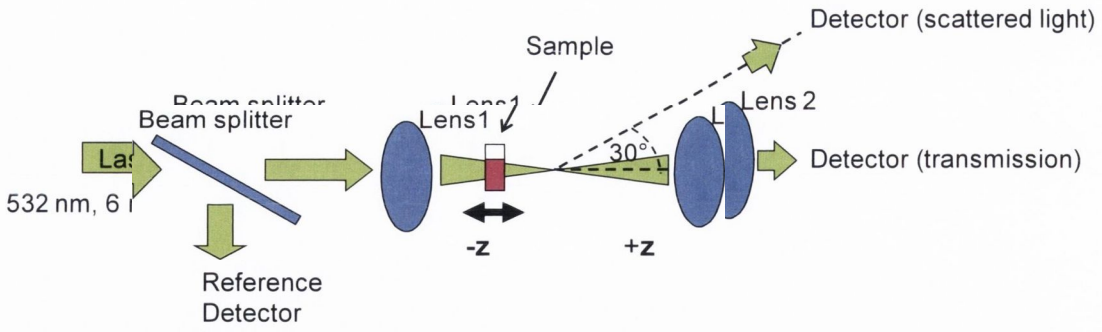



Figure **70** Schematic representation of the Z-scan technique.

UV/vis absorption spectra were performed on Shimadzu multiSpec-1505 using dichloromethane (unless indicated otherwise).

## 10.2 Syntheses

2,5-bis(hydroxymethylpyrrole) (**70**), tripyranne (**79**) and 5,10-di(*p*-tolyl)porphyrin (**48**) were obtained according to procedures reported in literature.[183, 182, 159]

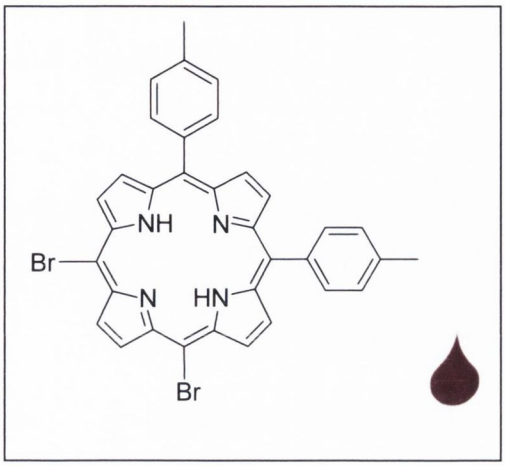
General procedure **A** – Sonogashira coupling:

A Schlenk tube was filled with Ar and charged with brominated porphyrin (1 equiv.) in dry THF/$NEt_3$. The solution was degassed by three freeze-pump-thaw cycles and put under Ar again. Alkynyl substrate (4 - 5 equiv.), copper(I) iodine (0.25 equiv.) and $Pd(PPh_3)_2Cl_2$ (0.1 or 0.25 equiv.) were added, and the reaction mixture was stirred at room temperature until the starting material was consumed. Then $CH_2Cl_2$ (30 mL) was added and the solution was washed with water and dried over $MgSO_4$. Further purification was carried out as indicated.

General procedure **B** – Pb(II) insertion with $Pb(acac)_2$:

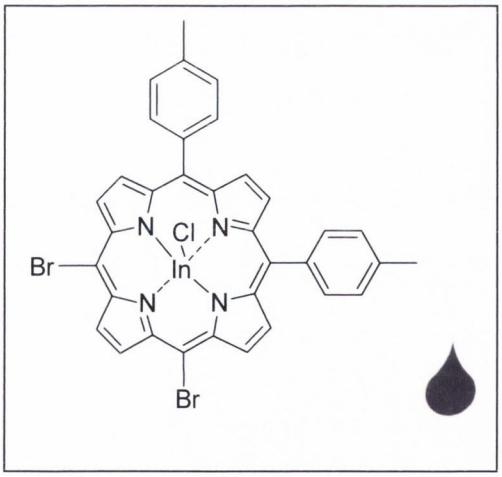
A solution of porphyrin (~100 mg, 1 equiv.) in toluene/MeOH (20 mL, 1:1 v/v) and $Pb(acac)_2$ (10-20 equiv.) was stirred at RT. The reaction was monitored by UV-vis spectroscopy. As soon as the reaction was completed water was added and the mixture was extracted with dichloromethane (DCM). The organic phase was subsequently washed twice with $H_2O$ and dried over $MgSO_4$. The solvent was removed under reduced pressure and the product was recrystallized from DCM/MeOH.

**5,10-Dibromo-15,20-di(*p*-tolyl)porphyrin (80):**




In 100 mL flask, 5,10-ditolylporphyrin **48** (100 mg, 0.204 mmol) was dissolved in $CHCl_3$ (50 mL) and pyridine was added (0.05 mL). Solution was cooled to 0 °C and NBS was added (91 mg, 0.512 mmol). The reaction was monitored by TLC. After 15 min reaction was stopped with acetone (5 mL). The volatiles were removed and the solid was solved in $CH_2Cl_2$, and then filtered through silica gel followed by recrystallization from $CH_2Cl_2$/MeOH to yield dark purple crystals of the title compound (103 mg, 0.159 mmol, 78%). M.p. = 261 °C; $R_f$ = 0.52 ($SiO_2$, $CH_2Cl_2$/*n*-hexane 1:3, v/v); $^1$H NMR (400 MHz, $CDCl_3$) δ = -2.77 (br, 2H, N*H*), 2.73 (s, 6H, C$H_3$), 7.59 (d, 4H, *J* = 7.6 Hz, $H_{arom}$), 8.06 (d, 4H, *J* = 7.6 Hz, $H_{arom}$) 8.79 (s, 2H, β-*H*), 8.89 (d, 2H, *J* = 4.7 Hz, β-*H*), 9.61 (d, 2H *J* = 4.7 Hz, β-*H*), 9.68 (s, 2H, β-*H*) ppm; $^{13}$C NMR (150.90 MHz, $CDCl_3$) δ = 21.4, 103.1, 121.7, 127.4, 132.1, 132.7, 134.2, 137.6, 138.4, 141.0, 143.9 ppm; UV-vis ($CH_2Cl_2$): $\lambda_{max}$ (log ε) = 423 (3.49), 523 (2.32), 558 (2.24), 602 (2.12), 660 nm (2.16); HRMS (ES+) calcd. for $C_{34}H_{25}Br_2N_4$ $[M+H]^+$ 647.0446, found 647.0446.

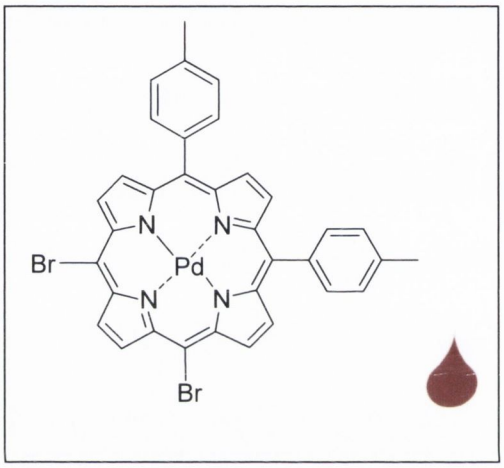
**Chloro[5,10-dibromo-15,20-di(*p*-tolyl)porphyrinato]indium(III) (InCl_Br) (81)**




5,10-Dibromo-15,20-di(*p*-tolyl)porphyrin **80** (100 mg, 0.154 mmol), $InCl_3$ (332 mg, 1.501 mmol) and sodium acetate (1.312 g, 0.015 mol) were dissolved in glacial acetic acid (50 mL). The reaction mixture was heated at reflux for 24 h. The solvent was removed under reduced pressure and the solid residue was dissolved in DCM. The solution was extracted with an aqueous solution of $NaHCO_3$ (5% w/v). The organic phase was washed twice with a saturated aqueous solution of NaCl and dried over $MgSO_4$. The solvent was removed and the solid residue was purified. Chromatographic separation was performed on silica gel. Traces of free base porphyrin were eluted with $CH_2Cl_2$/*n*-hexane (1:2, v/v) followed by elution of the metalloporphyrin with DCM to yield 119 mg (0.150 mmol, 98%) of a dark blue solid. M.p. > 300 °C; $R_f$ = 0.2 ($SiO_2$, $CHCl_3$); $^1$H

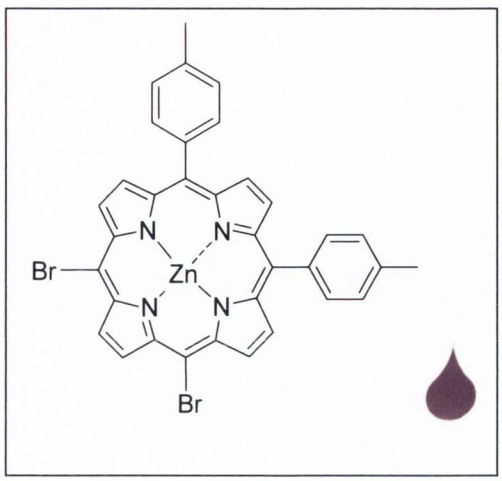
NMR (400 MHz, $CDCl_3$) δ = 2.75 (s, 6H, $CH_3$), 7.59 (d, 2H, $J$ = 7.6 Hz, $H_{arom}$), 7.65 (d, 2H, $J$ = 7.6 Hz, $H_{arom}$), 7.97 (d, 2H, $J$ = 7.6 Hz, $H_{arom}$), 8.23 (d, 2H, $J$ = 7.6 Hz, $H_{arom}$); 9.04 (s, 2H, β-*H*), 9.14 (d, 2H, $J$ = 4.8 Hz, β-*H*), 9.85 (d, 2H, $J$ = 4.7 Hz, β-*H*), 9.93 (s, 2H, β-*H*) ppm; $^{13}$C NMR (150.90 MHz, $CDCl_3$) δ = 21.5, 105.0, 123.5, 127.6, 127.7, 133.5, 133.9, 134.1, 134.5, 134.7, 135.0, 138.1, 138.2, 149.2, 149.3 ppm; UV-vis ($CH_2Cl_2$): $\lambda_{max}$ (log ε) = 431 (3.86), 571 (2.69), 612 nm (2.64); HRMS (MALDI LD+): calcd. for $C_{34}H_{22}N_4ClBr_2In$ $[M]^+$ 793.8938, found 793.8903.

**[5,10-Dibromo-15,20-di(*p*-tolyl)porphyrinato]palladium(II) (82)**




5,10-Dibromo-15,20-di(*p*-tolyl)porphyrin **80** (100 mg, 0.154 mmol) and $Pd(acac)_2$ (52 mg, 0.171 mmol) were dissolved in toluene (15 mL) and heated under reflux for 5 h. The progress of the reaction was monitored by TLC using $CH_2Cl_2$/*n*-hexane (4:1). Upon completion of the metalation the solvent was removed *in vacuo* and the product isolated after passage through a plug of silica gel using $CHCl_3$ as eluent. Product recrystallization using $CH_2Cl_2$/MeOH yielded 83 mg of red crystals (0.110 mmol, 63%). M. p. > 300° C; $R_f$ = 0.42 ($SiO_2$, $CH_2Cl_2$/*n*-hexane 4:1, v/v); $^1$H NMR (400 MHz, $CDCl_3$) δ = 2.73 (s, 6H, $CH_3$), 7.57 (d, 4H, $J$ = 7.8 Hz, $H_{arom}$), 8.01 (d, 4H, $J$ = 7.8 Hz, $H_{arom}$) 8.76 (s, 2H, β-*H*), 8.85 (d, 2H $J$ = 4.9 Hz, β-*H*), 9.57 (d, 2H, $J$ = 4.9 Hz, β-*H*), 9.62 (s, 2H, β-*H*) ppm; $^{13}$C NMR (100.6 MHz, $CDCl_3$) δ = 21.5, 105.2, 123.0, 127.6, 131.7, 132.2, 132.5, 132.8, 133.9, 137.8, 138.2, 141.5, 141.6, 142.3, 142.6 ppm; UV-vis ($CH_2Cl_2$): $\lambda_{max}$ (log ε) = 422 (3.66), 531 (2.73), 656 nm (2.18); HRMS (MALDI LD+): calcd. for $C_{34}H_{22}N_4Br_2Pd$ $[M]^+$ 749.9246, found 749.9268.

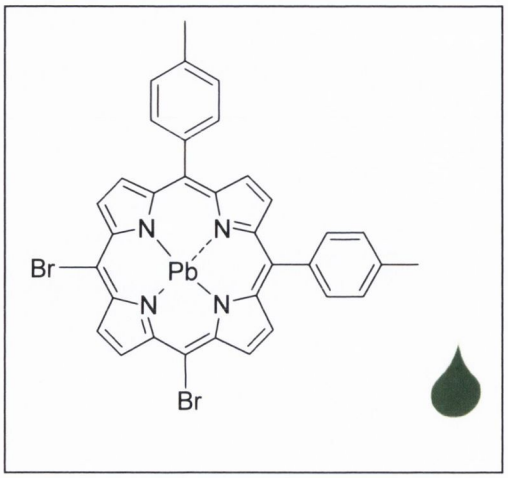
**[5,10-Dibromo-15,20-di(*p*-tolyl)porphyrinato]zinc(II) (83)**




1. Insertion of zinc(II) using $Zn(OAc)_2$: 5,10-Dibromo-15,20-di(*p*-tolyl)porphyrin **80** (250 mg, 0.386 mmol) was dissolved in chloroform (50 mL) and brought to reflux. $Zn(OAc)_2$ (126 mg, 0.574 mmol) was dissolved in small amount of MeOH (2 mL) and added dropwise. The progress of the reaction was monitored with TLC using $CHCl_3$/*n*-hexane (3:7 v/v) as eluent. After 2.5 h reaction was completed. The reaction mixture was allowed to cool. The solvent was removed, and the product was isolated after passage through a plug of silica gel using $CHCl_3$ as the eluent. Recrystallisation of the residue from $CHCl_3$/MeOH yielded 190 mg (267 mmol) of the title product as shinny purple crystals, which stands for the yield of 70%.

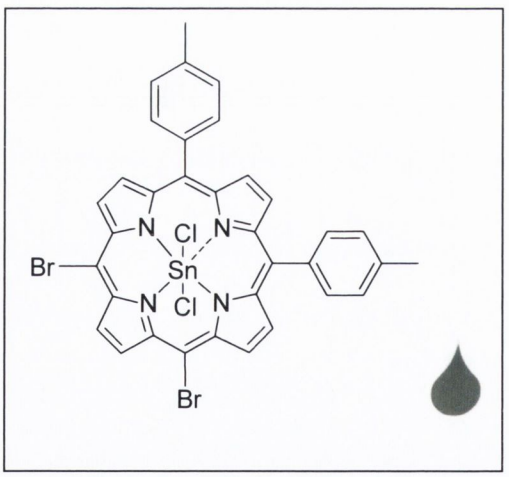
2. Insertion of zinc(II) using $Zn(acac)_2$: 5,10-Dibromo-15,20-di(*p*-tolyl)porphyrin **80** (100 mg, 0.154 mmol) and $Zn(acac)_2$ (203 mg, 0.770 mmol) in 50 mL of toluene was brought to reflux. The progress of the reaction was monitored with TLC using $CHCl_3$/*n*-hexane (3:7, v/v) as eluent. The reaction was complete after 2 h. The solvent was removed and the product was isolated after passage through a plug of silica gel using $CHCl_3$ as eluent. Recrystallization of the residue from $CHCl_3$/MeOH yielded 108 mg (0.152 mmol) of the title product as shiny purple crystals (98%). M. p. > 300° ; $R_f$= 0.3 ($SiO_2$, $CHCl_3$/*n*-hexane 3:7, v/v); $^1$H NMR (400 MHz, $CDCl_3$, 1% pyridine-$d_5$) δ = 2.68 (s, 6H, C*H*$_3$), 7.50 (d, 4H, *J* = 7.6 Hz, *H*$_{arom}$), 7.99 (d, 4H, *J* = 7.6 Hz, *H*$_{arom}$), 8.77 (s, 2H, β-*H*), 8.87 (d, 2H *J* = 4.7 Hz, β-*H*), 9.62 (d, 2H, *J* = 4.7 Hz, β-*H*), 9.73 (s, 2H, β-*H*) ppm; $^{13}$C NMR (100.6 MHz, $CDCl_3$, 1% pyridine-$d_5$) δ = 21.5, 104.3, 122.2, 127.2, 132.3, 132.7, 133.3, 133.7, 134.4, 137.1, 139.9, 149.9, 151.0, 151.1 ppm; UV-vis ($CH_2Cl_2$): $\lambda_{max}$ (log ε) = 393 (4.83), 424 (5.59), 517 (3.73), 554 (4.33), 595 nm (3.69); HRMS (MALDI LD+) calcd. for $C_{34}H_{22}N_4Br_2Zn$ $[M]^+$ 707.9503, found 707.9478, HRMS (ES+) $C_{34}H_{22}N_4Br_2Zn$ $[M]^+$ calcd. 707.9503, found 707.9529.

**[5,10-Dibromo-15,20-di(*p*-tolyl)porphyrinato]lead(II) (84)**




Following the general procedure **B**, 90 mg (0.139 mmol) of 5,10-dibromo-15,20-di(*p*-tolyl)porphyrin **80** and 1.125 g (2.776 mmol) of $Pb(acac)_2$ in 40 mL of toluene/MeOH (1:1, v/v) were stirred at room temperature for 30 min. Recrystallization yielded 118 mg (0.138 mmol, 99%) of a dark green product. M.p. >300 °C; $R_f$ = 0.25 ($Al_2O_3$, $CHCl_3$/*n*-hexane 3:20, v/v); $^1$H NMR (400 MHz, $CDCl_3$) δ = 2.74 (s, 6H, C*H*$_3$), 7. 58 (s, 4H, *H*$_{arom}$), 8.06 (br, 4H, *H*$_{arom}$), 8.91 (s, 2H, β-*H*), 8.99 (d, 2H *J* = 4.7 Hz, β-*H*), 9.74 (d, 2H, *J* = 4.7 Hz, β-*H*), 9.85 (s, 2H, β-*H*) ppm; $^{13}$C NMR (100.6 MHz, $CDCl_3$) δ = 21.6, 105.3, 124.0, 127.4, 127.6, 132.8, 132.9, 133.7, 133.8, 134.4, 137.5, 139.3, 149.0, 149.1, 150.1 ppm; UV-vis ($CH_2Cl_2$): $\lambda_{max}$ (log ε) = 358 (4.62), 470 (5.43), 623 (3.76), 669 nm (4.15); HRMS (MALDI LD+) calcd. for $C_{34}H_{22}N_4Br_2Pb$ $[M]^+$ 851.9978, found 851.9951.

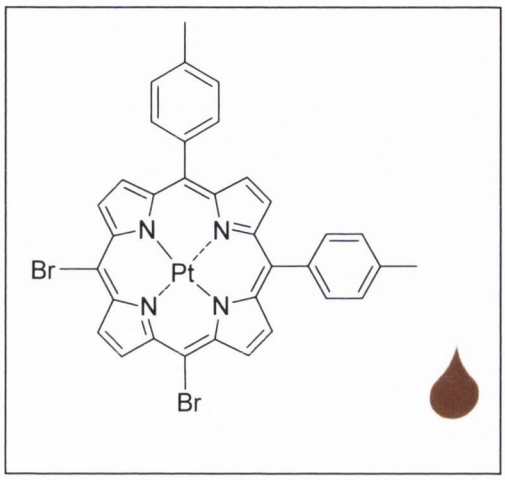
**Dichloro[5,10-dibromo-15,20-di(*p*-tolyl)porphyrinato]tin(IV) (85)**




5,10-Dibromo-15,20-di(*p*-tolyl)porphyrin **80** (180 mg, 0.278 mmol) and $SnCl_2$ (526 mg, 2.774 mmol) were dissolved in 15 mL DMF and heated to reflux for 1.5 h. The solvent was removed under reduced pressure and the product was isolated after passage through a plug of alumina using $CHCl_3$ as eluent. The solution was concentrated and the product was precipitated out *via* addition of MeOH. After filtration the product was washed with MeOH and dried to yield 193 mg (0.231 mmol, 83%) of a dark blue product. M.p. > 300 °C; $R_f$ = 0.8 ($Al_2O_3$, $CHCl_3$); $^1$H NMR (400 MHz, $CDCl_3$) δ = 2.77 (s, 6H, C*H*$_3$), 7.66 (d, 4H, *J* = 7.6 Hz, *H*$_{arom}$), 8.17 (d, 4H, *J* = 7.6 Hz, *H*$_{arom}$), 9.17 (s, 2H, β-*H*), 9.28 (d, 2H *J* = 4.7 Hz, β-*H*), 9.98 (d, 2H, *J* = 4.7 Hz, β-*H*), 10.10 (s, 2H, β-*H*) ppm; $^{13}$C NMR (100.6 MHz, $CDCl_3$) δ = 21.6, 104.3, 123.1, 128.0, 133.5, 134.0, 134.4, 134.9, 137.0, 138.9, 146.1, 146.2, 147.3 ppm; UV-vis ($CH_2Cl_2$): $\lambda_{max}$ (log ε) = 434 (5.69),

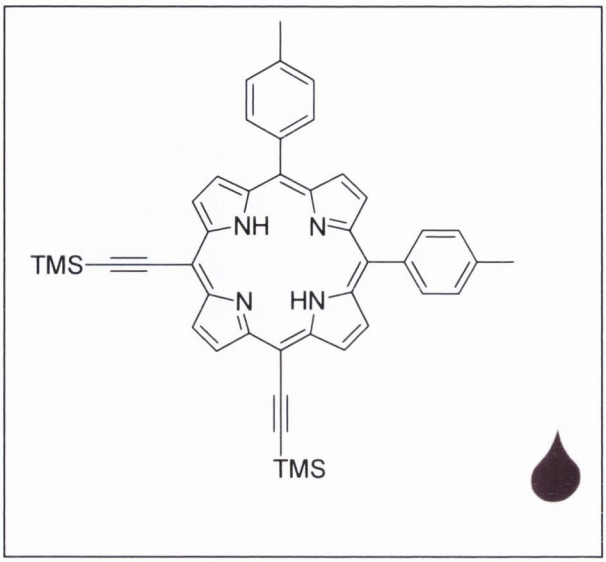
570 (4.27), 615 nm (4.31); HRMS (MALDI LD+) calcd. for $C_{34}H_{22}N_4ClBr_2Sn$ $[M\text{-}Cl]^+$ 798.8922, found 798.894.

**[5,10-Dibromo-15,20-di(*p*-tolyl)porphyrinato]platinum(II) (86)**



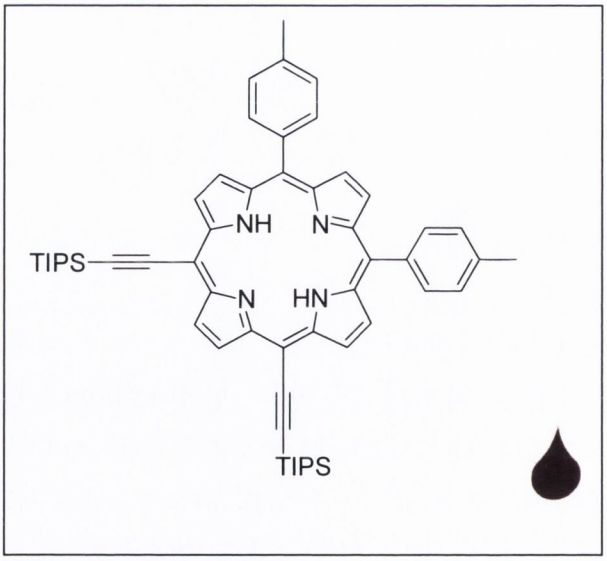

5,10-Dibromo-15,20-di(*p*-tolyl)porphyrin **80** (30 mg, 0.046 mmol), $PtCl_2$ (36 mg, 0.135 mmol) was heated in benzonitrile (10 mL) under Ar at 170 °C. The progress of the reaction was monitored by TLC using $CHCl_3$/*n*-hexane (1:4). Upon completion after 12 h the solution was cooled to room temperature and MeOH was added to precipitate the product which was filtered off and isolated after passage through a plug of silica gel using $CHCl_3$ as eluent. The solvent was removed under reduced pressure and the product was recrystallized from $CHCl_3$/MeOH to yield 23 mg (0.0277 mmol, 60%) of bright red crystals. M.p. = 292 °C; $R_f$ = 0.25 ($SiO_2$, $CHCl_3$/*n*-hexane 1:4, v/v); $^1$H NMR (400 MHz, $CDCl_3$) δ = 2.73 (s, 6H, $CH_3$), 7.58 (d, 4H, $J$ = 7.6 Hz, $H_{arom}$), 8.00 (d, 4H, $J$ = 7.6 Hz, $H_{arom}$), 8.69 (s, 2H, β-*H*), 8.74 (d, 2H $J$ = 5.3 Hz, β-*H*), 9.25 (s, 2H, β-*H*), 9.36 (d, 2H, $J$ = 5.3 Hz, β-*H*), ppm; $^{13}$C NMR (100.6 MHz, $CDCl_3$) δ = 21.6, 114.8, 123.0, 127.7, 128.6, 128.7, 131.2, 131.6, 133.8, 137.8, 137.9, 139.0, 139.3, 141.4, 141.5 ppm; UV-vis ($CH_2Cl_2$): $\lambda_{max}$ (log ε) = 405 (5.38), 516 nm (4.33); HRMS (MALDI LD+) calcd. for $C_{34}H_{22}N_4Br_2Pt$ $[M]^+$ 838.9857, found 838.9861.

**5,10-Di(*p*-tolyl)-15,20-bis[(trimethylsilyl)ethynyl]porphyrin (87)**




Following the general procedure for Sonogashira coupling, 90 mg (0.139 mmol) of porphyrin 5,10-dibromo-15,20-di(*p*-tolyl)porphyrin **80**, 0.096 mL (0.692 mmol) of TMS-acetylene, 6 mg (0.032 mmol) of CuI and 9 mg (0.013 mmol) of $Pd(PPh_3)_2Cl_2$ in 40 mL of THF/$NEt_3$ (1:3, v/v) after 12 h gave 64 mg (0.093 mmol, 67%) of a dark green solid after purification by column chromatography on silica gel ($CH_2Cl_2$/*n*-hexane 1:3 v/v). M. p. = 294 °C; $R_f$ = 0.43 ($SiO_2$, $CH_2Cl_2$/n-hexane 1:3, v/v); $^1$H NMR (400 MHz, $CDCl_3$) δ = -2.11 (br, 2H, N*H*), 0.65 (s, 18H, C$H_3$), 2.73 (s, 6H, C$H_3$), 7.58 (d, 4H, *J* = 7.8 Hz, $H_{arom}$), 8.06 (d, 4H, *J* = 7.8 Hz, $H_{arom}$), 8.73 (s, 2H, β-*H*), 8.86 (d, 2H, *J* = 4.9 Hz, β-*H*), 9.57 (d, 2H, *J* = 4.9 Hz, β-*H*), 9.69 (s, 2H, β-*H*) ppm; $^{13}$C NMR (150.90 MHz, $CDCl_3$) δ = 0.2, 21.4, 99.6, 102.0, 106.5, 122.8, 127.4, 134.2, 137.5, 138.5 ppm; UV-vis ($CH_2Cl_2$): $\lambda_{max}$ (log ε) = 439 (2.92), 541 (1.7), 581 (1.89), 618 (1.61), 679 nm (1.64); HRMS (ES+) $C_{44}H_{43}N_4Si_2$ $[M+H]^+$ calcd. 683.3026, found 683.3031.

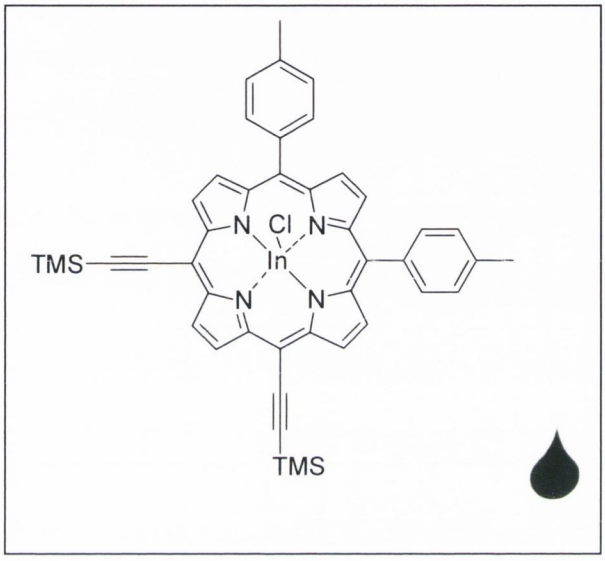
**5,10-Di(*p*-tolyl)-15,20-bis[(triisopropylsilyl)ethynyl]porphyrin (88)**




Following the general procedure **A**, 30 mg (0.046 mmol) of 5,10-dibromo-15,20-di(*p*-tolyl)porphyrin **80**, 0.05 mL (0.230 mmol) of TIPS-acetylene, 2 mg (0.012 mmol) of CuI and 8 mg (0.011 mmol) of $Pd(PPh_3)_2Cl_2$ in 12 mL of THF/$NEt_3$ (1:3, v/v) after 12 h gave 19 mg (0.022 mmol, 48%) of a dark green solid after purification by column chromatography on silica gel ($CH_2Cl_2$/*n*-hexane 1:2 v/v). M. p. > 300 °C; $R_f$ = 0.45 ($SiO_2$, $CH_2Cl_2$/*n*-hexane 1:3, v/v); $^1$H NMR (400 MHz, $CDCl_3$) δ= -2.08 (br, 2H, N*H*), 1.41 - 1.56 (m, 42H, TIPS), 2.72 (s, 6H, C$H_3$), 7.57 (d, 4H, *J* = 7.6 Hz, $H_{arom}$), 8.05 (d, 4H,

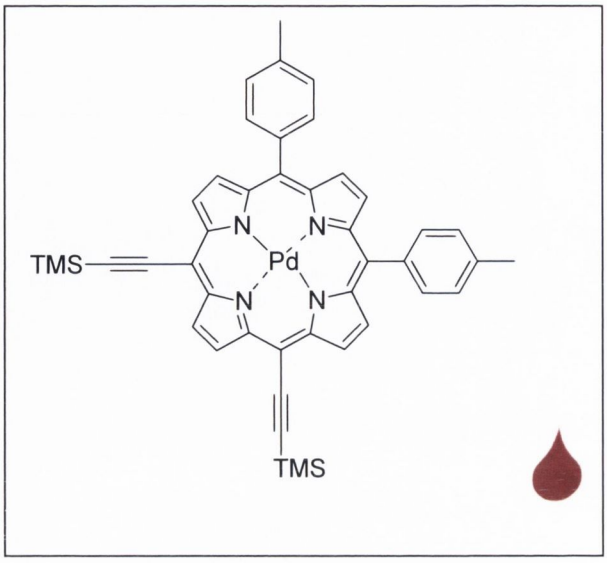
$J$ = 7.6 Hz, $H_{arom}$), 8.74 (s, 2H, β-*H*), 8.87 (d, 2H, $J$ = 4.7 Hz, β-*H*), 9.63 (d, 2H, $J$ = 4.7 Hz, β-*H*), 9.63 (s, 2H, β-*H*) ppm; $^{13}$C NMR (150.90 MHz, $CDCl_3$) δ = 11.9, 19.1, 21.5, 98.9, 100.2, 108.4, 122.8, 127.5, 134.2, 137.6, 138.6 ppm; UV-vis ($CH_2Cl_2$): $\lambda_{max}$ (log ε) = 440 (5.67), 545 (4.20), 583 (4.51), 619 (3.84), 679 nm (3.97); HRMS (MALDI LD+) calcd. for $C_{56}H_{67}N_4Si_2$ $[M+H]^+$ 851.4904, found 851.4901.

**Chloro{5,10-di(*p*-tolyl)-15,20-bis[(trimethylsilyl)ethynyl]porphyrinato}idium(III) (89)**



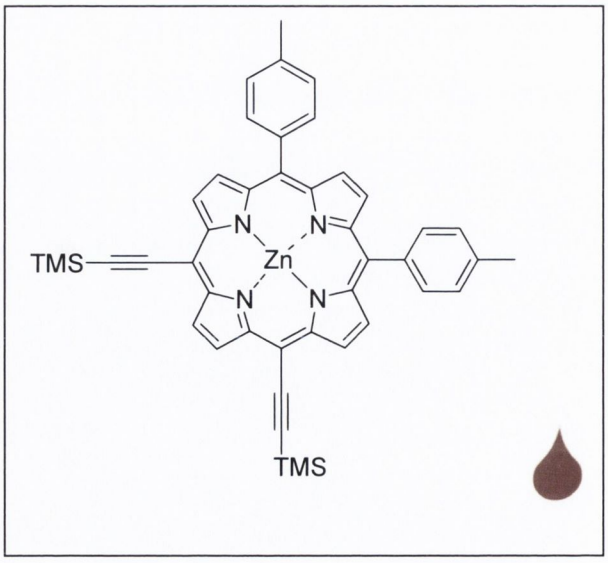

Following the general procedure **A**, 100 mg (0.126 mmol) of chloro[5,10-dibromo-15,20-di(*p*-tolyl)porphyrinato]indium(III) **81**, 0.087 mL (0.627 mmol) of TMS-acetylene, 6 mg (0.031 mmol) of CuI and 22 mg (0.031 mmol) of $Pd(PPh_3)_2Cl_2$ in 40 mL of THF/$NEt_3$ (1:3, v/v) after 24 h gave 16.7 mg (0.020 mmol, 16%) of a purple solid after purification by column chromatography on silica gel (THF/*n*-hexane 3:17 v/v). M.p. >300 °C; $R_f$ = 0.2 ($SiO_2$, THF/*n*-hexane 1:4, v/v); $^1$H NMR (400 MHz, $CDCl_3$) δ = 0.67 (s, 18H, C$H_3$), 2.75 (s, 6H, C$H_3$), 7.58 (d, 2H, $J$ = 7.6 Hz, $H_{arom}$), 7.65 (d, 2H, $J$ = 7.6 Hz, $H_{arom}$), 7.95 (d, 2H, $J$ = 7.6 Hz, $H_{arom}$), 8.25 (d, 2H, $J$ = 7.6 Hz, $H_{arom}$), 8.97 (s, 2H, β-*H*), 9.09 (d, 2H $J$ = 4.7 Hz, β-*H*), 9.79 (d, 2H $J$ = 4.7 Hz, β-*H*), 9.90 (s, 2H, β-*H*) ppm; $^{13}$C NMR (150.90 MHz, $CDCl_3$) δ = 0.3, 21.5, 101.5, 103.5, 106.1, 124.5, 127.6, 127.7, 131.6, 132.6, 133.0, 134.0, 134.1, 135.0, 138.0, 138.2, 149.0, 149.8, 151.5, 152.0 ppm; UV-vis ($CH_2Cl_2$): $\lambda_{max}$ (log ε) = 449 (5.82), 588 (4.29), 632 nm (4.47); HRMS (MALDI LD+) calcd. for $C_{44}H_{40}N_4ClInSi_2$ $[M]^+$ 830.1522, found 830.1519.

**{5,10-Di(*p*-tolyl)-15,20-bis[(trimethylsilyl)ethynyl]porphyrinato}palladium(II) (90)**




Following the general procedure **A**, 50 mg (0.066 mmol) of [5,10-dibromo-15,20-di(*p*-tolyl)porphyrinato]palladium(II) (**82**), 0.046 mL (0.326 mmol) of trimethylsilylacetylene, 3 mg (0.016 mmol) of CuI and 4.6 mg (0.006 mmol) of $Pd(PPh_3)_2Cl_2$ in 20 mL of THF/$NEt_3$ (1:3, v/v) after 12 h gave 30.2 mg (0.038 mmol, 57%) of a red solid after purification by column chromatography on silica gel (EtOAc/*n*-hexane = 1:24, v/v). M.p. >300 °C; $R_f$ = 0.56 ($SiO_2$, EtOAc/*n*-hexane 1:19, v/v); $^1$H NMR (400 MHz, $CDCl_3$) δ = 0.63 (s, 18H, $CH_3$), 2.72 (s, 6H, $CH_3$), 7.56 (d, 4H, $J$ = 7.8 Hz, $H_{arom}$), 8.01 (d, 4H, $J$ = 7.8 Hz, $H_{arom}$), 8.72 (s, 2H, β-*H*), 8.83 (d, 2H $J$ = 4.9 Hz, β-*H*), 9.56 (d, 2H $J$ = 4.9 Hz, β-*H*), 9.67 (s, 2H, β-*H*) ppm; $^{13}$C NMR (150.90 MHz, $CDCl_3$) δ = 0.1, 21.4, 101.6, 101.9, 105.7, 123.8, 127.4, 129.9, 130.8, 130.9, 131.9, 133.8, 137.5, 138.1, 141.2, 141.8, 143.5, 143.8 ppm; UV-vis ($CH_2Cl_2$): $\lambda_{max}$ (log ε) = 438 (2.68), 547 (1.81), 584 (1.59); HRMS (ES+) $C_{44}H_{41}N_4PdSi_2$ $[M+H]^+$ calcd. 787.1905, found 787.1921.

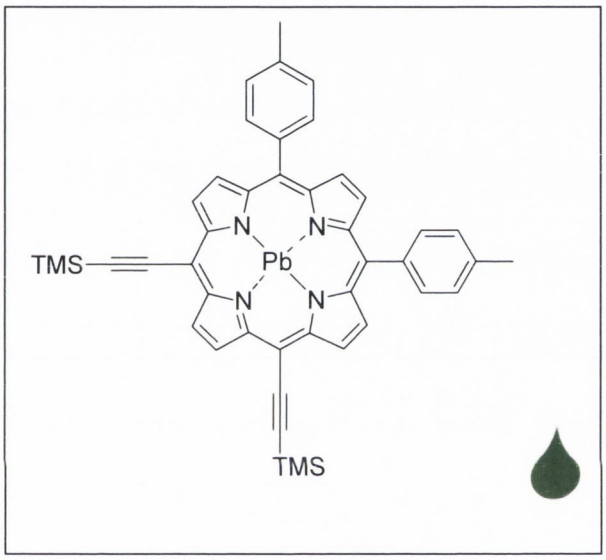
**{5,10-Di(*p*-tolyl)-15,20-bis[(trimethylsilyl)ethynyl]porphyrinato}zinc(II) (91)**




Following the general procedure for Sonogashira coupling, 240 mg (0.377 mmol) of porphyrin [5,10-dibromo-15,20-di(*p*-tolyl)porphyrinato]zinc(II) (**83**), 0.233 mL (1.679 mmol) of TMS-acetylene, 16 mg (0.084 mmol) of CuI and 24 mg (0.034 mmol) of $Pd(PPh_3)_2Cl_2$ in 45 mL of THF/$NEt_3$ (1:2, v/v) after 12 h gave 235 mg (0.315 mmol, 84%) of a violet solid after isolation of the product after passage through a plug of alox using $CHCl_3$ as eluent. M. p. > 300 °C; $R_f$ = 0.4 ($SiO_2$, EtOAc/*n*-

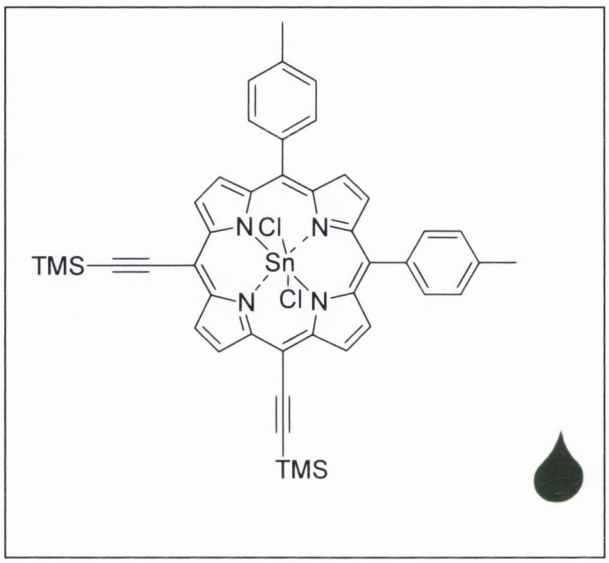
hexane 1:9, v/v); $^1$H NMR (400 MHz, $CDCl_3$, 1% pyridine-$d_5$) δ = 0.56 (s, 18H, $CH_3$), 2.63 (s, 6H, $CH_3$), 7.46 (d, 4H, $J$ = 7.6 Hz, $H_{arom}$), 7.96 (d, 4H, $J$ = 7.6 Hz, $H_{arom}$), 8.69 (s, 2H, β-*H*), 8.82 (d, 2H $J$ = 4.1 Hz, β-*H*), 9.56 (d, 2H $J$ = 4.1 Hz, β-*H*), 9.67 (s, 2H, β-*H*) ppm; $^{13}$C NMR (150.90 MHz, $CDCl_3$, 1% pyridine-$d_5$) δ = 0.4, 21.4, 99.3, 100.2, 108.4, 123.7, 127.1, 130.3, 131.5, 131.6, 132.8, 134.3, 136.9, 139.8, 149.6, 150.2, 152.5, 152.7 ppm; UV-vis ($CH_2Cl_2$): $\lambda_{max}$ (log ε) = 441 (5.7), 5.72 (4.5), 615 nm (4.5); HRMS (ES+) $C_{44}H_{41}N_4ZnSi_2$ $[M+H]^+$ calcd. 745.2161, found 745.2197.

**{5,10-Di(*p*-tolyl)-15,20-bis[(trimethylsilyl)ethynyl]porphyrinato}lead(II) (92)**



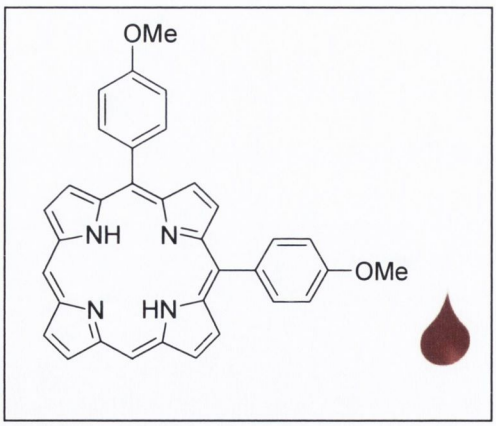

Following the general procedure **B**, 73 mg (0.106 mmol) of 5,10-di(*p*-tolyl)-15,20-bis[(trimethylsilyl)ethynyl]porphyrin (**87**) and 433 mg (1.069 mmol) of $Pb(acac)_2$ in 30 mL of toluene/MeOH (1:1, v/v) were stirred for 40 min at room temperature. Recrystallization from DCM/MeOH yielded 89 mg (0.100 mmol, 94%) of a dark green product. M.p. >300 °C; $R_f$ = 0.2 ($Al_2O_3$, $CHCl_3$/*n*-hexane 3:20, v/v); $^1$H NMR (400 MHz, $CDCl_3$) δ = 0.65 (s, 18H, $CH_3$), 2.73 (s, 6H, $CH_3$), 7.58 (br, 4H, $H_{arom}$), 7.91 (br, 2H, $H_{arom}$), 8.19 (br, 2H, $H_{arom}$), 8.86 (s, 2H, β-*H*), 8.96 (d, 2H $J$ = 4.7 Hz, β-*H*), 9.69 (d, 2H $J$ = 4.7 Hz, β-*H*), 9.81 (s, 2H, β-*H*) ppm; $^{13}$C NMR (150.90 MHz, $CDCl_3$) δ = 0.2, 21.4, 101.0, 101.2, 107.5, 125.4, 127.2, 127.4, 130.4, 131.6, 132.2, 133.3, 134.2, 137.3, 139.2, 148.5, 149.5, 151.4, 152.0 ppm; UV-vis ($CH_2Cl_2$): $\lambda_{max}$ (log ε) = 368 (4.61), 484 (5.47), 636 (3.94), 687 nm (4.40); HRMS (MALDI LD+) calcd. for $C_{44}H_{40}N_4Si_2Pb$ $[M]^+$ 888.2558, found 888.2598.

**Dichloro{5,10-di(*p*-tolyl)-15,20-bis[(trimethylsilyl)ethynyl]porphyrinato}tin(IV) (93)**




5,10-Di(*p*-tolyl)-15,20-bis[(trimethylsilyl)ethynyl]porphyrin (**87**) (67 mg, 0.098 mmol) and $SnCl_2$ (186 mg, 0.981 mmol) in 7 mL of DMF were heated at reflux for 1.5 h. The solvent was removed under reduced pressure and the solid residue was dissolved in $CH_2Cl_2$. The solution was washed twice with water and with a saturated, aqueous solution of NaCl and dried over $MgSO_4$ to yield 70 mg (0.0804 mmol, 89%) of a blue solid. M.p. >300 °C; $^1$H NMR (400 MHz, $CDCl_3$) δ = 0.67 (s, 18H, $CH_3$), 2.76 (s, 6H, $CH_3$), 7.64 (d, 4H, $J$ = 8.2 Hz, $H_{arom}$), 8.17 (d, 4H, $J$ = 8.2 Hz, $H_{arom}$), 9.09 (s, 2H, β-*H*), 9.22 (d, 2H $J$ = 4.7 Hz, β-*H*), 9.89 (d, 2H $J$ = 4.7 Hz, β-*H*), 10.01 (s, 2H, β-*H*) ppm; $^{13}$C NMR (150.90 MHz, $CDCl_3$) δ = 0.3, 21.5, 101.5, 103.5, 106.1, 124.5, 127.6, 127.7, 131.6, 132.6, 133.0, 134.0, 134.1, 135.0, 138.0, 138.2, 149.0, 149.8, 151.5, 152.0 ppm; UV-vis ($CH_2Cl_2$): $\lambda_{max}$ (log ε) = 450 (5.31), 591 (3.87), 636 nm (4.15); HRMS (MALDI LD+) calcd. for $C_{44}H_{40}N_4Si_2ClSn$ $[M\text{-}Cl]^+$ 835.1502, found 835.1536.

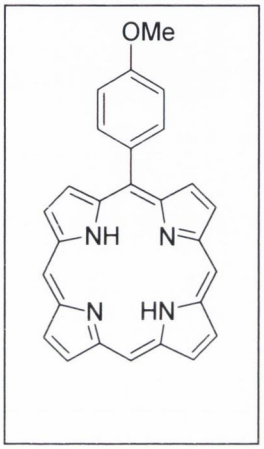
**5,10-Di(*p*-methoxyphenyl)porphyrin (95)**




A solution of *p*-anisaldehyde (1.2 mL, 9.937 mmol), paraformaldehyde (0.448 g, 14.905 mmol), pyrrole (2 mL, 29.811 mmol) in dry $CH_2Cl_2$ (200 mL) was stirred at RT under Ar atmosphere and shielded from light, and then TFA (0.076 mL, 0.994 mmol) was added. The mixture was stirred overnight followed by treatment with DDQ (15 g, 66.079 mmol). Stirring was continued for 1h, followed by addition of $NEt_3$ and stirring for another 5 min. The reaction mixture was filtered through plug of silica gel and washed with $CH_2Cl_2$. The solvent was removed *in vacuo* and the residue was purified by column chromatography on silica gel ($CH_2Cl_2$/*n*-hexane 1:2). The title product was eluted as second fraction. 51 mg (0.0976 mmol, 1.9%) of product was obtained as purple solid. M. p. > 300 °C; $R_f$ = 0.55 ($SiO_2$, EtOAc/*n*-hexane

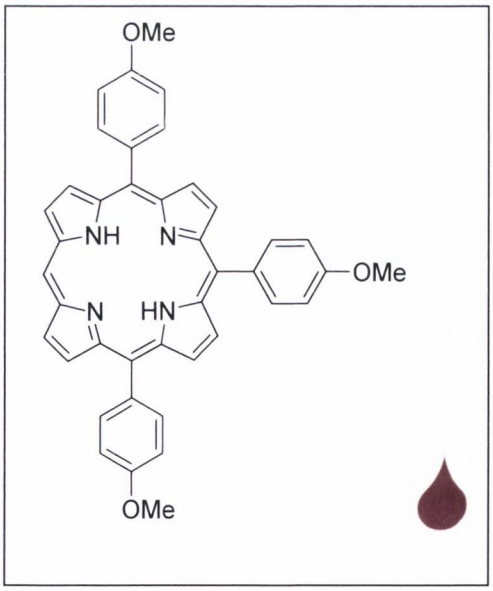
3:7, v/v); $^1$H NMR (400 MHz, $CDCl_3$) δ= -3.31 (br, 2H, N*H*), 4.15 (s, 6H, C$H_3$), 7.34 (d, 4H, *J* = 8.2 Hz, $H_{arom}$), 8.18 (d, 4H, *J* = 7.6 Hz, $H_{arom}$), 8.98 (s, 2H, β-*H*), 9.09 (d, 2H, *J* = 4.7 Hz, β-*H*), 9.38 (d, 2H, *J* = 4.7 Hz, β-*H)*, 9.48 (s, 2H, β-*H*), 10.26 (s, 2H, meso-*H*) ppm; $^{13}$C NMR (150.90 MHz, $CDCl_3$) δ = 29.8, 104.0, 112.3, 119.9, 131.0, 131.1, 134.6, 135.7, 159.5 ppm; UV-vis ($CH_2Cl_2$): $\lambda_{max}$ (log ε) = 408 (5.53), 504 (4.23), 538 (3.68), 577 nm (3.81); HRMS (MALDI LD+) calcd. for $C_{34}H_{26}N_4O_2$ $[M]^+$ 522.2056, found 522.2057.

**5-*p*-Methoxyphenylporphyrin (96)**




The title product was obtained following procedure reported above for 5,10-di(*p*-methoxyphenyl)porphyrin (**95**). It was eluated as a first fraction of the column. 30 mg (0.0574 mmol, 1.1%) of the title product was obtained in the form of purple solid. Analytical data were as reported by Ryppa *et. al.*[196]

**5,10,15-Tri(*p*-methoxyphenyl)porphyrin (97)**




The title product was obtained following procedure reported above for 5,10-di(*p*-methoxyphenyl)porphyrin (**95**). It was eluated as a third fraction of the column. 58 mg (0.0923 mmol, 2.8%) of the title product was obtained in the form of purple solid. M. p. > 300 °C; $R_f$ = 0.45 ($SiO_2$, EtOAc/*n*-hexane 3:7, v/v); $^1$H NMR (400 MHz, $CDCl_3$) = - 2.95 (br, 2H, N*H*), 4.13 (s, 3H, C$H_3$), 4.14 ( s, 6H, C$H_3$), 7.29 – 7.37 (m, 6H, $H_{arom}$), 8.13 – 8.21 (m, 6H, $H_{arom}$), 8.91 – 8.97 (m, 4H, β-*H*), 9.07 (d, *J* = 5.9, 2H, β-*H*), 9.36 (d, *J* = 5.9, 2H, β-*H*), 10.22 (s, 1H, meso-*H*); $^{13}$C NMR (150.90 MHz, $CDCl_3$) δ = 29.73, 104.57, 112.07, 112.38, 119.32, 120.35, 130.64 (br), 131.16, 131.45 (br),134.21, 135.07, 135.55, 135.75, 159.41, 159.46; UV-vis ($CH_2Cl_2$): $\lambda_{max}$ (log ε) = 416 (5.54), 511 (4.17), 548 (3.87), 587

(3.73), 640 nm (3.58); HRMS (MALDI LD+) calcd. for $C_{41}H_{32}N_4O_3$ $[M]^+$ 628.2474, found 628.2468.

# Appendix

Additional plots for cases A-M

- Absorption coefficient $\alpha$ and $d\alpha/dF$ plotted *versus* input fluence $F$ for varying $\kappa_1$

case A:

$\kappa_2 = 8\ \mathrm{cm^2.GW^{-1}}$

$I_1 = 0.15\ \mathrm{GW.cm^{-2}}$

$I_2 = 0.35\ \mathrm{GW.cm^{-2}}$

$I_3 = 2.5\ \mathrm{GW^2.cm^{-4}}$

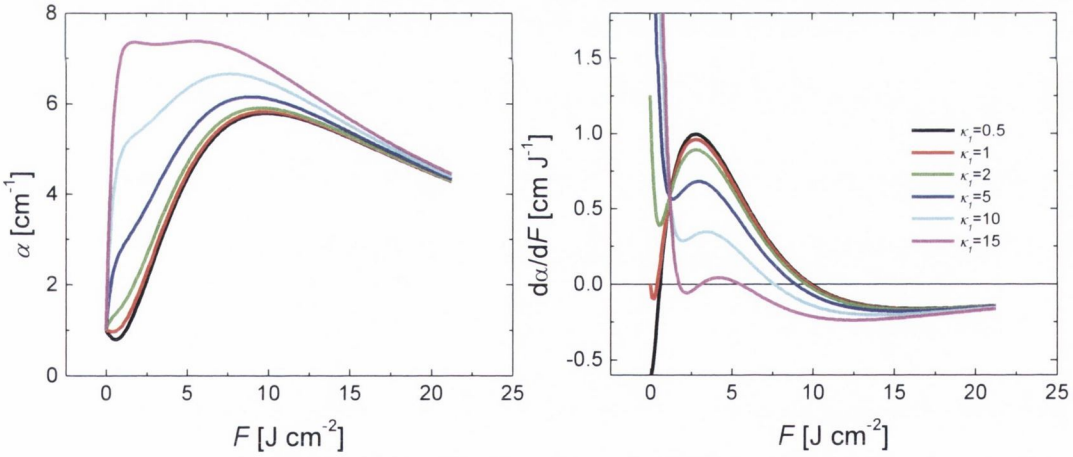



**Figure 71** Absorption coefficient $\alpha$ and $d\alpha/dF$ plotted *versus* input fluence $F$ for varying $\kappa_1$ – case A.

case C:

$\kappa_2 = 8\ \text{cm}^2.\text{GW}^{-1}$

$I_1 = 0.15\ \text{GW.cm}^{-2}$

$I_2 = 0.35\ \text{GW.cm}^{-2}$

$I_3 = 0.3\ \text{GW}^2.\text{cm}^{-4}$

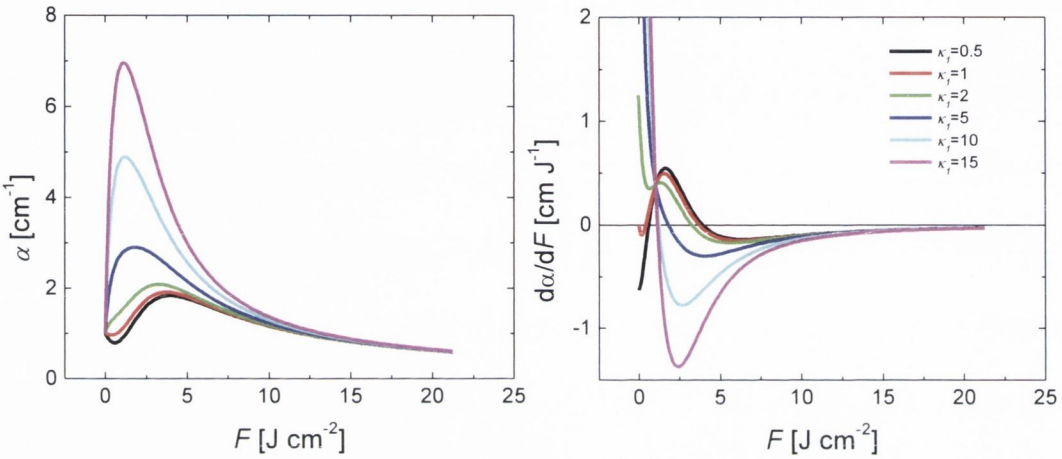



**Figure 72** Absorption coefficient $\alpha$ and $d\alpha/dF$ plotted *versus* input fluence $F$ for varying $\kappa_1$ – case C.

case E:

$\kappa_2 = 2\ \text{cm}^2.\text{GW}^{-1}$

$I_1 = 0.15\ \text{GW.cm}^{-2}$

$I_2 = 0.35\ \text{GW.cm}^{-2}$

$I_3 = 2.5\ \text{GW}^2.\text{cm}^{-4}$

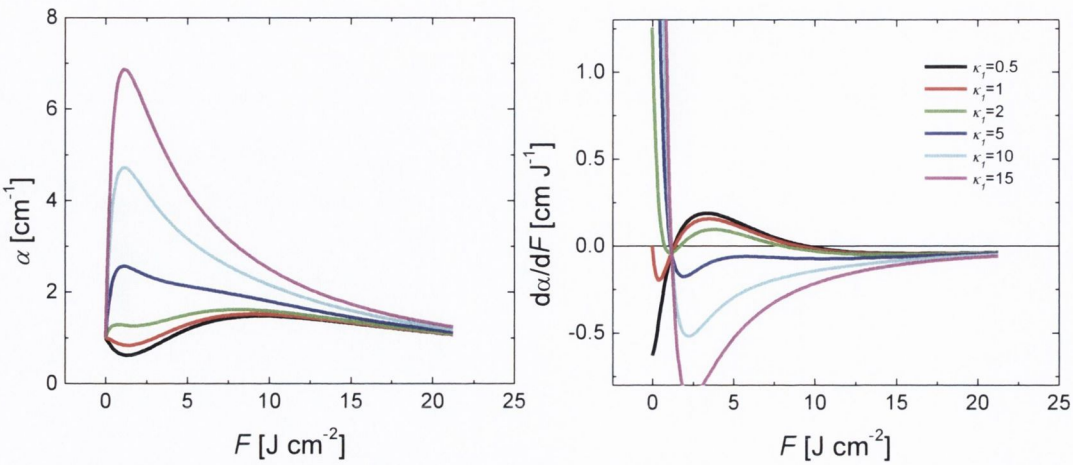



**Figure 73** Absorption coefficient $\alpha$ and $d\alpha/dF$ plotted *versus* input fluence $F$ for varying $\kappa_1$ – case C.

- Absorption coefficient $\alpha$ and $d\alpha/dF$ plotted *versus* input fluence $F$ for varying $\kappa_2$

case B:

$\kappa_1 = 4$ cm$^2$.GW$^{-1}$

$I_1 = 0.15$ GW.cm$^{-2}$

$I_2 = 0.35$ GW.cm$^{-2}$

$I_3 = 2.5$ GW$^2$.cm$^{-4}$

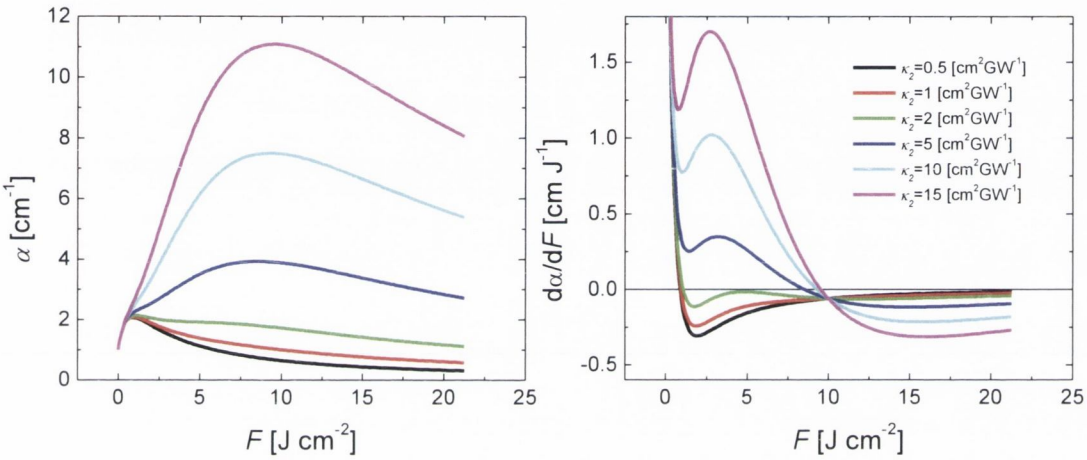



**Figure 74** Absorption coefficient $\alpha$ and $d\alpha/dF$ plotted *versus* input fluence $F$ for varying $\kappa_2$ – case B.

case D:

$\kappa_1 = 4\ \text{cm}^2.\text{GW}^{-1}$

$I_1 = 0.15\ \text{GW.cm}^{-2}$

$I_2 = 0.35\ \text{GW.cm}^{-2}$

$I_3 = 0.3\ \text{GW}^2.\text{cm}^{-4}$

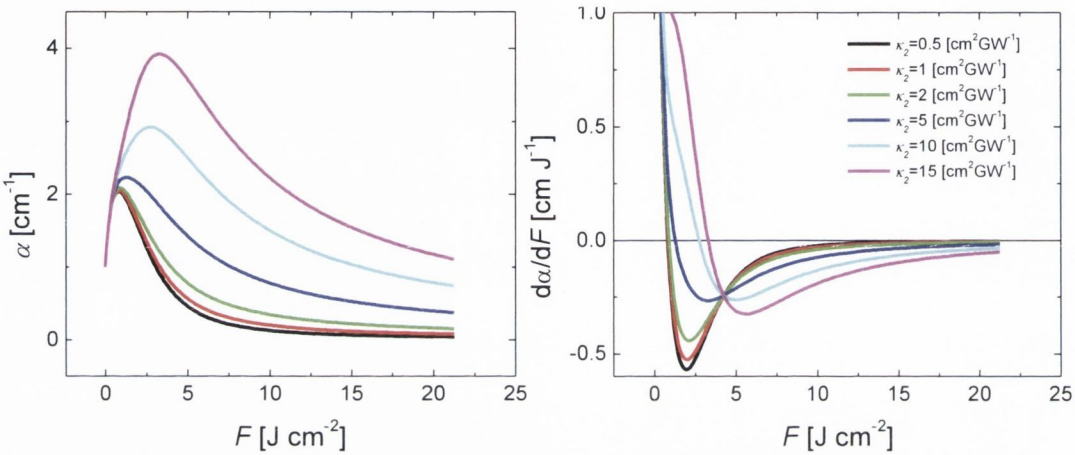



**Figure 75** Absorption coefficient $\alpha$ and $d\alpha/dF$ plotted *versus* input fluence $F$ for varying $\kappa_2$ – case D.

- Absorption coefficient $\alpha$ and $d\alpha/dF$ plotted *versus* input fluence $F$ for varying $I_1$

case F:

$\kappa_1 = 4\ \text{cm}^2.\text{GW}^{-1}$

$\kappa_2 = 8\ \text{cm}^2.\text{GW}^{-1}$

$I_2 = 0.35\ \text{GW.cm}^{-2}$

$I_3 = 2.5\ \text{GW}^2.\text{cm}^{-4}$

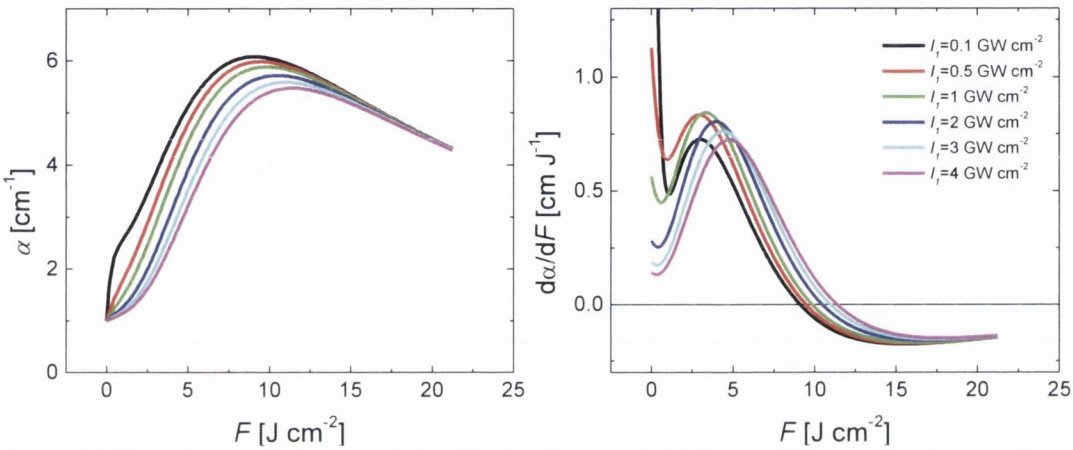



**Figure 76** Absorption coefficient $\alpha$ and $d\alpha/dF$ plotted *versus* input fluence $F$ for varying $I_1$ – case F.

case I:

$\kappa_1 = 8\ \text{cm}^2.\text{GW}^{-1}$

$\kappa_2 = 4\ \text{cm}^2.\text{GW}^{-1}$

$I_2 = 0.35\ \text{GW.cm}^{-2}$

$I_3 = 2.5\ \text{GW}^2.\text{cm}^{-4}$

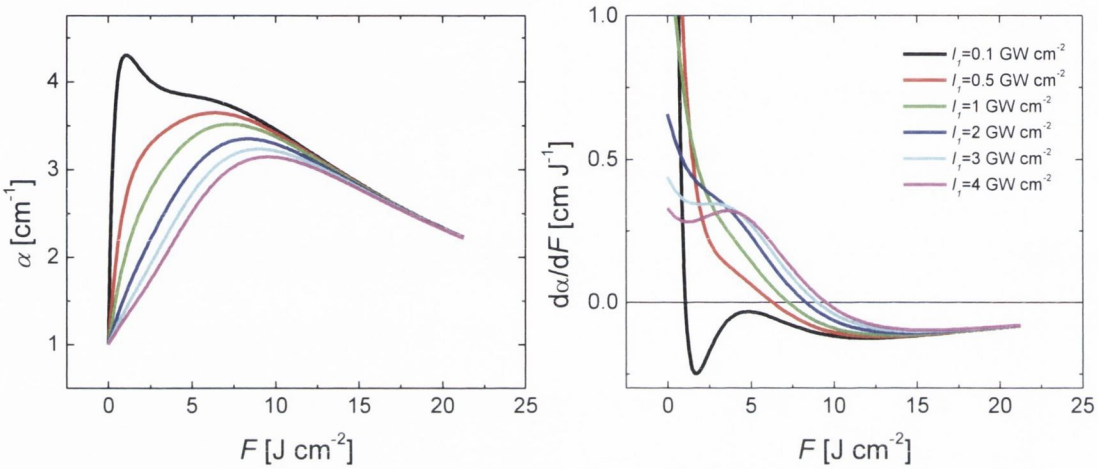



**Figure 77** Absorption coefficient $\alpha$ and $d\alpha/dF$ plotted *versus* input fluence $F$ for varying $I_1$ – case I.

case L:

$\kappa_1 = 4\ \text{cm}^2.\text{GW}^{-1}$

$\kappa_2 = 8\ \text{cm}^2.\text{GW}^{-1}$

$I_2 = 0.35\ \text{GW.cm}^{-2}$

$I_3 = 0.3\ \text{GW}^2.\text{cm}^{-4}$

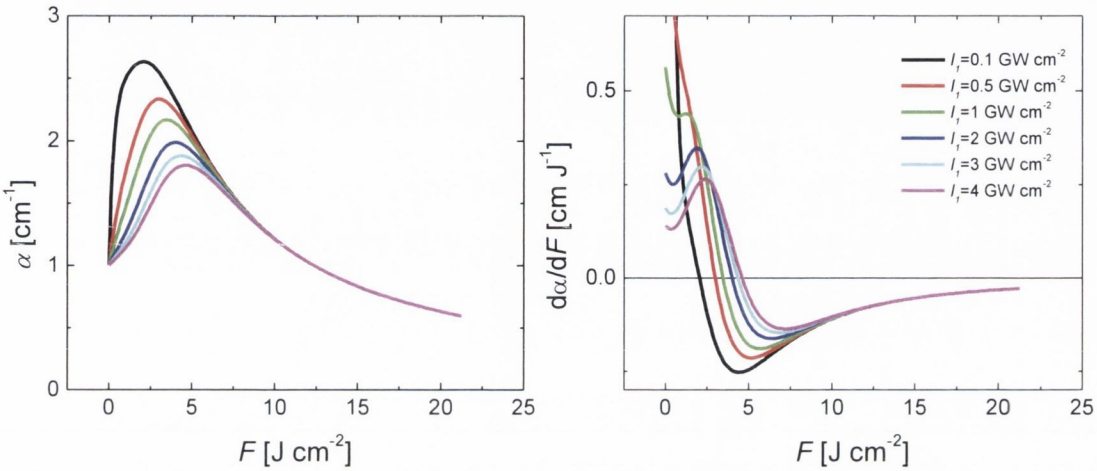



**Figure 78** Absorption coefficient $\alpha$ and $d\alpha/dF$ plotted *versus* input fluence $F$ for varying $I_1$ – case L.

- Absorption coefficient $\alpha$ and $d\alpha/dF$ plotted *versus* input fluence $F$ for varying $I_2$

case G:

$\kappa_1 = 4$ cm$^2$.GW$^{-1}$

$\kappa_2 = 8$ cm$^2$.GW$^{-1}$

$I_1 = 0.15$ GW.cm$^{-2}$

$I_3 = 2.5$ GW$^2$.cm$^{-4}$

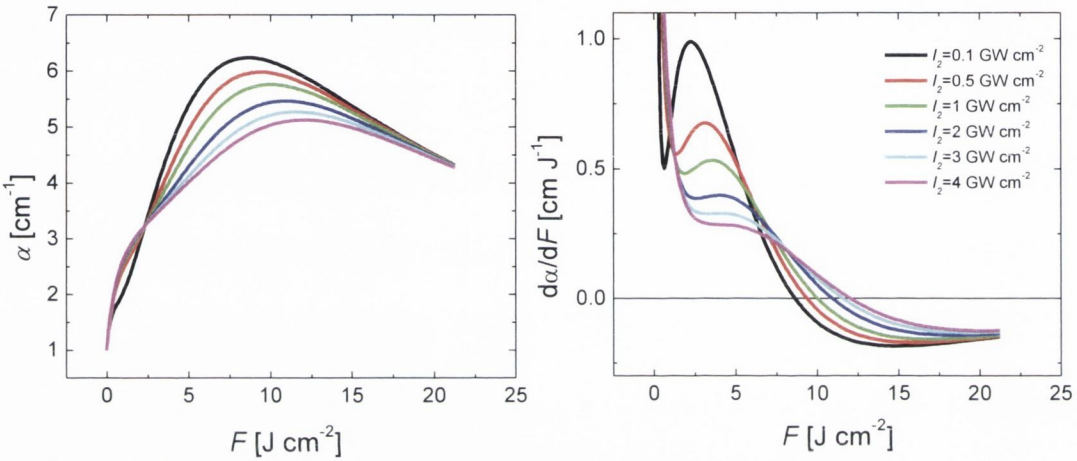



**Figure 79** Absorption coefficient $\alpha$ and $d\alpha/dF$ plotted *versus* input fluence $F$ for varying $I_2$ – case G.

case J:

$\kappa_1 = 8\ \text{cm}^2.\text{GW}^{-1}$

$\kappa_2 = 4\ \text{cm}^2.\text{GW}^{-1}$

$I_1 = 0.15\ \text{GW.cm}^{-2}$

$I_3 = 2.5\ \text{GW}^2.\text{cm}^{-4}$

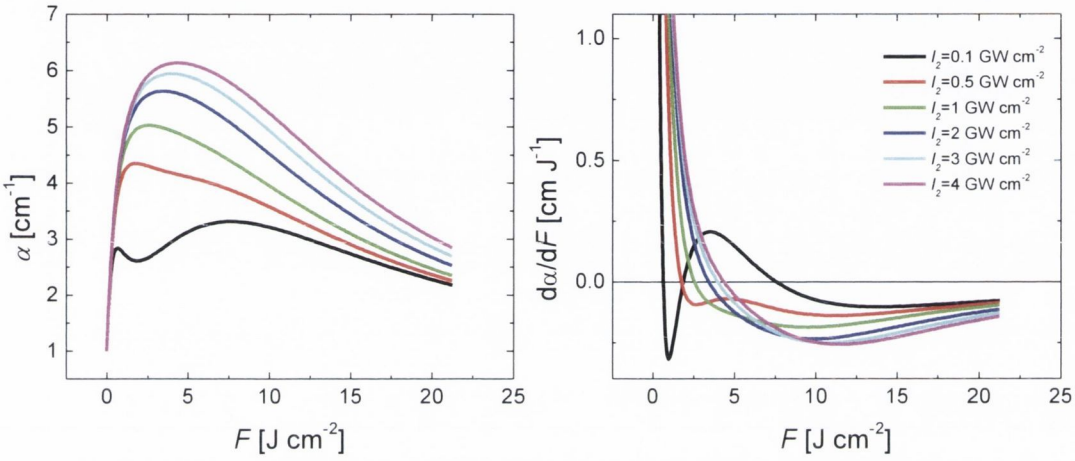



**Figure 80** Absorption coefficient $\alpha$ and $d\alpha/dF$ plotted *versus* input fluence $F$ for varying $I_2$ – case J.

case M:

$\kappa_1 = 4\ \text{cm}^2.\text{GW}^{-1}$

$\kappa_2 = 8\ \text{cm}^2.\text{GW}^{-1}$

$I_1 = 0.15\ \text{GW.cm}^{-2}$

$I_3 = 0.3\ \text{GW}^2.\text{cm}^{-4}$

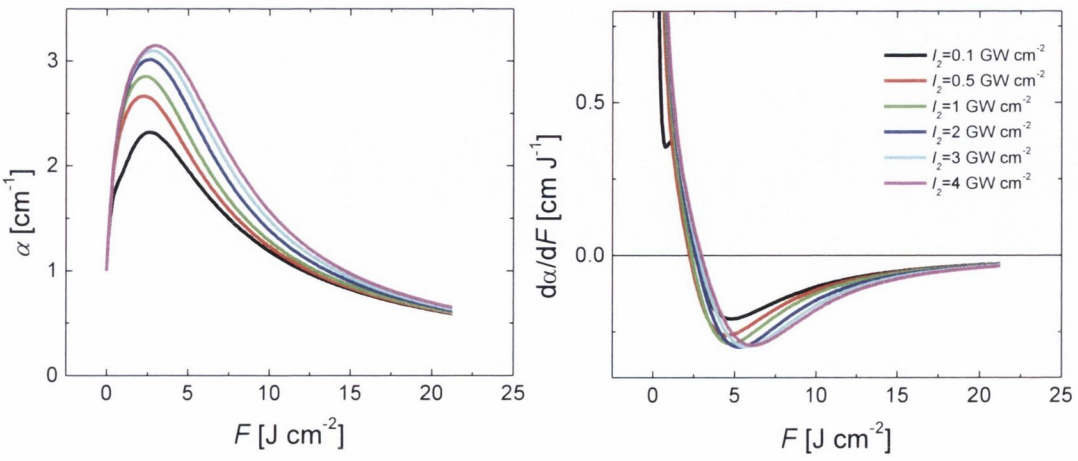



**Figure 81** Absorption coefficient $\alpha$ and $d\alpha/dF$ plotted *versus* input fluence $F$ for varying $I_2$ – case M.

- Absorption coefficient $\alpha$ and $d\alpha/dF$ plotted *versus* input fluence $F$ for varying $I_3$

case H:

$\kappa_1 = 4$ cm$^2$.GW$^{-1}$

$\kappa_2 = 8$ cm$^2$.GW$^{-1}$

$I_1 = 0.15$ GW.cm$^{-2}$

$I_2 = 0.35$ GW.cm$^{-2}$

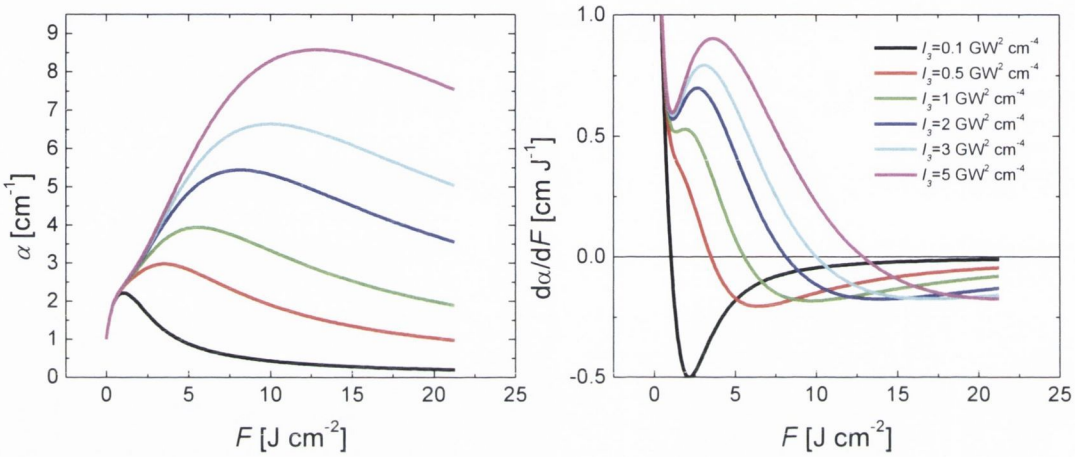



**Figure 82** Absorption coefficient $\alpha$ and $d\alpha/dF$ plotted *versus* input fluence $F$ for varying $I_3$ – case H.

case K:

$\kappa_1 = 8$ cm$^2$.GW$^{-1}$

$\kappa_2 = 4$ cm$^2$.GW$^{-1}$

$I_1 = 0.15$ GW.cm$^{-2}$

$I_2 = 0.35$ GW.cm$^{-2}$

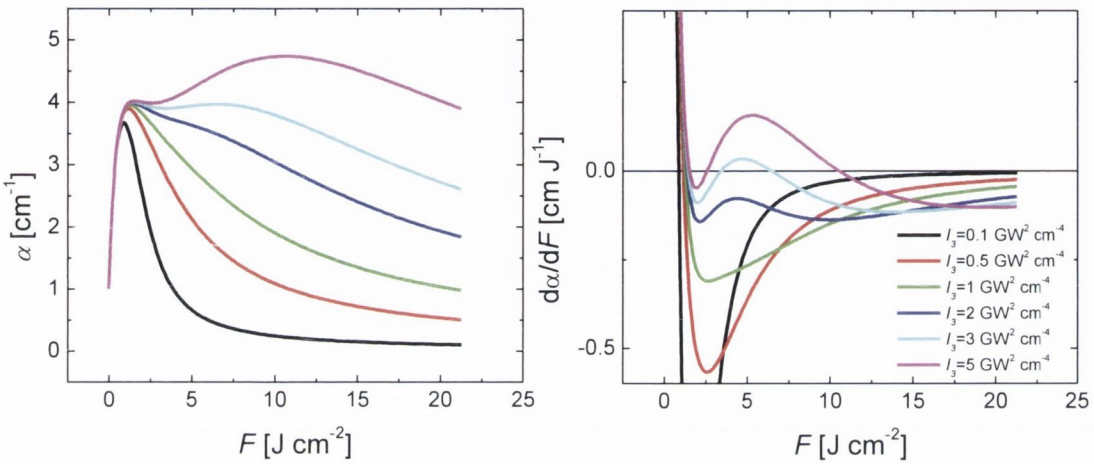



**Figure 83** Absorption coefficient $\alpha$ and $d\alpha/dF$ plotted *versus* input fluence $F$ for varying $I_3$ – case K.

# Bibliography


1. Boyd, R. W. *Nonlinear optics*, 2nd ed.; Academic Press: San Diego, CA, 2003.
2. Kerr, J., *Philos. Mag.* **1875,** *50*, 337-348.
3. Maiman, T. H., *Nature* **1960,** *187*, 493-494.
4. Franken, P. A.; Weinreich, G.; Peters, C. W.; Hill, A. E., *Phys. Rev. Lett.* **1961,** *7*, 118-119.
5. Bass, M.; Ward, J. F.; Weinreich, G.; Franken, P. A., *Phys. Rev. Lett.* **1962,** *9*, 446-448.
6. Pinnow, M., *Acta Polym.* **1993,** *44* (2), 112-112.
7. Jha, S. S., *Perspectives in optoelectronics*; World Scientific: Singapore; River Edge, NJ, 1995.
8. Degiorgio, V.; Flytzanis, C., *Nonlinear optical materials : principles and applications : Proceedings of the International School of Physics "Enrico Fermi" course CXXVI.* IOS Press: Amsterdam, 1995.
9. Marder, S. R., *Chem. Commun.* **2006,** 131-134.
10. He, G.; Liu, S., *Physics of nonlinear optics*; World Scientific: River Edge, NJ, 1999.
11. Bloembergen, N. *Nonlinear optics : a lecture note and reprint volume.* W.A. Benjamin: New York, 1965.
12. Davydov, B. L.; Derkacheva, L. D.; Dunina, V. V.; Zhabotinskii M. E.; Zolin, V. F.; Koreneva, L. G.; Samokhina M. A, *JETP Lett.* **1970,** *12*, 16-18.
13. Sauteret, C.; Hermann, J. P.; Frey, R.; Pradere, F.; Ducuing, J.; Baughman, R. H.; Chance, R. R., *Phys. Rev. Lett.* **1976,** *36*, 956-959.
14. Rustagi, K. C.; Ducuing, J., *Opt. Commun.* **1974,** *10*, 258-261.
15. Chen, Y.; Lin, Y.; Liu, Y.; Doyle, J.; He, N.; Zhuang, X. D.; Bai, J. R.; Blau, W. J., *J. Nanosci. Nanotechnol.* **2007,** *7*, 1268-1283.
16. Hollins, R. C., *Curr. Opin. Solid State Mater. Sci.* **1999,** *4*, 189-196.
17. Leite, R. C. C.; Porto, S. P. S.; Damen, T. C., *Appl. Phys. Lett.* **1967,** *10*, 100-101.
18. Hasselbeck, M. P.; VanStryland, E. W.; SheikBahae, M., *J. Opt. Soc. Am. B: Opt. Phys.* **1997,** *14*, 1616-1624.
19. Khoo, I. C.; Wood, M. V.; Chen, P. H.; Shih, M. Y., *Appl. Opt.* **1997,** *36*, 4110-22.
20. Elim, H. I.; Yang, J.; Lee, J. Y.; Mi, J.; Ji, W., *Appl. Phys. Lett.* **2006,** 88-90.
21. Calvete, M.; Yang, G. Y.; Hanack, M., *Synth. Met.* **2004,** *141*, 231-243.

22. Balaji, G.; Rekha, R. K.; Ramalingam, A., *Acta Phys. Polonica., A* **2011,** *119*, 359-363.

23. Chari, R.; Mishra, S. R.; Rawat, H. S.; Oak, S. M., *Appl. Phys. B: Lasers Opt.* **1996,** *62*, 293-297.

24. Giuliano, C. R.; Hess, L. D., *IEEE J. Quant. Electron.* **1967,** *QE 3*, 358-367.

25. Harter, D. J.; Shand, M. L.; Band, Y. B., *J. Appl. Phys.* **1984,** *56*, 865-868.

26. Jablonski, A., *Nature (London, U. K.)* **1933,** *131*, 839-40.

27. Mishra, S. R.; Mehendale, S. C., *Handbook of Advanced Electronic and Photonic Materials and Devices*, Nalwa, H. S., Ed. Academic Press: San Diego, 2001; Vol. 9, p 347.

28. McEwan, K. J.; Bourhill, G.; Robertson, J. M.; Anderson, H. L., *J. Nonlinear Opt. Phys. Mater.* **2000,** *9*, 451-468.

29. McKerns, M. M. Characterization of molecular structure, excited state absorption, and nonlienar opical response of metallotexaphyrin complexes. Ph. D. Dissertation, The University of Alabama, Birmingham, 2002.

30. Sun, Y. P.; Riggs, J. E., *Int. Rev. Phys. Chem.* **1999,** *18*, 43-90.

31. Kimball, B. R.; Nakashima, M.; DeCristofano, B. S., *Proc. SPIE* **2000,** *4106*, 264-271.

32. Koudoumas, E.; Ruth, A. A.; Couris, S.; Leach, S., *Mol. Phys.* **1996,** *88*, 125-133.

33. Kost, A.; Tutt, L.; Klein, M. B.; Dougherty, T. K.; Elias, W. E., *Opt. Lett.* **1993,** *18*, 334-336.

34. Fuqua, P. D.; Mansour, K.; Alvarez, D. J.; Marder, S. R.; Perry, J. W.; Dunn, B., *Proc. SPIE – Int. Soc. Opt. Eng.* **1992,** *1758,* 499-506.

35. Ebbesen, T. W.; Tanigaki, K.; Kuroshima, S., *Chem. Phys. Lett.* **1991,** *181*, 501-504.

36. Klimov, V.; Smilowitz, L.; Wang, H.; Grigorova, M.; Robinson, J. M.; Koskelo, A.; Mattes, B. R.; Wudl, F.; McBranch, D. W., *Res. Chem. Intermed.* **1997,** *23*, 587-600.

37. Tutt, L. W.; Boggess, T. F., *Progr. Quantum Electron.* **1993,** *17*, 299-338.

38. Kohlman R.; Klimov V.; Grigorova M.; Shi X.; Mattes B. R.; McBranch D. W.; Wang H.; Wudl F.; Nogues J.-L.; Moreshead W., *Proc. SPIE - Int. Soc. Opt. Eng.* **1997,** *3142,* 72-82.

39. McBranch, D. W., *Curr. Opin. Solid State Mater. Scie.* **1998,** *3*, 203-208.

40. Song, Y. L.; Fang, G. Y.; Wang, Y. X.; Liu, S. T.; Li, C. F.; Song, L. C.; Zhu, Y. H.; Hu, Q. M., *Appl. Phys. Lett.* **1999,** *74*, 332-334.

41. Tutt, L. W.; Kost, A., *Nature* **1992,** *356*, 225-226.

42. Mishra, S. R.; Rawat H. S.; Joshi M. P.; Mehendale S. C.; Rustagi K. C., *Proc. SPIE* **1994**, *2284*, 220-229.

43. Senge, M. O.; Fazekas, M.; Notaras, E. G. A.; Blau, W. J.; Zawadzka, M.; Locos, O. B.; Mhuircheartaigh, E. M. N., *Adv. Mater.* **2007,** *19*, 2737-2774.

44. Krivokapic, A.; Anderson, H. L.; Bourhill, G.; Ives, R.; Clark, S.; McEwan, K. J., *Adv. Mater.* **2001,** *13*, 652-656.

45. Dini, D.; Calvete, M. J. F.; Hanack, M.; Chen, W. Z.; Ji, W., *ARKIVOC* **2006**, 77-96.

46. Qureshi, F. M.; Martin, S. J.; Long, X.; Bradley, D. D. C.; Henari, F. Z.; Blau, W. J.; Smith, E. C.; Wang, C. H.; Kar, A. K.; Anderson, H. L., *Chem. Phys.* **1998,** *231*, 87-94.

47. Mendonca, C. R.; Gaffo, L.; Misoguti, L.; Moreira, W. C.; Oliveira, O. N.; Zilio, S. C., *Chem. Phys. Lett.* **2000,** *323*, 300-304.

48. Zakharova, I. B.; Kvyatkovskii, O. E.; Ermolaeva, G. M.; Spitsyna, N. G.; Shilov, V. B., *J. Opt. Tech.* **2010,** *77*, 1-5.

49. Dupuis, B.; Michaut, C.; Jouanin, I.; Delaire, J.; Robin, P.; Feneyrou, P.; Dentan, V., *Chem. Phys. Lett.* **1999,** *300*, 169-176.

50. Kaiser, W.; Garrett, C. G. B., *Phys. Rev. Lett.* **1961,** *7*, 229-231.

51. Göppert-Mayer, M., *Ann. der Physik, Ann. Phys.* **1931,** *401*, 273-294.

52. Ralston, J. M.; Chang, R. K., *Appl. Phys. Lett.* **1969,** *15*, 164-166.

53. Schwartz, J.; Naiman, C. S.; Chang, R. K., *Appl. Phys. Lett.* **1967,** *11*, 242-244.

54. Hasselbeck, M. P.; VanStryland, E. W.; SheikBahae, M., *Phys. Rev. B* **1997,** *56*, 7395-7403.

55. Rumi, M.; Perry, J. W., *Adv. Opt. Photon.* **2010,** *2*, 451-518.

56. He, G. S.; Yuan, L. X.; Cheng, N.; Bhawalkar, J. D.; Prasad, P. N.; Brott, L. L.; Clarson, S. J.; Reinhardt, B. A., *J. Opt. Soc. Am. B: Opt. Phys.* **1997,** *14*, 1079-1087.

57. Shirk, J. S., *Opt. Photon. News* **2000,** *11*, 19-23.

58. Khoo, I. C.; Wood, M. V.; Shih, M. Y.; Chen, P. H., *Opt. Express* **1999,** *4*, 432-442.

59. Mansour, K.; Soileau, M. J.; Vanstryland, E. W., *J. Opt. Soc. Am. B: Opt. Phys.* **1992,** *9*, 1100-1109.

60. Xia, T. J.; Dogariu, A. C.; Mansour, K.; Hagan, D. J.; Said, A. A.; Van Stryland, E. W.; Shi, S. In *Nonlinear optical properties of the inorganic metal cluster* $MO_2Ag_4S_8(PPh_3)_4$, Lawson, C. M., Ed. SPIE: Denver, CO, USA, 1996; pp 142-148.

61. McEwan, K. J.; Milsom, P. K.; James, D. B. In *Nonlinear optical effects in carbon suspension*, Lawson, C. M., Ed. SPIE: San Diego, CA, USA, 1998; pp 42-52.

62. Goedert, R. V.; Becker, R. J.; Clements, A. F.; Whittaker Iii, T. A. In *Overview of the shadowgraphic imaging technique and results for various materials*, Lawson, C. M., Ed. SPIE: San Diego, CA, USA, 1998; pp 2-12.

63. Justus, B. L.; Campillo, A. J.; Huston, A. L., *Opt. Lett.* **1994,** *19*, 673-675.

64. Sutherland, R. L., *Handbook of nonlinear optics*. Marcel Dekker: New York, 1996.

65. Bass, M.; Li, G.; Van Stryland, E. W.; *Handbook of optics.* McGraw-Hill: New York, 2010; Vol. IV.

66. Sheikbahae, M.; Said, A. A.; Wei, T. H.; Hagan, D. J.; Vanstryland, E. W., *IEEE J. Quantum Electron.* **1990,** *26*, 760-769.

67. Kuzyk, M. G.; Dirk, C. W., *Characterization techniques and tabulations for organic nonlinear optical materials*. Marcel Dekker: New York, 1998.

68. Wood, G. L.; Miller, M. J.; Mott, A. G., *Opt. Lett.* **1995,** *20*, 973-975.

69. Kwak, C. H.; Lee, Y. L.; Kim, S. G., *J. Opt. Soc. Am. B: Opt. Phys.* **1999,** *16*, 600-604.

70. Milgrom, R. L., *The colours of life*. Oxford University Press Inc.: New York, 1997.

71. Senge, M. O., *Chem. Commun.* **2011,** *47*, 1943-1960.

72. Kalisch, W. W.; Senge, M. O., *Angew. Chem., Int. Ed.* **1998,** *37*, 1107-1109.

73. Kadish, K. M.; Smith, K. M.; Guilard, R., *Handbook of porphyrin science;* World Scientific: New Jersey, London, 2010.

74. Kadish, K. M.; Smith, K. M.; Guilard, R., *The porphyrin handbook.* Academic: San Diego, Calif. ; London, 2000; Vol.1.

75. Kadish, K. M.; Smith, K. M.; Guilard, R., *The porphyrin handbook.* Academic: San Diego, Calif. ; London, 2000; Vol.3.

76. Kadish, K. M.; Smith, K. M.; Guilard, R., *The porphyrin handbook.* Academic: San Diego, Calif. ; London, 2000; Vol.6,

77. Kadish, K. M.; Smith, K. M.; Guilard, R., *Multiporphyrins, multiphthalocyanines, and arrays*. Academic Press: Amsterdam ; London, 2003.

78. Kruk, N. N., *J. Appl. Spectrosc.* **2008,** *75*, 461-482.

79. Suslick, K. S.; Chen, C. T.; Meredith, G. R.; Cheng, L. T., *J. Am. Chem. Soc.* **1992,** *114*, 6928-6930.

80. Albert, I. D. L.; Marks, T. J.; Ratner, M. A., *Chem. Mater.* **1998,** *10*, 753-762.

81. LeCours, S. M.; Guan, H. W.; DiMagno, S. G.; Wang, C. H.; Therien, M. J., *J. Am. Chem. Soc.* **1996,** *118*, 1497-1503.

82. Zhang, T. G.; Zhao, Y. X.; Asselberghs, I.; Persoons, A.; Clays, K.; Therien, M. J., *J. Am, Chem. Soc.* **2005,** *127*, 9710-9720.

83. Yamada, S.; Kuwata, K.; Yonemura, H.; Matsuo, T., *J. Photochem. Photobiol., A* **1995,** *87*, 115-119.

84. Uyeda, H. T.; Zhao, Y. X.; Wostyn, K.; Asselberghs, I.; Clays, K.; Persoons, A.; Therien, M. J., *J. Am. Chem. Soc.* **2002,** *124*, 13806-13813.

85. Huber, M., *Eur. J. Org. Chem.* **2001,** 4379-4389.

86. Sen, A.; Ray, P. C.; Das, P. K.; Krishnan, V., *J. Phys. Chem.* **1996,** *100*, 19611-19613.

87. Yamada, S.; Iida, H.; Matsuo, T., *Chem. Lett.* **1995,** 655-656.

88. Collman, J. P.; Kendall, J. L.; Chen, J. L.; Eberspacher, T. A.; Moylan, C. R., *Inorg. Chem.* **1997,** *36*, 5603-5608.

89. Misra, R.; Kumar, R.; PrabhuRaja, V.; Chandrashekar, T. K., *J. Photochem. Photobiol., A* **2005,** *175*, 108-117.

90. Maloney, C.; Byrne, H.; Dennis, W. M.; Blau, W.; Kelly, J. M., *Chem. Phys.* **1988,** *121*, 21-39.

91. Kandasamy, K.; Shetty, S. J.; Puntambekar, P. N.; Srivastava, T. S.; Kundu, T.; Singh, B. P., *J. Porphyrins Phthalocyanines* **1999,** *3*, 81-86.

92. Rao, D.; Aranda, F. J.; Roach, J. F.; Remy, D. E., *Appl. Phys. Lett.* **1991,** *58*, 1241-1243.

93. Rao, S. V.; Srinivas, N.; Rao, D. N.; Giribabu, L.; Maiya, B. G.; Philip, R.; Kumar, G. R., *Opt. Commun.* **2000,** *182*, 255-264.

94. Kiran, P. P.; Reddy, D. R.; Maiya, B. G.; Rao, D. N., *Opt. Mater.* **2003,** *21*, 565-568.

95. Kandasamy, K.; Shetty, S. J.; Puntambekar, P. N.; Srivastava, T. S.; Kundu, T.; Singh, B. P., *Chem. Commun.* **1997,** 1159-1160.

96. Qihuang, G.; et al., *J. Phys. D: Appl. Phys.* **1994,** *27*, 911.

97. Hosoda, M.; Wada, T.; Garito, A. F.; Sasabe, H., *Jpn. J. Appl. Phys. Lett.* **1992,** *31*, L249-L251.

98. Singh, B. P.; Vijaya, R.; Shetty, S. J.; Kandasamy, K.; Puntambekar, P. N.; Srivastava, T. S., *J. Porphyrins Phthalocyanines* **2000,** *4*, 659-664.

99. Ryppa, C.; Senge, M. O., *Heterocycles* **2004,** *63*, 505-508.

100. Kumar, G. R.; Ravikanth, M.; Banerjee, S.; Sevian, A., *Opt. Commun.* **1997,** *144*, 245-251.

101. Anderson, H. L., *Chem. Commun.* **1999,** 2323-2330.

102. Kuebler, S. M.; Denning, R. G.; Anderson, H. L., *J. Am. Chem. Soc.* **2000,** *122*, 339-347.

103. Screen, T. E. O.; Thorne, J. R. G.; Denning, R. G.; Bucknall, D. G.; Anderson, H. L., *J. Mater. Chem.* **2003,** *13*, 2796-2808.

104. Beljonne, D.; Okeefe, G. E.; Hamer, P. J.; Friend, R. H.; Anderson, H. L.; Bredas, J. L., *J. Chem. Phys.* **1997,** *106*, 9439-9460.

105. Matsuzaki, Y.; Nogami, A.; Tsuda, A.; Osuka, A.; Tanaka, K., *J. Phys. Chem. A* **2006,** *110*, 4888-4899.

106. Kim, D.; Osuka, A., *J. Phys. Chem. A* **2003,** *107*, 8791-8816.

107. Collini, E.; Ferrante, C.; Bozio, R.; Lodi, A.; Ponterini, G., *J. Mater. Chem.* **2006,** *16*, 1573-1578.

108. Si, J.; Wang, Y.; Yang, Q.; Ye, P.; Tian, H.; Zhou, Q.; Xu, H., *App. Phys. Lett.* **1996,** *69*, 1832-1834.

109. Blau, W.; Byrne, H.; Dennis, W. M.; Kelly, J. M., *Opt. Commun.* **1985,** *56*, 25-29.

110. McEwan, K.; Lewis, K.; Yang, G. Y.; Chng, L. L.; Lee, Y. W.; Lau, W. P.; Lai, K. S., *Adv. Funct. Mater.* **2003,** *13*, 863-867.

111. O'Flaherty, S. M.; Hold, S. V.; Cook, M. J.; Torres, T.; Chen, Y.; Hanack, M.; Blau, W. J., *Adv. Mater.* **2003,** *15* (1), 19-32.

112. Dini, D.; Barthel, M.; Hanack, M., *Eur. J. Org. Chem.* **2001,** 3759-3769.

113. Kiran, P. P.; Reddy, D. R.; Maiya, B. G.; Dharmadhikari, A. K.; Kumar, G. R.; Desai, N. R., *Appl. Opt.* **2002,** *41*, 7631-7636.

114. Kiran, P. P.; Srinivas, N.; Reddy, D. R.; Maiya, B. G.; Dharmadhikari, A.; Sandhu, A. S.; Kumar, G. R.; Rao, D. N., *Opt. Commun.* **2002,** *202*, 347-352.

115. Kiran, P. P.; Reddy, D. R.; Dharmadhikari, A. K.; Maiya, B. G.; Kumar, G. R.; Rao, D. N., *Chem. Phys. Lett.* **2006,** *418*, 442-447.

116. Bonnett, R.; Harriman, A.; Kozyrev, A. N., *J. Chem. Soc., Faraday Trans.* **1992,** *88*, 763-769.

117. Dini, D.; Yang, G. Y.; Hanack, M., *Targets Heterocycl. Syst.* **2004,** *8*, 1-32.

118. Bergkamp, M. A.; Dalton, J.; Netzel, T. L., *J. Am. Chem. Soc.* **1982,** *104*, 253-259.

119. Liu, Y. L.; Liu, Z. B.; Tian, J. G.; Zhu, Y.; Zheng, J. Y., *Opt. Commun.* **2008,** *281*, 776-781.

120. Jiang, L.; Jiu, T.; Li, Y.; Li, Y.; Yang, J.; Li, J.; Li, C.; Liu, H.; Song, Y., *J. Phys. Chem. B* **2008,** *112*, 756-759.

121. Su, W.; Cooper, T. M.; Nguyen, K.; Brant, M. C.; Brandelik, D. M.; McLean, D. G. In *Structure-optical property relationships of porphyrins*, Lawson, C. M., Ed. SPIE: San Diego, CA, USA, 1998; pp 136-143.

122. Notaras, E. G. A.; Fazekas, M.; Doyle, J. J.; Blau, W. J.; Senge, M. O., *Chem. Commun.* **2007,** 2166-2168.

123. Frampton, M. J.; Akdas, H.; Cowley, A. R.; Rogers, J. E.; Slagle, J. E.; Fleitz, P. A.; Drobizhev, M.; Rebane, A.; Anderson, H. L., *Org. Lett.* **2005,** *7*, 5365-5368.

124. Sevian, A.; Ravikanth, M.; Kumar, G. R., *Chem. Phys. Lett.* **1996,** *263*, 241-246.

125. Gong, Q.; Wang, Y.; Yang, S.; Xia, Z.; Zhou, Y. H.; Sun, W.; Dong, S.; Wang, D., *J. Phys. D: Appl. Phys.* **1994,** *27*, 911-913.

126. Vagin, S.; Yang, G. Y.; Lee, M. K. Y.; Hanack, M., *Opt. Commun.* **2003,** *228*, 119-125.

127. Liu, Z.-B.; Zhu, Y.-Z.; Zhu, Y.; Chen, S.-Q.; Zheng, J.-Y.; Tian, J.-G., *J. Phys. Chem. B* **2006,** *110*, 15140-15145.

128. Xu, Y. F.; Liu, Z. B.; Zhang, X. L.; Wang, Y.; Tian, J. G.; Huang, Y.; Ma, Y. F.; Zhang, X. Y.; Chen, Y. S., *Adv. Mater.* **2009,** *21*, 1275-1279.

129. Liu, Z. B.; Xu, Y. F.; Zhang, X. Y.; Zhang, X. L.; Chen, Y. S.; Tian, J. G., *J. Phys. Chem. B* **2009,** *113*, 9681-9686.

130. Guo, Z.; Du, F.; Ren, D. M.; Chen, Y. S.; Zheng, J. Y.; Liu, Z. B.; Tian, J. G., *J. Mater. Chem.* **2006,** *16*, 3021-3030.

131. Mamidala, V.; Polavarapu, L.; Balapanuru, J.; Loh, K. P.; Xu, Q. H.; Ji, W., *Opt. Express* **2010,** *18*, 25928-25935.

132. Ni Mhuircheartaigh, E. M.; Giordani, S.; Blau, W. J., *J. Phys. Chem. B* **2006,** *110*, 23136-23141.

133. Aloukos, P.; Iliopoulos, K.; Couris, S.; Guldi, D. M.; Sooambar, C.; Mateo-Alonso, A.; Nagaswaran, P. G.; Bonifazi, D.; Prato, M., *J. Mater. Chem.* **2011,** *21*, 2524-2534.

134. Jia, M. L.; Wan, Y.; Wang, X. F.; Xia, A. D., *Sci. China: Chem.* **2010,** *53*, 419-425.

135. Kruk, M.; Karotki, A.; Drobizhev, M.; Kuzmitsky, V.; Gael, V.; Rebane, A., *J. Lumin.* **2003,** *105*, 45-55.

136. Kim, D. Y.; Ahn, T. K.; Kwon, J. H.; Kim, D.; Ikeue, T.; Aratani, N.; Osuka, A.; Shigeiwa, M.; Maeda, S., *J. Phys. Chem. A* **2005,** *109*, 2996-2999.

137. Rath, H.; Sankar, J.; PrabhuRaja, V.; Chandrashekar, T. K.; Nag, A.; Goswami, D., *J. Am. Chem. Soc.* **2005,** *127*, 11608-11609.

138. Drobizhev, M.; Stepanenko, Y.; Rebane, A.; Wilson, C. J.; Screen, T. E. O.; Anderson, H. L., *J. Am. Chem. Soc.* **2006,** *128*, 12432-12433.

139. Drobizhev, M.; Karotki, A.; Kruk, M.; Mamardashvili, N. Z.; Rebane, A., *Chem. Phys. Lett.* **2002,** *361*, 504-512.

140. Luo, Y.; Rubio-Pons, O.; Guo, J. D.; Agren, H., *J. Chem. Phys.* **2005,** *122*, 2.

141. Zhou, X.; Ren, A. M.; Feng, J. K.; Liu, X. J., *THEOCHEM* **2004,** *679*, 157-164.

142. Ray, P. C.; Sainudeen, Z., *J. Phys. Chem. A* **2006,** *110*, 12342-12347.

143. Screen, T. E. O.; Thorne, J. R. G.; Denning, R. G.; Bucknell, D. G.; Anderson, H. L., *J. Am. Chem. Soc.* **2002,** *124*, 9712-9713.

144. Zhang, X. B.; Feng, J. K.; Ren, A. M.; Sun, C. C., *THEOCHEM* **2007,** *804*, 21-29.

145. Tanihara, J.; Ogawa, K.; Kobuke, Y., *J. Photochem. Photobiol., A* **2006,** *178*, 140-149.

146. Karotki, A.; Drobizhev, M.; Dzenis, Y.; Taylor, P. N.; Anderson, H. L.; Rebane, A., *Phys. Chem. Chem. Phys.* **2004,** *6*, 7-10.

147. Ahn, T. K.; Kim, K. S.; Kim, D. Y.; Noh, S. B.; Aratani, N.; Ikeda, C.; Osuka, A.; Kim, D., *J. Am. Chem. Soc.* **2006,** *128*, 1700-1704.

148. Hanack, M.; Dini, D.; Barthel, M.; Vagin, S., *Chem. Rec.* **2002,** *2*, 129-148.

149. Henari, F. Z.; Blau, W. J.; Milgrom, L. R.; Yahioglu, G.; Phillips, D.; Lacey, J. A., *Chem. Phys. Lett.* **1997,** *267*, 229-233.

150. Gao, Y. C.; Zhang, X. R.; Li, Y. L.; Liu, H. F.; Wang, Y. X.; Chang, Q.; Jiao, W. Y.; Song, Y. L., *Opt. Commun.* **2005,** *251*, 429-433.

151. Gao, Y.; Chang, Q.; Ye, H.; Jiao, W.; Song, Y.; Wang, Y.; Qin, J., *Appl. Phys. B: Lasers Opt.* **2007,** *88*, 89-92.

152. Su, W. J.; Cooper, T. M.; Tang, N.; Krein, D.; Jiang, H.; Brandelik, D.; Fleitz, P.; Brandt, M. C.; Mclean, D. G., *Mater. Res. Soc. Symp. Proc.* **1997,** *479*, 313.

153. Rothemund, P., *J. Am. Chem. Soc.* **1935,** *57*, 2010-2011.

154. Rothemund, P., *J. Am. Chem. Soc.* **1939,** *61*, 2912-2915.

155. Adler, A. D.; Longo, F. R.; Shergalis, W., *J. Am. Chem. Soc.* **1964,** *86*, 3145-3149.

156. Celli, J. P.; Spring, B. Q.; Rizvi, I.; Evans, C. L.; Samkoe, K. S.; Verma, S.; Pogue, B. W.; Hasan, T., *Chem. Rev.* **2010,** *110*, 2795-2838.

157. Gust, D.; Moore, T. A.; Moore, A. L., *Acc. Chem. Res.* **2009,** *42*, 1890-1898.

158. Arsenault, G. P.; Bullock, E.; Macdonald, S. F., *J. Am. Chem. Soc.* **1960,** *82*, 4384-4389.

159. Hatscher, S.; Senge, M. O., *Tetrahedron Lett.* **2003,** *44*, 157-160.

160. Rao, P. D.; Dhanalekshmi, S.; Littler, B. J.; Lindsey, J. S., *J. Org. Chem.* **2000,** *65*, 7323-7344.

161. Rao, P. D.; Littler, B. J.; Geier, G. R.; Lindsey, J. S., *J. Org. Chem.* **2000,** *65*, 1084-1092.

162. Dogutan, D. K.; Ptaszek, M.; Lindsey, J. S., *J. Org. Chem.* **2008,** *73*, 6187-6201.

163. Taniguchi, M.; Balakumar, A.; Fan, D. Z.; McDowell, B. E.; Lindsey, J. S., *J. Porphyrins Phthalocyanines* **2005,** *9*, 554-574.

164. Fan, D. Z.; Taniguchi, M.; Yao, Z.; Dhanalekshmi, S.; Lindsey, J. S., *Tetrahedron* **2005,** *61*, 10291-10302.

165. Dogutan, D. K.; Zaidi, S. H. H.; Thamyongkit, P.; Lindsey, J. S., *J. Org. Chem.* **2007,** *72*, 7701-7714.

166. Senge, M. O.; Shaker, Y. M.; Pintea, M.; Ryppa, C.; Hatscher, S. S.; Ryan, A.; Sergeeva, Y., *Eur. J. Org. Chem.* **2010,** 237-258.

167. Drach, J. E.; Longo, F. R., *J. Org. Chem.* **1974,** *39*, 3282-3284.

168. Sugiura, K.; Fujimoto, Y.; Sakata, Y., *Chem. Commun.* **2000,** 1105-1106.

169. Brinas, R. P.; Bruckner, C., *Tetrahedron* **2002,** *58*, 4375-4381.

170. Goncalves, D. P. N.; Ladame, S.; Balasubramanian, S.; Sanders, J. K. M., *Org. Biomol. Chem.* **2006,** *4*, 3337-3342.

171. Heo, P. Y.; Lee, C. H., *Bull. Korean Chem. Soc.* **1996,** *17*, 515-520.

172. Senge, M. O.; Ryppa, C.; Fazekas, M.; Zawadzka, M.; Dahms, K., *Chem.--Eur. J.* **2011,** *17*, 13562-13573.

173. Dogutan, D. K.; Lindsey, J. S., *J. Org. Chem.* **2008,** *73*, 6728-6742.

174. Buchler, J. W. In *Porphyrins and Metalloporphyrins*; Smith K. M., Ed.; Elsevier: Amsterdam, 1975, p 157-231.

175. Ball, R. G.; Lee, K. M.; Marshall, A. G.; Trotter, J., *Inorg. Chem.* **1980,** *19*, 1463-1469.

176. Lemon, C. M.; Brothers, P. J.; Boitrel, B., *Dalton Trans.* **2011,** *40*, 6591-6609.

177. Arnold, D. P.; Blok, J., *Coord. Chem. Rev.* **2004,** *248*, 299-319.

178. Sonogashira, K.; Tohda, Y.; Hagihara, N., *Tetrahedron Lett.* **1975,** 4467-4470.

179. Ali, H.; van Lier, J. E., *Tetrahedron* **1994,** *50*, 11933-11944.

180. Boyle, R. W.; Johnson, C. K.; Dolphin, D., *J. Chem. Soc., Chem. Commun.* **1995,** 527-528.

181. Ryan, A.; Gehrold, A.; Perusitti, R.; Pintea, M.; Fazekas, M.; Locos, O. B.; Blaikie, F.; Senge, M. O., *Eur. J. Org. Chem.* **2011,** 5817-5844.

182. Taniguchi, S.; Hasegawa, H.; Yanagiya, S.; Tabeta, Y.; Nakano, Y.; Takahashi, M., *Tetrahedron* **2001,** *57*, 2103-2108.

183. Katritzky, A. R.; Law, K. W., *Magn. Reson. Chem.* **1988,** *26*, 129-133.

184. Lindsey, J. S.; Schreiman, I. C.; Hsu, H. C.; Kearney, P. C.; Marguerettaz, A. M., *J. Org. Chem.* **1987,** *52*, 827-836.

185. Dimagno, S. G.; Lin, V. S. Y.; Therien, M. J., *J. Org. Chem.* **1993,** *58* , 5983-5993.

186. Raptopoulou, C.; Daphnomili, D.; Karamalides, A.; Di Vaira, M.; Terzis, A.; Coutsolelos, A. G., *Polyhedron* **2004,** *23*, 1777-1784.

187. Mink, L. M.; Neitzel, M. L.; Bellomy, L. M.; Falvo, R. E.; Boggess, R. K.; Trainum, B. T.; Yeaman, P., *Polyhedron* **1997,** *16*, 2809-2817.

188. Adler, A. D.; Longo, F. R.; Kampas, F.; Kim, J., *J. Inorg. Nucl. Chem.* **1970,** *32*, 2443-2445.

189. Plater, M. J.; Aiken, S.; Bourhill, G., *Tetrahedron* **2002,** *58*, 2415-2422.

190. Maya, E. M.; Snow, A. W.; Shirk, J. S.; Pong, R. G. S.; Flom, S. R.; Roberts, G. L., *J. Mater. Chem.* **2003,** *13*, 1603-1613.

191. Syrbu, S. A.; Ageeva, T. A.; Semeikin, A. S.; Koifman, O. I., *Russ. Chem. Bull.* **2007,** *56*, 707-731.

192. Strohalm, M.; Kavan, D.; Novák, P.; Volný, M.; Havlíček, V., *Anal. Chem.* **2010,** *82*, 4648-4651.

193. Stulz, E.; Mak, C. C.; Sanders, J. K. M., *J. Chem. Soc., Dalton Trans.* **2001,** 604-613.

194. Crossley, M. J.; Thordarson, P.; Wu, R. A. S., *J. Chem. Soc., Perkin Trans. 1* **2001,** 2294-2302.

195. Abraham, R. J., *Mol. Phys.* **1961,** *4*, 145-152.

196. Ryppa, C.; Senge, M. O.; Hatscher, S. S.; Kleinpeter, E.; Wacker, P.; Schilde, U.; Wiehe, A., *Chem.--Eur. J.* **2005,** *11*, 3427-3442.

197. Abraham, R. J.; Eivazi, F.; Pearson, H.; Smith, K. M., *J. Chem. Soc., Chem. Commun.* **1976,** 699-701.

198. Abraham, R. J.; Eivazi, F.; Pearson, H.; Smith, K. M., *J. Chem. Soc., Chem. Commun.* **1976,** 698-699.

199. Zhang, Y. H.; Wu, Y., *Chin. Chem. Lett.* **2005,** *16*, 534-536.

200. Maiti, N. C.; Mazumdar, S.; Periasamy, N., *J. Phys. Chem. B* **1998,** *102*, 1528-1538.

201. George, R. D.; Snow, A. W.; Shirk, J. S.; Barger, W. R., *J. Porphyrins Phthalocyanines* **1998,** *2*, 1-7.

202. Si, J. H.; Yang, M.; Wang, Y. X.; Zhang, L.; Li, C. F.; Wang, D. Y.; Dong, S. M.; Sun, W. F., *Appl. Phys. Lett.* **1994,** *64*, 3083-3085.

203. Swatton, S. N. R.; Welford, K. R.; Till, S. J.; Sambles, J. R., *Appl. Phys. Lett.* **1995,** *66* , 1868-1870.

204. Przhonska, O. V.; Lim, J. H.; Hagan, D. J.; Van Stryland, E. W.; Bondar, M. V.; Slominsky, Y. L., *J. Opt. Soc. Am. B: Opt. Phys.* **1998,** *15*, 802-809.

205. Deng, X. X.; Zhang, X. R.; Wang, Y. X.; Song, Y. L.; Liu, S. T.; Li, C. F., *Opt. Commun.* **1999,** *168*, 207-212.

206. Srinivas, N.; Rao, S. V.; Rao, D.; Kimball, B. K.; Nakashima, M.; Decristofano, B. S.; Rao, D. N., *J. Porphyrins Phthalocyanines* **2001,** *5*, 549-554.

207. Dini, D.; Vagin, S.; Hanack, M.; Amendola, V.; Meneghetti, M., *Chem. Commun.* **2005,** 3796-3798.

208. George, M.; Muneera, C. I.; Singh, C. P.; Bindra, K. S.; Oak, S. M., *Opt. Laser Technol.* **2008,** *40*, 373-378.

209. Konstantaki, M.; Koudoumas, E.; Couris, S.; Laine, P.; Amouyal, E.; Leach, S., *J. Phys. Chem. B* **2001,** *105*, 10797-10804.

210. Srinivas, N.; Rao, S. V.; Rao, D. N., *J. Opt. Soc. Am. B: Opt. Phys.* **2003,** *20*, 2470-2479.

211. McKerns, M. M.; Sun, W. F.; Lawson, C. M.; Gray, G. M., *J. Opt. Soc. Am. B: Opt. Phys.* **2005,** *22*, 852-861.

212. Dini, D.; Calvete, M. J. F.; Hanack, M.; Amendola, V.; Meneghetti, M., *J. Am. Chem. Soc.* **2008,** *130*, 12290-12298.

213. Venkatram, N.; Rao, D. N.; Giribabu, L.; Rao, S. V., *Appl. Phys. B-Lasers Opt.* **2008,** *91*, 149-156.

214. Azenha, E. G.; Serra, A. C.; Pineiro, M.; Pereira, M. M.; de Melo, J. S.; Arnaut, L. G.; Formosinho, S. J.; Gonsalves, A., *Chem. Phys.* **2002,** *280*, 177-190.

215. Duarte, F. J.; Hillman, L. W. *Dye laser principles : with applications*. Academic Press: Boston ; London, 1990.

216. Röder, B.; Buchner, M.; Ruckmann, I.; Senge, M. O., *Photochem. Photobiol. Sci.* **2010,** *9*, 1152-1158.

217. Rao, D. N., *Opt. Mater.* **2003,** *21*, 45-49.

218. Zawadzka, M.; Wang, J.; Blau, W. J.; Senge, M. O., *Chem. Phys. Lett.* **2009,** *477*, 330-335.

219. Barzda, V.; Peterman, E. J. G.; van Grondelle, R.; van Amerongen, H., *Biochemistry* **1998,** *37*, 546-551.

220. Damoiseau, X.; Tfibel, F.; Hoebeke, M.; Fontaine-Aupart, M. P., *Photochem. Photobiol.* **2002,** *76*, 480-485.

221. Dini, D.; Barthel, M.; Hanack, M., *Eur. J. Org. Chem.* **2001,** 3759-3769.

222. Unnikrishnan, K. P.; Thomas, J.; Nampoori, V. P. N.; Vallabhan, C. P. G., *Opt. Commun.* **2003,** *217*, 269-274.

223. Yuksek, M.; Elmali, A.; Durmus, M.; Yaglioglu, H. G.; Unver, H.; Nyokong, T., *J. Opt.* **2010,** *12*.

224. Su, W. J.; Cooper, T. M.; Brant, M. C., *Chem. Mater.* **1998,** *10*, 1212-1213.

225. Kimball, B. R.; Altshuler, K.; Cohen, S.; DeCristofano, B., *Proc. SPIE* **2001,** *4462*, 54-64.

226. Elim, H. I.; Ouyang, J. Y.; Goh, S. H.; Ji, W., *Thin Solid Films* **2005,** *477*, 63-72.

227. Doyle, J. J.; Wang, J.; O'Flaherty, S. M.; Chen, Y.; Slodek, A.; Hegarty, T.; Carpenter, L. E.; Wöhrle, D.; Hanack, M.; Blau, W. J., *J. Opt. A: Pure Appl. Opt.* **2008,** *10*, 9.

228. Dou, K.; Sun, X. D.; Wang, X. J.; Parkhill, R.; Guo, Y.; Knobbe, E. T., *IEEE J. Quantum Electron.* **1999,** *35*, 1004-1014.

229. He, C. Y.; Wu, Y. Q.; Shi, G.; Jiang, L.; Duan, W.; Song, Y.; Chang, Q., *J. Porphyrins Phthalocyanines* **2007,** *11*, 496-502.

230. Stone, A.; Fleische.Eb, *J. Am. Chem. Soc.* **1968,** *90*, 2735-2748.

231. Senge, M. O.; Forsyth, T. P.; Nguyen, L. T.; Smith, K. M., *Angew. Chem. Int. Ed. Engl.* **1995,** *33*, 2485-2487.

232. Chirvony, V. S.; van Hoek, A.; Galievsky, V. A.; Sazanovich, I. V.; Schaafsma, T. J.; Holten, D., *J. Phys. Chem. B* **2000,** *104*, 9909-9917.

233. Liu, Z. B.; Zhu, Y.; Zhu, Y. Z.; Tian, J. G.; Zheng, J. Y., *J. Phys. Chem. B* **2007,** *111*, 14136-14142.

234. Goncalves, P. J.; Borissevitch, I. E.; Zilio, S. C., *Chem. Phys. Lett.* **2009,** *469*, 270-273.

235. Gupta, I.; Ravikanth, M., *J. Photochem. Photobiol., A* **2006,** *177*, 156-163.

236. Goncalves, P. J.; De Boni, L.; Neto, N. M. B.; Rodrigues, J. J.; Zilio, S. C.; Borissevitch, I. E., *Chem. Phys. Lett.* **2005,** *407*, 236-241.

237. Mhuircheartaigh, E. M. N.; Blau, W. J.; Prato, M.; Giordani, S., *Carbon* **2007,** *45*, 2665-2671.

238. Senge, M. O.; Kalisch, W. W., *Z. Naturforsch. B Chem. Sci.* **1999,** *54*, 943-959.

239. Senge, M. O., *Z. Naturforsch. B Chem. Sci.* **2000,** *55*, 336-344.

240. Poveda, J. C.; Guerrero, A.; Alvarez, I.; Cisneros, C., *J. Photochem. Photobiol., A* **2011,** *220*, 31-38.

241. Bhardwaj, V. R.; Rajgara, F. A.; Vijayalakshmi, K.; Kumarappan, V.; Mathur, D.; Sinha, A. K., *Phys. Rev. A* **1998,** *58*, 3849-3855.

242. Baldo, M. A.; O'Brien, D. F.; You, Y.; Shoustikov, A.; Sibley, S.; Thompson, M. E.; Forrest, S. R., *Nature* **1998,** *395*, 151-154.

243. Zhu, L. J.; Wang, J.; Reng, T. G.; Li, C. Y.; Guo, D. C.; Guo, C. C., *J. Phys. Org. Chem.* **2010,** *23*, 190-194.

244. O'Brien, D. F.; Giebeler, C.; Fletcher, R. B.; Cadby, A. J.; Palilis, L. C.; Lidzey, D. G.; Lane, P. A.; Bradley, D. D. C.; Blau, W., *Synth. Met.* **2001,** *116*, 379-383.

245. Tuffy, B. Porphyrin Materials for Organic Light Emitting Diodes. M.S. Dissertation, Trinity College Dublin, Dublin, 2010.

246. Virgili, T.; Lidzey, D. G.; Bradley, D. D. C., *Adv. Mater.* **2000,** *12*, 58-62.